DESCRIPTIONS OF THREE NEW SPECIMENS OF CIMOLODONTANS AND A PHYLOGENETIC STUDY OF THE POSTCRANIAL ANATOMY OF MULTITUBERCULATA (MAMMALIA, SYNAPSIDA)

By

BOLORTSETSEG MINJIN

A dissertation submitted to the Graduate Faculty in Earth and Environmental Sciences
in partial fulfillment of the requirement for the degree of Doctor of Philosophy,
The City University of New York

2008

UMI Number: 3303791

ProQuest Information and Learning Company
300 North Zeeb Road
P.O. Box 1346
Ann Arbor, MI 48106-1346

This manuscript has been read and accepted for the
Graduate Faculty in Earth and Environmental Sciences in satisfaction of the
dissertation requirement for the degree of Doctor of Philosophy.

Dr. Meng Jin

[**required signature**]

Date 01/23/2008 — Chair of Examining Committee

Prof. Yehuda Klein

[**required signature]**

Date 01/23/2008 — Executive Officer

Dr. Michael J. Novacek

Dr. Guillermo W. Rougier

Dr. John H. Wahlert

Prof. Nehru E. Cherukupalli

Supervisory Committee

THE CITY UNIVERSITY OF NEW YORK

Abstract

DESCRIPTIONS OF THREE NEW SPECIMENS OF CIMOLODONTANS AND A PHYLOGENETIC STUDY OF THE POSTCRANIAL ANATOMY OF MULTITUBERCULATA (MAMMALIA, SYNAPSIDA)

By

Bolortsetseg Minjin

Advisor: Dr. Meng Jin

The position of Multituberculata within Mammalia and the phylogenetic relationships among multituberculates remain controversial. Previous comparative studies on the postcranial skeletons of multituberculates have suggested that this part of the skeleton is highly conserved and provides little phylogenetic information for resolving relationships within Multituberculata; however, detailed examination of published specimens and anatomical descriptions of three new partial multituberculate skeletons demonstrate that this is not the case.

Three new skeletons are described 1) a partial skeleton of *Ectypodus* sp. from the newly discovered Bangtail-2 locality (Early-Late Paleocene, Montana, USA), 2) partially articulated skeleton of an undescribed taxon referred to as the Udan Multi, which is closely related to *Tombaatar sabuli*, from the Udan Sayr locality (Late Cretaceous, Mongolia), and 3) a nearly complete and articulated skeleton of *Kryptobaatar dashzevegi* from the locality of

Ukhaa Tolgod (Late Cretaceous, Mongolia). The skeleton of *Kryptobaatar* includes the only multituberculate manus preserved in 3 dimensions, and it displays a mosaic of features; large centrale, contact of metacarpal V and cuneiform as in monotremes, enlarged trapezium and cranial displacement of metacarpal I as in trechnotherians (symmetrodonts and therian mammals), a fairly minor degree of humeral torsion, and fusion of cervical ribs to form transverse foramina of the cervical vertebrae. The new specimen of *Ectypodus* has a surprisingly derived ankle; its lateral astragalotibial facet on the astragalus is pulley-shaped. The calcaneus of the Udan Multi has a well developed calcaneal crest, reminiscent of the morphology seen in early mammaliaforms.

Previous phylogenetic hypotheses for the relationships within Multituberculata were tested with a data matrix of 35 taxa coded for 95 postcranial characters, of which 77 are new. Noteworthy findings include: 1) postcranial evidence for a clade of Late Cretaceous Mongolian multituberculates excluding *Djadochtatherium*, 2) morphology of the tibial articular surface on the astragalus supports a close phylogenetic relationship between *Ectypodus* and *Stygimys*, which previously had been placed in separate families, 2) discovery of eight new postcranial autapomorphies for Multituberculata, and 3) strong support for a close relationship between two Mongolian multituberculates, the Udan Multi and *Catopsbaatar*.

ACKNOWLEDGEMENTS

I want to thank my parents, Minjin and Urjin, whose support I have always been able to depend on and who have always given me sound advice. I would like to thank my advisor and committee members for their help and support. I appreciate Drs. Michael Novacek and Mark Norell, who allowed me to work on some amazing fossils from Mongolia and gave me the opportunity to study in the United States. I would like to thank my adviser, Dr. Meng Jin, who was always there when I needed help. Dr. Guillermo Rougier was my first teacher of cranial anatomy of mammals and frequently gave me good advice. I greatly enjoyed taking classes with Dr. John Wahlert and Prof. Nehru Cherukupalli. I want to thank my husband Jonathan Geisler, who did many drawings for the figures used in my dissertation and spent many hours editing my dissertation.

I want to extend my thanks to the 1996-2000 field crews of the joint expedition between the Mongolian Academy of Sciences and American Museum of Natural History (AMNH), particularly to Dr. Cathy Forster (Stony Brook University) who found the nearly complete skeleton of *Kryptobaatar dashzevegi* that is described in my dissertation. I want to thank Doug Boyer (Stony Brook University) and Dr. Jonathan Bloch (Florida Museum of Natural History) for allowing me to work on the specimen *Ectypodus* sp. from their newly discovered site in Montana. Fossils that I described in my dissertation were skillfully prepared by Amy Davidson (AMNH), Santiago Reuil (University of Louisville), and Doug Boyer (Stony Brook University). Photography of specimens was done by several talented individuals: Mick Ellison (AMNH), Doug Boyer (Stony Brook University), Ed Heck

(AMNH), Benjamin Burger (AMNH), Rick Edwards (AMNH) and Marian Dziewiński (Institute of Paleobiology, Polish Academy of Sciences, Poland).

I want to thank several people who helped me during my visits to museum collections: Daniel Brinkman, Marilyn Fox, Dr. Walter Joyce, and Vicki Fitzgerald (Peabody Museum of Natural History); Dr. Charles R. Schaff (Museum of Comparative Zoology); Dr. David Fox (University of Minnesota); Drs. Richard Fox, Craig Scott, Phil Currie, Eva Koppelhus, and Michael Caldwell (University of Alberta, Canada); Dr. Williams Clemens, Dr. Pat Holroyd, Dr. Kevin Padian, and Brian Kraatz (University of California, Berkeley); Dr. Zofia Kielan-Jaworowska (Institute of Paleobiology, Polish Academy of Sciences, Poland); Dr.Yuanqing Wang (Institute of Vertebrate Paleontology and Paleoanthropology, China).

I want to thank several individuals for discussions that helped me clarify my own thoughts on multituberculate evolution during the course of my dissertation research: Drs. Meng Jin, Guillermo Rougier, Michael Novacek, Zofia Kielan-Jaworowska, Yaoming Hu, Jonathan Geisler, Doug Boyer, Demberel Dashzeveg, Ann Weil, John Wahlert and Luo Zhe-Xi. I have received so much help while being a graduate student, and I am grateful to all of the following individuals: Dr. Ines Horovitz, Mick Ellison, Oyuntsetseg Waskin, Batbold Minjin, Batbayar Minjin, Susan Bell, Diana Bynum, Carl Mehling, Fiona Brady, Dr. Chris Norris, Dr. Zofia Kielan-Jaworowska, Dr. Zbigniew Jaworowski, Dr. Matthew Milhbachler, Dr. Sunny Hwang, Sumru Arcanli, Jennifer Lane, Dr. Robert Asher, Dr. Peter Makovicky, Yumiko Iwasaki, Dr. Diego Pol, Dr. Tom Rothwell, Dr. Keqin Gao, Dr. Yaoming Hu, Dr. Dallas Rhodes, Sarita Warren, Gabriella Rosen, Jessica Breeler, Alejandra Lora, Loraine Meeker, Chester Tarka, Munkhbileg Namsrai, Tergel Badraa, Brian Kraatz, and Illsa Lund.

This work was supported by a Frick Graduate Student Fellowship from the American Museum of Natural History (AMNH), a Theodore Roosevelt Memorial Grant (AMNH), the Carter Fund of the Department of Vertebrate Paleontology (AMNH), an Ernst Mayr Travel Grant in Animal Systematics (Museum of Comparative Zoology, Harvard University), and the Doris O. and Samuel P. Welles Research Fund (University of California's Museum of Paleontology).

TABLE OF CONTENTS

FIGURES

TABLES

INTRODUCTION

Multituberculata is an extinct clade of mammals known from the Late Jurassic through Late Eocene, with specimens being collected from Asia, North America, South America, Europe, and Africa (Kielan-Jaworowska et al., 2004). Although in most of the latest studies (e.g. Rowe, 1988; Rougier et al., 1996; Hu et al., 1997; Ji et al., 1999; Luo et al., 2002; Luo and Wible, 2005) Multituberculata form a stem group to Theria (the clade that includes Metatheria and Eutheria) the position of Multituberculata within Mammalia is still controversial (Luo et al., 2002). Teeth, which comprise the majority of the Mesozoic mammal record and are the sole basis for many multituberculate type specimens, are highly derived in multituberculates making comparisons with other taxa difficult. Among other mammaliamorph groups, multituberculate teeth resemble those of haramiyidans (Simpson, 1947; Hahn, 1973; Butler, 2000). The latter have frequently been placed with multituberculates in the Subclass Allotheria (e.g. Kielan-Jaworowska et al., 2004). However, there are substantial differences between the teeth and dental occlusion in the two groups, and unlike multituberculates, haramiyidans retain attachment of the postdentary bones on the medial surface of the dentary (Jenkins et al., 1997).

Cranial data as a whole support a multituberculate and monotreme sister-group relationship (Kielan-Jaworowska, 1971; Meng 1992; Wible and Hopson, 1993; Meng and Wyss, 1995; Wang et al., 2001; Hu et al., 2005; but see Rougier et al., 1996a,b), even though individual cranial characters within the cranial partition support affinities with eutriconodontans or therian mammals (Kielan-Jaworowska, 1986; Rowe, 1989; Wible and

Hopson, 1993; Rougier et al., 1996c; Luo et al., 2002; Rougier and Wible, 2006). The inclusion of postcranial data into studies on the higher-level phylogeny of mammals has stabilized the position of multituberculates as the sister-group to a clade that includes Theria plus symmetrodonts and possibly eutriconodontans (Rowe 1988, 1993; Sereno and McKenna 1995; Hu et al. 1997), with both hind limb (Luo et al., 2002) and forelimb characters supporting this position (Rowe, 1989; Sereno and McKenna, 1995; Sereno, 2006). Despite the emerging and still controversial consensus on the phylogenetic position of Multituberculata, the postcranial data for this clade is based on relatively few specimens, and additional fossils are needed to test the hypothesis that multituberculates and trechnotherians are closely related.

Even though multituberculate skeletons are exceedingly rare in North America, isolated bones are common and over the years various authors have tentatively referred some of these bones to cimolodontan multituberculates (e.g. Gidley, 1909; Broom, 1914; Simpson, 1928; Simpson and Elftman, 1928; Granger and Simpson, 1929; Deischl, 1964; Clemens, 1963; Krause and Jenkins, 1983). Taxonomic allocation of these isolated bones is difficult and has generally been based on their relatives sizes, frequencies, and geographic and geologic distribution (e.g. Granger and Simpsons, 1929; Deischl, 1964; Sahni, 1972). Although isolated postcranial specimens can provide unique information for resolving mammalian systematics (for an example with marsupials see Szalay, 1993), they have not been included in previous phylogenetic analyses of multituberculates because of the difficulty in assigning isolated postcrania to named taxa (e.g. Simmons, 1993; Rougier et al., 1997; Kielan-Jaworowska and Hurum, 1997).

Most studies on multituberculate postcrania have relied on isolated, or in rare cases, partially articulated, specimens (e.g. Gidley, 1909; Broom, 1914; Simpson, 1926; Simpson, and Elftman, 1928; Granger, and Simpson, 1929; McKenna, 1961; Clemens, 1963; Sloan, and Van Valen, 1965; Kielan-Jaworowska, 1979; Kielan-Jaworowska, 1989; Sahni, 1972; Jenkins, 1973; Kielan- Jaworowska and Dashzeveg, 1977; Krause and Baird, 1979; Krause and Jenkins, 1983; Jenkins and Krause, 1983; Kielan-Jaworowska and Qi, 1990). There are about 10 taxa represented by postcranial bones associated with craniodental remains (McKenna, 1961; Krause and Jenkins, 1983; Kielan-Jaworowska and Tao, 1990; Meng and Miao, 1992; Kielan-Jaworowska and Gambaryan, 1994; Sereno and McKenna, 1995; Hu and Wang, 2002; Sereno, 2006). Of these 10 taxa, all are from Asia except for the cimolodontan *Ptilodus kummae* (Jenkins and Krause, 1983; Krause and Jenkins, 1983). The association of postcranial bones with craniodental specimens is important because the type specimens of nearly all multituberculate species consist of isolated teeth or partial upper and/or lower jaws. Without such associations, the identification of isolated postcrania to genera and even families is often tenuous.

PREVIOUS WORK ON MULTITUBERCULATE POSTCRANIA

To date, Krause and Jenkins (1983) and Kielan-Jaworowska and Gambaryan (1994) are the only studies that have compared in detail the postcrania of different multituberculates. Krause and Jenkins (1983) described the skeleton of *Ptilodus kummae* and compared it with other North American multituberculates, including isolated specimens as well as a partial skeleton from the San Juan Basin of New Mexico, which although not associated with

craniodental material, was referred to *Eucosmodon* by Granger and Simpson (1929). They concluded that the postcrania of multituberculates are fairly uniform in morphology and suggested that at least some North American forms (e.g. *Ptilodus* and *Eucosmodon*) were aboreal. The evidence they cited in favor of arboreality included a dorsally open acetabulum suggestive of pronounced femoral abduction, ankle that accommodates a large range of abduction and eversion, divergent hallux, and long tail with robust transverse processes and hemal arches.

Kielan-Jaworowska and Gambaryan (1994) described postcrania of *Kryptobaatar dashzevegi, Nemegtbaatar gobiensis, Chulsanbaatar vulgaris, Sloanbaatar mirabilis, Catopsbaatar catopsaloides*, and an indeterminate taeniolabidoid from Late Cretaceous deposits of Mongolia. Most of the specimens were partially articulated. They supported Krause and Jenkins' (1983) conclusion that the postcrania of multituberculates vary little; however, they did not find arboreal adaptations in the postcrania of the Mongolian Late Cretaceous multituberculates that they studied and questioned much of the evidence listed by Krause and Jenkins (1983). They reconstructed the postcranial muscles of multituberculates and compared them to living groups of mammals, and based on that, they interpreted Mongolian multituberculates as terrestrial with an asymmetrical gait, steep jumps, and sprawling posture. The main features that support their reconstruction are the relatively long spinous and transverse processes on the posterior lumbar vertebrae. They also listed plesiomorphic and apomorphic character states of Multituberculata.

Sereno and McKenna (1995) were the first to describe a fairly complete and articulated forelimb of a multituberculate. The specimen they described included the skull, scapula, clavicle, interclavicle, manubrium, humerus, radius, and ulna and was referred to

Bulganbataar, although now is thought to be *Kryptobaatar* (Sereno, 2006). Based on their study, they concluded that Multituberculata had a parasagittal stance and that this posture evolved in the most recent common ancestor of Theria and Multituberculata. However, not all authors agree that the orientation of the forelimb in multituberculates was parasagittal (e.g Kielan-Jaworowska and Qi, 1990; Gambaryan and Kielan-Jaworowska, 1997), instead these other authors describe them as having the sprawling posture, like that seen in monotremes.

Minjin (2001) reported the hand of *Kryptobaatar dashzevegi* (MAE00-22). Preserved portions of the specimen she described include the skull, dentary, vertebrae, ribs, left and right forelimbs with articulated manus, right hind limb, and pelvis. Using 15 hand characters scored for 9 synapsid taxa, she tested the following phylogenetic hypotheses for the position of Multituberculata: 1) Monotremata and Multituberculata are sister-groups, 2) Multituberculata is the sister-group to all other mammals, and 3) Multituberculata is the sister-group to Theria. Of these three, the first two hypotheses received equal support, while the third hypothesis was one step longer. A potential synapomorphy of a monotreme and multitubercule clade is contact between the cuneiform and metacarpal V. This specimen is described in detail in the present study.

More recently, Hu and Wang (2002) described a new taxon, *Sinobaatar lingyuanensis*, from the Early Cretaceous of China. The specimen consists of a partially articulated, crushed skeleton with skull, from the Yixian Formation. More importantly, this specimen preserves an articulated right and left manus, making it the second multituberculate known to preserve this anatomical region. As in *Kryptobaatar* (Minjin, 2001), Hu and Wang found that the centrale in *Sinobaatar* is larger than the trapezoid and that the trapezium is enlarged. Hu and Wang (2002) also described the articulated pes, and unlike the

reconstruction of Kielan-Jaworowska and Gambaryan (1994), they determined that metatarsal V did not contact the calcaneus and that the calcaneal tuber and metatarsal III are parallel to each other.

In a series of papers (Kielan-Jaworowska et al., 2002, 2005; Kielan-Jaworowska and Hurum, 2006; Hurum et al., 2006) Kielan-Jaworowska and co-authors reported and/or figured a skull and partial skeleton of *Catopsbaatar catopsaloides* from the Mongolian Late Cretaceous locality, Khermiin Tsav. A detailed description of the postcrania has not been completed, but an ongoing project on the calcaneus (Bolortsetseg and Kielan-Jaworowska, in prep.) and published photos (Kielan-Jaworowska et al., 2005: fig. 4) allows some aspects of its postcrania to be compared to that of other multituberculates. Somewhat unexpectedly, the elbow of this specimen has a small sesamoid bone (Kielan-Jaworowska et al., 2002). Kielan-Jaworowska and Hurum (2006) focused on the limb posture of multituberculates. They concluded that multituberculate limbs were held in a sprawling posture based on the taphonomy of articulated specimens from the Yixian Formation of China and the morphology of their limb bones.

The most recent study of multituberculate postcrania is a paper by Sereno (2006), where he provides detailed descriptions and comparisons of the specimen of *Kryptobaatar* initially described by Sereno and McKenna (1995). As in their previous paper, Sereno argues that Multituberculata had a parasagittal stance and that characters of the forelimb place them as the sister-group to Trechnotheria. Key features that Sereno (2006) describes that support a parasagittal posture in multituberculates are: ventrally facing glenoid fossa of the scapula, moveable shoulder joint and reduction of many elements of the pectoral girdle, and increased flexion and extension of the elbow.

CLADISTIC ANALYSES WITHIN MULTITUBERCULATA

Given that few multituberculate specimens have postcrania associated with craniodental material and that it is widely thought that multituberculate postcrania are relatively invariant (e.g. Krause and Jenkins, 1983; Kielan-Jaworowska and Gambaryan, 1994; Sereno, 2006), it is not suprising that previous attempts to determine the phylogeny within Multituberculata have focused exclusively on craniodental characters. The first cladistic analyses of Multituberculata were conducted by Archibald (1982) and Simmons (1986), but the first comprehensive analysis was that of Simmons (1993). She analyzed a matrix of 67 characters for 49 taxa and found that Cimolodonta was monophyletic while Plagiaulacoidea was paraphyletic. Despite the importance advance this paper represents, analyses that included all taxa could not be completed because of the large number of most parsimonious trees. Heuristic searches were ended after 10,000 trees were saved, and it is unclear if the strict consensus she figured is consistent with all the most parsimonious trees.

Rougier et al., (1997) revised the matrix of Simmons (1993) and described and then added a new taxon, *Tombaatar sabuli*, to the matrix. Unlike Simmons (1993), they found a clade of mostly Mongolian multituberculates, subsequently named Djadochtatheria by Kielan-Jaworowska and Hurum (1997) and then in a later study changed to Djadochtatheroidea (Kielan-Jaworowska and Hurum, 2001). Like Simmons (1993), Rougier et al. (1997) found large numbers of most parsimonious trees and was not able to save all of them. The difficulties that these authors have had in resolving the phylogeny of multituberculates is caused by homoplasy in the dental characters and the fact that so many

taxa are known from just a few teeth, and can only be coded for a few characters in their matrices.

Kielan-Jaworowska and Hurum (1997) conducted cladistic analyses that focused on the relationships of multituberculates from Mongolia. Unlike previous authors, they obtained a fairly small number of most parsimonious trees; however, this can be attributed to the fact that their data matrix only included 17 taxa. When the same authors applied cladistic methods to a much larger dataset of 62 characters coded for 32 taxa, they obtained a strict consensus that had only two nodes resolved (Kielan-Jaworowska and Hurum, 2001). Instead of publishing this result, they displayed a cladogram drawn by hand, not the result of a computer-aided parsimony analysis. Similarly, in an unpublished PhD dissertation, Weil (1999) also found large numbers of most parsimonious trees when conducting phylogenetic analyses of multituberculates based solely on dental characters.

OBJECTIVES

Despite significant work on multituberculates, 1) the phylogeny within this group remains controversial, 2) variation among the postcrania of multituberculates has not been adequately documented and studied, and 3) although a consensus is emerging that Multituberculata is closer to Theria than to Monotremata, this result remains controversial. To contribute to the resolution of these problems, I will, describe three new, partial, cimolodontan multituberculate skeletons that are associated with diagnostic craniodental material: 1) a specimen of *Ectypodus* sp. from the newly discovered Bangtail-2 locality (Early-Late Paleocene, Montana, USA), 2) a partially articulated skeleton of an undescribed taxon referred to as the Udan Multi, from the Udan Sayr locality (Late Cretaceous,

Mongolia), and 3) a nearly complete and articulated skeleton of *Kryptobaatar dashzevegi* from the locality of Ukhaa Tolgod (Late Cretaceous, Mongolia). Then I will document variation among the postcrania of multituberculates by creating a character/taxon matrix comprised solely of postcranial characters. In doing so, I will incorporate isolated specimens from the Cretaceous and Paleogene of North America. Then I will analyze this matrix to test previous hypotheses for the phylogeny of Multituberculata.

SPECIMENS STUDIED

In this dissertation, I examined 129 specimens, including all described multituberculate skeletons (Tables 1, 2): *Ptilodus kummae* (UA 9001), *Eucosmodon* sp. (AMNH 16325), *Kryptobaatar dashzevegi* (ZPAL MgM I/41), *Nemegtbaatar gobiensis* (ZPAL MgM I/82), *Chulsanbaatar vulgaris* (ZPAL MgM I/83, I/99b), *Catopsbaatar catopsaloides* (PM 120/107) and *Sinobaatar lingyuanensis* (IVPP V12517). In addition, I studied three new specimens that are described in this dissertation. The first is a partial skeleton of the genus *Ectypodus* sp. collected in 2001 by an expedition led by Jonathan Bloch (Florida Museum of Natural History) from the newly discovered Bangtail-2 locality (Early-Late Paleocene, Montana, USA). The second specimen is a partially articulated skeleton of an undescribed taxon referred to as the Udan Multi, collected by the joint expedition between the Mongolian Academy of Sciences and the American Museum of Natural History in 1996 from the Udan Sayr locality (Late Cretaceous) of Mongolia. The third is a nearly complete and articulated skeleton of *Kryptobaatar dashzevegi* from the locality of Ukhaa Tolgod (Late Cretaceous, Mongolia) collected by the joint expedition between the Mongolian Academy of Sciences and the American Museum of Natural History in 2000. Additional details about the specimens and taxa studied are provided in TAXON SAMPLING under **PHYLOGENETIC ANALYSES**.

METHODS

Measurements were made with digital calipers and observations made with stereomicroscopes, predominantly a Wild M7A. The specimen from the Bangtail II locality was prepared using a combination of acid and mechanical preparation while the two new multituberculate skeletons from Mongolia were prepared mechanically. Photographs were taken with a digital camera installed on a microscope, a scanning electron microscope, and larger elements with a mounted digital camera. Postcranial anatomical terminology generally follows Evans (1993) except for tarsal anatomy, which follows Szalay (1993), and carpal anatomy, which follows Stafford and Thorington (1998). As in Evans (1993), anglicized versions of the Latin terms from the 1983 version of the Nomina Anatomica Veterinaria are used. Phylogenetic methods are described in METHODS under **PHYLOGENETIC ANALYSES**.

INSTITUTIONAL ABBREVIATIONS

AMNH, American Museum of Natural History, New York, USA; **BT**, Bangtail-2 locality, Park County, Montana, USA; **GSM**, Georgia Southern Museum, Statesboro, GA; **MCZ**, The Museum of Comparative Zoology, Harvard University, Cambridge, MA, USA; **PM**, Paleontological Center of the Mongolian Academy of Sciences, Ulaanbaatar, Mongolia; **PSS-MAE**, Paleontological and Stratigraphic Section (**PSS**) of the Geological Institute, Mongolian Academy of Sciences, Ulaanbaatar, Mongolia and collections of the joint Mongolian Academy of Sciences-American Museum of Natural History Paleontological Expedition (**MAE**); **UA** , University of Alberta, Edmonton, Canada; **UA Astr.,** uncatalogued

astragalus housed in the University of Alberta, Edmontan, Canada; **UCMP**, University of California Museum of Paleontology, Berkeley, California, USA; **UM Astr.,** uncatalogued astragalus housed in the University of Minnesota, Minneapolis, MN, USA; **UM Calc.**, uncatalogued calcaneus housed in University of Minnesota, Minneapolis, MN, USA; **UMVP**, Vertebrate Paleontology collection in University of Minnesota, Minneapolis, MN, USA; **USNM**, U.S. National Museum of Natural History, Washington, D.C., USA.

Anatomical Abbreviations

ab	astragalar buttress
ac	astragalar canal
aca	astragalocalcaneal facet
ace	acetabulum
acp	acromion process of scapula
afi	astragalofibular facet
an	astragalonavicular facet (on navicular or astragalus)
ant	acetabular notch
ap	articular process
arc	articular circumference
as	auricular surface
ast	astragalus
atil	lateral astragalotibial facet
atim	medial astragalotibial facet
bf	peroneus brevis fossa of calcaneus (new term)
c#	cervical vertebra, 1, 2, 3, etc.
ca	calcaneus
caa	calcaneoastragalar facet (on calcaneus or astragalus)
caf	cranial costal fovea
cas	stop for calcaneoastragalar joint
cc	caudal crest of humerus
ccf	calcaneocuboid facet
ce	centrale
cf	caudal fossa of calcaneus (new term)
cff	calcaneofibular facet
cfe	cuboid facet for ectocuneiform

cfn	cuboid facet for navicular
cl	clavicle
clp	caudolateral process of astragalus (new term)
cm5	contact for metatarsal V on calcaneus
cn	caudal notch
cop	coracoid process
cpt	cranioplantar tuberosity of calcaneus (new term)
cr	cranial ridge of calcaneus (new term)
crf	capitular facet on the radius
crtp	cranial transverse process
ctp	caudal transverse process
cu	cuboid
cuf	caudal costal fovea
cun	cuneiform
cur	caudal ridge of calcaneus (new term)
cvis	caudal ventral iliac spine
dpc	deltopectoral crest of humerus
ecc	ectepicondyle of humerus
ecf	facet for ectepicondyle of humerus on radius
ect	ectocuneiform
efn	ectocuneiform facet for navicular
enc	entepicondyle of humerus
enfn	entocuneiform facet for navicular
ent	entocuneiform
ep	epipubic bone
exf	extensor fossa
extt	extensor tubercle for distal phalanx
fac	facet for fibular contact on tibia
fas	facet for astragalus
fcb	facet for cuboid on metatarsal V
fcs	facet for calcaneus on metatarsal V
fcu	facet for cuneiform

fe	femur
fent	facet for entocuneiform
fi	fibula
ffib	facet for fibula (on parafibula)
flxt	flexor tubercle on distal phalanx
fmiv	facet for metatarsal IV on metatarsal V
fr	facet for radius
gl	glenoid fossa of scapula
gtr	greater trochanter of femur
gtu	greater tubercle of humerus
ha	hemal arch
hc	hemal canal
hd	head of femur
hh	head of humerus
hlp	hook-like lateral process of fibula
hp	hemal process
hs	hemal spine
hu	humerus
ia	interarticular sulcus on astragalus
iab	interarticular bulge
ice	intercondyloid eminence
icf	intercondyloid fossa of femur
icft	intercondyloid fossa of tibia
icl	interclavicle
ifo	infraspinous fossa
il	ilium
inc	interosseous crest
ipe	iliopubic eminence
ips	ischiopubic symphysis
isfo	incipient supraspinous fossa
it	ischiatic tuberosity
itb	ischiatic table

itg	intertubercular groove of humerus
lac	lateral condyle
L#	lumbar vertebra 1, 2, 3, etc.
lc	lateral crest of calcaneus
lco	lateral condyle of tibia
lf	lateral fossa of calcaneus (new term)
lgr	longitudinal groove
llp	lateral lip (of radial head)
lpc	lateral epicondyle
ltr	lesser trochanter
ltu	lesser tubercle of humerus
lu	lunate
m#	metacarpal I, II, III, IV, or V
m3fe	metatarsal III facet for ectocuneiform
mc	mesocuneiform
mco	medial condyle of tibia
mec	medial condyle of femur
mfe	mesocuneiform facet for ectocuneiform
mfn	mesocuneiform facet for navicular
mgm	origin of dorsal part of muscle gluteus medius
mgn	magnum
mm	medial malleolus of tibia
mp	mammillary process
mpc	medial epicondyle
ms	mesosternum
mt#	metatarsal I, II, III, IV, or V
na	navicular
nfe	navicular facet for ectocuneiform
ntf1-3	nutrient foramen 1-3 of distal phalanx
of	obturator foramen
olf	olecranon fossa
op	olecranon process of ulna

pff	parafibular facet of fibula
pg	peroneal groove of calcaneus
ph#	proximal phalanx I, II, III, IV, or V
pi	pisiform
ppdm	proximal phalanx articulation dorsal margin
pon	postobturator notch
poz	postzygapophysis
pp	peroneal process of calcaneus
prp	peroneal process of metatarsal V
prz	prezygapophysis
ps	pubis
pt	pubic tubercle
ptf	posttrochanteric fossa
ra	radius
rco	radial condyle of humerus
rss	ridge for fourth aponeurosis of muscle subscapularis
sa	sacrum
sb	sternebra
sc	sulcus calcanei
sca	scaphoid
ses	sesamoid bone
shc	suprahemal process
ss	scapular spine
sp	spinous process
spu	spur
stp	styloid process
stt	subtrochanter tubercle
sua	sustentacular facet for astragali
suc	supinator crest of the humerus
t#	thoracic vertebra 1, 2, 3, 4, 5 etc. or unknown
ta	anticlinal thoracic
tc	tuber calcis

td	trapezoid
ti	tibia
tl	last thoracic
tm	trapezium
trc	trochlear ridge of calcaneus
trf	trochanteric fossa
trh	trochlea of the femur
ttu	tibial tuberosity
uco	ulnar condyle of humerus
ul	ulna
un	unciform
vc	vertebral canal
vgr	ventral groove

GEOLOGICAL SETTINGS

BANGTAIL-2

This is a new locality in the western Crazy Mountains Basin of South Central Montana, approximately 1 mile northwest of the original Bangtail locality described by Gingerich et al. (1983) (fig. 1). The new partial skeleton of *Ectypodus* described in this dissertation came from this locality. It is Early-Late Paleocene age based on the co-occurence of the plesiadapid primate *Nannodectes intermedius* and the pentacodontid pantolestid *Aphronorus orieli* (Gingerich et al., 1983). The Bangtail-2 locality was discovered by an expedition led by Jonathan Bloch, Florida Natural History Museum, and work at the site is still ongoing. The geology of the area is still under investigation; however, preliminary results suggest that the Bangtail-2 section is at least 200 m below the exposures at the original Bangtail locality (fig. 2). Fossils are found in limestone nodules, and in some cases include partial skeletons. This locality is important because it is one of the few places in North America to study faunal changes during the Early-Late Paleocene transition.

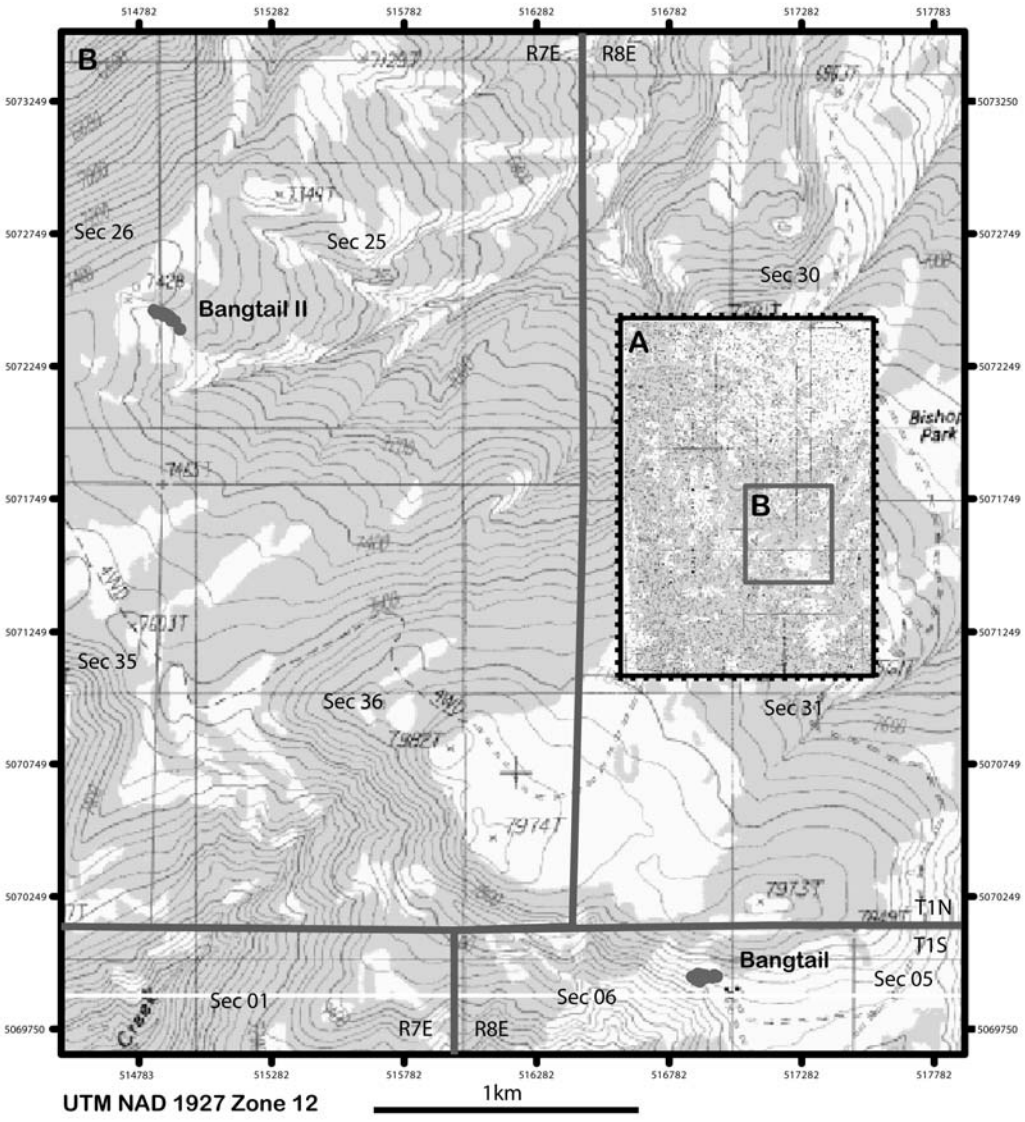

Fig. 1. Location of the Bangtail and Bangtail II quarries in the Crazy Mountains Basin, Montana. The partial skeleton of *Ectypodus* described in the present study was recovered from the Bangtail II quarry. **(A)** Grassy Mountain 7.5' USGS quadrangle, **(B)** Enlarged view of a part of the map in **A** showing the location of the two quarries.

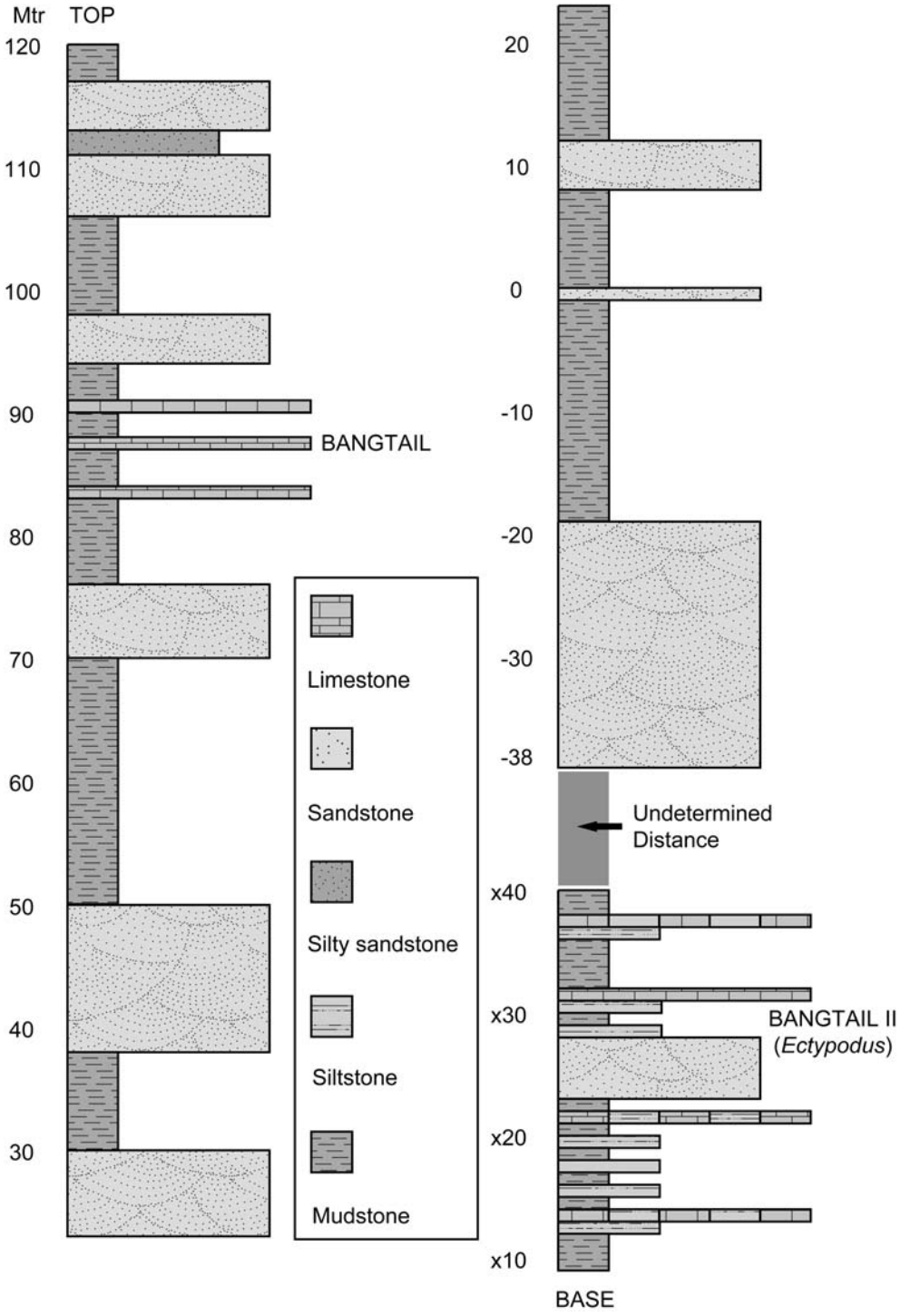

Fig. 2. Composite geologic section of the Fort Union Formation in the Crazy Mountain Basin showing the relative stratigraphic positions of the Bangtail and Bangtail II quarries. The section on the right fits directly underneath the section on the left.

UKHAA TOLGOD

This famous locality is located in the fossiliferous Nemegt Valley of the Umnugovi Province, Mongolia. It was discovered by a joint paleontological expedition between the Mongolian Academy of Sciences and the American Museum of Natural History in 1993 (Dashzeveg et al., 1995). Previously, many spectacularly preserved amniotes have been found from this locality (Novacek et al., 1997; Rougier et al., 1997; Rougier et al., 1998; Clark et al., 1999; Clark et al., 2002; Norell et al., 2000; Horovitz, 2000, 2003; Norell et al., 2001; Clarke and Norell, 2002; Makovicky et al., 2003; Joyce and Norell, 2005). Exposures of the Djadokhta Formation occur at Ukhaa Tolgod and have produced a fauna somewhat different from Bayn Dzak (i.e. Flaming Cliffs) the type locality of this formation (Makovicky, 2007). The Djadokhta Formation has recently been restudied by Dashzeveg et al. (2005), and they have divided it into two members, the Bayn Dzag and Tugrugyin Members. They did not specify which, if either, of the members is exposed at Ukhaa Tolgod, although the exposures at Ukhaa Tolgod are more similar in lithology to the Bayn Dzag Member. Based on preliminary paleomagnetostratigraphic results, Dashzeveg et al. (2005) interpret the Djadokhta Formation to be Late Campanian in age.

UDAN SAYR

This locality is a series of small outcrops distributed over a relatively large area. Located about 90 km west of Bayn Dzag in Umnugovi Province, Mongolia, Udan Sayr was first discovered by the Soviet Mongolian Paleontological Expedition in the 1980's

(Benton et al., 2000) and two joint expeditions have worked there, one between the Mongolian Academy of Sciences (MAS) and the American Museum of Natural History and another between the MAS and Hayashibara Museum of Natural Sciences. The undescribed multituberculate referred to as the Udan Multi was collected from this locality by the joint expedition between the MAS and AMNH. The exposures at Udan Sayr are similar to those of the Djadokhta and Barun Goyot Formations. The types of the ceratopsian dinosaur *Udanoceratops tschizhovi* (Kurzanov, 1992) and the metatherian *Asiatherium reshetovi* (Szalay and Trofimov, 1996) are from Udan Sayr.

SYSTEMATIC PALEONTOLOGY

CLASS MAMMALIA LINNAEUS, 1758

ORDER MULTITUBERCULATA COPE, 1884

SUBORDER CIMOLODONTA MCKENNA, 1975

SUPERFAMILY PTILODONTOIDEA SLOAN AND VAN VALEN, 1965

FAMLIY PTILODONTIDAE COPE, 1887

Ptilodus kummae Krause, 1977

HOLOTYPE: UA 9001, teeth associated with a partially articulated skeleton. See Krause and Jenkins (1983) for more details.

TYPE LOCALITY AND HORIZON: UAR2g locality, Saskatchewan, Canada.

DIAGNOSIS: See Krause (1977).

REVISED DESCRIPTION

During examination of the holotype specimen of *Ptilodus kummae*, it was discovered that the original description of the carpal bones by Krause and Jenkins (1983) is in need of revision. They interpreted the partially articulated and incomplete manus of *Ptilodus kummae* as representing the right side based on the following observations: "metacarpal I" having two phalanges, "metacarpal I" diverging from "metacarpal II," and the presence of a prepollex adjacent to "metacarpal I." Based on this interpretation, they described the adjacent carpal bones as the lunate, magnum, trapezoid, and trapezium. However, based on comparisons to the nearly complete manus of *Kryptobaatar* (MAE 00-22) and *Sinobaatar* (Hu and Wang, 2002), which were not available at the time

Krause and Jenkins (1983) did their study, I suggest that the partial manus of *Ptilodus kummae* is the left manus (fig. 3), not the right one as originally described.

Three key lines of evidence support the interpretation that the left manus is preserved in the partial skeleton of *Ptilodus kummae* (UA 9001). First are the relative positions of metacarpal I and II in *Kryptobaatar* and *Sinobaatar*. In both taxa, the trapezium is elongate proximodistally, causing the proximal end of metacarpal I to be clearly distal to the proximal end of metacarpal II, instead of being aligned. Even though metacarpal I is not preserved in a new specimen of *Kryptobaatar* (MAE00-22), the trapezium is and remains articulated with the rest of carpals, demonstrating that it too has a metacarpal I more distal than metacarpal II (fig. 4A: tm). In contrast, the two preserved metacarpals in *Ptilodus* are aligned (fig. 3: m4, m5), more like the condition seen with metacarpals IV and V of *Kryptobaatar* and *Sinobaatar*. The second observation that supports my interpretation is the morphology of the carpal bones that Krause and Jenkins (1983) identified as the trapezium and trapezoid. In *Kryptobaatar* and *Sinobaatar* the trapezium is transversely compressed and is significantly larger than the trapezoid. In contrast, the putative trapezoid and trapezium in *Ptilodus* are wider transversely than proximodistally and are subequal in size. Thus, I interpret the "trapezium" and "trapezoid" as the cuneiform and unciform (fig. 3: cun, un), based on the similarity to these bones as observed in *Kryptobaatar*. Finally, *Kryptobaatar* and *Sinobaatar* do not have a prepollex, whereas Krause and Jenkins (1983) identified the large bone projecting away from the two metacarpals in *Ptilodus* as a prepollex. This bone is almost certainly a pisiform (fig. 3: pi), based on marked similarity to this bone in *Kryptobaatar* (fig. 4: pi)

Regarding Krause and Jenkins' (1983) original reasons for identifying the metacarpals as I and II, one of them, the prepollex, is better interpreted as a pisiform. While they are correct in noting that the first metacarpal is divergent in many mammals, a similarity shared with one of the complete metacarpals preserved in the holotype of *Ptilodus*, the fifth metacarpal in the left manus of *Kryptobaatar* also diverges from the fourth (fig. 4 B: m4, m5). Thus this particular observation is inconclusive. In *Sinobaatar* the fifth metacarpal does not diverge from the fourth, but considering the crushed nature of this specimen, it is difficult to know whether this is the original anatomical position. Finally, Krause and Jenkins noted that only two phalanges are preserved in the manus of *Ptilodus* and suggested that these belong to what they interpret as metacarpal I. The fifth metacarpal of *Kryptobaatar* does have 3 phalanges; however, this part of the manus of *Ptilodus* is disarticulated and one phalanx could easily be missing, and it is unclear whether these phalanges belong to the putative first metacarpal or to another digit. I agree with Krause and Jenkins (1983) that the lunate and magnum are preserved in *Ptilodus*, but I interpret these as from the left side instead of the right (fig. 3: lu, mgn). Other aspects of the original description of *Ptilodus kummae* do not need revision. For the description of the rest of the skeleton, see Krause and Jenkins (1983) and Jenkins and Krause (1983).

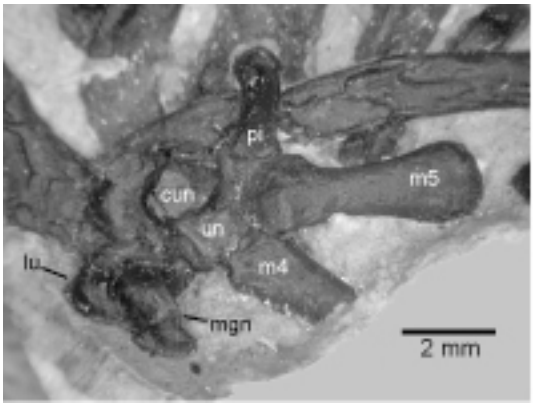

Fig. 3. Dorsal view of the left manus of a cast of the holotype of *Ptilodus kummae* (UA 9001). The labels and interpretation presented here differ from that of Krause and Jenkins (1983).

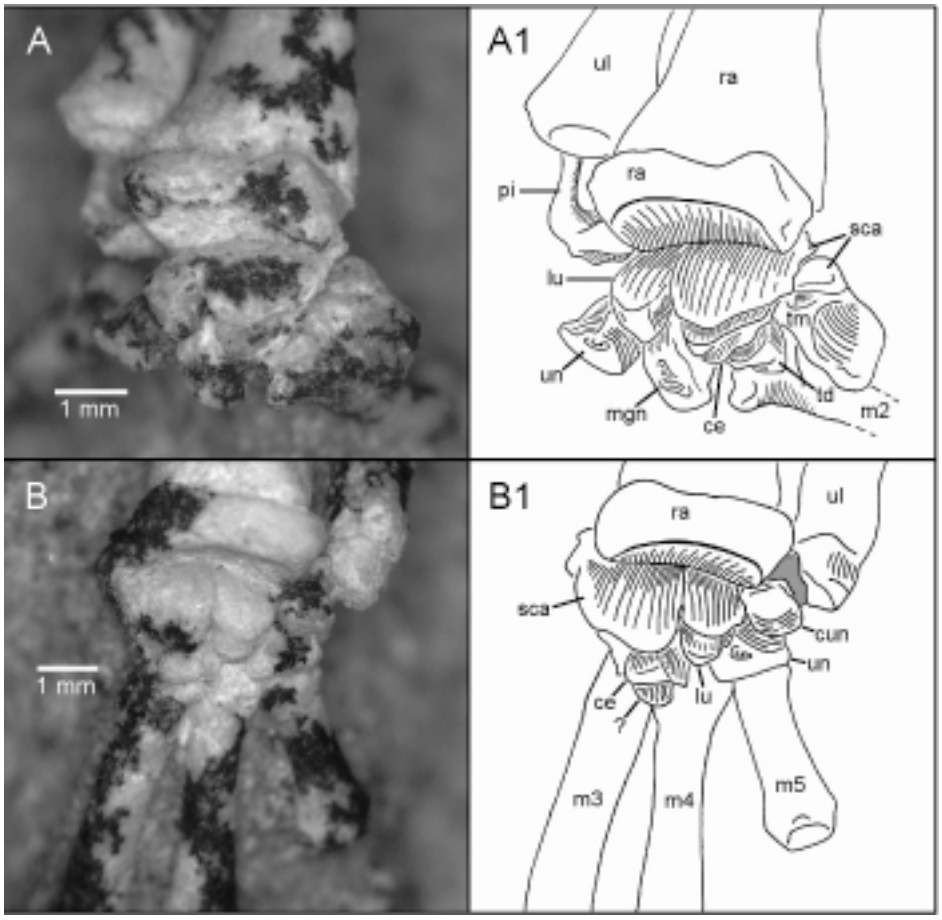

Fig. 4. Photograph **(A)** and interpretive drawing **(A1)** of the right wrist and photograph **(B)** and interpretive drawing **(B1)** of the left wrist. **A** is in proximodorsal view while **B** is in dorsal view.

FAMILY NEOPLAGIAULACIDAE AMEGHINO, 1890

GENUS ECTYPODUS MATTHEW AND GRANGER, 1921

Ectypodus sp. Matthew and Granger, 1921

REFERRED SPECIMEN: BT03049, an associated partial skeleton including right M_1, right scapula, head and neck of the right radius, distal portions of the left and right ulnae, left unciform?, left scaphoid?, two articulated thoracic vertebrae (including the probable anticlinal vertebra), seventh caudal vertebra, pelvis, right femur, left tibia, parafibula, right astragalus, right navicular, right ectocuneiform, left metatarsal I and V, and 9 phalanges; four proximal, three middle, and two distal. Several bones are lacking including the skull, humerus, manus, and calcanei.

LOCALITY AND HORIZON: Bangtail-2, Bangtail Plateau, Western Crazy Mountain Basin, Park County, Montana (See figs.1, 2).

DESCRIPTION

DENTITION

(fig. 5)

Only the right M_1 was preserved (fig. 5). The apex of the crown and the mesial, distal, and lingual surfaces of the roots are broken. In addition, the distal end of the crown is broken. The M_1 is double rooted, and the mesial portion of the tooth is much narrower than the distal portion. The length of the tooth is 1.98 mm, its mesial width is 0.41mm,

and its distal width is 0.81mm, yielding a length/ width ratio of 2.4 (table 1). The molar has two longitudinal rows of cusps; the lingual row has four cusps and the labial row has seven or eight, the ambiguity being caused by breakage of the crown. Mesially, the lingual and labial rows of cusps converge and eventually the space between the rows disappears (fig. 3.1). All four cusps on the lingual side are larger and more separated from each other than the cusps on the labial side; therefore, in lateral view, all four lingual cusps are visible. In lingual view, all the labial cusps are not visible because they are heavily worn (fig. 5.2). The cusps in the lingual and labial rows decrease in size mesially. The mesial-most cusp on the labial row is located mesial to the mesial-most cusp on the lingual side, while the distal-most cusp of the labial row is positioned slightly lingual as compared to rest of the cusps on the labial row. The lingual cusps have vertical wear facets on their labial sides, while their lingual sides do not and are inclined, not vertical. From mesial to distal, the cusps of the lingual row become more blunt, especially the apex of the last cusp, which is wide mesiodistally. There are well developed basins between the cusps on the lingual row. All the labial cusps have bulbous tips, and all are clearly separate from each other except for the distal two, which are twinned.

Table 1. Measurements (in millimeters) m1 of *Ectypodus* sp. (BT03049) from the Bangtail II quarry.

Dimension Measured	
Mesodistal length	1.98
Mesial width	0.41
Distal width	0.81
Ratio between the length and the greatest width	2.40
Ratio between the tooth length and femur length	0.12

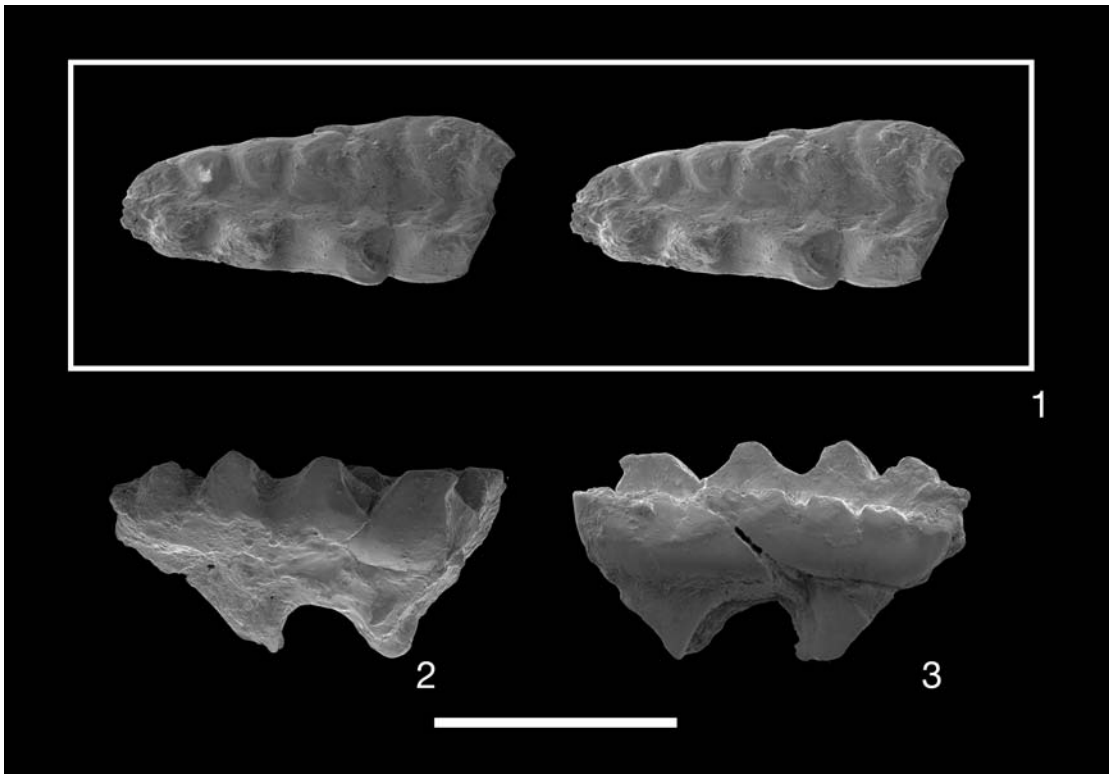

Fig. 5. Right M_1 of *Ectypodus* sp. (BT03049): **(1)** stereopairs of occlusal view, **(2)** lingual view, and **(3)** labial view. Mesial is to the left in **(1)** and **(2)** and to the right in **(3)**. Scale bar is 1 mm in length.

VERTEBRAE

(fig. 6)

Only two partially articulated posterior thoracic vertebrae are preserved (fig. 6 A, B). During preparation the two vertebrae were separated. I tentatively assign these two vertebrae as the anticlinal and the post-anticlinal vertebrae based on the vertical neural spine in the former and the cranially inclined spine in the latter (table 2). The anticlinal vertebra is complete except for the craniomedial part of the right prezygapophysis (fig. 6 A). The post-anticlinal vertebra is missing the left postzygapophysis along with most of the cranial part of the left pedicle and lamina and the caudal part of the centrum (fig. 6 B).

Both vertebrae share many aspects of their morphology, which are described here. Unique aspects of each vertebra are detailed in subsequent paragraphs. Anapophyses (accessory processes) are present but metapophyses (mammilary processes) are not (fig. 6 B5: ap). In lateral view, the caudal notch (i.e. the gap between the arch and centrum) is pronounced and reaches the longitudinal half-way point of the centrum. The dorsal surface of the centrum is nearly flat and has two foramina for the basivertebral veins, located on either side of the midline. The vertebral canal is large, and in cranial view, the pedicles are mostly vertical but have dorsal and ventral ends that curve slightly medially (fig. 6 A1, B1). The dorsal sides of the laminae are nearly flat. Both vertebrae have cranial and caudal costal fovea (see below for details on each vertebra).

ANTICLINAL VERTEBRA (6A1-6A5): In cranial view, the centrum is rectangular in shape except for the ventral corners, which are rounded, and the ventral side, which has a small ventrally oriented keel along the midline. The width of the cranial face of the

centrum is greater than its dorsoventral height. The cranial face of the centrum is concave and its dorsal margin is sharp. The ventral surface of the centrum is saddle-shaped, with the "saddle" being oriented craniocaudally. The cranial costal fovea is located between the pedicle and the centrum (fig. 6 A1: caf). It faces craniolaterally and has a caudal border that is convex caudally. The cranial costal fovea is separated from the cranial face of the centrum by a small pit. The caudal costal fovea of the anticlinal vertebra is larger than the cranial costal fovea, and the cranial border of the former bows cranially (fig. 6 A2: cuf). The prezygapophyses face laterally and slightly dorsally. The notch between the prezygapophyses is trapezoid-shaped. The postzygapophyses are wide and face ventromedially. The neural spine is vertical, short, centrally located in lateral view, and tapers to a point (fig. 6 A5).

POST-ANTICLINAL VERTEBRA (6B1-6B5): The caudal fovea faces more laterally than the corresponding facet on the anticlinal vertebra. The prezygapophyses are narrow, face dorsally, and are separated by a notch, which differs from that of the anticlinal vertebra in being wider and triangular shaped, with a rounded apex (fig. 6 B4). The postzygapophyses face ventrally. The neural spine is short, inclined craniodorsally, and is slightly taller than the spine of the anticlinal vertebra (fig. 6 B5: sp).

CAUDAL VERTEBRA: Only one caudal vertebra is preserved. Based on comparisons with the articulated caudal series of *Ptilodus kummae* (Krause and Jenkins, 1983), it is tentatively determined to be the seventh caudal (fig. 6 C). Unlike the sixth caudal vertebra of *P. kummae*, it lacks prezygopophyses and unlike the eighth, it has cranial transverse processes as well as caudal ones.

The seventh caudal vertebra of *Ectypodus* sp. is complete and has a centrum that is 6.7 mm in length. In cranial view, the centrum is hexagonal while in caudal view it is cordiform, with the top of the "heart" along the ventral margin (fig. 6 C1, C2). Metapophyses are present (fig. 6 C5: mp). Faint parallel ridges run from the caudal end of each metapophysis. A weak neural spine starts from between the metapophyses and reaches caudally to the postzygopophyses, which are significantly reduced in size. Cranial transverse processes are larger and more laterally extended than the caudal transverse processes. In the dorsal view, cranial and caudal transverse processes meet at the level of the longitudinal midpoint of the centrum. In cranial view, it can be seen that the transverse processes are positioned towards the ventral side of the centrum. As seen in ventral view, the centrum has hemal processes at its cranial and caudal ends (fig. 6 C4: hp). These hemal processes are for the articulation of hemal arch, which may be preserved (see below). The ventral surface of the centrum has a canal that opens into the cranial and caudal haemal processes. Two parallel ridges on the ventral surface of the centrum run caudally from the cranial hemal processes to the caudal margin of the centrum.

Fig. 6. Vertebrae of *Ectypodus* sp. (BT03049): **(A1-A5)** anticlinal thoracic vertebra, **(B1-B5)** post-anticlinal thoracic vertebra, and **(C1-C5)** caudal vertebra. **(A1, B1, C1)** cranial views, **(A2, B2, C2)** caudal views, **(A3, B3, C3)** dorsal views, **(A4, B4, C4)** ventral views, and **(A5, B5, C5)** lateral views. Scale bar is 2 mm in length.

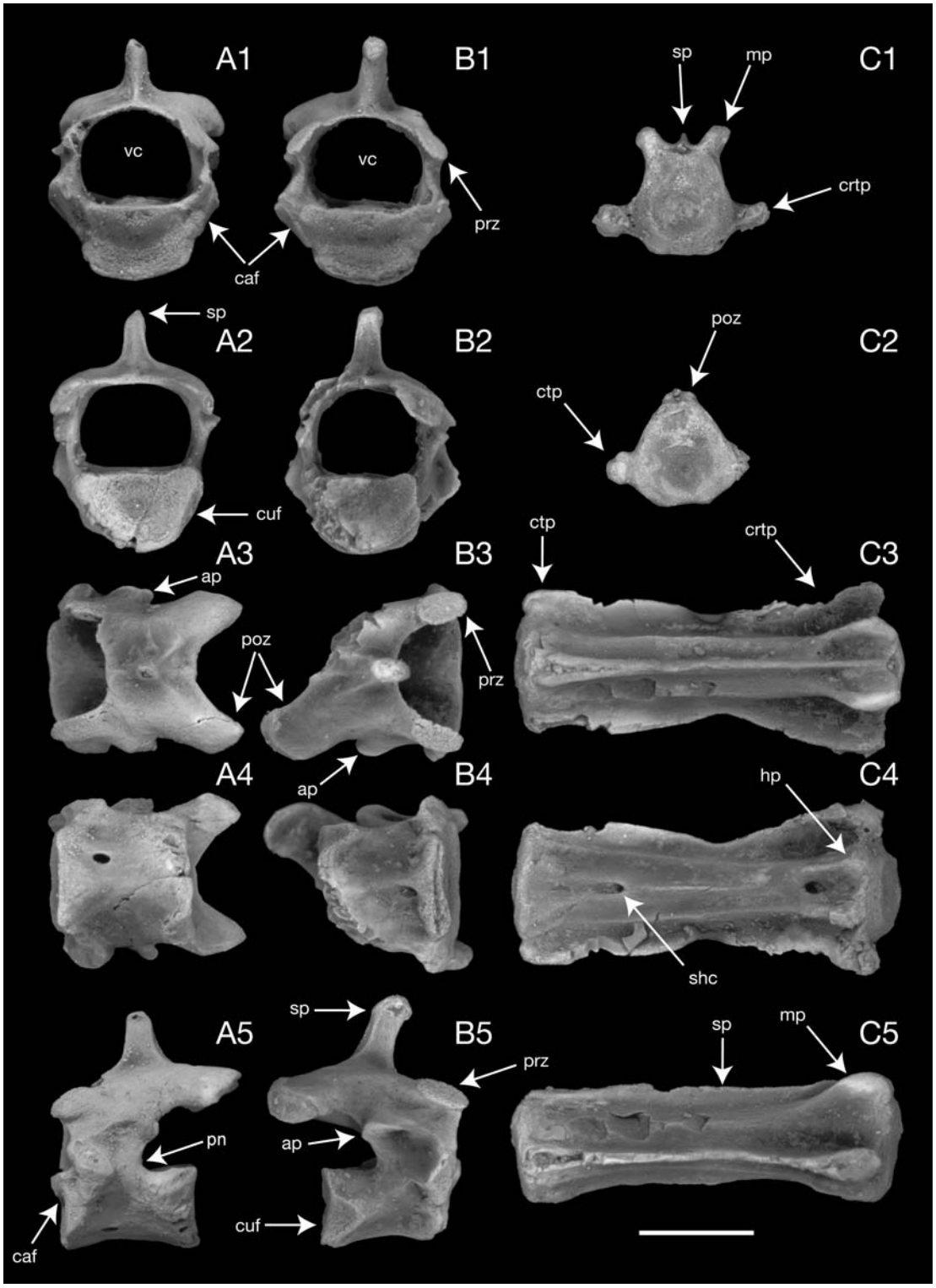
A1
B1
C1
vc
vc
sp
mp
crtp
prz
caf
sp
A2
B2
C2
poz
ctp
cuf
ctp
crtp
A3
B3
C3
ap
poz
prz
A4
ap
B4
hp
C4
shc
sp
A5
B5
sp
mp
C5
prz
pn
ap
cuf
caf

Table 2. Measurements (in millimeters) of thoracic vertebrae of *Ectypodus* sp. (BT03049). Abbreviations: a = length of neural spines; b = distance between prezygopophyses; c = length of body; d = distance between prezygopophysis and neural spine. Method of measuring vertebrae is based on Kielan-Jaworowska and Gambaryan (1994).

Vertebra	**a**	**b**	**c**	**d**
Anticlinal	0.9	3.4	2.4	0.8
Post-Anticlinal	1.3	3.2	2.3	0.7

HEMAL ARCH

(fig. 7)

An incomplete hemal arch is preserved (fig. 7); this is similar to the hemal arches of the caudal vertebrae posterior to the sixth caudal of *Ptilodus kummae*. It is possible that this arch belongs to the caudal described above, but this cannot be confirmed. The anterior and posterior ends of the arch are missing. The hemal canal is triangular-shaped (fig. 7.3: hc). The hemal spine is elongate, compressed dorsoventrally, bears a shallow groove on its dorsal surface, and has a narrow groove on the ventral surface towards the preserved distal end (fig. 7.2: vgr).

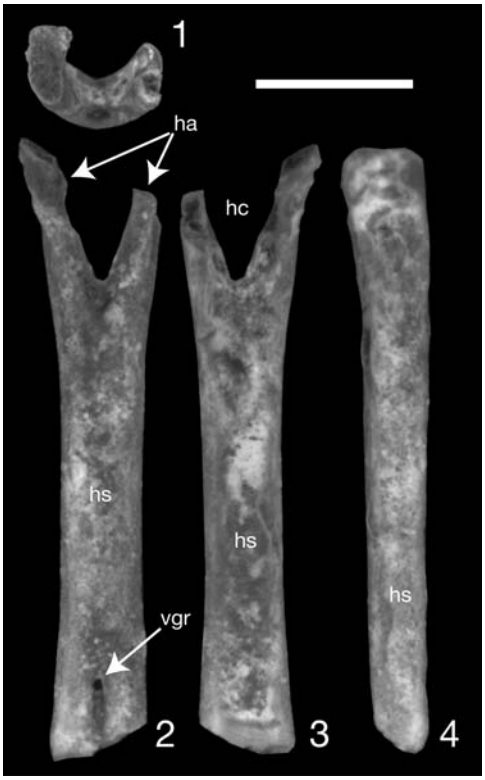

Fig. 7. Hemal arch (chevron) of *Ectypodus* sp. (BT03049): **(1)** cranial view, **(2)** ventral view, **(3)** dorsal view, and **(4)** lateral view. Scale bar is 1 mm in length.

SCAPULA

(fig. 8)

The right scapula is incomplete; the glenoid fossa, coracoid process, base of the spine, and ventral part of the infraspinous fossa are preserved while the acromion and metacromion are not (fig. 8). An incipient supraspinous fossa occurs dorsal to the glenoid fossa and ventrocranial to the spine (fig. 8.2: isfo), while the infraspinous fossa is caudal to the spine and trough-shaped (fig. 8.4: ifo). The medial side of the scapula is generally flat. The ventral portion of the spine projects directly laterally, but more dorsal portions strongly project caudolaterally, so that the infraspinous opens more caudally than laterally.

The glenoid fossa is oval and slightly concave. The scapula and coracoid are fused, and the glenoid fossa continues onto the latter. The long coracoid process is centered on the transverse diameter of the glenoid fossa and its distal end projects medially (fig. 8.5: cop). The cranial side of the distal end of the coracoid is flat. The medial edge of the coracoid is slightly concave and thinner than its lateral edge. In lateral view, the lateral margin of the coracoid splits into cranial and caudal ridges, with the former being better developed. Between these two ridges is a flat lateral side of the coracoid. The lateral margin of the coracoid is positioned more caudally than the medial margin; therefore, the whole coracoid is slightly twisted clockwise when viewed dorsally. On the craniomedial side and dorsal to the glenoid fossa, there is short ridge that is oriented caudodorsally. This is likely for the attachment of the fourth aponeurosis of subscapularis muscle (fig. 8.3: rss). Just cranial to this ridge is a small nutrient foramen.

Fig. 8. Right scapulocoracoid of *Ectypodus* sp. (BT03049): **(1)** cranial view, **(2)** lateral view, **(3)** medial view, **(4)** dorsal view, and **(5)** ventral view. In **4** and **5**, lateral is to the bottom of the figure. Scale bar is 2 mm in length.

ULNA

(fig. 9)

The distal two thirds of each ulna are preserved. The bodies of the preserved parts have three sides: cranial, caudomedial and caudolateral. A prominent interosseous crest occurs on the medial side of the proximal preserved half of the cranial surface (figs. 9.1 and 4: inc). Lateral to the crest is a longitudinal groove and lateral to the groove the cranial surface is convex. The remaining distal half of the cranial surface of the ulna lacks an interosseous crest and groove, instead the cranial surface is entirely convex. The posterocaudal surface of the body is concave proximally then gradually becomes convex distally. In medial view, the body of the ulna is narrow distally with a slightly concave caudal margin, but then begins to broaden substantially near the preserved proximal end. The proximal half of the caudolateral surface is flat and tapers distally.

The distal epiphyses are not fused. The styloid process is well developed and it too has three surfaces (fig. 9.3: stp). The cranial surface has a facet for the radius and another for the cuneiform, but the separation between the facets is poorly developed (fig. 9.6: fcu, fr). The facet for radius is small, flat, transversely elongated, and proximodistally short, and does not continue onto the medial side of the ulna. The facet for the cuneiform is elongated proximodistally, slightly convex, and faces craniodistally. The facet for the radius is just proximal to the facet for cuneiform bone, and both facets face craniomedially. The medial side of the styloid process is concave and the lateral side of the styloid is very flat.

Fig. 9. Left ulna of *Ectypodus* sp. (BT03049): **(1)** cranial view, **(2)** caudal view, **(3)** medial, **(4)** lateral, **(5)** distal view, and **(6)** cranial view of distal end of the left ulna. Scale bars are 2 mm (for **1-4**) and 1 mm (**5 and 6**) in length.

RADIUS

(fig. 10)

Only the head and neck of the right radius is preserved. The head is circular in outline and the capitular facet is concave and bowl shaped (fig. 10.1: crf). The articular circumference faces caudally, and it is proximodistally deep along caudolateral quarter of the head's circumference. The facet is deepest in the middle and decreases in depth medially and caudally. There is no flat facet on the head for the ectepicondyle of the humerus.

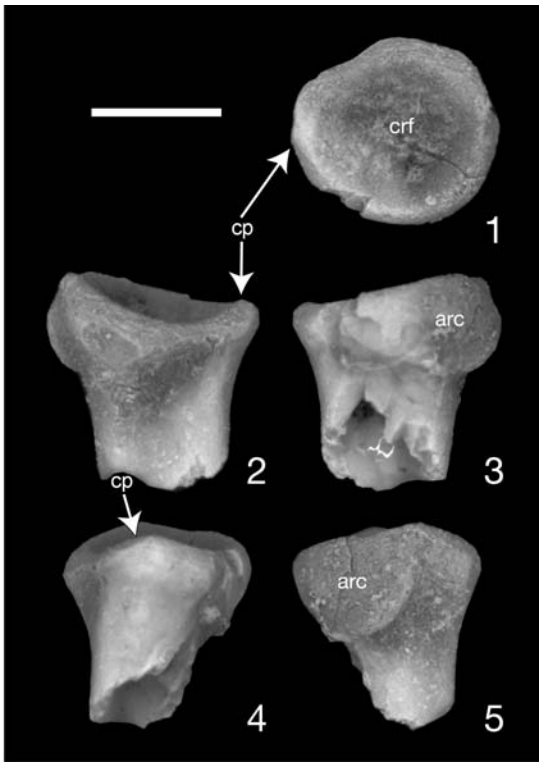

Fig. 10. Head of the right radius *Ectypodus* sp. (BT03049): **(1)** proximal view, **(2)** lateral view, **(3)** caudomedial view, **(4)** cranial view, and **(5)** caudolateral view. Scale bar is 1 mm in length.

CARPAL BONES

(fig. 11)

Two isolated carpal bones are preserved, and I tentatively identify these bones as the left unciform and left scaphoid (fig. 11). The carpal bones were compared with the type of *Ptilodus kummae* (Krause and Jenkins, 1983), a specimen of *Kryptobaatar* described in the present study (Minjin, 2001), and *Sinobaatar* (Hu and Wang, 2002). The unciform? of *Ectypodus* resembles those of the above taxa in tapering in thickness, similar to the dorsal face of the unciform of *Kryptobaatar* (fig. 4 A1, B1).

The scaphoid? of *Ectypodus* is an irregular shaped bone. Like that of *Kryptobaatar*, one side is large, convex, and may have articulated with the radius (fig. 11 A2). It also has what appears to be a scaphoid tubercle, although it is unclear if this structure occurs in other multituberculates. The opposite side is concave and likely articulated with the centrale (fig. 11: A1).

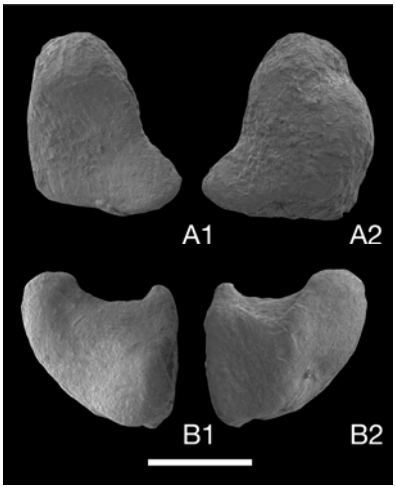

Fig. 11. Isolated carpal bones of *Ectypodus* sp. (BT03049): Left scaphoid? in **(A1)** distal and **(A2)** proximal views. Left unciform? in **(B1)** distal and **(B2)** proximal views. Scale bar is 0.5 mm in length.

PELVIS

(fig. 12)

The pelvis is complete except for the caudal dorsal and ventral iliac spines and the portion of the pelvic symphysis cranial to the postobturator notch (fig. 12). The right and left pelvic bones are separated and dislocated. The sutures of the pelvis are synostosed; therefore, the sutures among the ilium, pubis, and ischium are not discernible. The left pelvis is crushed dorsoventrally, with a crack between the ilium and pubis just ventral to the acetabular fossa, and the pubis is distorted so that it is oriented laterally. Because of the crushing, the acetabulum is elongated craniocaudally and its cranioventral border is broken. Pieces of the left ischiatic table (sensu Evans, 1993) sit broken between the ischiatic tuberosity and the postobturator notch.

The body of the ilium is long and slender. The caudal ventral iliac spine is prominent, and it is situated 7.30 mm cranial to the cranial border of the acetabular fossa (fig. 12.2: cvis). The lateral side of the preserved part of the ilium is flat; cranially it faces mostly dorsally while caudally it faces dorsolaterally. On the medial side of the ilium, the caudal part of the auricular surface has a strongly developed ridge that runs cranially.

The ischiatic table is fan shaped, with its dorsal border quite concave, its caudal and caudoventral borders convex, and the ventral border emarginated at the postobturator notch. The caudodorsal corner of the table is formed by a large ischiatic tuberosity (fig. 12.2: it). The lateral surface of the ischiatic table varies in morphology; its cranial portion is slightly convex, its caudodorsal portion is fairly flat, while its ventral portion, especially in the area of the postobturator notch, is strongly concave. The postobturator

notch emarginates the ventral margin of the ischium and is located caudal to the obturator foramen (fig. 12.3: pon). Its opening is narrow, because the notch's caudal edge comes ventrally to a sharp, cranially-projecting point. The ischia articulate along the edges of the postobturator notches, and the articulation surface is widest along the cranial edges of the notches.

The acetabular fossa is cup-shaped and its ventral side bears a notch that opens ventrocaudally (fig. 12.5: ant). The fossa is not centered but is closer to the dorsal margin of the pelvis. The margins of the acetabulum are defined by a prominent ridge on the caudal, cranial, and ventral sides, but not the dorsal side. The attachment for the round tendon in the acetabular fossa is located at the craniodorsal end of the acetabular notch. The pectineal tubercle is rudimentary.

Fig. 12. Innominate of *Ectypodus* sp. (BT03049): **(1)** cranial view, **(1.1)** enlarged image of cranial end of left ilium, **(2)** lateral view of the right pelvis and medial view of the left pelvis, **(2.1)** enlarged medial view of the ilium, **(3)** lateral view of the left pelvis and medial view of the right pelvis, **(3.1)** ischiopubic symphysis and postobturater notch of the right pelvis, **(4)** ventral view, **(5)** dorsal view, and **(5.1)** enlarged dorsal and lateral views of the acetabulum. Scale bar is 5 mm in length.


as
mgm
2.1
cvis
mgm
1
mgm
as
cvis
1.1
cvis
il
ps
of
itb
it
2
ace
3
ips
ips
pon
3.1
itb
4
5
ps
ace
ant
of
5.1
ps
ace
ant

FEMUR

(fig. 13)

A complete right femur was preserved, but the left was not. The right femur's total length is 16.83 mm, while its distal width is 3.65 mm (fig. 13). In cranial view, the head of the femur is spherical, but in caudal view, it can be seen that its posterocaudal side is flattened. The dorsoventral diameter of the head 2.10 mm and the depth of the head varies from 1.76 mm (cranial side) to 1.34 mm (caudal side). The head lacks a clear fovea. In cranial view, the basal margin of the head, where it connects to the neck, is almost parallel to the shaft. The neck is short and its craniocaudal width (1.01 mm) is thinner than its dorsoventral diameter (1.24 mm). The angle between the neck and the shaft of the femur is 42°, in craniolateral view. The distance between the head and the greater trochanter is 1.19 mm, while the height of the latter is 1.70 mm, including 0.95 mm above the head (table 3). The greater trochanter is curved and points craniomedially as well as dorsally. The tip of the greater trochanter is gently convex, faces dorsally as well as caudolaterally, and its cranial edge just slightly overhangs the shaft of the trochanter (fig. 13.1: gtr). A well-defined ridge originates near the tip of the greater trochanter, courses distally on the caudal side of the trochanter, and then forms the lateral edge of the postrochanteric fossa. The postrochanteric fossa is situated just lateral to the lesser trochanter (fig. 13.4: ptf). This fossa is elongate proximodistally and narrows transversely; therefore, lateral side of the shaft of the femur in this region faces laterally instead of craniolaterally, as seen in other multituberculate femora (e.g. *Nemegtbaatar*; Kielan-Jaworowska and Gambaryan, 1994).

The lesser trochanter is prominent and starts just distal to the neck and greater trochanter (fig. 13.5: ltr). The base of the lesser trochanter is centered on the transverse width of the shaft and protrudes caudally, with the tip expanded and pointing medially well beyond the shaft. The transverse width of the lesser trochanter is 2.26 mm, and its lateral end is thicker proximodistally (1.44 mm) than its medial end (0.89 mm) (table 3). The caudal surface of the lesser trochanter is separated by a faint, proximodistal ridge into two distinct surfaces; a caudolaterally-facing and convex surface and a caudally-facing flat surface. The trochanteric fossa, between the two trochanters, is very deep, excavates to the base of the greater trochanter, and is continuous with a poorly developed groove that runs medially between the lesser trochanter and the neck of the femoral head (fig. 13.5: trf). In cranial view, the subtrochanter tubercle (fig. 13.1) is present where the femoral neck and greater trochanter join the shaft, but it is poorly developed. Lateral to that tubercle is a proximodistally elongate groove.

The suture between the distal epiphysis and the shaft is discernable. On the distal end of the femur, the trochlea is poorly developed, with its distal surface transversely concave and its cranial surface nearly flat. In cranial view, the trochlea (i.e. patellar groove) is oriented medioproximally to laterodistally (fig. 13.1: trh). The medial and lateral borders of the trochlea are not well defined. The lateral epicondyle is much larger and more bulbous than the medial epicondyle. A well developed extensor fossa, or possibly a fossa for the collateral ligament, occurs on the distolateral side of the lateral epicondyle (fig. 13.3: ?ext). In cranial view, a deep fossa, which is triangular in shape with the apex pointed proximally, is situated proximal to the trochlea. The medial condyle is small, oval shaped, and is proximodistally convex (fig. 13.6: mec). Medial to

the medial condyle is a small ridge that runs proximally. The lateral side of the medial condyle is elevated above the intercondyloid fossa, which separates the medial and lateral condyles. The proximal part of the lateral condyle has a transverse facet on its medial side that is proximal to the intercondyloid fossa.

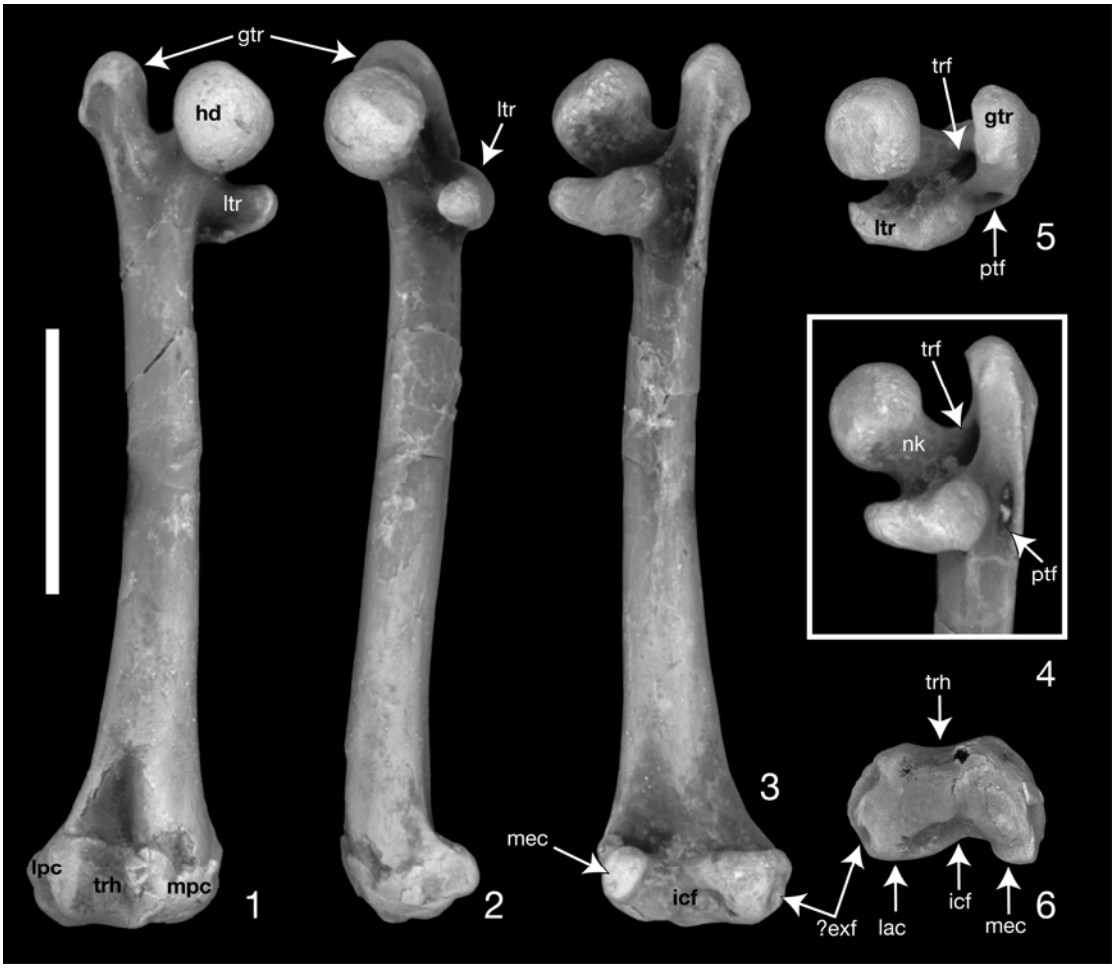

Fig. 13. Right femur of *Ectypodus* sp. (BT03049): **(1)** cranial view, **(2)** medial view, **(3)** caudal view, **(4)** enlarged caudomedial view of the proximal part of the femur, **(5)** proximal view, and **(6)** distal view of the distal end. Scale bar is 5 mm in length.

Table 3. Measurements (in millimeters) of femur of *Ectypodus* sp. (BT03049).

Dimension Measured	**(mm)**
Body	
Total length	16.83
Width of the distal end	3.65
Head	
Diameter of the head (dorsoventral)	2.1
Depth of the head (cranial side)	1.76
Depth of the head (caudal side)	1.34
Distance between head and greater trochanter	1.19
Neck	
Craniocaudal thickness	1.01
Dorsoventral thickness	1.24
Greater Trochanter	
Height	1.7
Distance extends beyond head	0.95
Lesser Trochanter	
Transverse length	2.26
Width at lateral end	1.44
Width at medial end	0.89

TIBIA

(fig. 14)

An incomplete, left tibia is preserved (fig. 14). Its distal end is not preserved, the proximal end is crushed on its medial side, and the caudolateral side of the shaft is cracked and crushed. On the proximal surface, the medial condyle is not preserved and the intercondyloid eminence only partially so. The shaft is flattened and has a slightly convex craniomedial side and a concave caudolateral side. In proximal view, the intercondyloid eminence runs craniocaudally. The lateral condyle articular surface faces proximocaudally (fig. 14.3: lco). Caudolateral to the lateral condyle articular surface is the fibular articular surface (fig. 14.2: fac), which faces laterally and slightly caudally. The tibial tuberosity is developed into a strong hook-like process that projects craniolaterally from the proximal end (fig. 14.1: ttu). In proximal view, the edge of the tibia is slightly notched between the tibial tuberosity and the fibular facet. A groove continues posterocaudally from this notch on the proximal surface, connects with a small intercondyloid fossa, and separates the lateral condyle from the tibial tuberosity.

Fig. 14. Left tibia of *Ectypodus* sp. (BT03049): **(1)** cranial view, **(2)** caudal view, **(3)** lateral view, **(4)** medial view, and **(5)** proximal view. In **5**, cranial is towards the left. Scale bar is 5 mm in length.

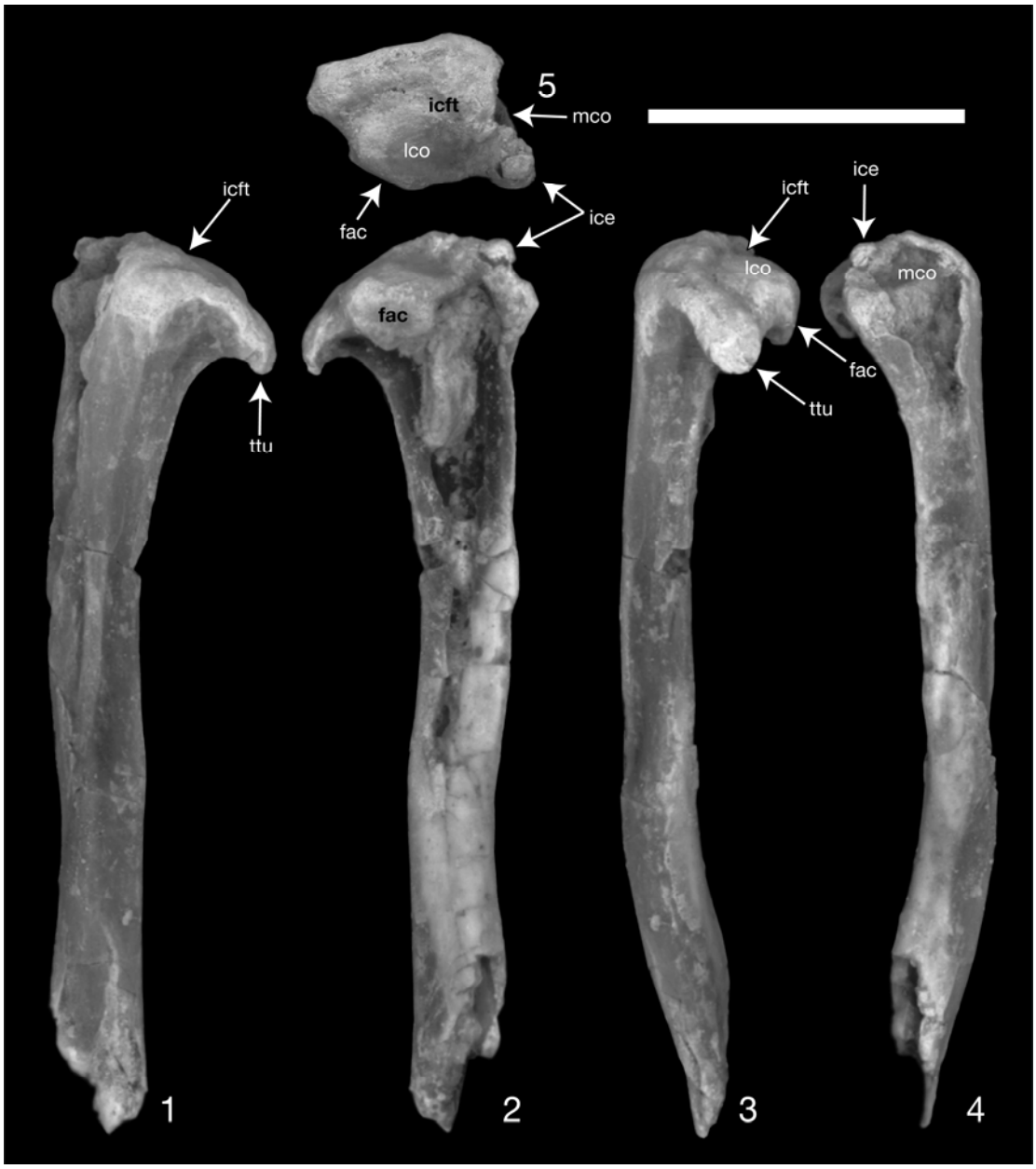

PARAFIBULA

(fig. 15)

A parafibula is preserved, although it is difficult to tell if it is the right or the left (fig. 15) (table 4). Even though this structure has been briefly described in *Ptilodus kummae*, *Kryptobaatar dashzevegi*, MCZ 20807 and 20806, and UA 11996, its exact

orientation in all of these taxa as well as the specimen of *Ectypodus* described here is unclear. In previous descriptions, three parts of the parafibula have been described: fibular facet, neck, and muscular process. The fibular facet articulates with the fibular head on the craniolateral surface (Krause and Jenkins, 1983; Kielan-Jaworowska and Gambaryan 1994). The fibular facet is almost circular shaped and slightly concave (fig. 15: ffib).

Fig. 15. Parafibula of *Ectypodus* sp. (BT03049). Orientation of all views uncertain. Scale bar is 2 mm in length.

TARSAL BONES

(fig. 16-18)

ASTRAGALUS: Only the right astragalus is preserved (fig. 16). Like other multituberculate astragali previously described (e.g. Granger and Simpson, 1929; Kielan-Jaworowska and Gambaryan, 1994; Minjin 2003), it has a buttress around the astragalar canal and a medially positioned astragalonavicular facet that is oriented transversally. In dorsal view, the lateral margin of the astragalus is craniocaudally longer than its medial margin (fig. 16.1) (table 4). In dorsal and plantar views, the buttress (fig. 13) is rectangular shaped. The astragalar canal is centered in the buttress and is circular (fig. 16.1: ac). The medial side of the buttress is straight, longer than its lateral side, and gently slopes craniolaterally. The lateral astragalotibial facet is a shallow, pulley-shaped trochlea (fig. 16.1: atil), but the upper ankle joint is not fully developed into the tenon-mortise. Two important difference from a fully-developed tenon-mortise joint are that the medial and lateral astragalotibial facets lie in the same plane and that the astragalofibular facet faces craniolaterally.

The well-defined lateral ridge of the lateral astragalotibial facet begins on the craniolateral side of the buttress, is aligned craniocaudally, and wraps around onto the cranial face of the astragalus. In lateral view, the ridge is convex dorsally. The ridge medial to the lateral astragalotibial facet is thicker, transversely, as compared to lateral ridge. The caudal end of the medial ridge is slightly more lateral than its cranial end. The caudal margin of the lateral astragalotibial facet is well defined, and it terminates just craniolateral to the buttress. Cranial to the astragalar foramen is a groove that continues

craniomedially to reach to the medial margin of the astragalus and runs along the caudal margin of the astragalotibial facet.

The medial astragalotibial facet is flat and is equal in width to the width of the lateral astragalo-tibial facet (fig. 16.1: atim). The astragalofibular facet is small and shaped like a boomerang in medial view (17.1: afi). Its cranial part runs next to the lateral astragalotibial ridge, while its more lateral part occurs on the caudolateral process. The *caudolateral process* of astragalus, new term, is located on the lateral side of the astragaulus and supports the caudal end of the calcaneoastragalar facet (fig. 16.2 and 17.1: clp). This should not be confused with the lateral process of some eutherians, which supports the cranial side of the calcaneoastragalar facet (e.g. *Phenacodus*, Geisler, 2001: fig. 4c and 5c). Caudal to this caudolateral process and lateral to the buttress the surface of the astragalus is concave. Cranial to the caudolateral process and plantar to the astragalofibular facet there is a distinct, but small fossa.

In plantar (ventral) view, the calcaneoastragalar facet is oval shaped and its long axis is oriented caudolaterally to craniomedially (fig. 16.2: caa). Unlike other described multituberculate astragali, the calcaneoastragalar facet is more caudally situated than the sustentacular facet, and it reaches the lateral side of the buttress. The sustentacular facet is irregular in shape, with its long axis oriented craniocaudally. The surface of the sustentacular facet is almost flat and faces plantarly, unlike other multituberculates, which have a more laterally facing facet (fig. 17.2: su). The angle between the long axes of the sustentacular and the calcaneoastragalar facets is about 40˚. There is no astragalar medial plantar tuberosity. A low *interarticular bulge*, new term, occurs between the sustentacular facet and the buttress on the plantar side of the astragalus (fig. 16.2: iab).

The interarticular sulcus is curved medially, in part because the calcaneoastragalar facet is angled, instead of being aligned craniocaudally. The astragalonavicular facet delineates a wide arc of rotation; it starts on the medial side of the astragalus and wraps onto the cranial side (fig. 17.2: an). Its surface is convex dorsoplantarly and medially, and unlike other multituberculates it is not saddle-shaped.

NAVICULAR: The proximal side of the navicular bears a dorsoplantarly concave facet for the astragalus (fig. 18: A6). The facet is wider dorsally. In lateral view, the dorsal end of the astragalar facet comes to a sharper point than the plantar end. The medial rim of the facet is more proximal than the lateral rim. In proximal view, the medial rim is straight, while lateral rim is convex. The proximodistal depth of the navicular is half of its total dorsoplantar length (table 4). The dorsolateral side of the navicular has large bulbous area, which bears facets for the cuboid and ectocuneiform. The cuboid facet on the navicular is large, slightly convex dorsoplantarly, and flat proximodistally (fig. 18 A3: cfn). It is restricted to the lateral side of the navicular. Distal to the cuboid facet is an ectocuneiform facet that is concave and extends dorsomedial to lateroplantar. The ectocuneiform facet covers the lateroplantar side of navicular (fig. 18 A5: efn). Distomedial to the ectocuneform facet and distal to the navicular is a facet for mesocuneiform. On the distocaudal side of the navicular is small bulbous facet for the entocuneiform (fig. 18 A5: enfn).

The distal surface of the navicular is divided into two convex areas, one dorsal and another plantar that join at the midpoint of the bone. The dorsal half of the distal surface is very wide, and plantar to that, the navicular narrows abruptly. On the plantar half of the medial side of the navicular, just distal to the astragalar facet, is a dorsopalmar

groove. Dorsodistal to this groove, is a small, bulbous convex area, possibly for articulation with the mesocuneiform (fig. 18 A2: mcfn).

ECTOCUNEIFORM: Only the right ectocuneiform was preserved. It is transversally compressed and proximodistally elongated (fig. 18 B1). In medial view, it is almost shaped like a quadrangle but with concave proximal and distal borders and a proximal border that is slightly shorter than the distal border (fig. 18 B3: mfe). In dorsal view, the proximal part of the ectocuneiform curves slightly medially and distally it widens (table 4). The distal border is convex in dorsal view. The ectocuneiform laterally contacts with the cuboid, proximally with the navicular, proximomedially with the mesocuneiform, and distomedially probably with metatarsal IV. Proximally, the ectocuneiform is pinched; therefore, the concave contact surface for the navicular is quite narrow. The plantar side of the ectocuneiform is narrow proximally and slightly broader distally.

On the lateral side there are two cuboid facets; the larger one at the proximodorsal corner and the smaller one on the distoplantar corner (fig. 18 B2: cfe). On the medial side of the ectocuneiform, there are also two facets. While it is possible that both facets on medial side are for the mesocuneiform, in *Eucosmodon* sp. (AMNH 16325) only the proximal facet is for the mesocuneiform while the distal facet is for metatarsal III (fig. 18 B3: m3fe). The more proximal of the two facets is situated on the proximodorsal corner of the medial side while the distal facet starts from the dorsodistal corner and continues proximoplantarly, but does not reach the plantar margin. The facets are separated from each other by a shallow, concave, nonarticular area.

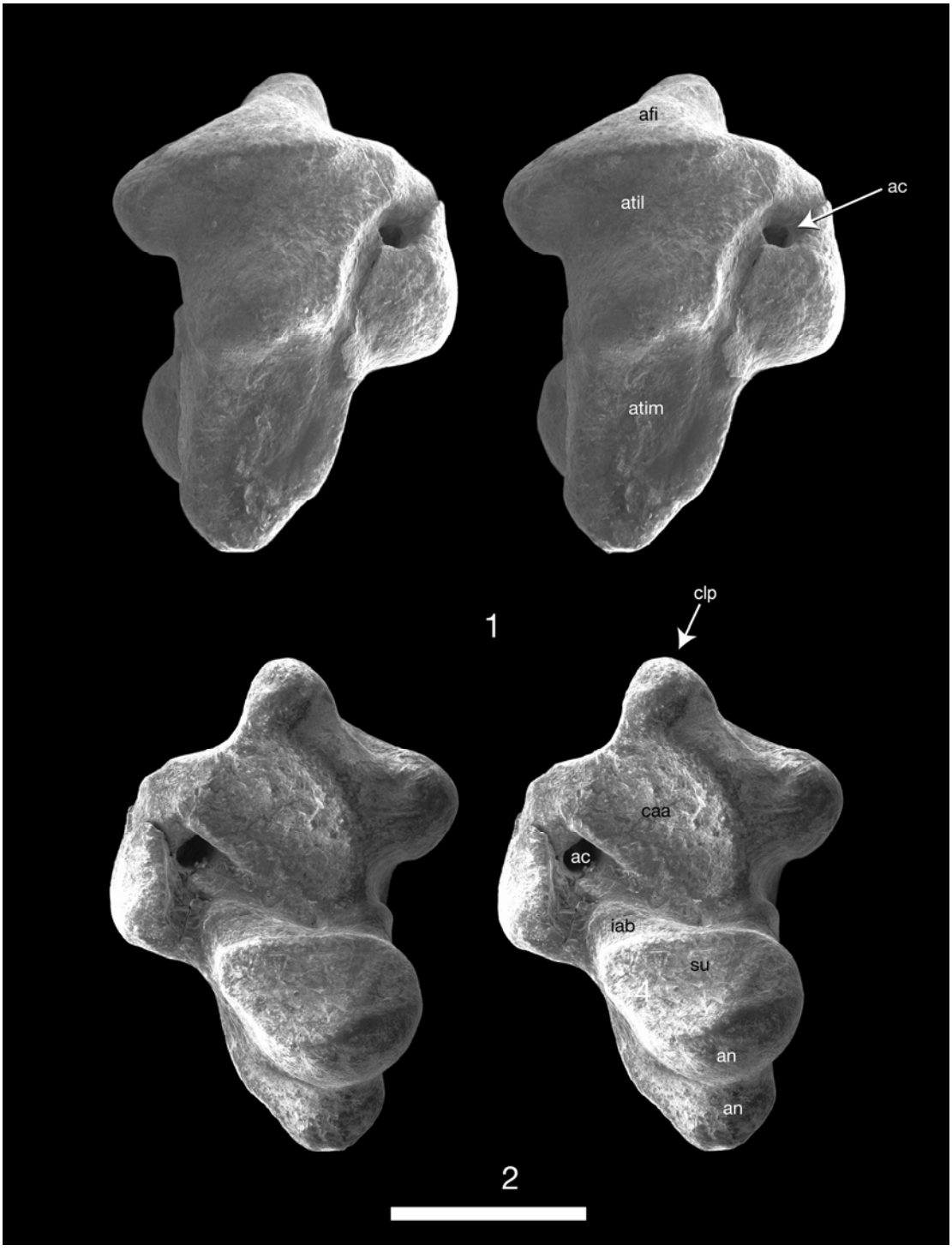

Fig. 16. Stereopairs of the right astragalus *Ectypodus* sp. (BT03049): **(1)** dorsal view, **(2)** plantar view. In **1** distal is towards the left while in **2** it is towards the right. Scale bar is 1 mm in length.

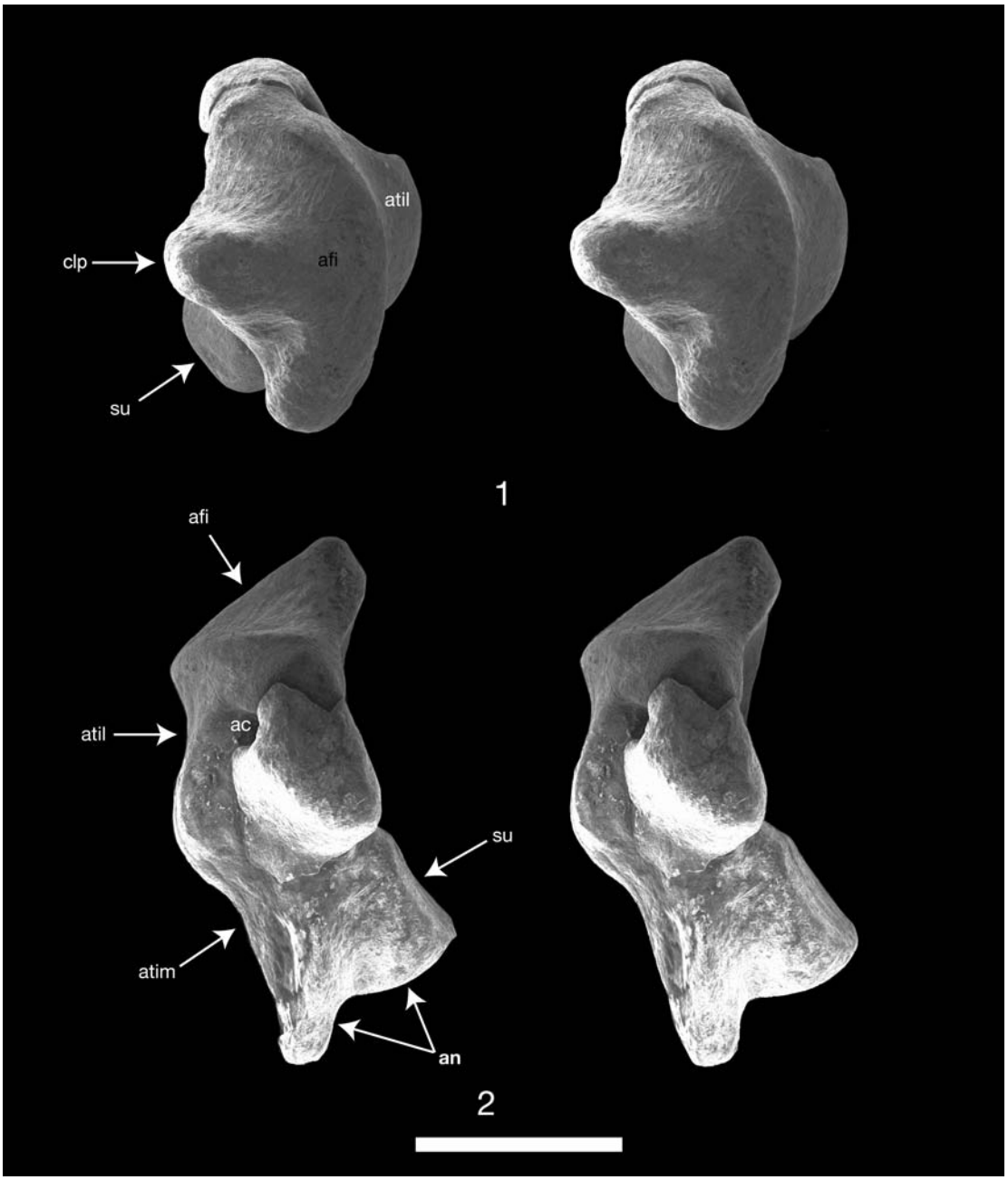

Fig. 17. Stereopairs of the right astragalus of *Ectypodus* sp. (BT03049): **(1)** medial view, **(2)** dorsal view. In **1** dorsal is to the right while in **2** it is to the left. Scale bar is 1 mm in length.

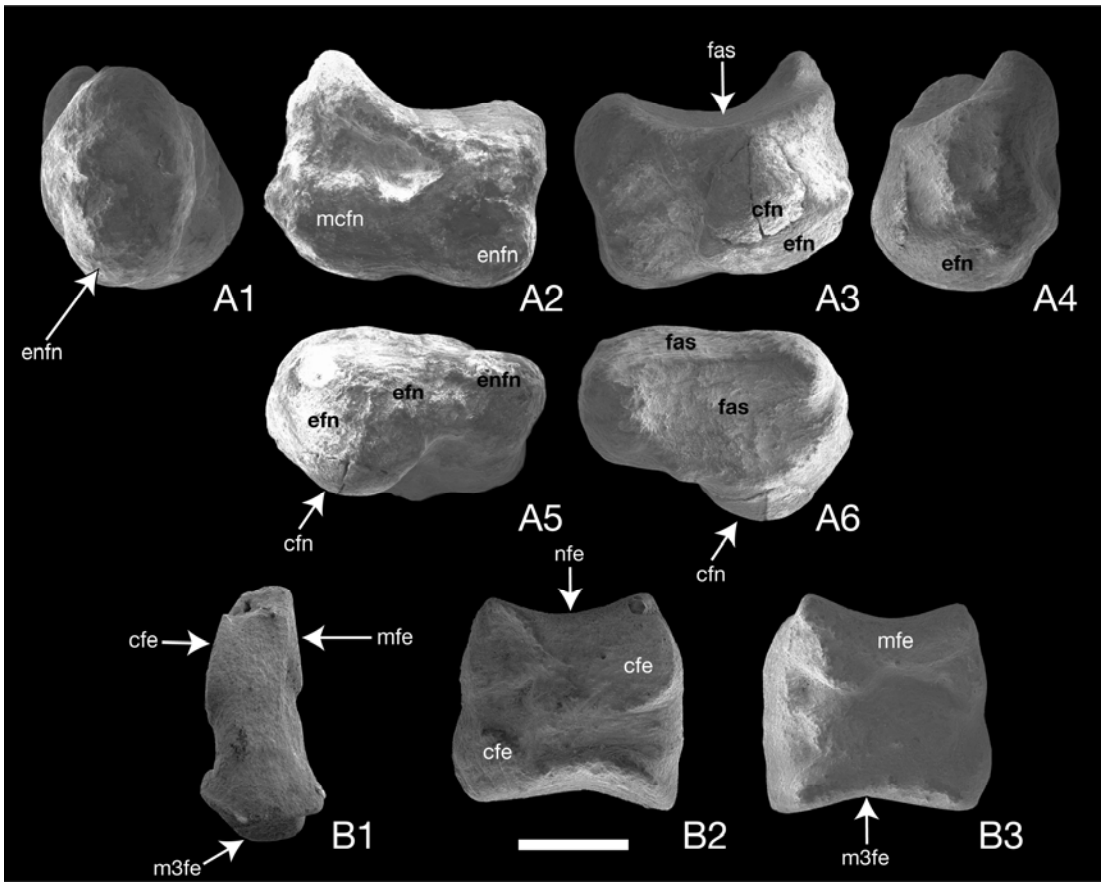

Fig. 18. Right navicular **(A1-A6)** and ectocuneiform **(B1-B3)** of *Ectypodus* sp. (BT03049): **(A1)** plantar view, **(A2, B3)** medial views, **(A3, B2)** lateral views, **(A4, B1)** dorsal views, **(A5)** distal view, and **(A6)** proximal view. Scale bar is 0.5 mm in length.

Table 4. Measurements (in millimeters) of hind limb bones of *Ectypodus* sp. (BT03049).

Dimension Measured	**(mm)**
Parafibula	
Length	2.65
Astragalus	
Transverse length	2.79
Medial width	1.22
Lateral width	0.51
Navicular	
Length	1.50
Ectocuneiform	
Craniocaudal length	1.09
Dorsoventral length	1.15
Craniodorsal transverse width	0.51
Caudodistal transverse width	0.47

METATARSAL

(figs. 19 and 20)

The identity of the two preserved metatarsals was based on direct comparison to the articulated metatarsal bones of *Ptilodus kummae* (Krause and Jenkins, 1983).

METATARSAL I: The left metatarsal I was preserved, but the distomedial part of its head is broken (fig. 19). The body of metatarsal I is transversely wider than its dorsoplantar dimension, and it widens towards its proximal and distal ends. In dorsal view, the articulation facet for the entocuneiform on the proximal end of this bone is saddle-shaped, with the saddle oriented transversely. In plantar view of the proximal end, there are two well developed tubercles; the medial one being slightly larger than the lateral one (fig. 19.5: fent). Moving to the distal end, there is a pit on the dorsal surface just proximal to the articulating facet for the proximal phalanx (fig. 19.2: ppdm)

METATARSAL V: A complete left metatarsal V was preserved (fig. 20). It is transversely wide and dorsoplantarly flattened. From its lateral side originates a laterally projecting peroneal process with a tubercle on its tip (fig. 20.4: prp). The process is close to but separated from the proximal end of the metatarsal. The small articulation facet for the cuboid is situated on the proximal end and faces proximodorsally. Lateral to this is a large articulating facet which, based on comparison to other multituberculates, likely articulated with the calcaneus (fig. 20.5: fcb). On the medial side of the proximal end is a medially-facing facet for metatarsal IV. Distal to this facet is a low flat-topped tubercle.

The head of metatarsal V is convex. On the dorsal side and just proximal to the head is a prominent and transversely elongated pit, which is for a collateral ligament. The head is shifted towards the lateral side; therefore, the medial side bears a pit between the body and the head. The distal face of the head faces distolaterally. In distal view, there is a parasagittal keel on the plantar side of the head (fig. 20.1). On both sides of, and just proximal to, the keel are two small pits, probably for sesamoid bones.

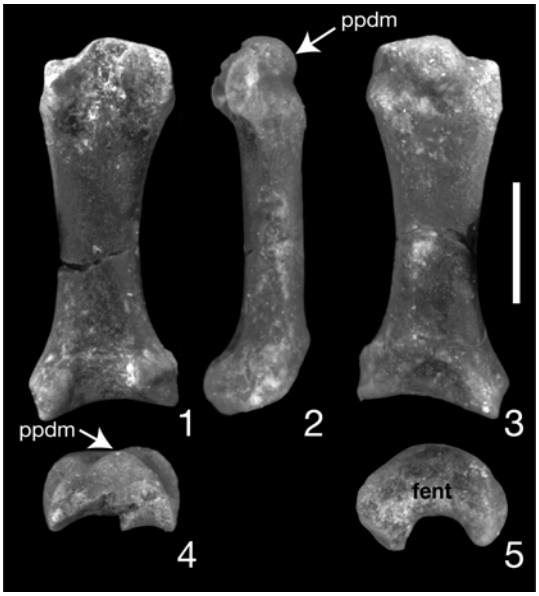

Fig. 19. Left metatarsal I of *Ectypodus* sp. (BT03049): **(1)** plantar view, **(2)** lateral view, **(3)** dorsal view, **(4)** distal view, and **(5)** proximal view. Scale bar is 1 mm in length.

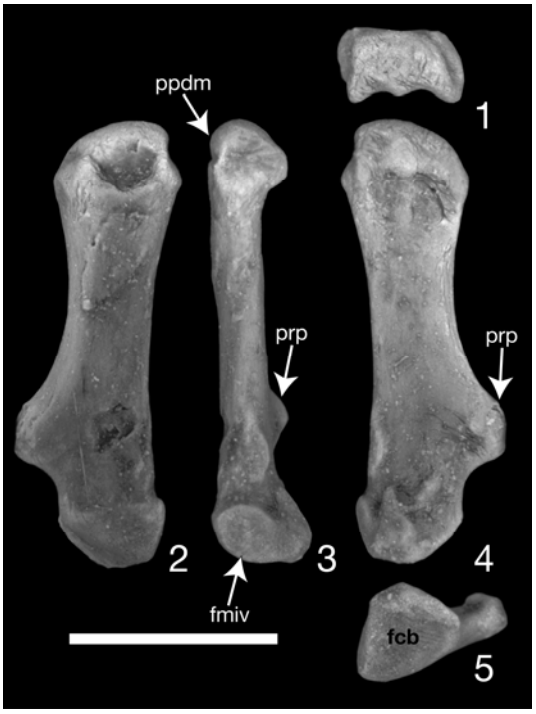

Fig. 20. Left metatarsal V of *Ectypodus* sp. (BT03049): **(1)** distal view, **(2)** dorsal view, **(3)** medial view, **(4)** plantar view, and **(5)** proximal view. In **5** lateral is to the right. Scale bar is 2 mm in length.

PHALANGES

(fig. 21)

Two proximal, five middle, and two distal phalanges are preserved (table 5). None are in articulation, thus it is hard to determine if they are manual or pedal phalanges. The bodies of the two proximal phalanges are sturdy and flat; thus based on comparison to the pedal phalanges of *Ptilodus kummae*, they are probably the first or fifth proximal phalanges. In contrast, the phalanges identified as middle phalanges are slender and slightly arched dorsally (fig. 21 B3). The articulation surfaces on the proximal ends of the proximal phalanges are concave and oval shaped, with the long axis oriented transversely. The articulation surfaces for the metatarsals are visible in dorsal view. On the middle phalanges, the articulation surfaces on their bases are similar to those of the proximal phalanges but are more circular shaped, more concave, and smaller. In addition, the dorsal margin of these facets is slightly more elevated; therefore, unlike the proximal phalanges, the articulation surfaces are not visible in dorsal view. The heads of the proximal and middle phalanges differ from each other. The proximal phalanges have proximodistally rounded heads, while the middle phalanges have trochlea-shaped heads. In plantar view, the proximal phalanges have a parasagittal ridge on the head, which separates two sesamoid bones. In contrast, the trochleated head of middle phalanges lacks a median ridge (fig. 21 B2).

The distal phalanx is a shaped like a claw, being narrow transversely and hooked (fig. 21). It has a well-developed flexor tubercle that is situated well distal of the articulating surface for the middle phalanx (fig. 21 A3: flxt). The extensor tubercle

overhangs the articulating surface for the middle phalanx (fig. 21 A2: extt). There are three nutrient foramina on the distal phalanx, two of which lead into long, curved grooves on the medial and lateral sides (fig. 21 A1, A3: nft1, nft2).

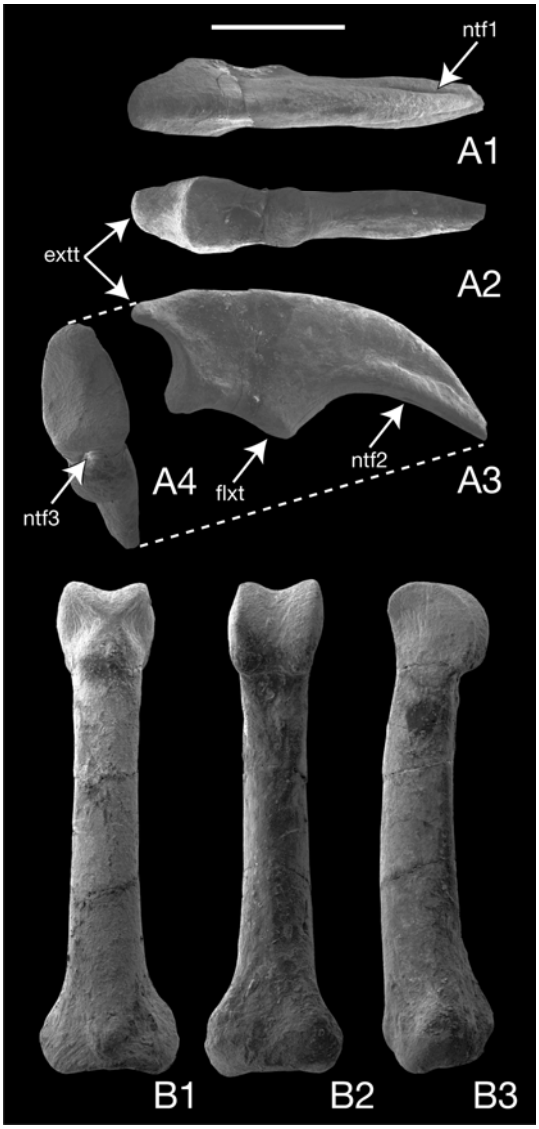

Fig. 21. Distal **(A1-3)** and middle **(B1-B3)** phalanges of *Ectypodus* sp. (BT03049): **(A1, B1)** dorsal views, **(A2, B2)**, plantar views, **(A3, B3)** medial and/or lateral views, **(A4)** proximal view. Scale bar is 1 mm in length.

Table 5. Measurements (in millimeters) of metatarsals and phalanges of *Ectypodus* sp. (BT03049).

Dimension Measured	**(mm)**
Metatarsal I	
Length	2.95
Length of the base	1.18
Craniocaudal width of the body	0.5
Transverse width of the body	0.71
Metatarsal V	
Length	4.29
Length of the base	1.25
Craniocaudal width of the body	0.47
Transverse width of the body	0.84
Phalanges	
Length of the proximal phalanx (025)	2.89
Length of the proximal phalanx (035)	3.67
Length of the proximal phalanx (041)	3.15
Length of the proximal phalanx (008)	3.17
Length of the middle phalanx (040)	3.56
Length of the middle phalanx (037)	3.42
Length of the middle phalanx (023)	3.00
Length of distal phalanx	2.7
Length of proximal phalanx (025)	2.7
Length of proximal phalanx (041)	3.1
Length of middle phalanx (800)	3.2
Length of middle phalanx (040)	3.6
Length of middle phalanx (035)	3.7
Length of middle phalanx (023)	3.3
Length of distal phalanx (045)	2.7

IDENTITY OF REFERRED SPECIMEN

Three multituberculates have been reported from the original Bangtail locality: *Ectypodus* sp. C, *Ptilodus*, and *Anconodon* (Gingerich et al., 1983; D. Boyer, pers. comm.). *Ectypodus* sp. C is an undescribed species of *Ectypodus* originally described by Rigby (1980) from the Swain quarry of the Washakie Basin, Wyoming and Gingerich et al (1983) referred seven specimens from the Bangtail quarry to this species: right M_1, P^1, partial snout with left P^{1-4}, cranial part of M^1, right maxilla with P^{1-4}, right M^1, and right I_1.

The M_1 of BT03049 differs from those of *Ptilodus* and *Anconodon*. Both genera have larger lower molars than that of BT03049, and *Ptilodus* has only five cusps in the external (labial) row of M_1, in contrast to seven in BT03049 (Krause, 1977). *Anconodon* has even more, with 8 cusps in the external row (Jepsen, 1940). Of the three taxa known from the Bangtail locality, BT03049 is most similar to *Ectypodus* sp. C. The M_1 of *Ectypodus* sp. C from the Bangtail locality (USNM 309868) is 2.3 x 1.0 mm (length x width) while that of BT03049 is slightly smaller, measuring 1.98 x 0.81 mm. Both specimens have the same number of external cusps, but BT03049 has four cusps in the internal row instead of five (fig. 5.2), as seen in USNM 309868. Given the variation in size and number of cusps seen in species of *Ectypodus* (Jepsen, 1930), BT03049 falls within the range of variation observed within this genus. More striking is the detailed similarity among the relative positions of the cusps as seen in BT03049 and in species of *Ectypodus*; in both, the internal and external rows diverge caudally and the internal cusps are widely separated. Given the morphological similarity between BT03049 and

Ectypodus and the fact that this genus has been reported from the nearby original Bangtail locality, I tentatively refer BT03049 to *Ectypodus*. However, it is conceivable that BT03049 could be a taxon that has not yet been reported from Bangtail locality, particularly given the difficulty in assigning a single tooth to a genus within Neoplagiaulacidae (Scott, 2005).

Other plausible genus-level referrals for BT03049 were discovered by referring to the character-taxon matrix of Rougier et al. (1997), modified from the original matrix developed by Simmons (1993) to resolve the phylogenetic relationships within Multituberculata. Following Simmons (1993), Rougier et al. (1997) included a character for M_1 cusp formula and another for M_1 size in their matrix, and of the 49 coded in their matrix, 14 of them, like BT03049, have a cusp formula of 7:4 (7 cusps in the external row and 4 cusps in the internal row): *Mesodma*, *Parectypodus*, *Ectypodus*, *Mimetodon*, *Neoplagiaulax*, *Prochetodon*, *Baiotomeus*, *Microcosmodon*, *Stygimys*, *Liotomus*, *Neoliotomus*, *Essonodon*, and *Cimolomys*. Of these 14 genera, seven are coded as having a M_1 that has a length between 1.0-2.9 mm, the same as BT03049: *Mesodma*, *Parectypodus*, *Ectypodus*, *Mimetodon*, *Neoplagiaulax*, *Prochetodon*, *Microcosmodon*. This list can further be narrowed down because only *Ectypodus*, *Microcosmodon*, *Neoplagiaulax* (Weil, 1999), and *Parectypodus* have distally-diverging cusp rows, like the Bangtail specimen. Furthermore, spaces occur between the internal cusps in *Neoplagiaulax* and *Ectypodus* (Scott, 2005), but in *Neoplagiaulax* the external row has more cusps and they are crowded together, unlike BT03049. Additional discoveries of more multituberculates from the Bangtail localities are needed to confirm our referral of

BT03049 to *Ectypodus* or to demonstrate that it occurs to a taxon not yet reported from this locality.

SUPERFAMILY DJADOCHTATHERIOIDEA KIELAN-JAWOROWSKA AND HURUM, 2001

FAMILY DJADOCHTATHERIIDAE KIELAN-JAWOROWSKA AND HURUM, 1997

Kryptobaatar dashevegi, Kielan-Jaworowska, 1970a

REFERRED SPECIMEN: MAE 00-22, an articulated skeleton with skull, including nearly complete forelimbs, right hind limb, lumbar vertebrae, sacrum, many ribs, and sternal elements, but not preserving the scapulae, most cervical vertebrae, some thoracic vertebrae, the left hind limb, and the tail (fig. 22).

LOCALITY AND HORIZON: Ukhaa Tolgod locality, Nemegt Basin, Umnugovi Province, Mongolia (see GEOLOGICAL SETTINGS for more details).

DESCRIPTION

SKULL

The skull of *Kryptobaatar daszevegi* has recently been described in great detail by Wible and Rougier (2000).

Fig. 22. Skeleton of *Kryptobaatar dashzevegi* (MAE 00-22) from Ukhaa Tolgod, Mongolia. Scale bar is 2 mm.

VERTEBRAE

(fig. 22-30)

The vertebral column is not complete and the specimen is missing most of the cervical and caudal series (fig. 22). Regarding the cervical vertebrae, only the last cervical and an articulated fragment of the right postzygapophysis of the sixth cervical are preserved. Eight thoracic vertebrae are preserved: five are cranial thoracics and three are the posterior-most thoracic vertebrae. The first three thoracic vertebrae are partially articulated, and the next two thoracics have become disarticulated from the first three, but remained closeby. The last two thoracics remain articulated with the caudal part of the vertebral column, but the third from the last is slightly dislocated towards the left side. There are eight lumbar vertebrae and all are articulated and remain in their original positions. The sacrum consists of four vertebrae, and this specimen ends after the first two caudal vertebrae.

CERVICAL VERTEBRAE: Only the right postzygopophysis is preserved from the sixth cervical vertebra (fig. 23: c6). There is a small facet on the craniodorsal side of the postzygopophysis, probably for contact with the fifth cervical vertebra. The right side of the arch of the seventh cervical vertebra is preserved but its body is not. The vertebra has a large transverse foramen and a transverse process that is short and robust. Just distal to the transverse foramen is a stout, cranially projecting ventral tubercle (= cranial tubercle of the human, called the ventral branch of the transverse process by Kielan-Jaworoska and Gambaryan, 1994). The body of the seventh cervical is not visible. The articulation surfaces of the post and prezygopophyses are in the same dorsal plane.

THORACIC VERTEBRAE: Eight vertebrae are preserved, but only the first three and the last three are articulated. The remaining two vertebrae are dislocated from the rest of the vertebral column, although their location near the first three thoracics suggests that they represent the 4th and 5th thoracic vertebrae (fig. 23: t4?, t5?). Although eight vertebrae are preserved, the original count was certainly more. The first thoracic vertebra is nearly complete. The body of the vertebra is compressed craniocaudally and transversally wide. The vertebral foramen is large, thus the laminae are transversally wide and the post- and prezygopophyses are positioned far apart. The postzygopophyses are slightly more dorsal than the prezygopophyses, are large, and project more laterocaudally than those on the last cervical vertebra. The first thoracic's spinous process is very short, bulbous, and oriented slightly caudally in addition to dorsally. Unlike the last cervical, where the pedicles are dorsoventrally tall, the pedicles below the prezygapophyses on the first thoracic are short. The transverse process of the first thoracic is very short and expanded craniocaudally. The costal fovea of the transverse process faces lateroventrally.

The morphologies of the second, third, and what is thought to be the fourth thoracics are similar. The laminae on each of the three vertebrae are narrower, craniocaudally, than the lamina of the first thoracic. In lateral view, the neural spines of the second and third thoracics are more inclined caudally as compared to that of the first (fig. 23: t5?); therefore, the space between the spines of the first and second thoracics is quite large. All three vertebrae have craniocaudally elongate costal fovea of the transverse process, although much less so than that of the first thoracic. The costal fovea of the transverse process is located at the junction between the pedicle and the body on the second and third vertebrae, but on the fourth? thoracic, it is located more dorsally.

The cranial and caudal costal fovea of these three vertebrae are not clearly defined, although they appear to be located near the dorsolateral corners of the cranial and caudal faces of the centrum. Parapophyses and accessory processes (i.e. anapophyses) are not present on the anterior thoracics. The exact locations of the postzygopophyses on these vertebrae are uncertain, either because they were broken off or the articular surfaces are not well defined.

The prezygopophyses of the second thoracic are located just dorsal and slightly cranial to the costal fovea of the transverse processes; therefore, the pedicles are quite short on this vertebra. The spinous process of the second thoracic is broken, but it appears to be as short as that of the first, third, and fourth? thoracics. The caudal face of the third thoracic and the cranial face of the fourth? thoracic are visible. Each is slightly concave and roughly triangular in shape, with the rounded-over apex pointing ventrally (fig. 23: t4?). The fourth? thoracic does not have a median ventral crest, instead the ventral surface of the body is pinched and triangular in shape with the apex pointing caudally. Thoracic 5? is similar to thoracic 3 and 4? except that the spinous process is longer, the lamina is wider craniocaudally, and the cranial costal fovea is well-defined.

Three caudal thoracic vertebrae are preserved. The cranial one is the anticlinal vertebra and the remaining two are post-anticlinal (fig. 23: ta). The spinous process of the anticlinal vertebra is vertical while the two post-anticlinal vertebrae clearly have cranially inclined processes, even though the tips of the processes are broken. The spinous process of the penultimate thoracic vertebra is very short, its cranial edge is straight, and its caudal edge is inclined cranially. Although the prezygopophyses of the anticlinal vertebra are broken, enough is preserved to tell that the distance between the prezygopophyses is

wider than on the post-anticlinal vertebrae. Prezygopophyses of the post-anticlinal vertebrae face dorsomedially, and all three of the preserved caudal thoracics have postzygopophyses that face ventrolaterally. The costal fovea of the transverse process and the cranial and caudal costal fovea are not well defined. The anticlinal vertebra has a small accessory process (i.e. anapophysis) between the postzygapophysis and the pedicle base. A ridge originates at the tip of the accessory process and then runs cranioventrally. Ventral to this ridge is a small concave area, which in turn is bordered ventrally by another weak ridge. As compared to the anticlinal vertebra, the penultimate thoracic has larger accessory processes and the ridge that runs from it is positioned more ventrally, thus making the concave area that is ventral to this ridge smaller. The ultimate thoracic has a rudimentary accessory process, and the two ridges described above are replaced by a single ridge that appears to be a small transverse process. The concave area ventral to the accessory process is absent on the ultimate thoracic. The last two thoracic vertebrae remain in articulation with the ribs on their right sides (figs. 23, 24).

LUMBAR VERTEBRAE: Eight lumbar vertebrae are preserved (figs. 25-29: L1-8), and given that this part of the vertebral column is intact, all seem represented. Transverse processes of the last four lumbars and the second one are complete, but these processes are not preserved on the first and the third, and the fourth is missing the left process only. As shown by Jenkins (1971), the lumbars in *Thrinaxodon* have ribs that articulate to the centra by parapophyses that diminish on each successive vertebra. Thus the transverse processes on the lumbars of multituberculates are most likely homologous to the lumbar ribs of more basal synapsids. In general, the transverse processes of *Kryptobaatar* are directed ventrolaterally as well as slightly cranially, and the lengths of the processes on

sequential vertebrae increase caudally, except for the last lumbar (fig. 25). The base of each transverse process is wide and gradually tapers towards a distal end that is pointed craniolaterally. The transverse process of the last lumbar is distinct from the others. Its transverse process is strongly bent cranially, and it is shorter than the transverse process of the seventh lumbar (fig 25: L8). The dorsal surface of the transverse process of the last lumbar is concave craniocaudally; with well defined ridges along its cranial and caudal margins. Even though the ends of the spinous processes of the fifth and sixth lumbar vertebrae are broken, it is clear that they were strongly inclined cranially (fig. 27: L6, L7). The spinous process on the seventh lumbar is also inclined cranially, but to a lesser degree than is seen in more cranial lumbars. The spinous process of the last lumbar vertebra is almost vertical and probably the tallest of the eight (figs. 28, 30: L8). Small accessory processes are present only on the first and second lumbar vertebrae. The postzygopophyses of the first five lumbar vertebrae face ventrolaterally, while the last three lumbar vertebrae have ventrally facing postzygopophyses. Mammillary processes are visible on the right side of the last three lumbars, and these processes were probably present on the other lumbars prior to post-mortem damage. As seen in dorsal view, the last three lumbar vertebrae are more square-shaped while the preceding lumbars are craniocaudally elongate (fig. 29).

SACRAL VERTEBRAE: The sacrum consists of four articulated or fused vertebrae (figs. 25, 30: sa). The first sacral vertebra is not fused to the second, but the second through fourth are completely fused to each other with just sutures tracing the boundaries between zygapophyses on separate vertebrae. Unlike the specimen of *Kryptobaatar* described by Kielan-Jaworowska and Gambaryan (1994), in this specimen only the

transverse process of the first sacral firmly articulates with the ilium (fig. 30: il, sa). The anterior-most point of the transverse process of the second sacral is thickened dorsoventrally, so it may have had a ligamentous attachment with the ilium. Alternatively both sides of the pelvis may have rotated outward post-mortem, removing direct contact between the second sacral and ilium, but this seems unlikely.

The prezygopophyses of the first sacrum are flat, face dorsally, and are located cranial to the cranial margins of the transverse processes and the centrum. Just caudal to the prezygopophysis is a distinct pit. The notch between the prezygopophyses of the first sacral is wide and deep craniocaudally. Its transverse processes are wide, directed caudolaterally, and unlike the other sacrals, it distal end is at a level well ventral to that of its base. The auricular surface is not visible. The first sacral is craniocaudally the shortest of all sacrals. By contrast, the second through fourth sacrals are elongated craniocaudally, and in dorsal view, the vertebrae are transversely narrow between the pre- and postzygopophyses. The spinous processes of all the vertebrae are not well preserved. Even so, the spinous process of the first sacral seems to point vertically. The spines of the second and third sacrals are fused, and the spine of the second points slightly more caudally. The spinous process of the fourth sacral is broken, even so, it has a thicker base than those of other vertebrae. The transverse process of the second sacral is wide and differs from the others in having its distal edge oriented caudomedially, as is seen in *Ptilodus kummae*. The transverse processes of the third and fourth sacrals are broken. That of the third has a laterally directed process while that of the fourth seems to be angled more cranially. Only the right postzygopophysis of the fourth sacral is preserved.

It is circular in shape and faces ventrally. The centrum of the fourth sacral is slightly compressed dorsoventrally to form an oval shape.

RIBS: Eleven right ribs are preserved, and all but the last two are dislocated from their anatomical positions (fig.23). On the left side, 5 ribs are preserved; three are entirely visible while the rest are either hidden under other bones or are only partially exposed. To the left of the vertebral column, seven ribs are preserved, but only three are completely exposed. Of the right ribs, 4 clearly have two heads, five have one or two heads that have partially merged, and two are not preserved well enough to tell. All the ribs are curved, although the curvatures in the last two ribs are subtle. Several of the middle ribs on the right side have a flattened dorsal surface that extends for approximately a quarter the distance down the shaft from the tuberculum and/or capitulum. Otherwise, the shafts are compressed craniocaudally. As preserved, the longest rib is on the left side side (21 mm), and this rib is probably close to its original length. The last two ribs on the right side are considerably shorter, being approximately 9 mm in length.

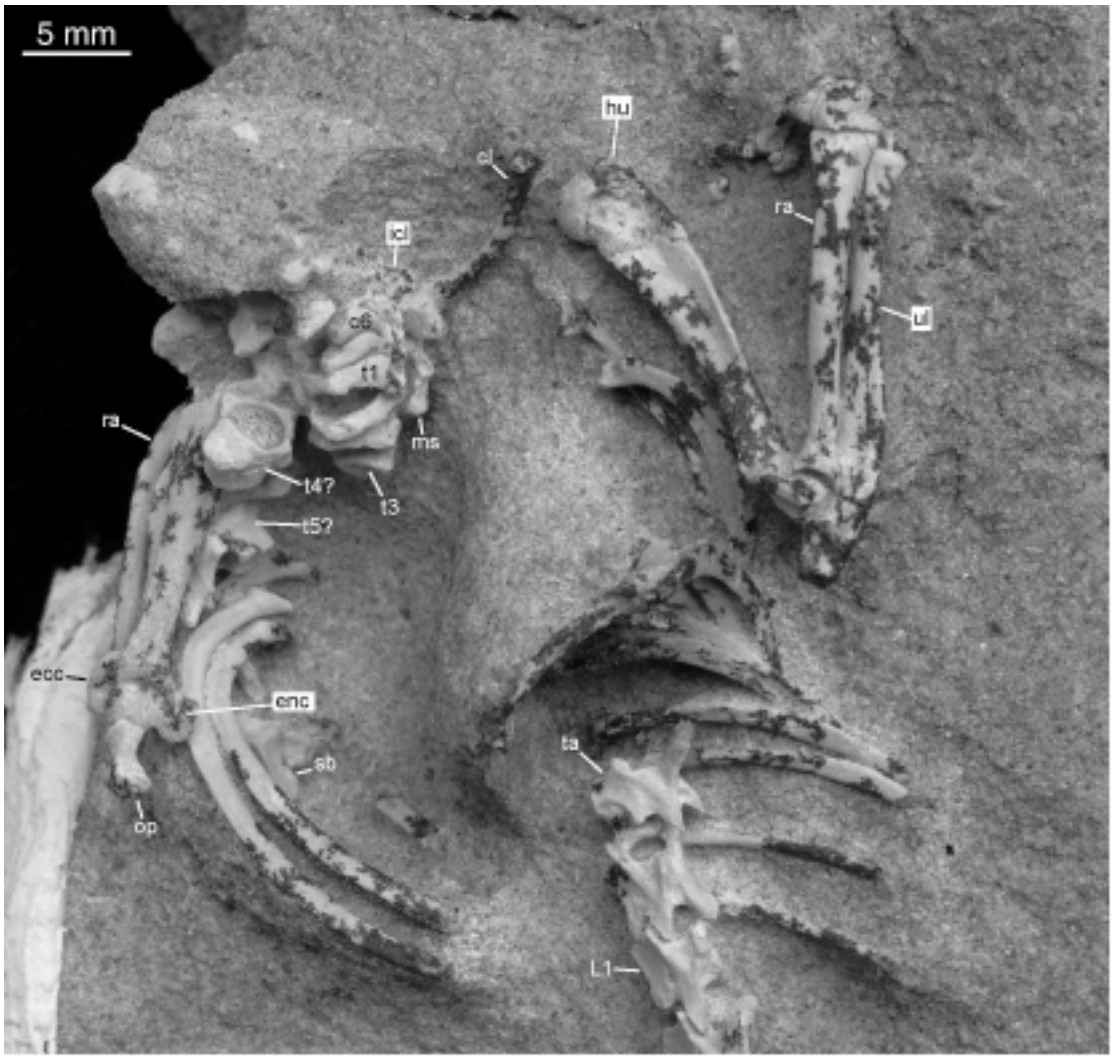

Fig. 23. Dorsal view of the partially articulated thorax and forelimbs of *Kryptobaatar dashzevegi* (MAE 00-22). See fig. 24 for stereophotographs of this image.

STERNUM

(fig. 23 and fig. 25)

Two sternebrae are preserved, but it is hard to tell which sternebrae they are because they are dislocated from their natural positions. A partial manubrium is also preserved. The manubrium is partially exposed beneath the first and second thoracic vertebrae, but little can be seen except for one or two articulation surfaces for costal cartilages (fig. 23: ms). Two middle sternebrae are preserved dislocated underneath the left ribs (fig. 23: sb). One of them has a low, but sharp median keel on its ventral surface. The body of each is about twice as long as wide. A third sternebra occurs to the left of the lumbar vertebrae (fig. 25: sb).

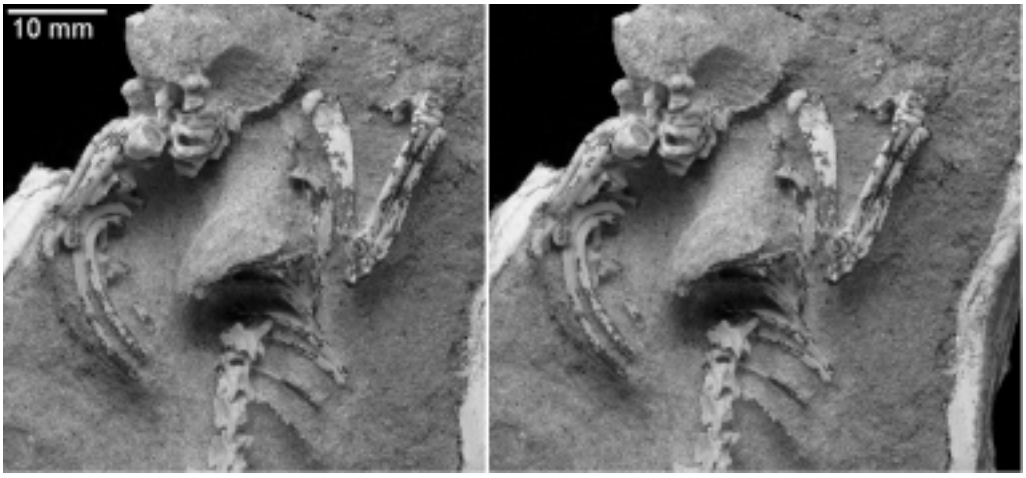

Fig. 24. Stereophotographs of the dorsal view of the partially articulated thorax and forelimbs of *Kryptobaatar dashzevegi* (MAE 00-22). See figs. 23 and 32 for labels of individual features.

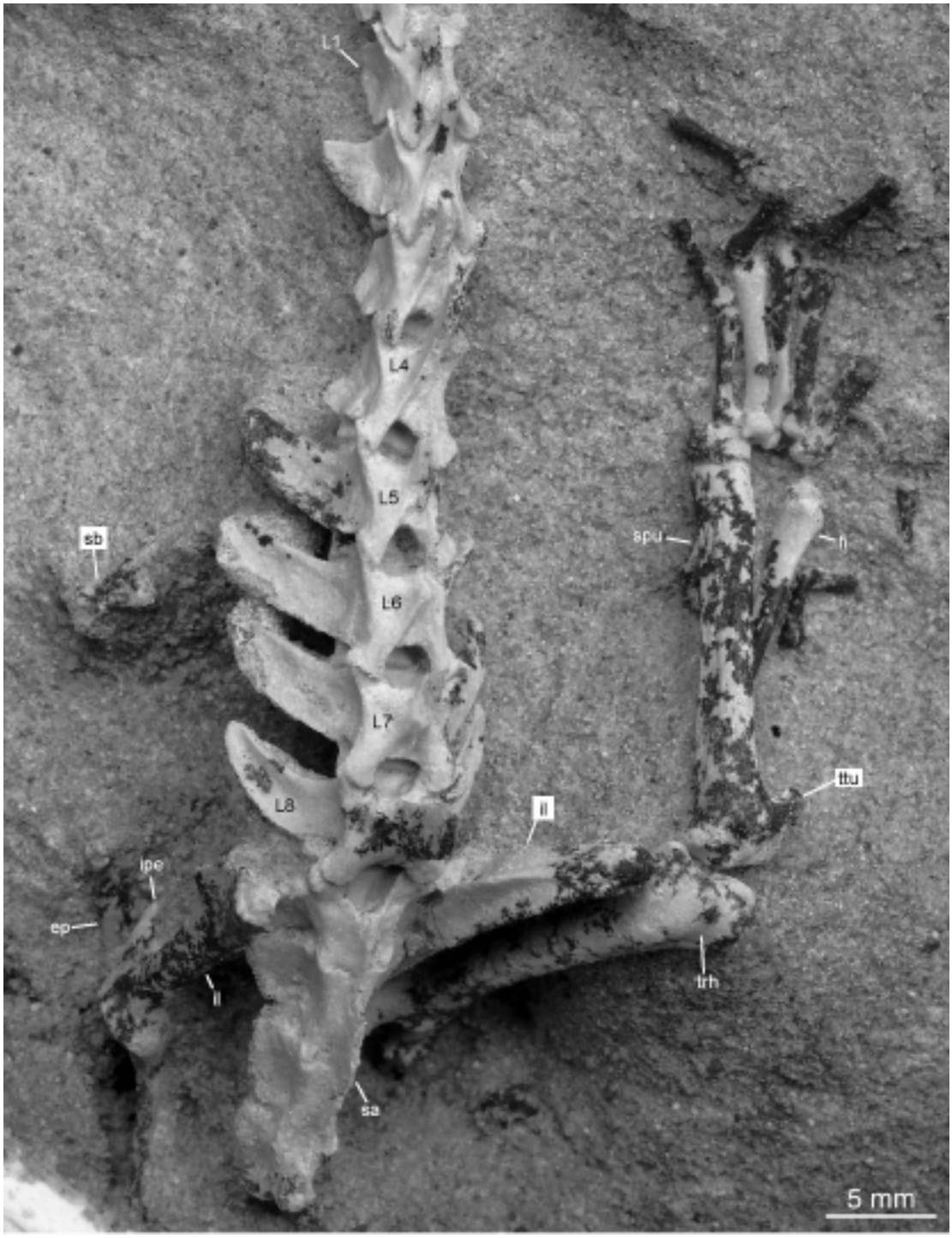

Fig. 25. Dorsal view of the lumbus, pelvis, and right hindlimb of *Kryptobaatar dashzevegi* (MAE 00-22). See fig. 26 for stereophotographs of this image and fig. 35 for labels of individual features on the right hindlimb.

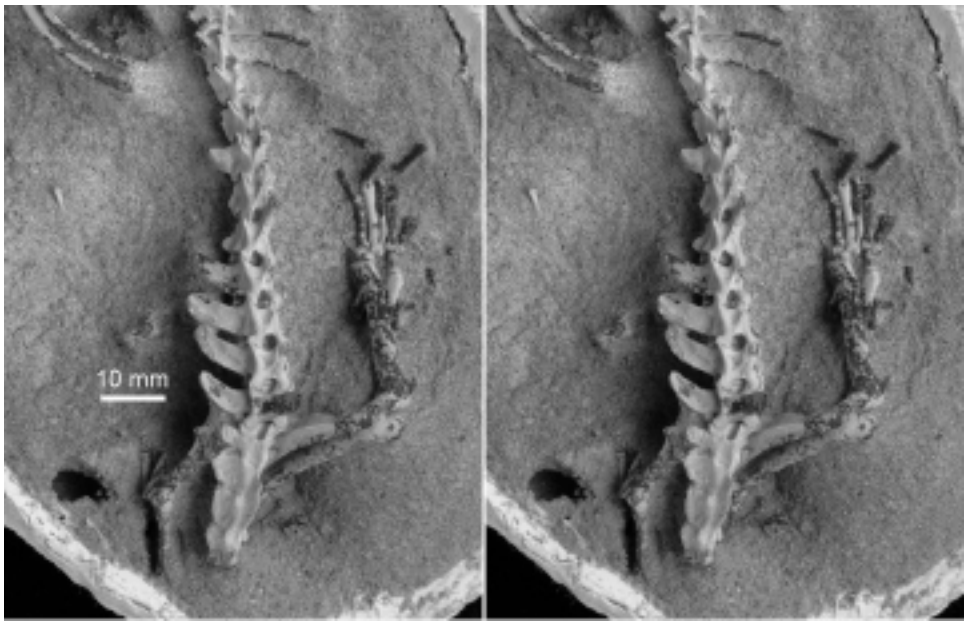

Fig. 26. Stereophotographs of the dorsal view of the pelvic girdle, and right hindlimb of *Kryptobaatar dashzevegi* (MAE 00-22). See figs. 25 and 35 for labels of individual features.

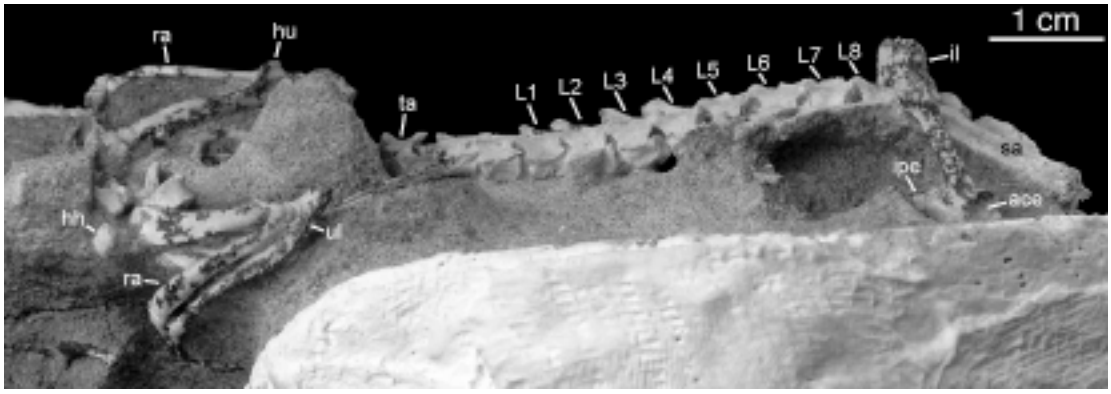

Fig. 27. View of the left side of the skeleton of *Kryptobaatar dashzevegi* (MAE 00-22). Cranial is to the left.

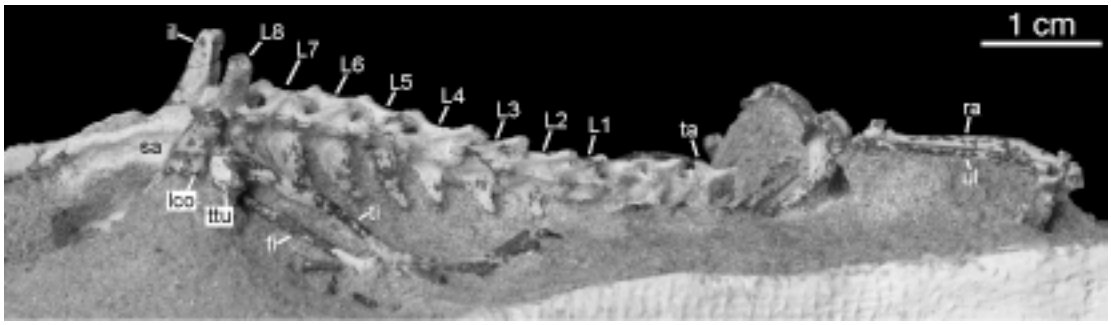

Fig. 28. View of the right side of the skeleton of *Kryptobaatar dashzevegi* (MAE 00-22). Cranial is to the right.

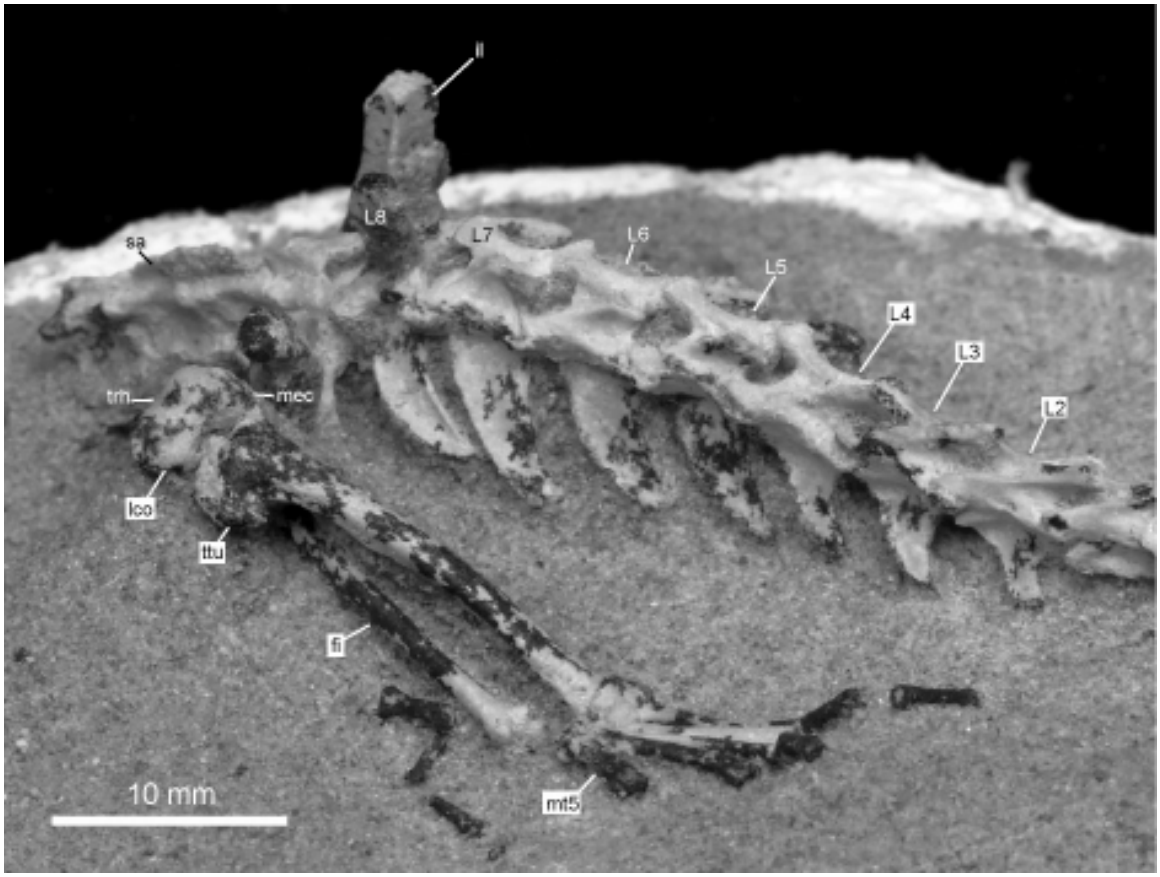

Fig. 29. Dorsolateral view of the right side of the lumbus, pelvic girdle, and right hindlimb of *Kryptobaatar dashzevegi* (MAE 00-22). Cranial is towards the lower right corner of the image.

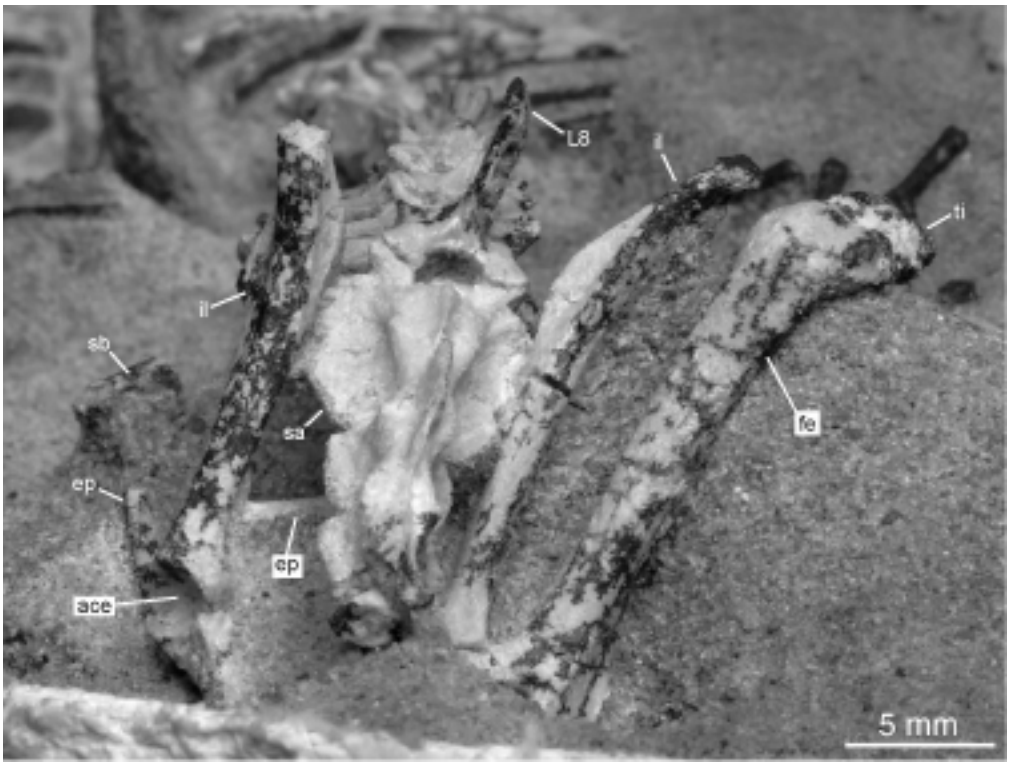

Fig. 30. Dorsal view of the pelvic girdle and right femur of *Kryptobaatar dashzevegi* (MAE 00-22). Cranial is towards the top of the image.

PECTORAL GIRDLE AND FORELIMB

(fig. 4, 23, 31-34)

Most bones of the forelimbs are preserved. On the right side, the scapula, 3 metacarpals, unciform, and all but 3 phalanges were not preserved. On the left side, the scapula, clavicle, trapezoid, trapezium, 2 metacarpals, and six phalanges were not preserved. The right clavicle is in natural contact with the interclavicle, which is partially hidden beneath the cervical vertebrae (fig. 23: cl, icl). Both humeri are preserved, but the

proximal end of left humerus is broken right below the head. Both humeri are articulated with the radii and ulnae, all in their natural positions. Both the right and left radius and the left ulna are complete; the right ulna is missing its distal epiphysis. The right and left carpals are displaced from the radii and ulnae. On the left manus, metacarpals I-III, their phalanges, including the distal ones, are still articulated with the carpal bones. On the right manus, only two metacarpals are preserved. The right metacarpal II and its proximal phalanx are articulated, but the distal phalanx is displaced. What is thought to be metacarpal V of this manus is displaced caudally. There are 5 sesamoid bones near the right manus; two are floating cranial to the manus, two are still articulated with the caudal end of metacarpal II, and one is articulated with the displaced second distal phalanx.

INTERCLAVICLE: It is not clear if the interclavicle is completely preserved because only the cranial part of the right interclavicle is exposed (fig. 23: icl). The cranial edge is convex and deflected ventrally so that the dorsal face of this part of the interclavicle actually faces partially cranially. This differs from the reconstruction presented by Sereno (2006), and indicates that the interclavicle had four, not three lobes: two lateral, one cranial (observed here) and a fourth caudal. Extending laterally from the body of the interclavicle is a wing-like process, with a squared-off tip. The clavicle articulates with the ventral surface of the interclavicle where the "wing" starts to extend laterally. Unfortunately the ventral surface is obscured, so the position and morphology of the clavicular facet can not be observed.

CLAVICLE: Only the right clavicle is preserved, and it articulates with the interclavicle in its natural position. The right clavicle is about 10 mm in length and is compressed dorsoventrally. It is boomerang-shaped, being strongly concave dorsally and

convex ventrally in cranial or caudal view (fig. 23: cl). In dorsal view it is also slightly sigmoidal. The cranial face of the clavicle bears a sharp ridge for the lateral three fourths of the bone's length. The medial end of the clavicle, which articulates with the interclavicle is broad. The distal end of the clavicle tapers and bears a large, laterally-facing, concave facet, presumably for the acromion of the scapula.

HUMERUS: Both humeri of MAE 00-22 are preserved, but the head of the left humerus is detached. In addition, the proximal end of the right humerus is partially obscured. The overall morphology of the humerus is typical of that seen in other multituberculates. Because the humeri were left in articulation with the radius and ulna and embedded in the matrix, it is difficult to estimate the degree of humeral torsion. The right humerus lies on its medial side, and the ectepicondyle appears to be roughly aligned with the junction of the humeral head and greater tuberosity. Using figure 10.7 of Sereno (2006) for comparison, this would imply that the degree of torsion is small, possibly even less than the 15 degrees reported in the specimen of *Kryptobaatar* described by Sereno (2006). The head of the humerus is globular in shape and does not strongly overhang the shaft (fig. 32: hh). The greater tubercle is positioned slightly cranial to the head. The deltopectoral crest is well developed and extends distally past the midpoint of the shaft (figs. 31, 32: dpc). Approximately ¼ of the way down from the humeral head on the medial side of the shaft is a low ridge for attachment of the teres major muscle. The lateral side of the humerus, caudal to the deltapectoral crest, is concave, although not as concave as in the Udan Multi.

Although the distal ends of both humeri are well preserved, only the caudal surfaces are visible. The flange of the ectepicondyle does not continue proximally up the

shaft (fig. 23: ecc), and in lateral view, it can be seen that the caudal surface of the ectepicondyle flange faces somewhat laterally. The distal edge of the flange is thickened, and the entepicondylar foramen is not visible because of the orientations of both humeri. In caudal view, it can be seen that the entepicondyle is well developed (fig. 23: enc). The articulation for the ulna on the caudal side of the humerus is well preserved and bears two parasagittal ridges, which are the continuations of the ulnar (medial) and radial (lateral) condyles. Between the ridges is a well defined trough. In caudal view, a strong notch separates the medial of the two ridges from the entepicondylar process. The olecranon fossa is well developed, transversely elongate, and extends medially slightly beyond the proximal end of the medial (ulnar) condyle/ridge. The supratrochlea foramen is absent (fig. 23).

RADIUS: Both radii remain articulated with the ulnae and they are still in contact with the humeri. In cranial view, the head of the radius is wide, the shaft abruptly narrows at the neck, and then the body gradually widens to reach its greatest width at the distal end (figs. 31, 32). Just distal to the neck is a low bicipital tuberosity. In lateral view, the shaft of the radius is slender, and its distal end curves caudally (fig. 33: ra). The entire shaft is slightly bowed craniolaterally. In cross-section, the shaft is ovoid proximally and rectangular distally, with the greatest axis shifting from craniocaudal proximally to transversely distally. The distal epiphyses of both radii are slightly offset; the right epiphysis is displaced cranially and the left distally. The outline of the proximal edge of the radius head is concave in cranial view and has upturned medial and lateral edges. The carpal atricular surface is concave and fairly featureless with confluent

scaphoid and lunate facets. The styloid process is present but small. Overall the radius is robust, more so than the ulna

ULNA: *Kryptobaatar* (MAE 00-22) includes a complete right and left ulna that in many respects resembles those of previously described multituberculates (i.e. *Nemegtbaatar*, *Chulsanbaatar*, and AMNH 118505, by Kielan-Jaworowska and Gambaryan, 1993; *Ptilodus kummae*, and 13 isolated ulnae, by Krause and Jenkins, 1983). Only the lateral, caudal, and a small portion of the medial sides of the right and left ulna are visible. The epiphysis of the right ulna is missing and the separation between the left ulna and its epiphysis is distinct. The ulna is transversally compressed, but widens transversely proximal to the trochlear notch (fig. 33). In caudal view, the shaft looks almost straight except for a slight medial curve located about one quarter of the way from its distal end. In lateral view, the proximal half of the caudal border of the ulna is convex while the distal half is slightly concave (figs. 31, 32). In contrast, the cranial border is almost straight.

In cranial view, the olecranon process has a wide and inflated end, is transversely narrow at the middle of its length (fig. 23: op), and then transversely widens to form a broad and blunt anconeal process. The medial and lateral sides of the olecranon process each bear a longitudinal fossa. The lateral fossa was likely for the insertion for the aconeus muscle while the medial one was likely for the origin for the flexor carpi ulnaris, at least based on canine anatomy (Evans, 1993). Distal to this the lateral side of the ulna is flat and then convex. The caudal side of the ulna is fairly flat and transversely broad at the olecranon process, and then it tapers in width distally so that the distal three fourth of the ulna's caudal side is formed by a ridge (fig. 33). Aspects of the medial side (i.e.

coronoid process, interosseous crest/border) were not visible on either ulna. The distal epiphysis is preserved on the left side only, and it bears a fairly blunt styloid process.

CARPAL BONES: As preserved, the articulated right manus of *Kryptobaatar* (MAE 00-22) includes eight elements in two rows: in the proximal row is the scaphoid, lunate, and pisiform and in the distal row is the unciform, magnum, trapezoid, and trapezium (fig. 4 A). There is also a large centrale that is situated between the proximal and distal carpal rows. At least one element, the right cuneiform, is missing based on a large gap in the proximal carpal row. It appears that all carpal bones have remained close to their original positions, except for the trapezium, which was displaced distomedially. Part of the craniomedial edge of the scaphoid is broken off from the rest of this bone, and remains in contact with the displaced trapezium. The articulated left manus includes the scaphoid, lunate, cuneiform, centrale, trapezoid, and unciform (figs. 4 B, 34). There is a small bone that could be the left magnum (fig. 4 B: ?) or it could be broken piece of third or fourth metatarsal. The centrale has been displaced distolaterally. In addition, the digits of the left hand appear to have been shifted medially so that they no longer contact the carpal bones.

As seen in both sides, the scaphoid is transversely wide and virtually lacks a distinct dorsal face (figs. 4, 34: sca). Instead, a gently convex proximal surface wraps onto the "dorsal" surface, consistent with a manus habitually flexed in a plantigrade posture. The proximodistal diameter of the scaphoid varies, being greatest near its lateral side, and then tapering medially. The scaphoid is also dorsopalmarly very deep and lacks a medial tubercle. The scaphoid contacts five bones: the radius, trapezium, lunate, magnum, and centrale. The radial articular surface contacts the medial 2/3 of the distal

end of the radius. Laterally, the scaphoid articulates with the lunate and internally may articulate with the magnum. Distally, the scaphoid articulates with the centrale along what appears to be a fairly flat facet. Medial to the centrale the scaphoid articulates with the trapezium along an articular surface that faces palmarly.

In dorsal view, the lunate is roughly triangular-shaped, with the apex pointed distally (figs. 4, 34: lu). Distal to its proximal articulating surface, the lunate also appears somewhat pinched, with concave medial and lateral sides. The lunate is as dorsopalmarly deep as the scaphoid, and its articular surface for the radius is convex dorsopalmarly and nearly flat transversely. Unlike the scaphoid, the lunate has a distinct dorsal surface, and on the left hand it appears that the proximal surface slightly overhangs it. In dorsal view, the proximal third of the lunate contacts the scaphoid medially, but the distal two thirds does not. It is possible that the magnum filled this void and is now displaced distally but the morphology of the magnum suggests this is not the case. Instead, it appears that there is a nonarticulating, external (i.e. dorsal) gap between the lunate and scaphoid that closes internally as the carpal bones come together. The articulation surface for the cuneiform is convex.

The cuneiform is only preserved in the left manus (figs. 4 B1, 34: cun). It is similar in size to the unciform and is roughly circular in dorsal view. Its cranial face is convex and very irregular. The cuneiform appears to be shorter proximodistally than the lunate and magnum while dorsopalmarly it is similar in depth. Its proximal surface is convex and it articulates with the styloid process of the ulna on its proximolateral side. The cuneiform also contacts distally with the uniciform and medially with the lunate.

The unciform is preserved on both sides and in dorsal view is roughly shaped like a right triangle, with the hypotenuse on the distolateral side (figs. 4, 34: un). The unciform deviates from this general shape in having a concave proximal margin, along which it contacts the cuneiform, and a slightly convex medial side, along which it contacts the lunate. The proximal side of the unciform, which contacts the cuneiform, is mostly flat except for the dorsal quarter, which is concave transversely. The unciform is as deep, dorsopalmarly, as the lunate and scaphoid, and palmarly it gets narrower. An irregular depression is situated on an otherwise fairly flat cranial face. A similar depression appears on the unciform of *Sinobaatar* (Hu and Wang 2002, fig. 1C). Distomedially, the unciform has a small contact with the magnum. The long distolateral surface of the unciform articulates primarily with metacarpal V and metacarpal V is roughly aligned directly cranial to unciform. Ji et al. (2002) interpreted this feature as synamorphy of Theria. Given the orientation of this surface, the fifth metacarpal would be directed distolaterally away from the rest of the manus.

The centrale is a large transversely elongate bone that tapers in proximodistal diameter medially (fig. 4: ce). Its articular surface for the scaphoid is flat, and distomedially, the centrale contacts the trapezoid and its extreme medial tip also touches the trapezium. Laterally the centrale has substantial contact with the magnum. The lateral third of the distal surface of the right centrale does not contact any bone. It seems likely that it used to have broad contact with the proximal lateral projection of metacarpal II. In the right hand, the second metacarpal is highly flexed in what is certainly an unnatural position, causing the centrale to no longer contact metacarpal II. Under this interpretation, the centrale would not contact metacarpal III.

The magnum is proximodistally elongate and ovoid in shape (fig. 4A: mgn). Its proximal end is pointed and reaches between the lunate and scaphoid. The magnum presumably had broad contact with metacarpal II on its medial side (see discussion above), and distally it contacted metacarpal III. The large size of the magnum suggests that metacarpal III may have been displaced distally relative to the other metacarpals; however, the magnum of *Ptilodus kummae* is highly concave, suggesting instead that the magnum dorsally overlapped the proximal surface of metacarpal III, as is seen in the multituberculate *Sinobaatar* (Hu et al. 2002, fig. 1A). The proximal surface of the magnum articulates with the lunate while its proximolateral corner articulates with the unciform.

The trapezoid is the smallest bone in the manus, and it is not as deep as the scaphoid, dorsopalmarly (fig. 4A: td). It contacts with the centrale proximally, the trapezium medially, and metacarpal II distally. Its dorsal face is quite narrow transversely and widens palmarly. Its contacts with the centrale and trapezium are flat. The trapezium articulates with and slightly overlaps dorsally the proximal end of metacarpal II. What is exposed suggests that the articular surface for metacarpal II is convex.

The trapezium is the largest bone in the manus (fig. 4 A: tm). Its cranial face is narrow transversely, but it has a large, roughly rectangular, medial face. The trapezium contacts with the scaphoid, centrale, trapezoid, presumably metacarpal I, and metacarpal II. Dorsopalmarly the trapezium is as deep as the scaphoid, but proximodistally it is much longer. The great length of the trapezium means that metacarpal I was not aligned with the other metacarpals but is in a more distal position. The same morphology is seen in *Sinobaatar* (Hu et al. 2002, fig. 1A) and various trechnotheres (Ji et al., 2002). The distal

surface of the trapezium is dorsopalmarly convex. A proximodistal strip of the lateral side articulates with metatarsal II.

The pisiform is a long bone, and its articulating end is bent medially, resembling the end of a golf club (figs. 4, 33: pi). The tubercle of the pisiform is compressed transversely, deep dorsopalmarly, and ends with a terminal swelling. This tubercle is long, equal to approximately 60% of the width of the distal epiphysis of the radius. The articulating portion is broken but appears to be convex.

METACARPALS: All the metacarpals are represented in MAE 00-22 except metacarpal I. These include right metacarpals II and IV and left metacarpals III, IV, and V. In terms of length, metacarpal III (5.7 mm) > metacarpal IV (4.9 mm) > metacarpal II (4.68 mm) > metacarpal V (3.28 mm). The bodies of metacarpals III-V are most slender in the middle of their shafts (fig. 34: m3-5). In contrast, the body of metacarpal II is most compressed transversely slightly distal to the middle of the shaft. Each metacarpal has a transversely wide head (i.e. distal end), lacks a keel on the dorsal face of the articular surfaces for the proximal phalanges, and bears a shallow, transversely wide pit proximal to the head. The metacarpals are long and slender except for metacarpal V, which is short and stout (fig. 34: m5). Like monotremes, the plantar part of the base (i.e. proximal end) of metatarsal V contacts the cuneiform. The base of metacarpal II still contacts with the trapezoid along a dorsopalmarly slightly convex surface (fig. 4 A1: td, mc) Lateral to the trapezoid facet on metacarpal II is a proximally directed tubercle that prior to post-mortem disarticulation, likely contacted the centrale on its proximal and medial sides and the magnum on its lateral side.

PHALANGES: The right hand includes one proximal and two distal phalanges, and the left hand preserves two proximal, three middle, and three distal phalanges. There are some disarticulated sesamoid bones in the vicinity of the right hand and on the left hand a sesamoid remains in place at the joints between the proximal and middle phalanges on the III and IV digits. In each case the sesamoid is in a lateral position and matrix obscures more medial portions of each joint; therefore, it is possible that each sesamoid has a more medial pair. On the left hand, the phalanges still articulate with each other and the metacarpals (fig. 34). Digits III-V have three phalanges, although a space occurs on digit V where the proximal phalanx should be.

From what is visible, the proximal phalanges closely resemble the metacarpals, except that they are much shorter. The middle phalanges taper in transverse width and dorsopalmar depth distally, but then slightly increase in both dimensions at their heads. Even so, the heads of the middle phalanges are much smaller than the heads of the proximal phalanges. The distal phalanges form long narrow, slightly recurved claws, with plantar sides that are flat transversely and curved proximodistally. On digits II-V, the distal phalanges are slightly longer than the proximal phalanges and much longer than the middle phalanges. On digit II, the distal phalanx is slightly shorter than the proximal phalanx. Each distal phalanx comes to a sharp point and at least on their lateral sides, there is a groove that shallows distally. The distal phalanges have a large flexor tubercle at the base of the palmar side, and each flexor tubercle is fairly long proximodistally. In lateral view, the joints between the distal and middle phalanges are curved, and the proximal end of the each distal phalanx dorsally overlaps the distal end of each middle phalanx.

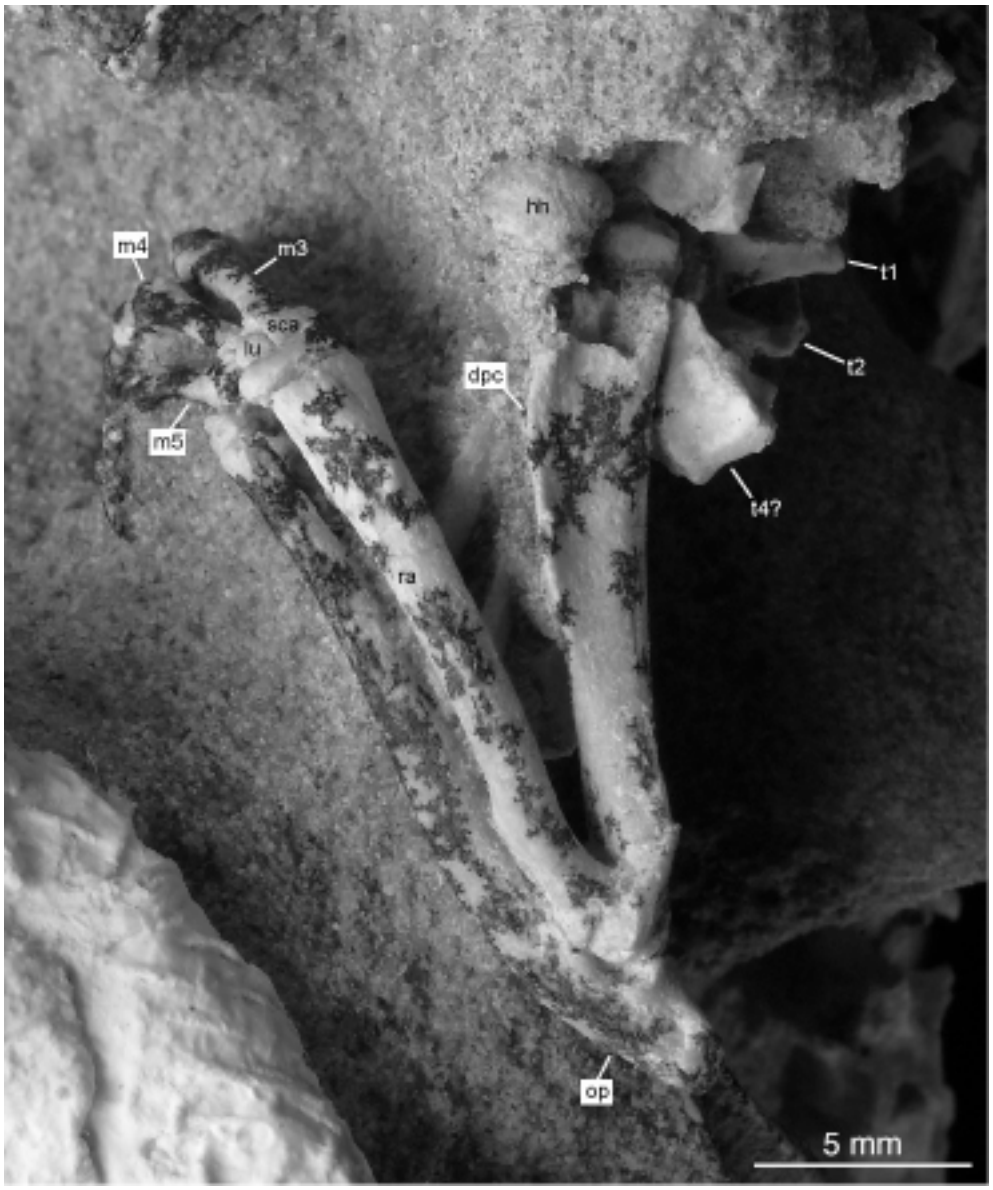

Fig. 31. Dorsal view of the left forelimb of *Kryptobaatar dashzevegi* (MAE 00-22). The orientation of the limb as preserved is not typical, and in this view, the lateral side of the humerus, craniolateral side of the radius, and lateral side of the ulna are visible.

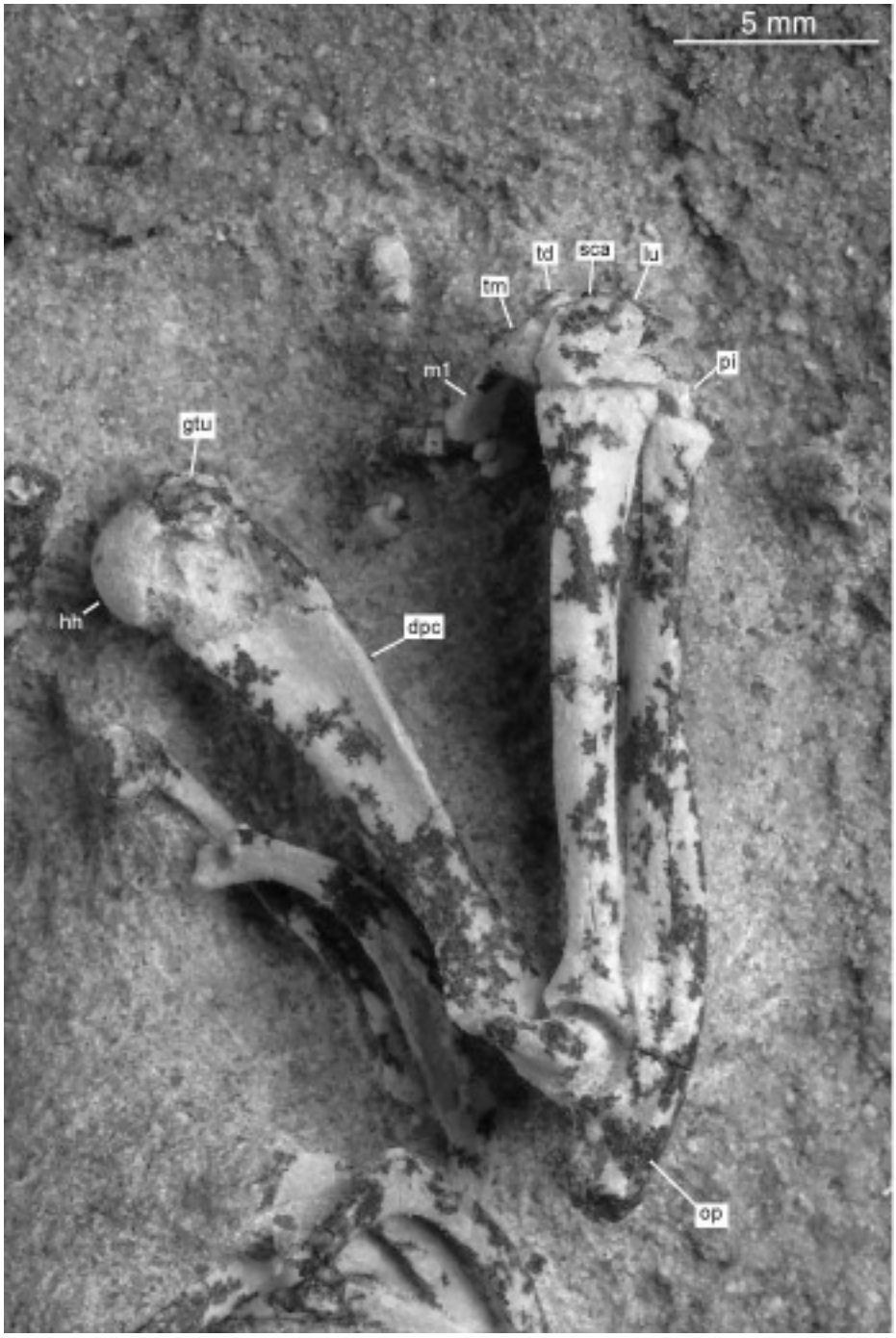

Fig. 32. Dorsal view of the right forelimb of *Kryptobaatar dashzevegi* (MAE 00-22). The orientation of the limb as preserved is not typical, and in this view, the lateral side of the humerus, craniolateral side of the radius, and lateral side of the ulna are visible. See fig. 24 for stereophotographs of this image.

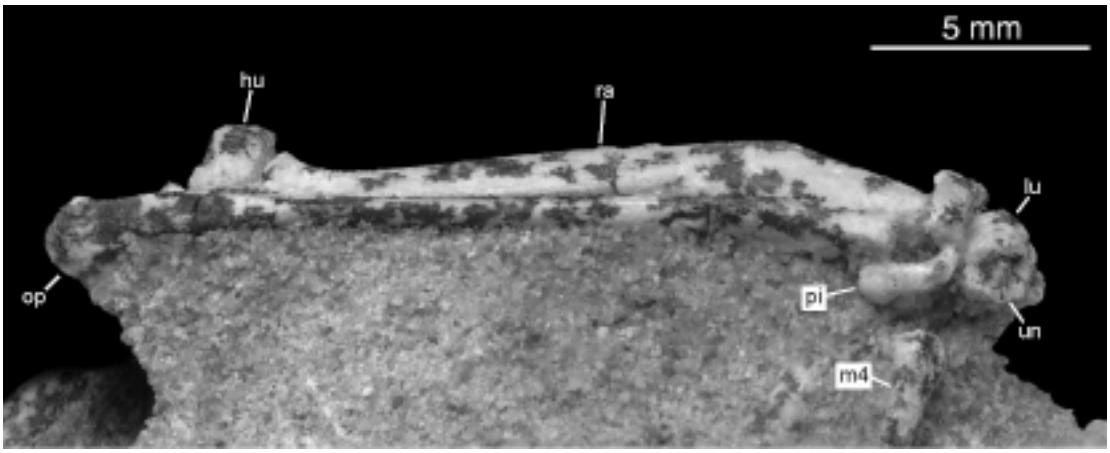

Fig. 33. Lateral view of the right forelimb of *Kryptobaatar dashzevegi* (MAE 00-22). The orientation of the limb as preserved is not typical, and in this view, the caudal side of the ulna is visible.

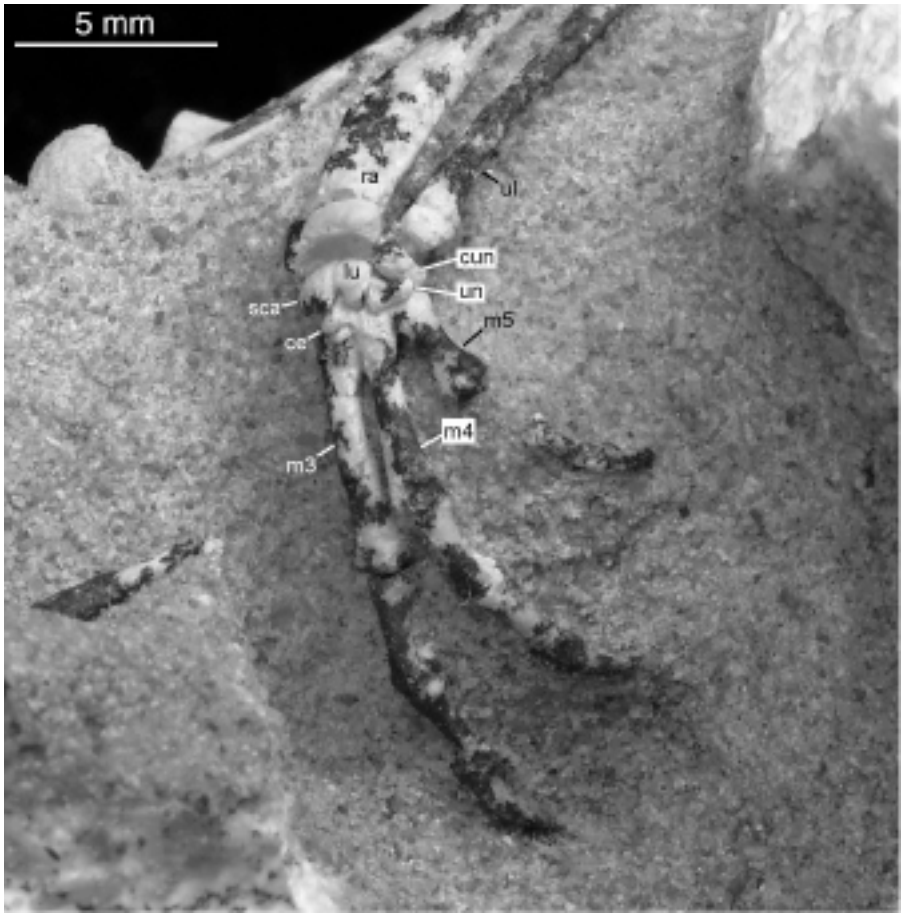

Fig. 34. Dorsal view of the left manus of *Kryptobaatar dashzevegi* (MAE 00-22).

HIND LIMB

(fig. 25-27, 29-30, 35-40)

The pelvic limbs are incomplete. The entire left hind limb is missing but the right hind limb is complete except for the cuboid, ectocuneiform, entocuneiform, mesocuneiform and seven phalanges. The pelvis is complete except for the cranial third of the right ilium and the tip of the left ilium. On both sides, the pelvis is partially exposed caudal to the acetabular fossa. The distal epiphysis of the right tibia is slightly offset cranially from the shaft while the distal epiphysis of the fibula has been slightly displaced laterally. The right astragalus and calcaneus were displaced several millimeters from their natural positions and the calcaneus was superimposed on top of the astragalus. The calcaneus and astragalus were removed from the jacketed block and fully prepared. Although the right metatarsals appear to be in their original positions, the phalanges are not.

PELVIS: The ilium is long and the wing of the illium is flared craniolaterally (fig. 30: il). In lateral view, the dorsal margin of the ilium is straight to slightly concave and the caudal dorsal iliac spine and the greater ischiatic notch are absent (fig. 27). The ventral caudal iliac spine is well developed, points ventrolaterally, and contributes to a dorsolaterally facing gluteal surface. The cranial end of the ilium is diamond-shaped in cross section, with a ventral crest that continues cranially from the ventral caudal iliac spine, a dorsal crest, a medial crest that originates at the dorsal edge of the auricular surface, and a convex lateral side. The body of ilium is rod-like. The acetabular fossa is large, semilunar in outline and has a prominent notch on its caudoventral side (fig. 30:

ace). The ridges forming the acetabular fossa are elevated only around the cranial half, causing the fossa to be open caudolaterally. Van Valen and Sloan (1966) and Krause and Jenkins (1983) describe the acetabalum as open dorsally in multituberculates. Although there are few differences in the acetabulum among the taxa they studied and the specimen of *Kryptobaatar* studied here, "opens caudally" is more appropriate because the entire pelvis of *Kryptobaatar* is oriented craniodorsally at an angle of 35°. This causes what may be considered dorsal to actually face caudally. With the head of the femur in the socket, as is seen on the right side, most of the dorsal side and all of the caudal side of the femoral head are exposed. The acetabular fossa is positioned close to the dorsal edge of the ilium and/or ischium. The iliopubic eminence (i.e. pectineal tubercle) is very large, triangular in shape, and situated cranioventral to the acetabular fossa (fig. 25: ipe). The lesser ischiatic notch is well developed, leading caudally to a prominent ischiatic tuberosity. The obturator foramen is present and the ischiatic table appears broad, although this part of the pelvis is only partially visible.

EPIPUBIC BONES: Both epipubic bones are preserved, but neither is in its original position (fig. 30: ep). What is presumably the right epipubic bone is oriented craniocaudally and lies ventral to the right acetabular fossa. The left epipubic bone has been shifted to lie transversely and occurs under the sacrum and just touches the medial side of the right ilium. The epipubic bone is transversely flattened and gradually tapers to what is presumably the cranial end.

FEMUR: Only the right femur is preserved, and it is complete. In cranial view, it has a globular head that is noticeably larger than its neck and a prominent greater tubercle that extends beyond the level of the head. The head and neck of the femur form an angle

of approximately 135°. The head of the right femur is nestled in the acetabulum, so the presence or absence of the pit for the round ligament could not be determined. The lateral side of the greater trochanter forms a sharp crest that becomes more pronounced proximally, continues to the top of the tubercle, and slightly overhangs its cranial face. At the junction of the femoral neck and the base of the greater tubercle is a small subtrochanter tubercle. In cranial view, the shaft of the femur is narrowest just distal to the femoral neck and then gradually widens distally. The shaft is slightly bowed medially (fig. 30: fe).

On the distal end, the trochlea (i.e. patellar groove) is quite broad and shallow and is offset laterally, such that the medial trochlear ridge is in line with the center of the shaft (fig. 25: trh). The medial trochlear ridge is broad, low, and rounded. In contrast, the lateral trochlear ridge is much higher and narrower. The medial epicondyle is poorly developed and slightly convex. The lateral epicondyle is more pronounced and distal to it is a small fossa. In distal view, the medial condyle points caudally and the lateral condyle is fairly low (fig. 29: mec, lco).

TIBIA: The right tibia is complete (figs. 25, 26, 29). It is broad and robust. The lateral side of the proximal end bears the tibial tuberosity, which is homologous with the lateral hook-like process of Kielan-Jaworowska and Gambaryan (1994) (fig. 25, 29: ttu). Extending distally from base of the tibial tuberosity is a short and low cnemial crest. The tibial tuberosity is short and has a distal tip that is recurved to point distally. The femur articulates with the medial and lateral condyles of the tibia, which are oriented posterocaudally to craniolaterally. The medial condyle is concave transversely while the lateral condyle is approximately flat. A small but relatively high intercondyloid eminence

separates the condyles. The intercondyloid area is transversely wider craniolaterally than caudomedially.

The shaft of the tibia is flattened, with its broad sides facing craniomedially and caudolaterally. In medial view, the entire shaft is slightly bowed craniolaterally. The distal epiphysis is thick proximodistally. The separation between the diaphysis and epiphysis is unfused, and the distal epiphysis has been slightly offset cranially from the diaphysis. The caudomedial end of the tibia extends distally slightly more than the craniolateral end. The distal face of the tibia is not visible.

FIBULA: A complete right fibula is preserved (fig. 25, 35: fi), but the morphology of the proximal end of the fibula cannot be studied because it is behind the tibia and obscured by matrix. Only the shaft and the distal end are exposed. The shaft is slender and widens distally. The distal epiphysis is not fused with the shaft. A parafibula is not visible, although it could be present and obscured by matrix, like the proximal end of the fibula.

ASTRAGALUS: The astragalus is described as being in a plantigrade position. Thus ventral equals plantar and the opposite side of the foot is dorsal. In dorsal view, the lateral and cranial borders of the astragalus form a right angle (fig. 36 A). The cranial border continues medially from its junction with the lateral border but then abruptly turns 60° cranially to contribute to an unamed process that forms the craniomedial corner of the astragalus. This process should not be confused with an astragalar neck, which is an extension of body, whereas this process is an extension of the medial astragalotibial facet. The lateral border of the astragalus is broadly convex. The dorsal surface of the astragalus is smooth, nearly flat, and slightly inclined with the lateral side higher than the

medial side. There is no separation between the medial and lateral tibial articular surfaces, and the medial articular surface narrows (craniocaudally) medially (fig. 36 A: atil, atim). The astragalar foramen is situated on the lateral half of the astragalus caudal to the tibial articular surface (fig. 36 A: ac). It opens caudodorsally. The arched buttress that encircles the astragalar canal is not bulbous like the Udan Multi, instead it is almost flat (figs. 37, 38 A: ab). The medial side of the buttress is not straight but is instead concave and faces caudally and slightly medially.

In the lateral view, there is a groove that goes dorsoplantarly around the base of the buttress and separates it from the calcaneoastragalar facet. The groove becomes more pronounced plantarly. Also visible in this view is a square, flat area that is lateral to the astragalar foramen and caudal to the tibial articular surface. This region likely contacted the fibula (fig. 37 B: afi?). The calcaneoastragalar facet is concave craniocaudally and nearly flat transversely (figs. 36 B: caa).

On the plantar side, the astragalar canal empties into a deep interarticular sulcus, which runs cranially and separates the sustentacular and calcaneoastragular facets (fig. 36 B: ia). The calcaneoastragalar facet is aligned craniocaudally, faces ventrally, has straight medial and lateral sides, has convex cranial and caudal sides, and its caudal width is slightly wider than its cranial width. The sustentacular facet is nearly circular and faces ventrolaterally (figs. 36 and 38 B: su). Just lateral to the caudolateral edge of the sustentacular facet is a small interarticular bulge that restricts the width of the interarticular sulcus (fig. 36 B: iab). The astragalonavicular facet is pulley-shaped, starts on the cranial side and then wraps around onto the medial side of the astragalus (fig 36 B; 37 A: an). Along its entire course it faces partially plantarly, but on the cranial side it

mostly faces cranially and on the medial side it mostly faces medially. It is separated by a thick ridge from the dorsal surface of the astragalus, unlike some other multituberculates where there is a groove in this position or a thin lip (see characters under **PHYLOGENETIC ANALYSIS**).

CALCANEUS: Only the right calcaneus is preserved, and it is also described following a plantigrade posture. The tuber calcis is straight and its lateral side gradually turns so that it faces laterally and slightly dorsally near its caudal end (fig. 39 A: tc). The tip of the tuber calcis is bulbous and transversely wide, with the medial side extended slightly more than the lateral side. The calcaneal lateral crest is more of a ridge and runs straight from the center of the distal end of the tuber calcis to the peroneal process (fig. 39 A: lc). The crest is pressed closely against the tuber calcis resulting in the calcaneus being fairly narrow in width. In lateral view, the tuber calcis is fairly deep, its plantar margin is fairly straight, its dorsal margin is concave, its caudal margin is convex, and the dorsal and caudal margins join to form an acute, dorsally pointing angle (fig. 40 A).

The peroneal process is short, directed craniolaterally and ventrally, and has a bulbous tip. Medial to the peroneal process is the peroneal groove, and the tip of the peroneal process extends outward to overhang part of the groove (figs. 39, 40: pg, pp). The craniomedial side of the groove is formed by the trochlear ridge (fig. 40 A: trc). The trochlear ridge continues onto the cranial end of the calcaneus and then forms a tuberosity on the plantar side of the calcaneus that is located just craniolateral to the calcaneocuboid facet. This tuberosity is herein named the *cranioplantar tuberosity*, new term (fig. 39 B: cpt). The calcaneocuboid facet is slightly concave and is almost circular in shape, except that it gradually tapers caudally (fig. 40 B: ccf). Medial to the calcaneocuboid facet and

on the ventral side of the calcaneus is a small distoplantar fossa, which is considered homologous to the ventrodistal groove of Horovitz (2000).

In the specimen of *Kryptobaatar* described by Kielan-Jaworowska and Gambaryan (1994) (i.e. ZPAL MgM-I/41), the opening of the peroneal groove is two to three times the size of the groove in the specimen described here. Based on ZPAL MgM-I/41, these authors concluded that metatarsal V fits in the medial side of this enlarged groove and articulates directly with the calcaneus. Based on the specimen described here, the calcaneus described by Kielan-Jaworowska and Gambaryan (1994) is almost certainly broken, causing the peroneal groove to appear much larger than it actually is. However, I still agree with them that the calcaneus and metatarsal V contact each other, but the region of contact in their specimen is missing. In MAE 00-22, metatarsal V presumably contacted the broadly convex cranial end of the calcaneus between the peroneal groove and the cuboid facet (fig. 40 A: cm5).

The sustentacular facet is located slightly caudomedial to, and slightly dorsal to, the calcaneocuboid facet (figs. 39, 40: su). Along the proximal margin of the sustentacular tali is a small tubercle, close to the caudomedial corner of the calcaneoastragalar facet. The sustentacular facet faces mostly medial, although it also faces slightly cranial and dorsal. It is flat, almost ovoid, and slightly tapers cranially. The calcaneoastragalar facet is separated from the sustentacular facet by a half moon shaped sulcus calcanei (fig. 40 B: sc). The calcaneoastragalar facet and the calcaneofibular facet are situated side by side onto top of a pedestal that elevates them above the surrounding parts of the calcaneus (fig. 39 A: caa, cff). The facets are separated by a faint step. Both taper cranially, are convex craniocaudally, nearly flat transversely, and are similar in size.

Just lateral to the calcaneofibular facet is a small tubercle. In dorsal view, a broad fossa occurs between the calcaneofibular facet and the peroneal groove.

NAVICULAR: The right navicular is preserved but has shifted craniodistally from its natural position. Only lateral and proximal views are available for study (fig. 35: na). The navicular is not as deep, dorsoventrally, as the navicular of *Ectypodus* sp. and *Ptilodus kummae.* The facet for the astragalus is dorsoplantarly concave and transversely nearly flat. The facet for the cuboid is located on the lateral side of the navicular, is dorsoplantarly elongate, and convex. The facets for the ectocuneiform and mesocuneiform are on the distal side of the navicular, appear to be flat, and are not separate.

OS CALCARIS OF EXTRATARSAL SPUR: The right spur is partially visible (fig. 35: spu). It has been displaced proximally and projects caudomedially from a point one quarter of the way up from the distal end of the tibia, assuming that it was originally situated near the ankle in articulation with the astragalus, as in extant monotremes (Hurum et al., 2006). The medial side of the os calcaris is formed by a high crest that decreases in height distally. The caudal end of the os calcaris is rounded over and convex. Lateral to the crest on the medial side is a longitudinal trough. The lateral side of the os calcaris also forms a crest, although unlike the medial side, the crest decreases in height proximally.

METATARSALS: Only the right metatarsals are preserved (fig. 35: mt1-5). They appear to be in their natural positions, except for metatarsal V which has been slightly shifted proximally, and metatarsals III and IV, which have been rotated so that their dorsal sides face slightly medial as well. The relative lengths of the metatarsals are: MtIII

> MtIV > MtII > MtI > MtV. In dorsal view, the articulation surface for metatarsal IV on metatarsal III faces proximolaterally as seen in *Eucosmodon* sp. but not in *Ptilodus kummae*, in which it faces directly laterally. The cuboid contact surface on the proximal end of metatarsal IV is convex craniocaudally, and its dorsomedial corner does not form a small process, as is seen in *Ptilodus kummae*. Metatarsal V has a peroneal process on the lateral side of its proximal end, but the separation between the process and the base is quite small, similar to the morphology seen in the Udan Multi.

The shaft of each metatarsal is narrowest transversely at approximately one quarter of the distance from each base, and then gradually widens distally. The shaft of metatarsal I is flat in lateral view, and that of metatarsal IV is slightly bowed dorsally. The distal articular surfaces for the middle phalanges lack median keels on the dorsal surfaces. On each metatarsal, a transversely wide and shallow fossa is situated just proximal to the articular surfaces for the phalanges. A pit occurs on the medial and lateral sides of the head of each metatarsal, presumably for collateral ligaments.

PHALANGES: Three proximal phalanges are preserved (fig. 35: ph1-3). Based on their positions relative to the metatarsals, they probably belong to digits I, II, and III. One middle phalanx is preserved near the second proximal phalanx. Three other phalanges, including one distal phalanx, occur caudal to the distal end of the fibula and likely belong to digit V. The phalanges are fairly long and taper distally, but then slightly widen at their distal ends. They are not bowed and have distal articular surfaces that narrow proximodorsally. As with the metatarsals, the distal ends bear central pits on the medial and lateral sides.

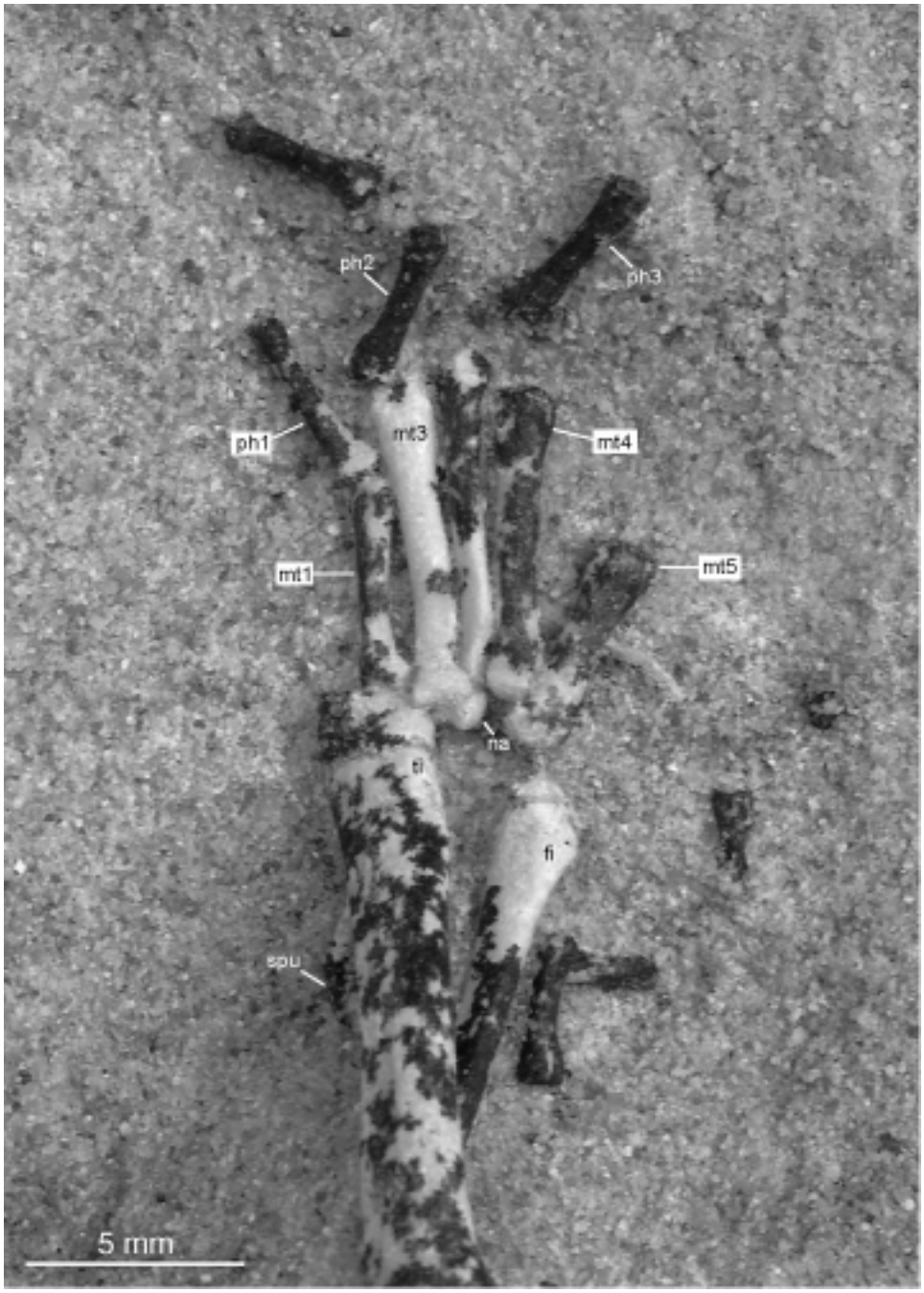

Fig. 35. Dorsal view of the right pes of *Kryptobaatar dashzevegi* (MAE 00-22). See fig. 26 for stereophotographs of this image.

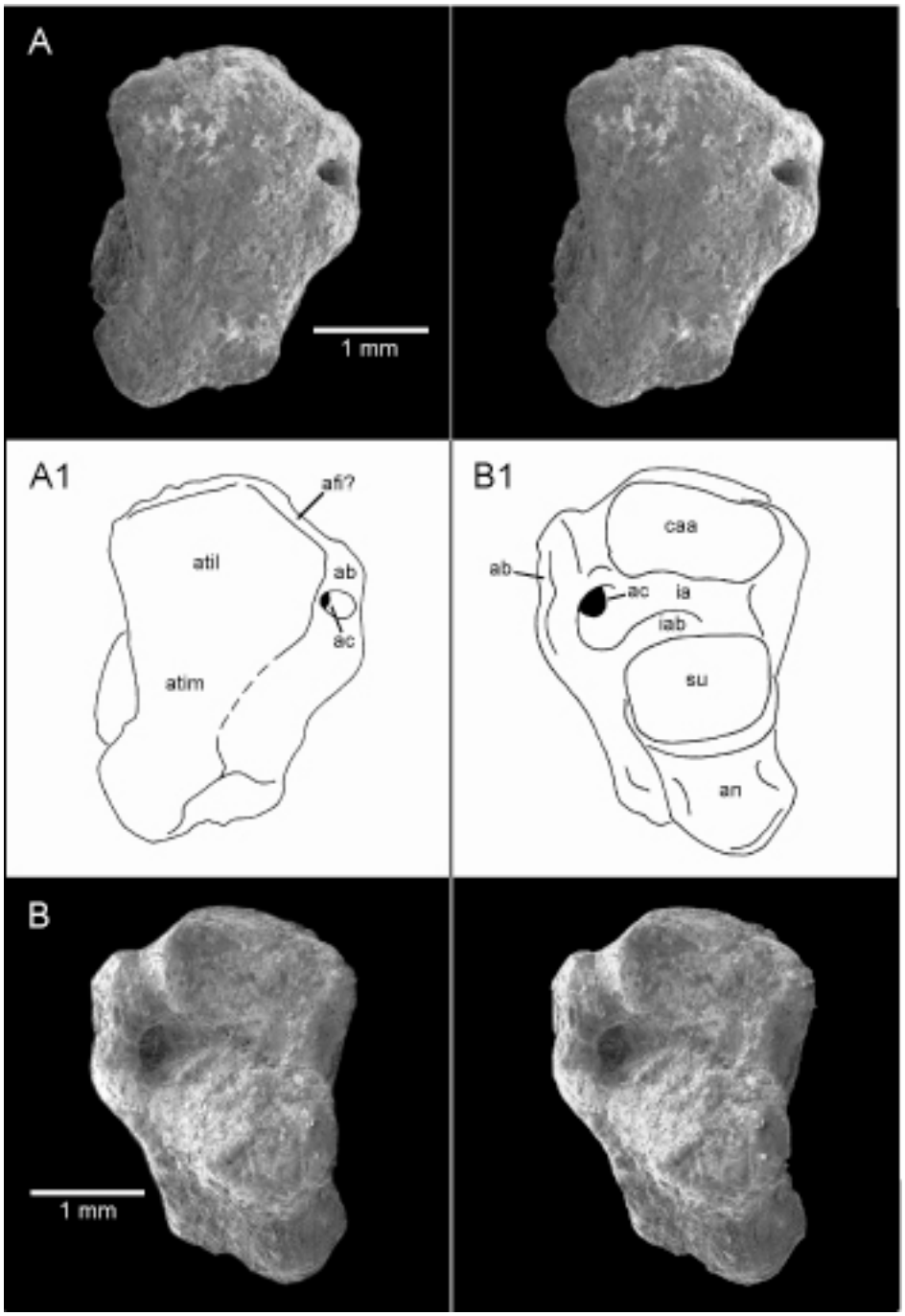

Fig. 36. Astragalus of *Kryptobaatar dashzevegi* (MAE 00-22): **(A)** SEM stereophotographs of the dorsal side, **(A1)** interpretive drawing of the same, **(B)** SEM stereophotographs of plantar side, **(B1)** interpretive drawing of the same. In all images, lateral is towards the top of the page.

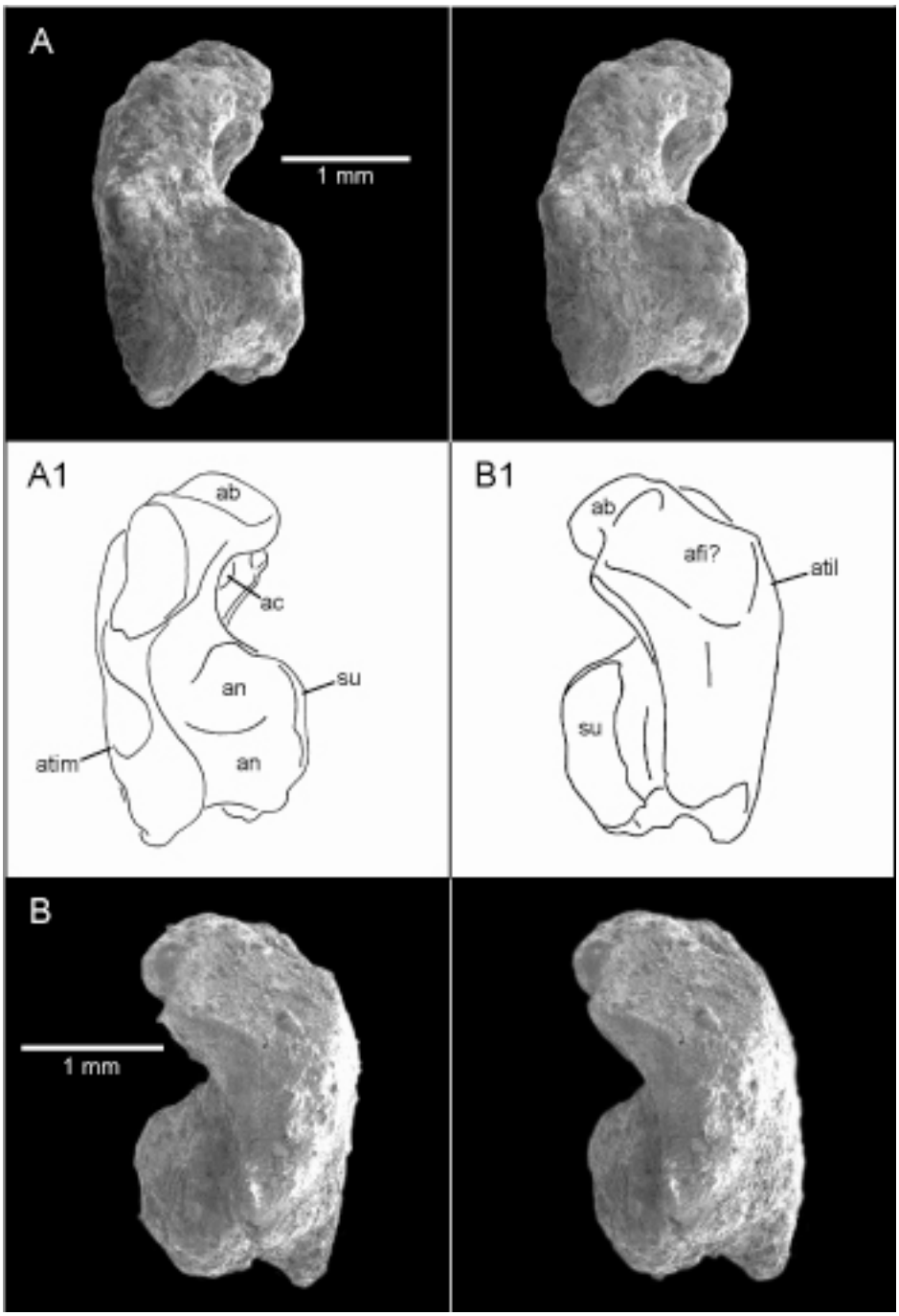

Fig. 37. Astragalus of *Kryptobaatar dashzevegi* (MAE 00-22): **(A)** SEM stereophotographs of medial side, **(A1)** interpretive drawing of the same, **(B)** SEM stereophotographs of lateral side, **(B1)** interpretive drawing of the same. In **A** and **A1** dorsal is to the left while in **B** and **B1** it is towards the right.

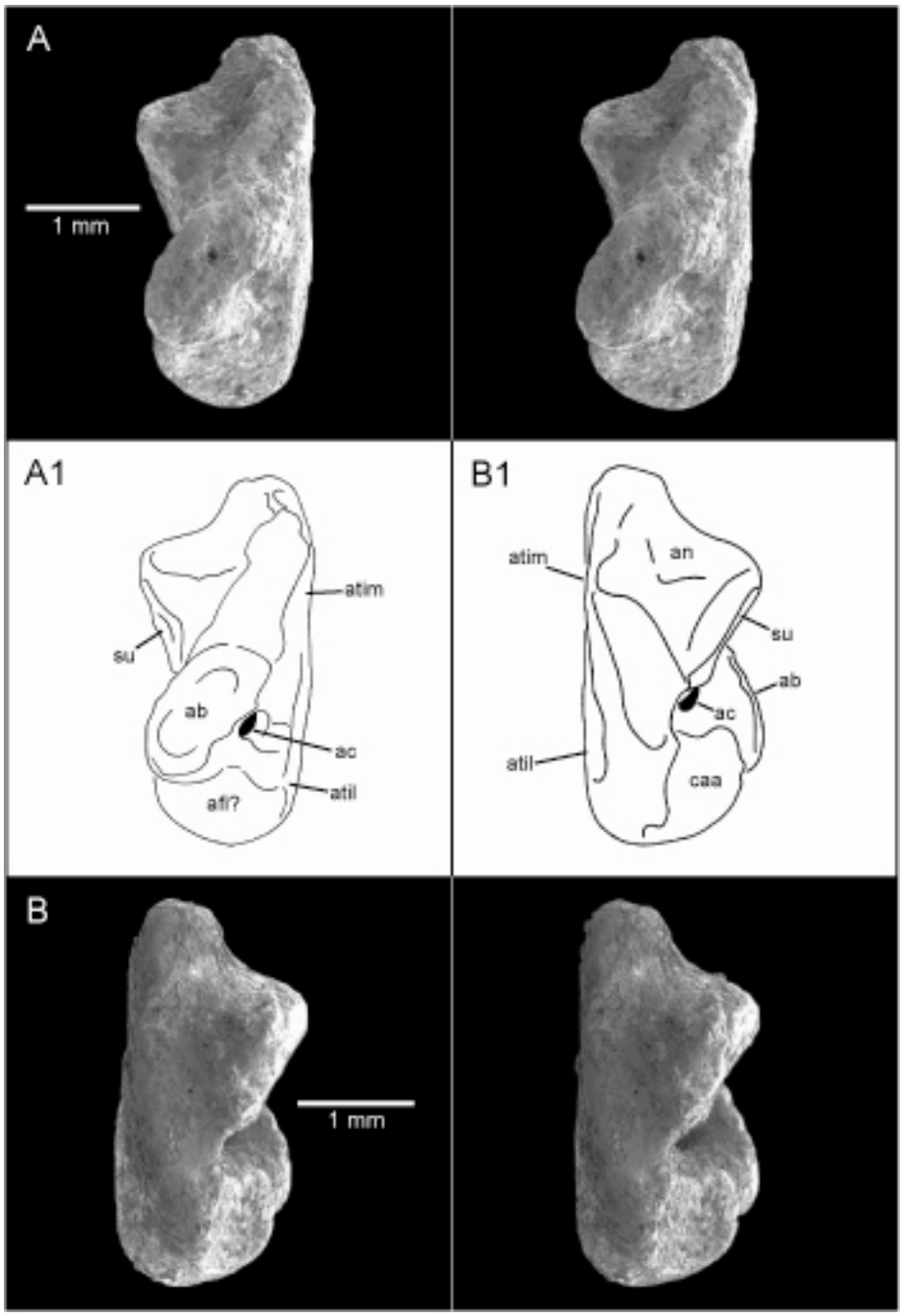

Fig. 38. Astragalus of *Kryptobaatar dashzevegi* (MAE 00-22): **(A)** SEM stereophotographs of caudal side, **(A1)** interpretive drawing of the same, **(B)** SEM stereophotographs of cranial/distal side, **(B1)** interpretive drawing of the same. In all images, medial is towards the top of the page.

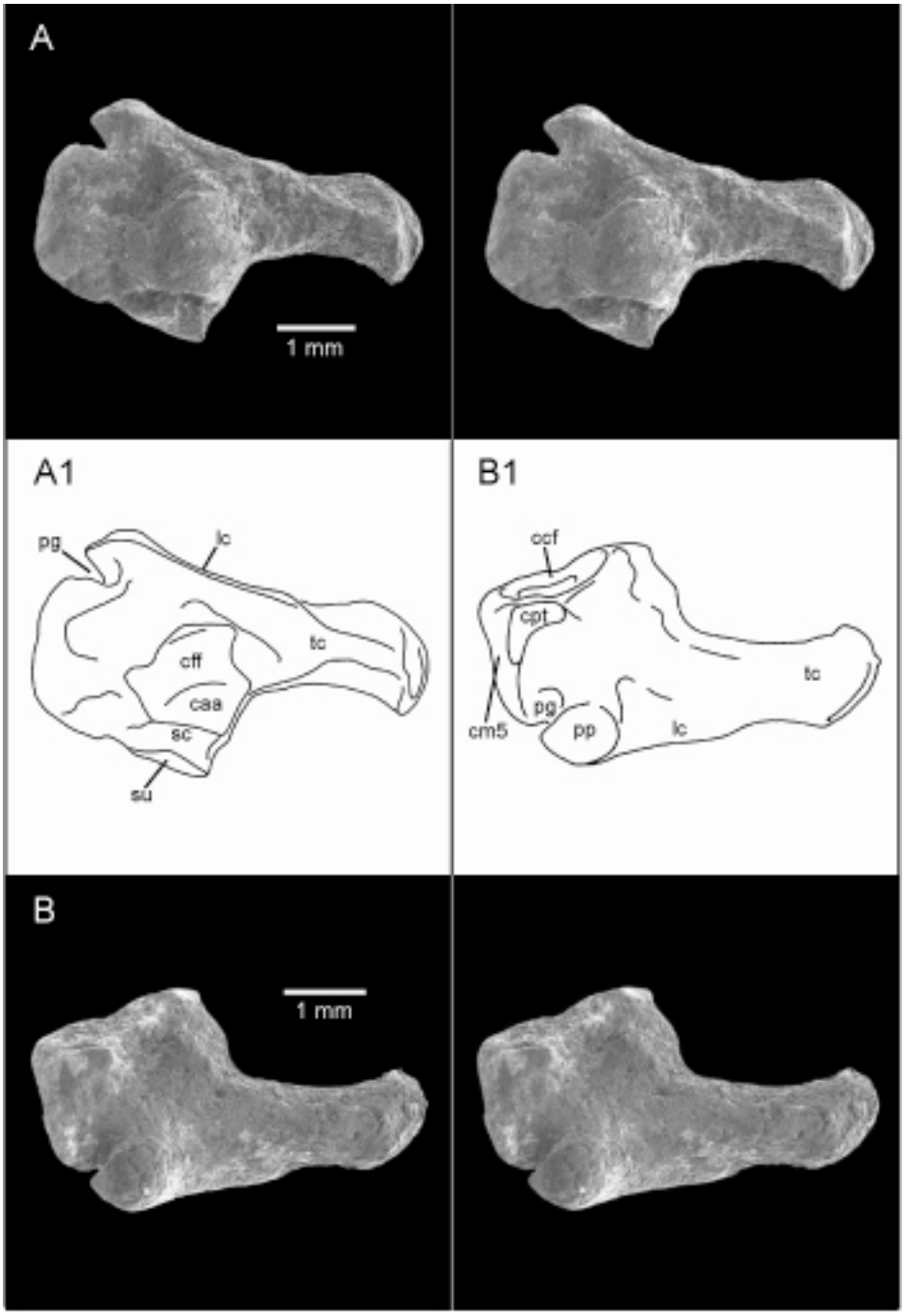

Fig. 39. Calcaneus of *Kryptobaatar dashzevegi* (MAE 00-22): **(A)** SEM stereophotographs of the dorsal side, **(A1)** interpretive drawing of the same, **(B)** SEM stereophotographs of plantar side, **(B1)** interpretive drawing of the same. In **A** and **A1** lateral is towards the top of the page while in **B** and **B1** it is towards the bottom of the page.

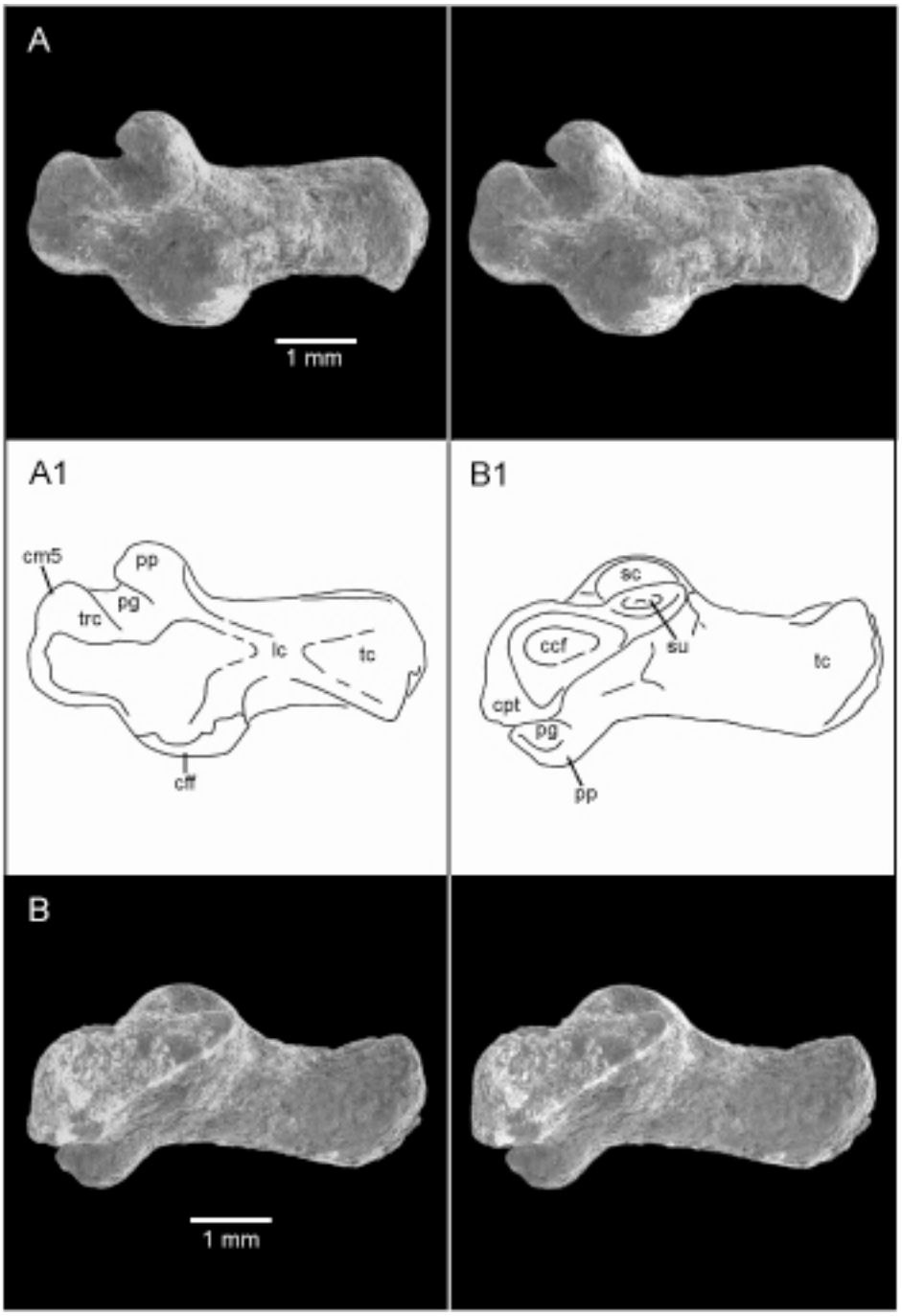

Fig. 40. Calcaneus of *Kryptobaatar dashzevegi* (MAE 00-22): **(A)** SEM stereophotographs of the lateral side, **(A1)** interpretive drawing of the same, **(B)** SEM stereophotographs of medial side, **(B1)** interpretive drawing of the same. In **A** and **A1** plantar is towards the top of the page while in **B** and **B1** it is towards the bottom of the page.

IDENTITY OF REFERRED SPECIMEN

MAE 00-22 can clearly be referred to the genus *Kryptobaatar* based on the morphology of its skull and size. The condylobasal length of the skull is approximately 29 mm, which falls within the range of variation described for *Kryptobaatar dashzevegi* (Wible and Rougier, 2001). Like *Kryptobaatar* and the much larger *Djadochtatherium* and *Catopsbaatar*, the sides of the snout of MAE 00-22 are straight in dorsal view, giving the snout a trapezoidal shape (Kielan-Jaworowska and Hurum, 1997) (fig. 22). Other features that this specimen shares with previously described specimens of *Kryptobaatar* are: large and blade-like P_4, small facial exposure of the lacrimal, absence of palatal fenestra, four upper premolars, and the alveolus for I^3 totally within the premaxilla. The morphology of M^1 is particularly useful for identifying this genus, but unfortunately the upper and lowers are still in occlusion, obscuring many details. The M^1 of *Kryptobaatar* abruptly widens at the beginning of the lingual row, and this can be observed in MAE 00-22. In addition, like this genus, the inner crest does have at least one weakly developed cusp.

Currently there are two recognized species of *Kryptobaatar*: *K. dashzevegi* and *K. mandahuensis*. The morphology of MAE 00-22 clearly shows that it can be referred to *K. dashzevegi*, the only species presently known from Ukhaa Tolgod (Wible and Rougier, 2001). Like this species and unlike *K. mandahuensis* (Smith et al., 2001), the suture between the palate and maxilla is straight transversely, the dentary is low under the diastema behind I_1, the coronoid process has a long (rostrocaudally) base, M_1 has four not five labial cusps, and P_4 is only slightly longer than M_1. In addition, the zygomatic arch in this specimen originates at the distal root of P^4; however, this feature may not be

diagnostic of *K. dashzevegi* as another specimen of this species (i.e. PSS-MAE 113; Wible and Rougier, 2001: fig. 15) has the zygomatic arch originating at the cranial root, similar to what has been described for *K. mandahuensis* (Smith et al., 2001).

Udan Multi, Rougier et al., *in prep*

REFERRED SPECIMEN: PSS-MAE 141, an associated partial skeleton with skull, including three cervical, ten thoracic, three lumbar, third and fourth caudal, and nine other caudal vertebrae; distal end of left scapula; humeral head and greater tubercle of right humerus as well as a fairly complete distal end, left humerus, the proximal third of the humerus including the head and tubercles; head and the distal end of the left radius and the distal end of the right radius; shaft of the left ulna and the distal end, distal end of the right ulna; left trapezoid?/magnum? metacarpal I and II; partial pelvis; left and right femur; left and right tibia; left and right fibula; left and right tarsal bones except right navicular, mesocuneiform; left and right metatarsals; phalanges.

LOCALITY AND HORIZON: Udan Sayr locality, Nemegt Basin, Umnugovi Province, Mongolia (see GEOLOGICAL SETTINGS for more details).

VERTEBRAE

CERVICAL VERTEBRAE: The cervical vertebral series of the Udan Multi is incomplete. Three cervical vertebrae are preserved in articulation, but the identities of these three vertebrae remain uncertain. None of them have the characteristic morphology

of the atlas or axis vertebra; therefore, the three vertebrae are the 3, 4, 5th or 4, 5, 6th or 5, 6, 7th. Based on similarities to the transverse processes of the cervicals in an unidentified multituberculate from Mongolia (Kielan-Jaworowska, 1989: ZPAL MgM-I/165), the vertebrae are tentatively identified as the 3, 4 and 5th cervicals. Only the ventral part of the right side of the body and the right transverse process of the third cervical is preserved. The fourth and fifth cervicals are represented by their vertebral bodies and the pre- and postzygopophyses, pedicles, and transverses processes of the right side.

The bodies of the cervicals are dorsoventrally compressed, transversally wide, and their lengths are twice their depths. The caudal face of the fifth body is visible and is distinctly concave. This concave area is either for an enlarged notochord depression or intervertebral disk. The third and fourth cervicals have weak median ventral crests, while there is no crest on the fifth cervical. There is a pair of foramina, one on each side of the sagittal plane, on the dorsal sides of the bodies of the fourth and the fifth cervical vertebrae. These pairs of foramina were for basivertebral veins. Each foramen is slightly longer craniocaudally than wide. The dorsal sides of the bodies of the fourth and fifth cervicals are more cranial than the ventral sides; therefore, in longitudinal section the bodies are procumbent.

The pre- and postzygopophyses of the fourth and fifth cervicals are quite large and lie in about same the dorsal plane. The three vertebrae have fairly short transverse processes that extend caudolaterally. Each process is perforated by a large transverse foramen. The transverse processes of all three vertebrae differ from each other. The 3rd cervical has the longest transverse process, and it extends well caudal to the body to terminate nearly at the level of the midpoint of the body of the 4th. The transverse process

of the fifth extends distinctly more ventrally than those of the third and fourth. As a consequence, the distance between the base of the transverse process and the level of the pre- and postzygopophyses is much greater than on the other two vertebrae. The presence or absence of a cranially projecting ventral tubercle of the transverse process could not be determined.

THORACIC VERTEBRAE: Ten thoracic vertebrae are preserved, but only two were found in articulation. The relative positions of the thoracics and the lumbar vertebrae are inferred based on comparison to those in *Ptilodus kummae* (Krause and Jenkins, 1983) and a skeleton of *Kryptobaatar dashzevegi* (MAE 00-22). The vertebrae are given letters with "A" signifying the most cranial of the preserved thoracics. Of particular use is the fact that the craniocaudal length of the vertebral bodies increases with each successive thoracic vertebra.

Thoracics (T) A, B, and C: These vertebrae have the shortest and smallest bodies of all the preserved thoracics, supporting their positions as cranial thoracics. The spinous processes and zygopophyses are broken on these vertebrae, although portions of the neural arch are preserved with TA and TC. In these two vertebrae, it can be seen that the transverse process originates from the neural pedicle and has an ovoid, ventrolaterally facing costal fovea. Only on TB and TC are the laterally-facing cranial costal fovea and caudal costal fovea well developed. TC differs from TA and TB in having a caudally protruding ventral margin of the caudal surface of the body and in having a longitudinal fossa on each lateral side of side of the body. Visible only in TB, the dorsal surface of the body bears two, large, craniocaudally elongate foramina for basivertebral veins, one on each side of the sagittal plane.

Thoracics D, E, and F: Of these three, TE and F are still articulated with each other. The tips of the spinous processes on all three are broken and the left transverse processes have been sheared off of TE and TF. Even so, it is apparent that the spinous processes are quite short and strongly inclined caudally. The cranial costal fovea face mostly laterally, but the caudal costal fovea face caudolaterally. The postzygopophyses face medioventrally and slightly caudally. The transverse processes are almost absent, originate from the pedicles, and have large, convex costal fovea that face laterally and slightly ventrally. TD has a median ventral crest on the vertebral body while TE and TF do not.

Thoracic G: The spinous process and zygopophyses were not preserved with this vertebra. The ventral crest and accessory process are absent. Cranial and caudal costal fovea are well developed and are situated at the same level. The transverse process originates from the junction of the arch and the body and its ventrolaterally-facing costal fovea contacts the cranial costal fovea. The cranial face of the body is rectangular and less concave than the ovoid caudal face. The lateral sides of the body are highly concave between the cranial and caudal costal fovea.

Thoracic H: This vertebra is almost completely preserved. The spinous process is inclined caudally, has a craniocaudally broad base, and is quite short. The distance between the prezygopophyses is much smaller than the distance between the postzygopophyses. The pre- and postzygapophyses face dorsolaterally and ventromedially respectively. The accessory process (i.e. anapophysis) is a small bump and is situated on the caudal margin of the pedicle. Cranial and caudal costal fovea are located at the same level. The transverse process is virtually absent and originates from

the upper part of the vertebral body, just ventral to the base of the pedicle. The costal fovea of the transverse processes face laterally and slightly ventrally. The ventral crest is present but low.

Thoracic I: This vertebra is entirely preserved. The prezygopophyses are flat and face dorsolaterally and slightly cranially. In contrast, the postzygapophyses face directly ventrally. The spinous process is inclined caudally, does not taper dorsally, and has a squared off tip. The accessory process is well developed and originates from the middle of the vertebral side at the level where the pedicle and body join. It extends caudolaterally to the level of the caudal edge of the body. The lateral side of the accessory process bears a fossa that extends cranioventrally to contact the cranial costal fovea. The cranial costal fovea is much larger than the caudal costal fovea, and the latter is at a level well ventral to the former. In dorsal view, the pre-and postzygapophyses are separated from each other by the same transverse distance. Between the postzygapophyses and running up the caudal face of the spine is a deep triangular fossa. The cranial and caudal faces of the body are ovoid and concave, although the latter is more concave than the former. The ventral crest is well developed.

Thoracic J: In this vertebra the spine is short and angled slightly cranially, unlike that of TI. Thus the anticlinal vertebra is not preserved. Based on comparisons to a skeleton of *Kryptobaatar* (MAE 00-22), TJ is the vertebra immediately caudal to the anticlinal vertebra. In dorsal view, a sharp ridge leads from the dorsal surface of each postzygapophysis up to the tip of the spine, defining a deep triangular fossa in between. The notch between the prezygopophyses is wider than the notch between the postzygopophyses. The prezygopophyses are concave transversally and face dorsally

while the postzygopophyses face ventrolaterally. Unlike the other thoracics, the mammillary processes are present.

In lateral view, the ventral part of the body of TJ is shifted caudal relative to the dorsal surface; therefore, the whole body has a rhomboidal shape. The cranial costal fovea is large, faces craniolaterally, and tapers caudally. A small crest begins at the caudal termination of the cranial costal fovea and continues to the ventral edge of the accessory process. As in TH, there is a fossa on the lateral side of the accessory process, but it is quite shallow. The dorsal margin of this fossa is defined by a prominent crest that continues from the dorsal edge of the accessory process (i.e. anapophysis) but then nearly disappears before reaching the dorsal edge of the cranial costal fovea. The accessory processes are long and well developed with thickened tips. The caudal costal fovea is absent. The cranial articular surface of the body is pentagonal in shape and concave, whereas the caudal surface of the body is cordiform in shape and is more concave than the cranial face. The ventral crest of the body is very well developed, and on either side of the crest, the surface of the vertebral body is concave, particularly just caudal to the cranial costal fovea. In cranial view, the pedicles are vertical, but in caudal view the pedicles are oriented dorsomedially, causing the vertebral foramen (i.e. neural canal) to narrow dorsally.

LUMBAR VERTEBRAE: Only three lumbar vertebrae (L) were found, none in articulation. As with the thoracics, they are labeled A, B, and C, with A being the most cranial. LA is probably the cranial-most lumbar, LC is probably the last, and LB is obviously somewhere between the other two. The transverse processes of all three vertebrae are broken, and only the base of the process is preserved on the left side of LA

and LB and on the right side of LC. Based on what is preserved, LA has a ventrolaterally directed transverse process while LB and LC have laterally directed processes. The transverse process is craniocaudally wider in LA than in the other two. The cranial edge of this process in LC rises to join the prezygopophysis, thus forming a deep fossa between the two processes. This morphology is also seen in last lumbar vertebra of *Kryptobaatar* (MAE 00-22).

In all three lumbars, the body in lateral view is rhomboidal with the cranial face in each facing slightly ventrally. In addition, the dorsoventral height of the cranial face is less than the height of the caudal face. The transverse width of the body is much greater in LB and LC as compared to LA. The ventral crest is very high and sharp in LA, more so than in any of the preserved thoracics; and although well developed, the crest is much lower on LB and LC.

The spinous process is broken in LB but mostly preserved in LA and LC. It is inclined cranially in LA while it is nearly vertical in LC. The transversely concave prezygopophyses of LA are only partially preserved, and it seems that mammillary processes were present on this vertebra, but it cannot be determined if they occurred on the other two lumbars. The prezygophyses are not preserved in LB, and the partially preserved prezygophyses of LC are larger and flatter than those of LA. The postzygopophyses of LA faces ventrally and slightly laterally. The postzygophyses face lateroventrally in LB and laterally but more ventrally in LC. On LA, there are crests that run from the spinous process caudoventrally to the dorsal surfaces of the postzygopophyses, as is seen in thoracics I and J.

SACRAL VERTEBRAE: The caudal part of the third and a nearly complete fourth sacral vertebra are preserved. The third and fourth sacrals are completely fused, but in dorsal view, a faint, matrix-filled line can be seen that traces the line of fusion between the prezygopophyses of the fourth and the postzygopophyses of the third. On the lateral side of the sacrum, right at the junction between the vertebrae, is a posteriorly-facing cleft. Another larger, more open depression occurs caudal to this notch on the body of the fourth sacral. The transverse processes of both sacrals are broken but they appear to have been directed straight laterally. The caudal face of the body of the fourth sacral is pentagonal. The ventral surface of the sacrum is quite narrow and on either side there is a longitudinal valley between the ventral surface and the transverse processes. On the ventral surface of the fourth sacral, there are two low, parallel ridges instead of a single median ventral crest. The spinous processes are vertical. The postzygopophyses of the fourth sacrum are large and face ventrally and slightly laterally.

CAUDAL VERTEBRAE: Nine caudal (Cd) vertebrae, inferred to be caudals 1 through 9, are preserved. Two of these are the first and second caudal, as evidenced by the right prezygapophyses of the first caudal still being attached to the postzygapophysis of the fourth sacral and the second caudal being in articulation with the first. Two other caudals that articulate with each other are probably the Cd3 and Cd4. Five more articulated caudals were found caudal to the pelvis, and based on their position and morphology as compared to *Ptilodus kummae* (Krause and Jenkins, 1983), they are likely Cd5 through Cd9.

The left transverse process of Cd1 is broken, but the process on the right side is partially preserved. It is craniocaudally wide, does not quite reach the caudal margin of

the body, and is directed ventrolaterally. The prezygopophyses of the first caudal face mediodorsally and are larger than the postzygopophyses, which face ventrolaterally. The tips of the zygopophyses are squared-off. Although the end of the spinous process is not preserved, it is clear that the entire process is slightly inclined caudally. The cranial surface of Cd1 is circular, and its ventral margin is positioned more caudal than its dorsal margin, giving the vertebral body a rhomboidal shape in lateral view. The ventral surface of the body is narrow and its lateral margins are delineated by faint ridges. Only the prezygopophyses of the second caudal are preserved and they are still in articulation with the first caudal. The prezygopophyses face mediodorsally and are slightly larger than those of the Cd1.

The third caudal is partially preserved. It still retains the spinous process, right transverse process, and postzygapophyses, but the prezygopophyses and the cranial part of the body were not preserved. The fourth caudal is nearly complete but the ends of the spinous and transverse processes were not preserved. The ventral surface of each caudal forms a longitudinal valley with a ridge bounding each lateral side. In ventral view, both Cd3 and Cd4 have a distinct pit just cranial to the base of the transverse process, and it is so well developed in Cd3, that it causes the cranial margin of the transverse process to be elevated as compared to the caudal margin. The transverse processes of both caudals point slightly ventrally and cranially, in addition to their primarily lateral direction. On Cd3 the cranial margin of the transverse process is directed straight laterally while the caudal margin curves craniolaterally, thus this process comes to a point. On the ventral side of the transverse process of Cd3 there is a low ridge that originates from the distal end of the transverse process and then continues for a short distance medially. The

postzygopophyses of the both Cd3 and Cd4 face ventrolaterally, and the spinous processes seem to be quite short.

The last five articulated vertebrae gradually increase in length caudally. The dorsal sides of all five caudals are exposed while only the ventral sides of Cd6 and Cd7 are exposed; the ventral sides of the other three are covered by matrix. Cd5 has a circular cranial face that is concave in the center with a surrounding, thickened rim. The vertebral canal of this vertebra is a narrow transverse slit. It appears that it has a small spinous process, although the exact size is uncertain because it is broken. The transverse processes and zygopophyses of Cd5 were not preserved. Cd6 is longer than Cd5 and has a large, fairly flat, and dorsomedially facing prezygapophysis. Cd7 through Cd9 have laterally projecting, short transverse processes, which originate from nearly the entire lengths of their vertebral bodies. The lateral extension of each transverse process is fairly consistent along the length of each vertebra but does slightly diminish near the caudal margin. The dorsal surfaces of these vertebrae are badly broken; therefore, the morphology of each is not described. On all caudals the transverse processes originate from the centrum and are located well below the vertebral canal.

FORELIMB

(fig. 41-44)

SCAPULA**:** The distal (ventral, the part where the glenoid fossa is located) part of the left scapula is preserved, including the coracoid process, glenoid fossa, acromion process, and ventral part of the scapular spine (fig. 41). In lateral view, the acromion

process is flat, triangular-shaped, and overhangs the caudal face of the scapular spine (fig. 41.3: acp). The scapular spine is quite high and forms the cranial border for the infraspinous fossa. The infraspinous fossa is craniocaudally narrow but quite concave, and unfortunately, more proximal (dorsal) portions of this fossa were not preserved. The supraspinous fossa is not developed except for a small shallow fossa just cranial to the base of the scapular spine (fig. 41.1 and 3: isfo).

The glenoid fossa is oval-shaped and not deep, with the long axis oriented transversely (fig. 41.4: gl). The edges of the fossa are elevated and sharp, and the fossa extends onto the caudal side of the coracoid process. The coracoid process extends ventromedially from the glenoid fossa by a long and stout neck. The tip of the coracoid process is transversally wide, forming a "L" shaped process in caudal view, with bottom of the "L" pointing medially (fig. 41.2: cop). The medial point of the "L" is likely homologous with the posterior (caudal) process of the coracoid, but now points medially as the glenoid fossa rotated from facing laterally primitively (e.g. monotremes), to facing ventrally and caudally, as is seen in multituberculates. On the cranial side of the tip of the coracoid process is a distinct fossa that is bordered laterally by a low tubercle. The lateral edge of this tubercle is formed by a sharp ridge, which continues proximally and then gradually shifts medially to become the cranial edge of the scapular blade. The caudal edge of the scapula shifts laterally as it approaches its ventral end, providing space for a fossa situated next to the glenoid and medial to the caudal edge. This fossa is possibly for the origin of the triceps muscle. The medial side of the ventral end of the scapula bears two, short, parallel, proximodistal ridges. Dorsal to this the medial side becomes flatter and wider.

HUMERUS: The humeral head and greater tubercle of the right humerus are preserved, as well as a fairly complete distal end. For the left humerus, the proximal half or third of the humerus is preserved, including the head and tubercles; its distal end is preserved as well. In proximal view, the head of humerus is ovoid with the main axis oriented craniomedially (fig. 42.2). The head faces proximocaudally. The greater tubercle has a convex and smooth dorsal face that just barely extends above the level of the head (fig. 42.1: gt). As compared to the greater tubercle, the lesser tubercle is lower than the head, sticks out medially from it, and faces caudally. Between the greater and lesser tubercles and on the cranial side of the proximal end is a broad and deep intertubercular groove (fig. 42.2: itg). This groove extends for a considerable distance down the humeral shaft. Just distal to the head, the intertubercular groove widens and excavates into the lesser tubercle, then it becomes shallower and very narrow, and finally its distal end is wide and of moderate depth. The humeral shaft is transversely compressed and triangular in cross-section, with a caudal crest that forms the caudal side (Fig. 42.1: cc). The caudomedial and caudolateral sides of the proximal third of the humerus each bear a longitudinal fossa that deepens proximally. The lateral fossa is the deeper of the two and is bordered laterally by a prominent deltopectoral crest.

On the preserved portion of the distal end of the humerus, the ectepicondyle is prominent and bears a continuation of the radial articular surface (fig. 43: ecc). This extension is concave and is adjacent to a large, globular radial condyle (fig. 43: rco). The lateral edge of the radial articular surface is marked by a sharp ridge. A deep groove separates the radial and ulnar condyles. The ulnar condyle is not globular but instead forms more of a high crest (fig. 43: uco). As seen in distal view, the articular surfaces of

the distal humerus are oriented craniomedial to caudolateral (fig. 43 A3). The entepicondyles of neither humeri were preserved. On the caudal surface is a wide and deep olecranon fossa with a supratrochlear foramen (fig. 43 A: olf). It is possible that the foramen was formed by breakage; however, the fact that the size and position are the same on both sides suggests that the foramen is natural. The ectepicondyle is continuous with a broad, well developed, and proximally extended supinator crest (fig. 43 A: suc).

RADIUS: The head and the distal end of the left radius and the distal end of the right radius are preserved. The outline of the head in proximal view is ovoid and the capitular facet is concave and circular in shape (fig. 44 B1: crf). The caudolateral side of the head has a narrow, curved, and flat to slightly convex facet for the ectepicondyle of the humerus, similar to the morphology in *Ptilodus kummae* (Krause and Jenkins, 1983) (fig. 44 B1: ecf). This facet parallels the rim of the capitular facet and faces proximally. The articular circumference (Evans, 1993) for articulation with the ulna is on the caudomedial side of the head, and is proximodistally deepest on the medial side (fig. 44 B2: arc). The articular circumference extends for 100° around the capitular head. In proximal view, the cranial margin of the head of the radius comes to a blunt point towards the medial side. There is almost no neck for a prominent bicipital scar of the tubercle.

On the distal end, the styloid process is present but small (fig. 44 A: stp). The articular surface for the carpals is shallow, transversely elongate, and concave craniocaudally and transversely. The articulation surfaces for the lunate and magnum are confluent. In medial view, the distal end of the radius appears to be bent caudally. The junction of the distal epiphysis and the diaphysis is visible, and the epiphysis is not thick

proximodistally. The distal end of the radius is much wider than the shaft. Just proximal to this widening, the cranial side of the shaft has a low median ridge. The ridge courses proximolaterally and quickly disappears.

ULNA: The shaft of the left ulna is broken just proximal to the radial notch, but the distal end is preserved. Only the distal end of the right ulna is preserved. The medial projection of the coronoid process is partially preserved, and the lateral projection of the coronoid process is poorly developed. The radial notch is not well preserved, but it appears to have been a fairly flat surface. The shaft of the ulna in cross-section is T-shaped just distal to the radial notch, with the top of the "T" being the cranial face. Distal to this, the shaft is C-shaped in cross-section, being bowed medially. The caudal margin of the shaft is convex, and at the level of the radial notch, a flattened caudal side appears and gradually widens proximally. The interosseous crest of the ulna is high and sharp.

The distal end of the ulnar shaft is compressed transversely with the medial side being concave. The facet for the ulnar notch of the radius is convex cranially. Mediodistal to this facet is mediodistally-facing and proximodistally elongate, flat facet for the cuneiform.

METACARPALS AND CARPAL BONES: Left metacarpal I and II are preserved. What is likely the left trapezoid was also recovered in the vicinity of metacarpal II, although this carpal bone could also be a magnum. For this description the carpal bone is described as the trapezoid based on a fairly close, but not perfect, fit with the proximal end of metacarpal II. The trapezoid is crescent shaped in medial and lateral view. Its distal surface is strongly concave dorsopalmarly and its proximal surface is strongly convex. The posterocaudal corner of the trapezoid has small facet, probably for

contacting the trapezium. It seems that the trapezoid and magnum had no direct contact with each other, as in *Kryptobaatar*, because there is no obvious facet on the lateral side of the trapezoid. In *Kryptobaatar*, the trapezoid contacts with the centrale proximally, but there is no obvious facet on the trapezoid of the Udan Multi.

The articular facet for the trapezoid on metacarpal II is similar to that of *Kryptobaatar*. The lateral half of the facet is elevated as compared to the rest of the surface, is oriented dorsopalmarly, and faces proximomedially. The elevated part of the facet is on the medial side of a distinct dorsolateral process projecting from the dorsolateral corner of the proximal end. Based on comparisons to the articulated right manus of *Kryptobaatar dashzevegi* (MAE 00-22) this process articulated with the magnum laterally and the centrale proximally. The facet for the trapezium on metacarpal I is flat and crescent-shaped in proximal view, with the points of the crescent pointing medially and laterally. The trapezium facet also faces slightly proximodorsally.

The distal head of metacarpal II is transversally wider than its proximal base, while the exact opposite is true of metacarpal I. The head of each metacarpal is convex proximodistally and slightly convex transversely. On the dorsal surfaces of both metacarpals, there is distinct pit just proximal to the articular surface for the proximal phalanx. The shafts of metacarpals I and II are compressed dorsopalmarly.

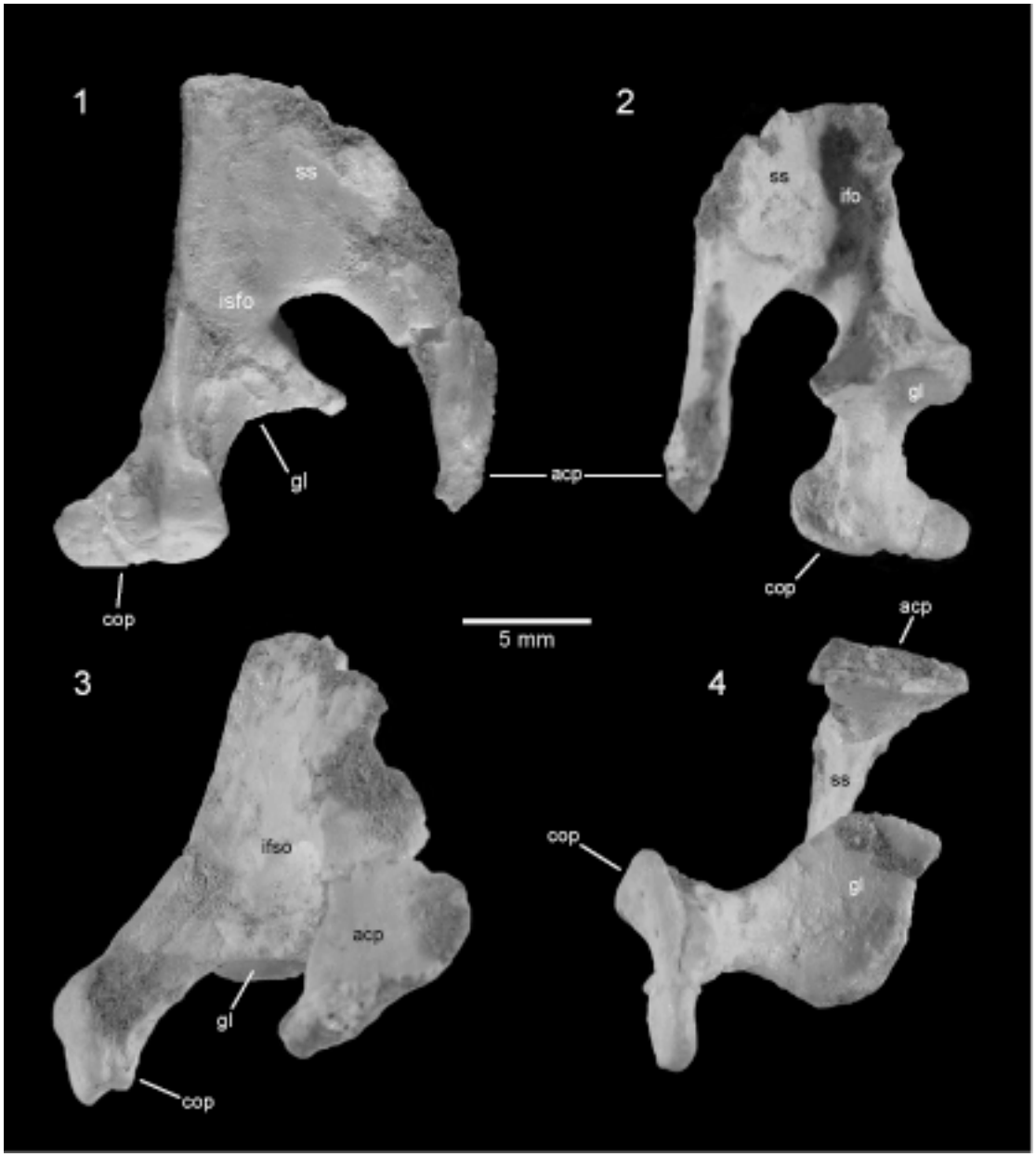

Fig. 41. Left scapulocoracoid of the Udan Multi (PSS-MAE 141): **(1)** cranial view, **(2)** caudal view, **(3)** lateral view, and **(4)** ventral view. In **1,** lateral is towards the right, in **2** it is towards the left, in **3** it is directed towards the viewer, and in **4** it is towards the top of the image.

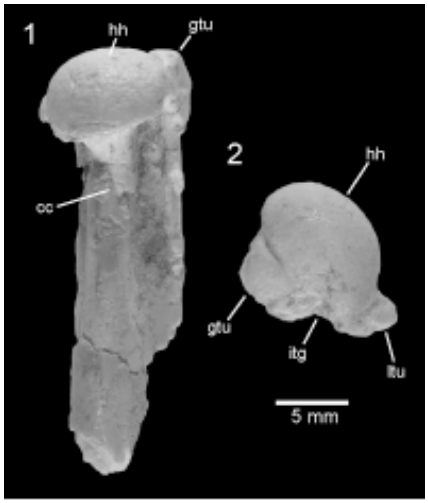

Fig. 42. Proximal end of left humerus of the Udan Multi (PSS-MAE 141): **(A1)** caudal view, **(A2)** proximal view. In **A2** caudal is towards the top of the image.

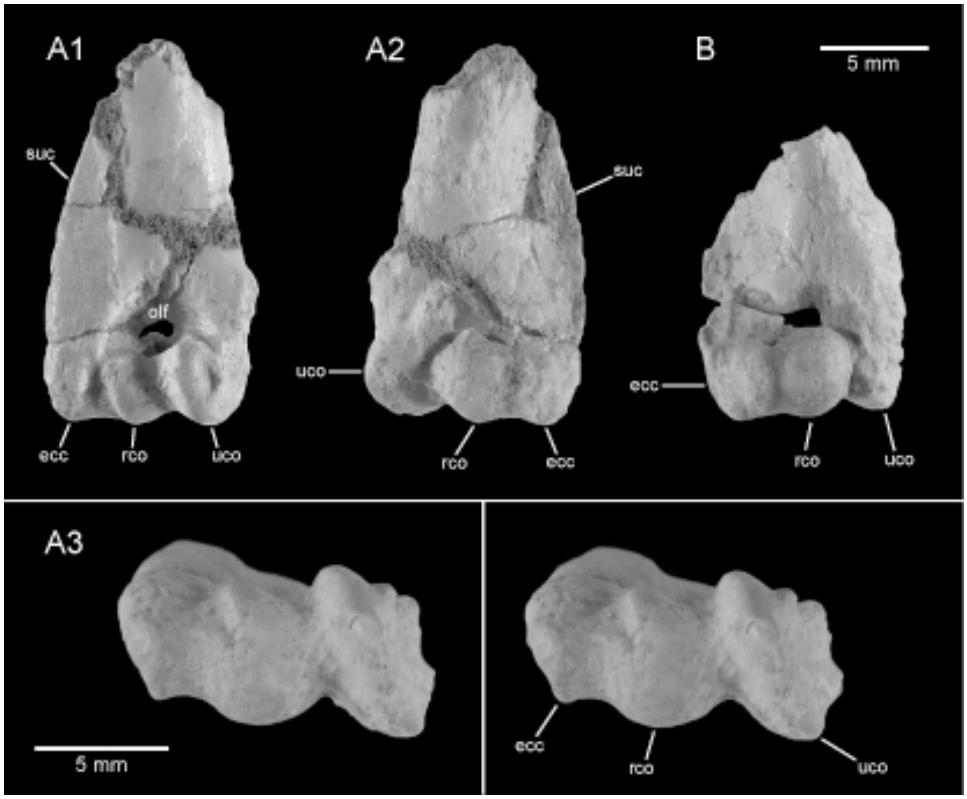

Fig. 43. Distal ends of the left **(A1, A2, A3)** and the right **(B)** humeri of the Udan Multi (PSS-MAE 141): **(A1)** caudal view, **(A2, B)** cranial views, **(A3)** distal view. In **A1**, **A3**, and **B** lateral is towards the left while in **A2** it is towards the right.

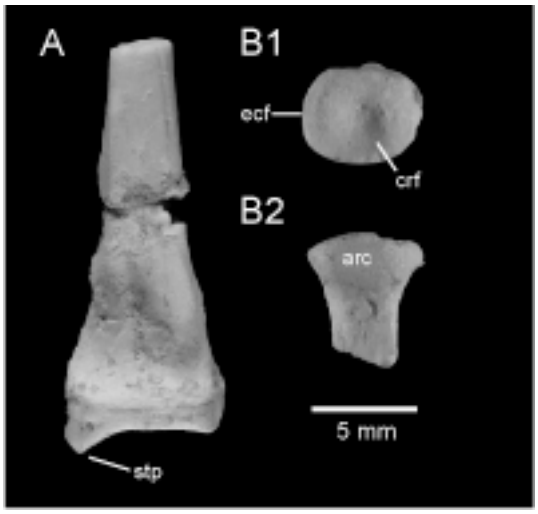

Fig. 44. Distal **(A)** and proximal **(B1, B2)** ends of left radius of the Udan Multi (PSS-MAE 141): **(A)** cranial view, **(B1)** proximal view, and **(B2)** caudal view. In **A** medial is towards the left while in **B1** and **B2** it is towards the right.

HIND LIMB

(fig. 45-55)

The pelvis is partially preserved; the right and left ilium are broken a short distance cranial to the acetabular fossae and the cranial portions were not preserved (fig. 45). Both femora are still in articulation with the pelvis, obscuring details of the acetabular fossa. The right side of the pelvis is less complete than the left, and in addition to other damage, it lacks the cranial and caudal ends of the ischium.

ILIUM: Only caudal ends of the ilia are preserved. Cross sections seen at breaks through the right and left ilium are ovoid, being deeper dorsoventrally than transversely (fig. 45:il). Cranioventral to the acetabulum is a low iliopubic eminence (i.e. pectineal

tubercle). The elements of the pelvis are fused so it is unclear how much of the acetabulum is formed by the ilium.

ISCHIUM: The left ischium is better preserved than the right one. The obturator foramen is small and ovoid, with the long axis oriented craniocaudally (fig. 45: of). This foramen is only two to two and a half times the size of the acetabulum. The ischium is narrow dorsal to the obturator foramen, but then caudal to the foramen, it expands forming a fan-shaped ischiatic table (fig. 45: itb). The ischial tuber is very small, and the caudal edge of the ischium is gently convex. The right and left ischia join at a craniocaudally long symphysis at a 50 °angle. Although the ventral side of the pelvis is not completely prepared, there was a fairly low ventral keel along the pelvic symphysis. The presence or absence of a postobturator notch could not be determined.

PUBIS: The left pubis is better preserved than the right. The iliopubic eminence is prominent, comes to a point, and occurs at the junction of the medial, subhorizontal portion of the pubis with the lateral and short vertical part (fig. 45: ipe). The right and left pubes are completely fused to each other at a sagittal and ventrally inflected pubic tubercle (fig. 45: pt).

FEMUR: Both femora are preserved (figs. 45, 46). The left femur is complete although it occurs in two pieces (table 6). The right femur is missing a central part of the shaft but is otherwise nearly complete. Its lateral epicondyle is broken as well as parts of the caudal surface of the distal end. The proximal ends of both femora are complete, although many details are obscured by matrix.

The neck of the femur forms approximately a 120° angle with the shaft. The head itself is slightly larger than the neck. The greater trochanter is vertical, robust, and

extends well above the level of the head (fig. 46 A: gtr). Its proximal end forms a large triangular surface that is flat craniocaudally. In cranial view this surface can be seen to overhang more distal parts of the greater trochanter, and in caudal view, it leads distally into a prominent ridge. Medial to this ridge is a fairly open and longitudinal posttrochanteric fossa on the caudal side of the femur. Medial to the posttrochanteric fossa is a fairly small lesser trochanter that juts postermedially. Unlike *Nemegtbaatar* (Kielan-Jaworowska and Gambaryan, 1994: fig. 16b), the subtrochanteric tubercle is absent.

The line separating the distal epiphysis and the diaphysis is very clear. The lateral condyle of the femur is transversally very wide with its long axis oriented proximomedially to distolaterally. In contrast, the medial condyle is much narrower transversely, aligned proximodistally, and extends caudally much more than the lateral condyle. The femoral trochlea (Evans, 1993) is saddle shaped but shallow with low medial and lateral trochlear crests (fig. 46 A: trh). In comparison to the lateral trochlear crest, the medial trochlea crest is transversally wider, much larger, and higher. The intercondyloid fossa is weakly developed, shallow, and transversally elongate. The lateral condyle has a large extensor fossa for the origin of the muscle extensor digitorum longus. Proximal to this is a well developed lateral epicondyle (fig. 46 A2: lpc). The medial epicondyle is nearly absent (fig. 46 A2: mpc).

Table 6. Measurements of the femur of the Udan Multi (PSS-MAE 142).

Dimension Measured	**(mm)**
Body	
Length	56.99
Width of the distal end	15.71
Head	
Diameter of the head (dorsoventral)	7.84
Distance between head and greater trochanter	4.31
Neck	
Dorsoventral thickness	6.37
Greater Trochanter	
Height	8.08
Distance extends beyond head	2.34

TIBIA: Elements of both the right and left tibia are preserved (fig. 46B, C, D) (table 7). The left tibia is nearly complete and articulated with fibula, which is slightly offset proximally from its natural position (fig. 46 D). The proximal and distal ends of the right tibia are preserved, although a part of the shaft is not (fig. 46 B, C). The tibia is flattened, with one side facing craniomedially and the other caudolaterally. Each of these faces is fairly wide, reflecting a very shout tibial shaft. The craniolateral and posterocaudal edges of the two main sides form sharp ridges. Consistent with the flattening of the bone, the long axis of the distal end is oriented from craniolateral to posterocaudal. Relative to the proximal third of the shaft, the distal third is bent medially. In lateral view, the tibia is convex cranially and the distal end abruptly curves to point distocaudally (fig. 46 D2).

The medial and lateral condyle facets of the proximal end are aligned craniolaterally to caudomedially and face proximocaudally. The intercondyloid eminence is low and obscure. The medial condyle facet is ovoid, concave, and at a lower level than the lateral condyle facet (fig. 46 D1: mco). The lateral condyle facet is large, ovoid, and

flat to slightly convex. Along the caudal margin of the proximal face is a wide popliteal notch between the two condyle facets. Caudolateral to the lateral condyle facet is a flat, caudolaterally-facing facet for the fibula (fig. 46 B: fac). The tibial tuberosity projects laterally from the proximal end, and is considered the homolog to the hook-like lateral process of Kielan-Jaworowska and Gambaryan (1994). This process is situated cranial to the lateral condyle and forms a stout process that is hooked distally. Between the lateral condyle facet and the tibial tuberosity is a broad concave region. The entire caudal margin of the proximal face overhangs the shaft, forming a deep fossa, which is best developed at the popliteal notch (fig. 46 B).

The separation between the distal epiphysis and diaphysis is clear on the craniomedial side of the tibia but is fused on the caudolateral side. The medial malleolus is low and is part of a continuous articular surface for the astragalus (fig. 46 C: mm). The articular surface is divided into two parts; a larger concave surface that faces laterally and a much smaller convex surface on the medial malleolus that faces medially. A faint ridge separates the two facets. The caudal side of the medial malleous is vertical and distinct from the rest of the caudal part of the distal end of the tibia.

FIBULA: Both the right and left fibulae are preserved (table 7). The left fibula is virtually complete and remains in partial articulation with the tibia (fig. 46 D). The right fibula is broken into two pieces with the shaft not preserved; an isolated proximal end and a distal end that is still in articulation with the astragalus.

The proximal head of the fibula is elongated craniolaterally to caudomedially. The craniolateral end of the head forms a large, flat process that comes to a blunt point and greatly overhangs the body of the fibula (fig. 46 D3: hlp). This process is homologous to

the hook-like process of the fibula as described by Kielan-Jaworowska and Gambaryan (1994). Supporting this process and continuing distally down the shaft of the fibula is a prominent ridge, with deep, pocketed fossae on either side that undercut the head. The medial fossa is bounded medially by a large flat surface that faces craniomedially and articulates with the tibia. The caudal side of the head has a rectangular, gently convex, posteroproximally facing surface that based on comparison to a specimen of *Kryptobaatar* (Kielan-Jaworowska and Gambaryan, 1994: ZPAL MgM-I/41) articulated with the parafibula (fig. 46 D3: pff), which was not preserved.

The caudal side of the fibular shaft, just distal to the head, is concave and bounded on each side by well defined ridges that then distally merge at the middle of the shaft. Distal to this, the caudal side is a rounded ridge. On the caudolateral side of the fibular body is a ridge that bears a low flange at about the midpoint of the shaft. In caudal view, the shaft narrows distally until widening at the distal end, while in caudolateral view, the fibula gradually widens distally until rapidly widening at the distal end.

The distal end of the fibula has a large, convex surface on its medial side, presumably for contact with the tibia and for the astragalus. The lateral side of the distal end has a cranial and a caudal tubercle with a concave area in between. In distal view, a ridge runs between the tubercles and medial to that is an elongate fossa. On the right side, the distal end of the caudal tubercle contacts the calcaneus and the distal end of the broad convex surface on the medial side touches the astragalus. It is unclear if either of these contacts is natural. On the right side there is a sesamoid between the astragalus and the distal fibula, and on the left fibula three sesamoids occur in the area between the tibia and fibula (fig. 46 D: ses). The sesamoids appear to have been slightly displaced and add to

the complexity of upper ankle joint. Based on their shape and size none of these sesamoids is the os calcaris.

PES: The Udan Multi is probably plantigrade (Bolortsetseg and Zhang, in prep.) while standing. Therefore, the astragalar facet on the calcaneus and the tibial facets on the astragalus would be facing dorsally and the tuber calcis of the calcaneus would be projecting caudally. On the metacarpals and phalanges, cranial is generally equivalent to distal and caudal to proximal. The tarsus is divided into proximal and distal tarsals. The former includes the calcaneus and astragalus, while the latter includes the navicular, cuboid, ectocuneiform, mesocuneiform, and entocuneiform.

All of the bones are preserved on the left pes. The left calcaneus and astragalus were articulated with each other and with the rest of the tarsus but they were separated for more detailed study. The distal tarsal bones on the left side are complete and articulate with each other, but all are partially separated from the metatarsals. Metatarsals I-IV appear to be in their original positions relative to each other. Metatarsal V was dislocated from the other metatarsals and was removed from the matrix during preparation. The left proximal phalanges for digits II through IV are preserved distal to their corresponding metatarsals, but they are not in their natural positions. Plantar to the tarsal bones are three dislocated sesamoid bones, one near the proximal end of the fourth phalanx, one near the distal end of this phalanx, and one near the middle of the third phalanx.

Unlike the left pes, the right pes is missing the navicular, mesocuneiform, and all but part of one phalanx. As with the left side, metatarsal V was dislocated and separated from rest of the metatarsal bones. Metatarsals I-IV articulate with each other, but the entire foot is partially dislocated from the ankle. Although the astragalus is shifted

distolaterally from its original position, the cuboid, calcaneus, and entocuneiform are locked together in their natural positions. The distal end of the fibula is still in contact with the right tarsals, but it is shifted proximally from its natural position.

CALCANEUS: Both right and left calcanei of PSS-MAE 142 are preserved (table 7). The tuber calcis of the calcaneus is dorsoplantarly deep and is transversely wide cranially and transversely narrow caudally (fig. 47: tc). Its caudal end is swollen. In caudal view, the entire tuber calcis is not oriented straight dorsopalmarly but instead is oriented mediodorsally to lateroplantarly (fig. 48 A: tc). In dorsal view, the caudal end of the tuber calcis is bent medially (fig. 47 A). In lateral view, the dorsal border of the tuber calcis is slightly convex while the plantar border is concave. The plantar border is longer than its dorsal border (fig. 49 A). On the dorsal border, just cranial to the terminus of the tuber calcis, is a small tubercle that is separated from the swelling at the end of the tuber by a faint, transverse groove.

The great width of the calcaneus is primarily attributed to the development of the lateral crest of the calcaneus. In other described multituberculates (e.g. *Ptilodus*, *Eucosmodon*) the lateral crest is apprised to the body of the calcaneus, but in the Udan Multi, it is laterally expansive, similar to the morphology seen *Oligokyphus* (Szalay, 1993). The lateral crest begins near the middle of the tuber calcis, runs craniolaterally for a short distance, then forms an obtuse angle where it turns to run more cranially, and finally leads to the peroneal process (fig. 47 A: lc). The peroneal process is short, directed craniolaterally as well as plantar. The end of the process is bulbous (figs 47-49: pp).

The calcaneoastragalar facet is elongated craniomedially to caudolaterally, transversely narrow, and strongly convex dorsally. It is located craniomedial to the tuber

calcis and far medial of the peroneal process (fig. 47: caa). The fibular facet appears to be absent, but on the right side the fibula does contact what is considered to be part of the calcaneoastragalar facet. It is possible that these two facets are present but lack the ridge that separates these facets as seen in other multituberculates. The right astragalus was preserved in contact with calcaneus. Later these two bones were separated, but before they were, the astragalus completely covered the central articular surface on the dorsal side of the calcaneus. Craniomedial to the calcaneoastragalar facet is a small, flat, dorsally-facing facet that acts as a stop to dorsiflexion of the pes (fig. 47 A: cas). The stop extends cranially to the margin of the cuboid facet.

There are three fossae on the dorsal side of the calcaneus, these occur caudal to, lateral to, and craniolateral to the calcaneoastragalar facet and are bounded laterally by the lateral crest. Separating these fossae are two ridges. The first of these, herein termed the *cranial ridge*, new term (cr: fig. 47 A), runs craniomedially across the calcaneal body starting from the lateral border caudal to the peroneal tubercle and ending just cranial to the caudolateral corner of calcaneoastragalar facet. The second ridge, herein termed the *caudal ridge of the calcaneus,* new term, runs caudally from caudolateral corner of the calcaneoastragalar facet to the craniolateral side of the tuber calcis (fig. 47 A: cur). Medial to the caudal ridge of the calcaneus and caudal to the calcaneoastragalar facet is a shallow small fossa herein termed the *caudal fossa* of the calcaneus, new term, (fig. 47 A: cf). Lateral to the caudal ridge of the calcaneus and caudal to the cranial ridge of the calcaneus is a large, triangular fossa with its apex pointing craniolaterally herein named the *lateral fossa*, new term, (fig. 47 A: lf). Cranial to the cranial ridge and lateral and craniolateral to the calcaneoastragalar facet is a large and well-developed irregular fossa.

This fossa is probably for the attachment of the brevis muscle; therefore, it is herein named the *peroneus brevis fossa*, new term, (fig. 47 A: bf).

The craniolateral side of the peroneus brevis fossa is delimited by a high trochlear ridge that borders much of the peroneal groove (fig. 47 A: trc). In dorsal view, the peroneal groove, for the tendon of the peroneus longus muscle, is a C-shaped notch bordered caudolaterally by the peroneal process and craniomedially by the trochlear ridge. The peroneal groove leads into a deep concavity on the plantar side of the calcaneus that is bordered dorsolaterally by the peroneal groove, caudally by the peroneal process, craniolaterally by a smooth facet for metatarsal V (see description of metatarsal V), and medially by the cranioplantar tuberosity (named in preceding description of *Kryptobaatar*) (figs. 47, 48 B). On the plantar side of the calcaneus, there is a small fossa of unknown function between the sustentacular tali and the cranioplantar tuberosity.

The sustentacular facet is on the craniomedial side of the sustentacular tali and it faces craniomedially and slightly dorsally (fig. 49 B: su). Along the proximal margin of the sustentacular tali is a broad rounded tubercle. The facet is craniocaudally elongate and approximately half the length of the calcaneoastragalar facet. The cranial margins of the calcaneoastragalar and sustentacular facets are approximately at the same level. The sulcus calcanei, separating the two facets, is ovoid and deep (fig. 47 B: sc). The caudal margin of the sulcus calcanei is longer than its cranial margin; therefore, the facets are closer cranially than they are caudally. The craniomedial side of the sustentacular facet contacts the calcaneocuboid facet.

The calcaneocuboid facet is rhomboidal in shape with the long axis oriented craniocaudally, and it faces medially and slightly plantarly (figs. 47, 48 B: ccf). The facet

is nearly flat dorsopalmarly but slightly concave craniocaudally. In dorsal view, the lateral edge of the calcaneocuboid facet forms a thick raised rim that borders the peroneus brevis fossa. The cranial and cranioventral margins of the calcaneocuboid facet are swollen, with the cranioventral margin being continuous with the cranioplantar tuberosity. The cranial end of the trochlear ridge forms a medially protruding tubercle. Between this tubercle and the swollen margin of the cuboid facet is a narrow concave facet for metatarsal V (fig. 48 B: cm 5).

ASTRAGALUS: In dorsal view, the astragalus is roughly rectangular in shape with the long axis oriented transversely to the axis of the foot except for its medial side, which is notched (fig. 50 A). The transverse diameter of the left astragalus is 7.17 mm, which was measured from the notch on its medial side to the greatest lateral extent of its lateral side. Its craniocaudal diameter is 5.54 mm, which was measured from along a craniocaudal line that intersects the caudal edge at a point just medial to the arched buttress (table 7).

The facets on the astragalus for the lateral and the medial tibial condyles and the fibula are confluent and are not separated by ridges or grooves. The articular surfaces on the dorsal side of the astragalus are comprised of a highly convex and bulbous area on the lateral third and a gently, transversely concave area on the medial two thirds (fig. 50 A: atil, atim). The entire articular surface narrows (craniocaudally) medially and appears to extend to the craniomedial corner of the proximal surface. The astragalofibular facet is most likely on the lateral side of the bulbous area, thus placing it at an angle relative to the lateral facet of the tibia on the astragalus (fig. 51 B: afi). It looks to be large, which might explain why the fibula seems to have little to no contact with the calcaneus. A

large astragalar foramen is situated just caudal to the bulbous tibial articular surface, and it is surrounded by a bulbous buttress (figs. 50, 52: ab, ac). The caudomedial corner of the astraglaus forms a distinct process. Although labeled as the astragalar medial plantar tuberosity by Szalay (1994: fig. 5.9), this may not be correct because the structure actually occurs on the dorsal, not plantar, side of the astragalus.

In lateral view, a wide groove runs plantarly from the astragalar foramen and separates the caudal side of the buttress from the convex facet for the fibula (fig. 51 B). In plantar view, this groove also separates the buttress from the calcaneoastragalar facet. The calcaneoastragalar facet is concave craniocaudally, has its long axis aligned craniocaudally, and is nearly flat transversely (figs. 50, 52 B: caa). A wide interarticular sulcus runs caudally into the astragalar canal and separates the calcaneoastragalar facet from the sustentacular facet (fig. 50 B: ia). The sustentacular facet is somewhat bean-shaped, flat, and faces ventrolaterally (fig. 50 B: su). On the medial side of the pedestal supporting the sustentacular facet is the medial side of the astragalonavicular facet (fig. 51 A: an). The astragalonavicular facet of the astragalus is slightly trochleated and wraps from the cranial to the medial side of the astragalus. In cranial view, its plantar edge forms a 40° angle relative to the sole of the foot (fig. 52 B: an). The lateral edge of the astragalonavicular facet of the astragalus may have contacted the cuboid.

CUBOID: In dorsal view, the cuboid is diamond shaped except that its lateral corner forms an elongate process that tapers laterally and is 1.72 mm in length (fig 53: B: cu) (table 7). The four sides of the cuboid are distolateral, proximolateral, distomedial, and proximomedial. Due to post-mortem disarticulation of the right tarsus, it can be seen that there is no noticeable separation between the facets for metatarsals IV and V on the

distolateral side of the cuboid. The distomedial side and surface, which contact the ectocuneiform, are concave. The cuboid is very deep dorsoplantarly, as is seen with the rectangular proximal side (fig. 54 B: cu). On this side, there is a deep L- shaped fossa with the vertical segment of the "L" oriented dorsoplantarly and the base directed laterally. The top of the “L” reaches the dorsal surface and forms a notch that accommodates the swollen distal margin of the calcaneocuboid facet on the calcaneus. The facet for the calcaneus is medial to the vertical leg of the L-shaped fossa, and it tapers dorsoplantarly. The facet is slightly convex transversely and flat dorsoplantarly. Opposite the main cuboid facet and on the medial side of the L-shaped fossa is a small facet that appears to have acted as a stop to the calcaneus during eversion. The facet where the navicular contacts the cuboid is triangular-shaped, tapers plantarly, and is 3.91 mm long on the left side, proximodistally. The dorsal surface of the cuboid is gently concave except towards its proximomedial side, where it is distinctly concave, and its proximal corner, which is distinctly convex.

NAVICULAR: Only the left navicular is preserved, and it is in its natural position relative to adjacent bones. The long axis of the navicular is oriented dorsolateral to medioplantar, and it is 5.45 mm in length (fig. 53 B: na) (table 7). If measured perpendicular to the long axis, the proximal end is 3.09 mm wide, the middle portion is 2.35 mm wide, and the distal end is 2.72 mm wide. The navicular is proximodistally 3.02 mm deep. The proximal side, which articulated with the astragalus, is saddle-shaped with the dorsal end of the saddle coming to a point (fig. 53 B: an). The plantar end of the astragalar articular surface comes to a tuberosity with a smooth, convex top. This tuberosity fits into an articular fossa on the astragalus and limits rotation at the

astragalonavicular joint. The astragalar facet on the navicular is smaller than the navicular facet on the astragalus. The navicular contacts with the entocuneiform and the mesocuneiform distally, and the ectocuneiform and cuboid distolaterally. The contact with the entocuneiform is particularly long.

ECTOCUNEIFORM: The ectocuneiform is rectangular-shaped, and its proximodistal diameter is 2.16 mm while its transverse diameter, as seen in dorsal view, is 2.73 mm (table 7). In dorsal view the ectocuneiform is positioned obliquely, and as seen on the right side, its distolateral corner fits between the metatarsals II and III (fig. 55 B: ect). Its lateral side contacts metatarsal II while its distal side contacts the mesocuneiform. The medial side contacts the navicular. The articulation surface for metatarsal II is flat.

MESOCUNEIFORM: Only the left mesocuneiform is preserved, and it is the smallest bone in the tarsus (figs. 53, 54: mc). It is nearly rectangular in shape, with its width being 1.56 mm while its length is 2.53 mm (table 7). Its lateral side contacts with the proximal third of the entocuneiform, its proximal side contacts the navicular, its medial side contacts the ectocuneiform, and its distal side contacts metatarsal II. The dorsal surface of the mesocuneiform is convex.

ENTOCUNEIFORM: The entocuneiform is large, roughly triangular shaped, and faces medially and slightly dorsally (figs. 53-56: ent) (table 7). The large medially-facing side is concave. The distal two thirds of its lateral side articulates with metatarsal II while the proximal third articulates with a small mesocuneiform (fig. 53 B: ent, mc). The proximal side has a concave ovoid fossa for the navicular and the plantar margin of this facet is swollen and forms a tuberosity (fig. 55 B: ent). The distal end of the

entocuneiform is wide transversely and convex, to fit into a corresponding fossa on the proximal end of metatarsal I. Plantar to this is a concave area that also articulates with metatarsal I.

Table 7. Measurements of the tibia and tarsals of the Udan Multi (PSS-MAE 142).

Dimension Measured	**(mm)**
Tibia	
Length	40.94
Width of distal end	7.62
Fibula	
Length	36.92
Width of distal end	7.04
Astragalus	
Transverse length	8.02
Medial width	5.15
Lateral width	4.74
Navicular	
Length	5.41
Ectocuneiform	
Proximodistal length	2.72
Dorsoplantar length	3.96
Craniodorsal transverse width	1.89
Caudodistal transverse width	1.98
Mesocuneiform	
Proximodistal length	2.27
Entocuneiform	
Proximodistal length	4.27
Cuboid	
Proximodistal length (dorsal)	4.24
Proximodistal length (plantar)	2.56

METATARSALS: The metatarsals, in order of decreasing length, are Mt II > Mt III > Mt I > Mt IV > Mt V (fig. 53-55 A: mt1-4). The proximal ends of metatarsals I and V are wider than their heads, while in the other metatarsals, the opposite is true (figs. 54 A, 56 B: mt 1; 57). Metatarsal V is the widest metatarsal, and its proximal end bears a flat medially facing facet for metatarsal IV, and lateral to that, a large, proximodorsally facing facet for the cuboid and the calcaneus (fig. 57: fcl, fcb). Although metatarsal V

was not found articulated with the rest of the pes, the cuboid and metatarsal IV were. Almost the entire cranial side of the cuboid articulates with metatarsal IV (fig. 53, 55 B: mt4, cu), leaving little room to articulate with the large proximal facet for metatarsal V. Based on this morphology, metatarsal V must have contacted the calcaneus, probably when the foot was everted. The large proximal facet on metatarsal V may accommodated the trochlear ridge of the calcaneus as indicated by a faint groove that traverses the facet. Slightly distal to base and on the lateral side of metatarsal V is a laterally projecting tuberosity, presumably for the insertion of the peroneous brevis muscle (fig. 57: prp). Contraction of this muscle may have caused the calcaneus and this metatarsal to engage.

All the metatarsals, except for metatarsal I, have a transversely elongate fossa on their dorsal sides just proximal to heads (fig. 53 A). The fossa is largest on metatarsal V. The articulation surface for the entocuneiform on metatarsal I is saddle-shaped. In dorsal view, the joint between metatarsal I and the entocuneiform is offset distally 4.62 mm as compared to the joint between metatarsal II and the mesocuneiform (fig. 55 A).

PHALANGES: Numerous phalanges were found in the matrix surrounding the partially articulated skeleton of the Udan Multi. Only the left proximal phalanges for digits II, III, and IV were found in their approximate natural positions (figs. 53, 54: ph 2-4). Each of these proximal phalanges has a transversely wide base that gradually narrows distally before slightly widening again at the distal end. The distal articular surfaces for the middle phalanges are convex dorsoventrally but flat transversely. The medial and lateral side of each bears a distinct pit. Fragments of two distal phalanges were found, although it is unclear if they are from the manus or pes. They are elongate claws that have a shallow longitudinal groove on the side.

Table 8. Measurements of the metatarsals and phalanges of the Udan Multi (PSS-MAE 142).

Dimension Measured	**(mm)**
Metatarsal Length	
Metatarsal I	12.55
Metatarsal II	13.00
Metatarsal III	13.77
Metatarsal IV	12.05
Metatarsal V	10.41
Proximal Phalanges Length	
Phalanx II	9.31
Phalanx III	9.09
Phalanx IV	8.26

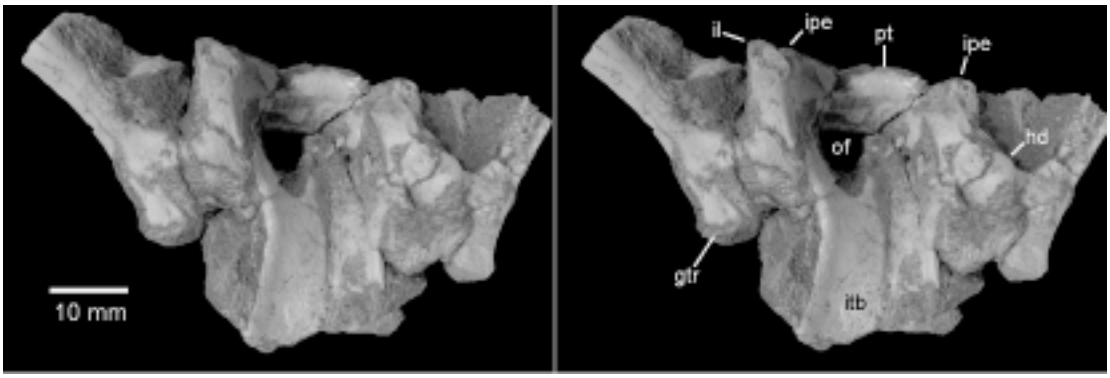

Fig. 45. Stereophotographs of the pelvic girdle of the Udan Multi (PSS-MAE 141) in dorsal view.

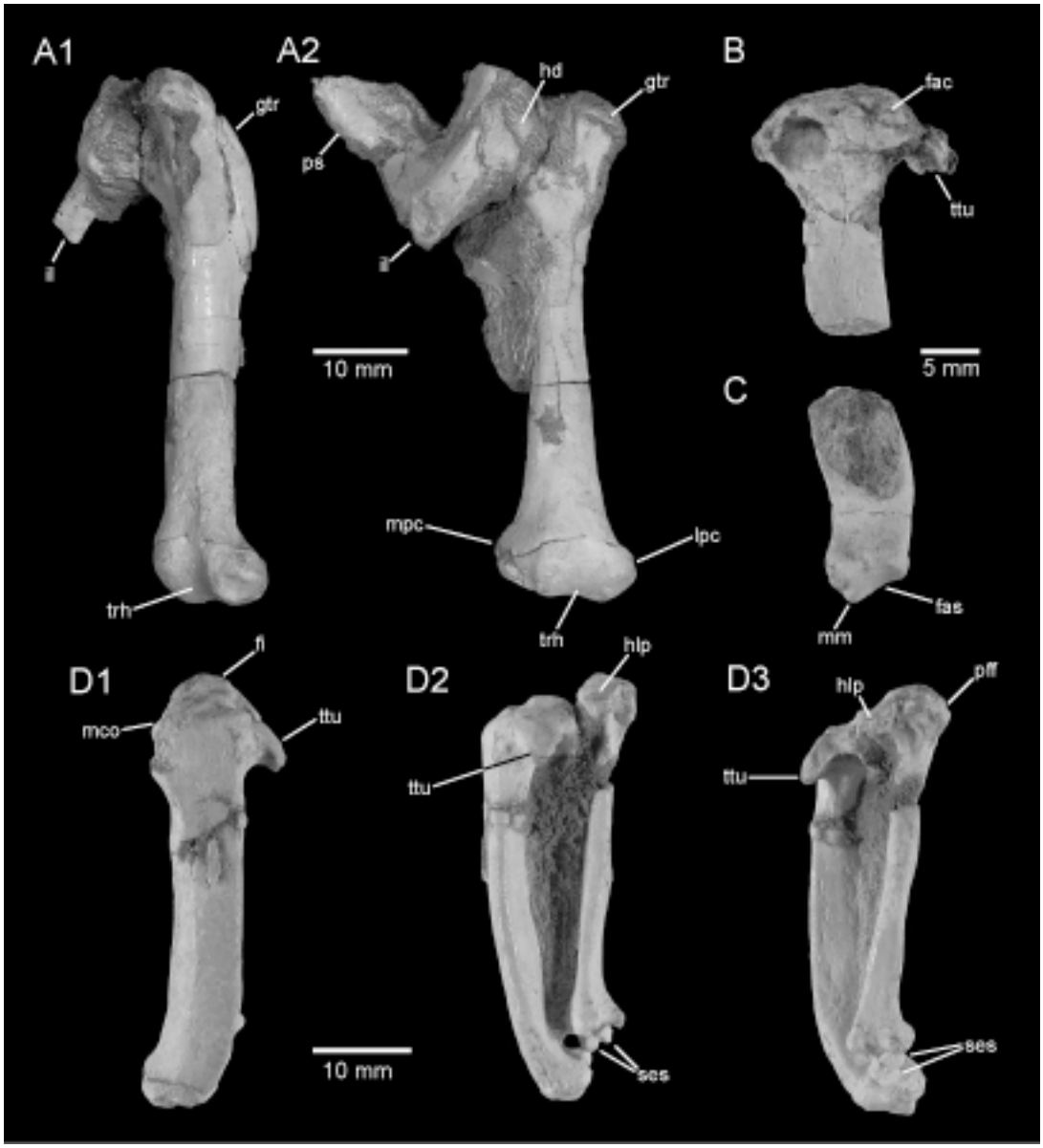

Fig. 46. Left femur **(A1, A2)**, right tibia **(B, C)** and left tibia and fibula **(D1-3)** of the Udan Multi (PSS-MAE 141): **(A1)** craniolateral views, **(A2)** cranial view, **(B)** caudolateral view of proximal end of right tibia, **(C)** caudolateral view of distal end of right tibia, **(D1)** craniomedial view, **(D2)** lateral view, and **(D3)** caudal view.

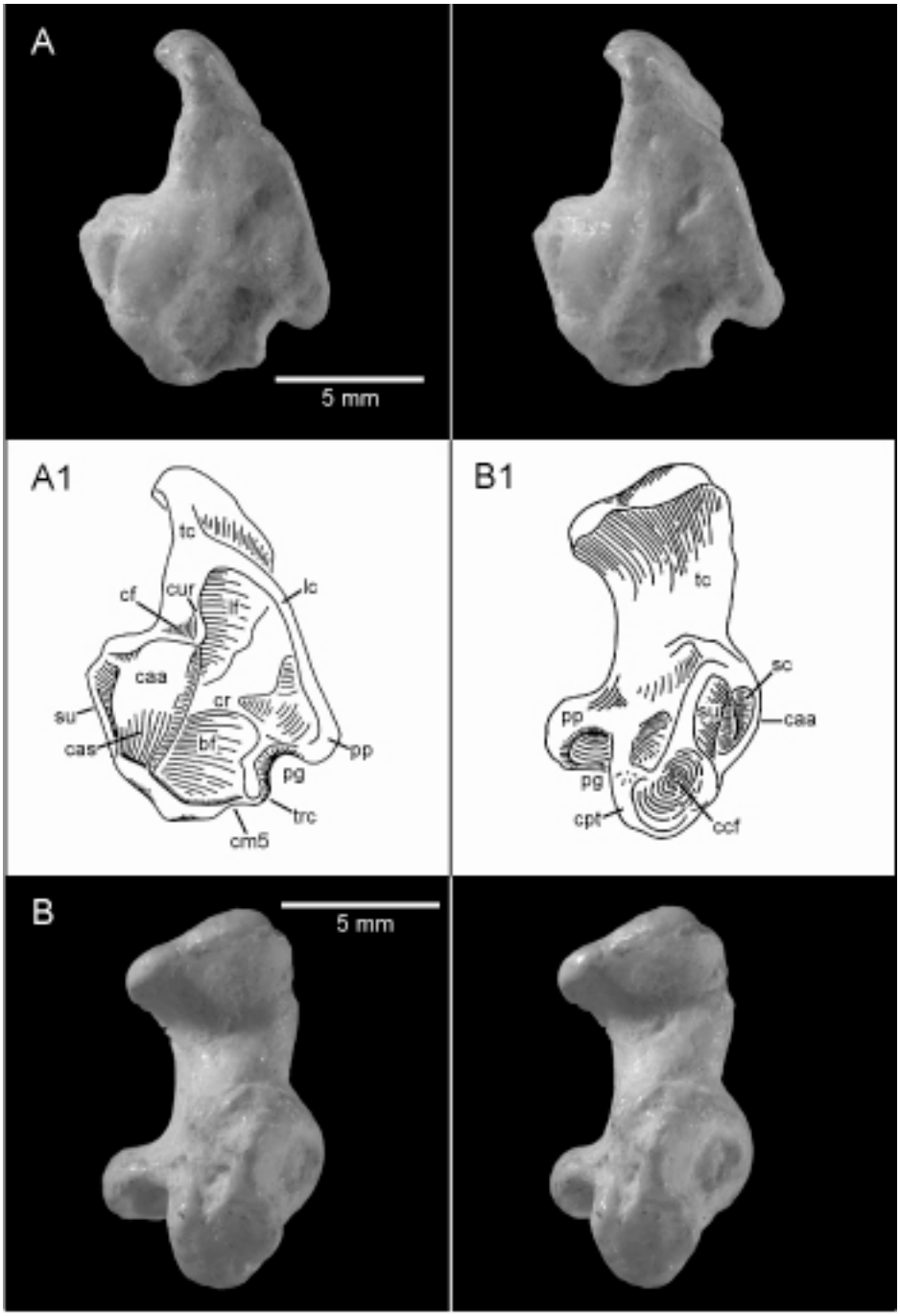

Fig. 47. Left calcaneus of the Udan Multi (PSS-MAE 141): **(A)** stereophotographs of the dorsal side, **(A1)** interpretive drawing of the same, **(B)** stereophotographs of plantar side, **(B1)** interpretive drawing of the same. In **A** and **A1** lateral is towards the right while in **B** and **B1** it is towards the left of the page.

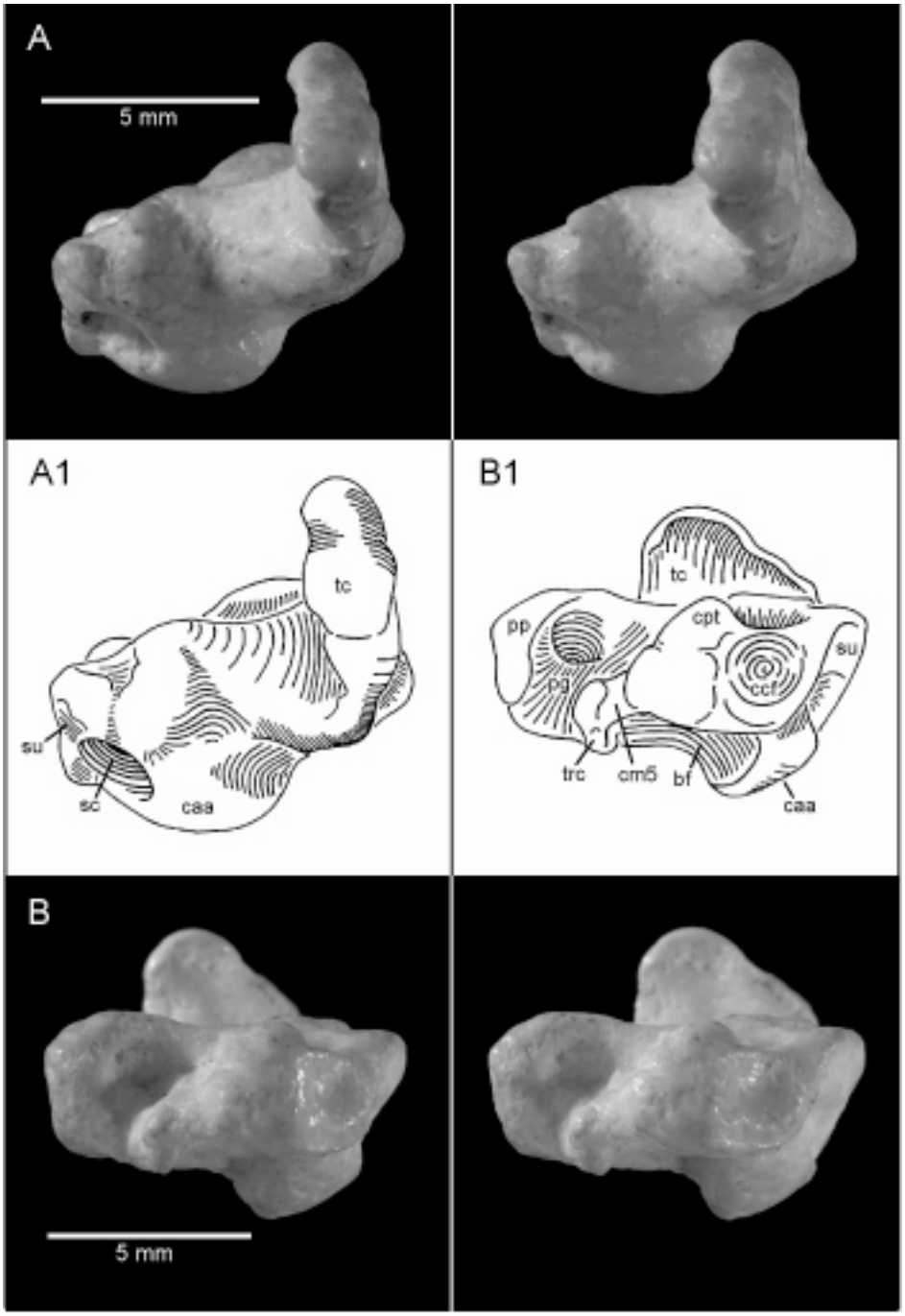

Fig. 48. Left calcaneus of the Udan Multi (PSS-MAE 141): **(A)** stereophotographs of the caudal side, **(A1)** interpretive drawing of the same, **(B)** stereophotographs of the distal side, **(B1)** interpretive drawing of the same. In **A** and **A1** medial is towards the left while in **B** and **B1** it is towards the right of the page.

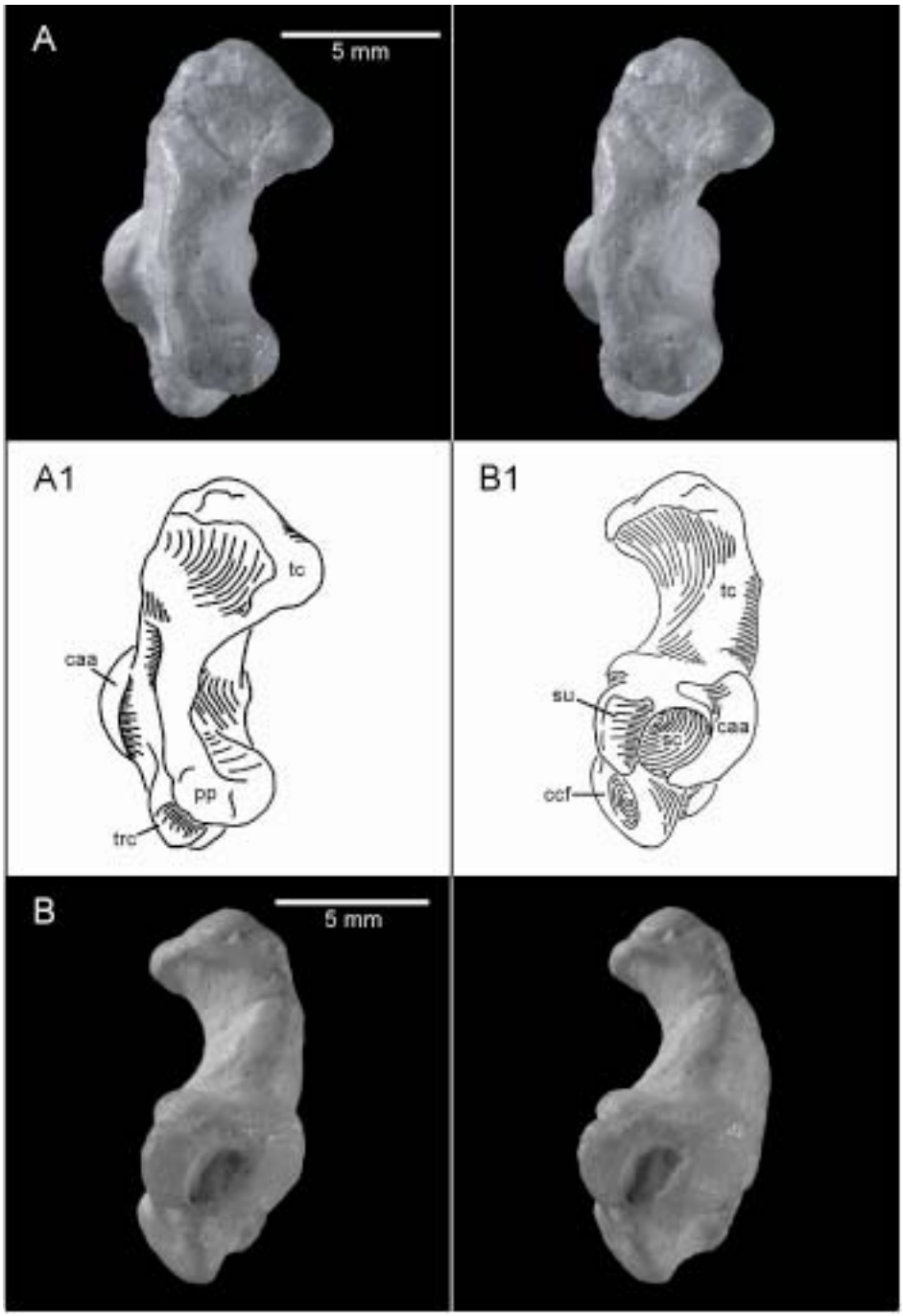

Fig. 49. Left calcaneus of the Udan Multi (PSS-MAE 141): **(A)** stereophotographs of the lateral side, **(A1)** interpretive drawing of the same, **(B)** stereophotographs of medial side, **(B1)** interpretive drawing of the same. In **A** and **A1** dorsal is towards the left while in **B** and **B1** it is towards the right of the page.

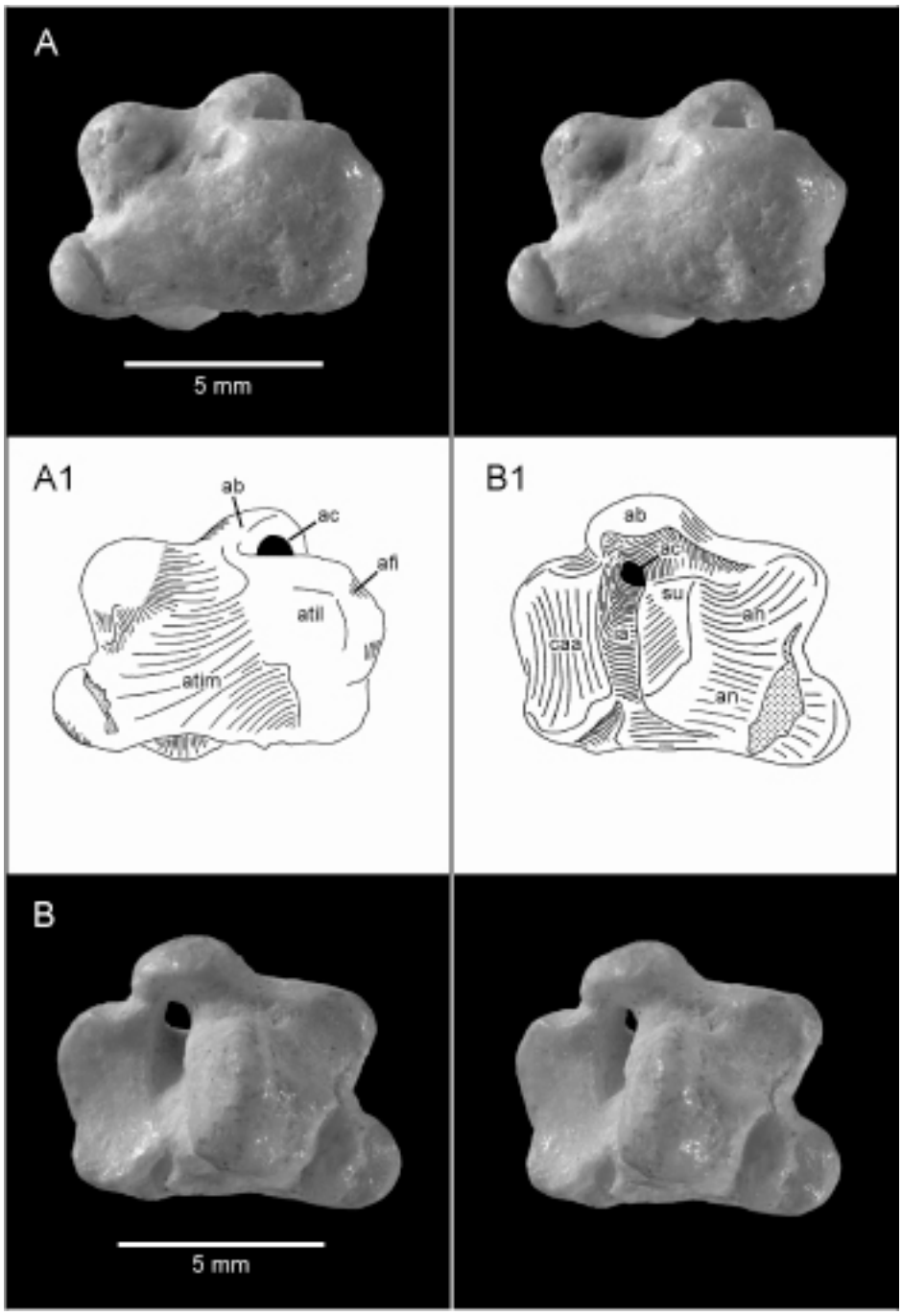

Fig. 50. Left astragalus of the Udan Multi (PSS-MAE 141): **(A)** stereophotographs of the dorsal side, **(A1)** interpretive drawing of the same, **(B)** stereophotographs of plantar side, **(B1)** interpretive drawing of the same. In **A** and **A1** lateral is towards the right while in **B** and **B1** it is towards the left of the page.

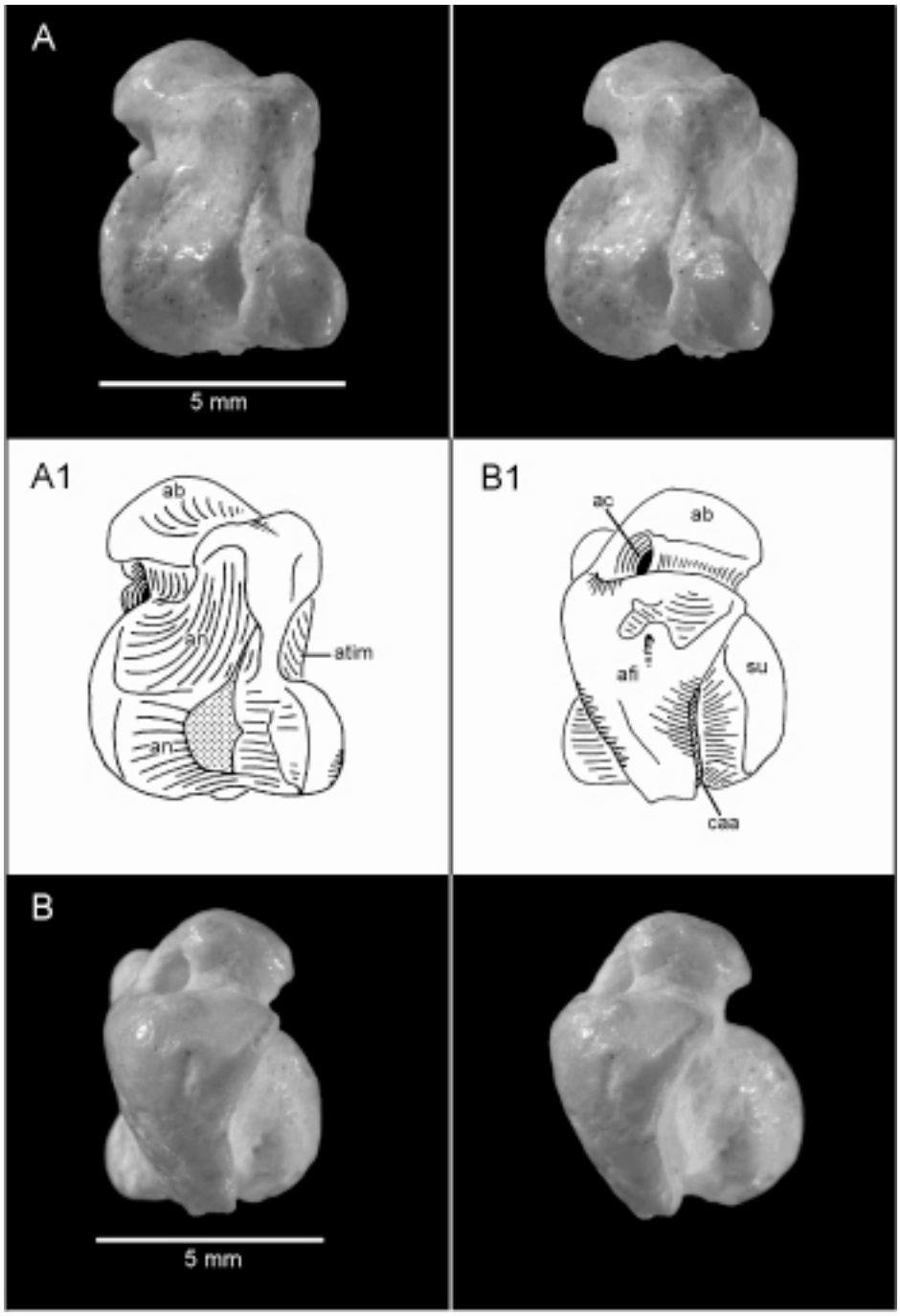

Fig. 51. Left astragalus of the Udan Multi (PSS-MAE 141): **(A)** stereophotographs of medial side, **(A1)** interpretive drawing of the same, **(B)** stereophotographs of the lateral side, **(B1)** interpretive drawing of the same. In **A** and **A1** dorsal is towards the right while in **B** and **B1** it is towards the left of the page.

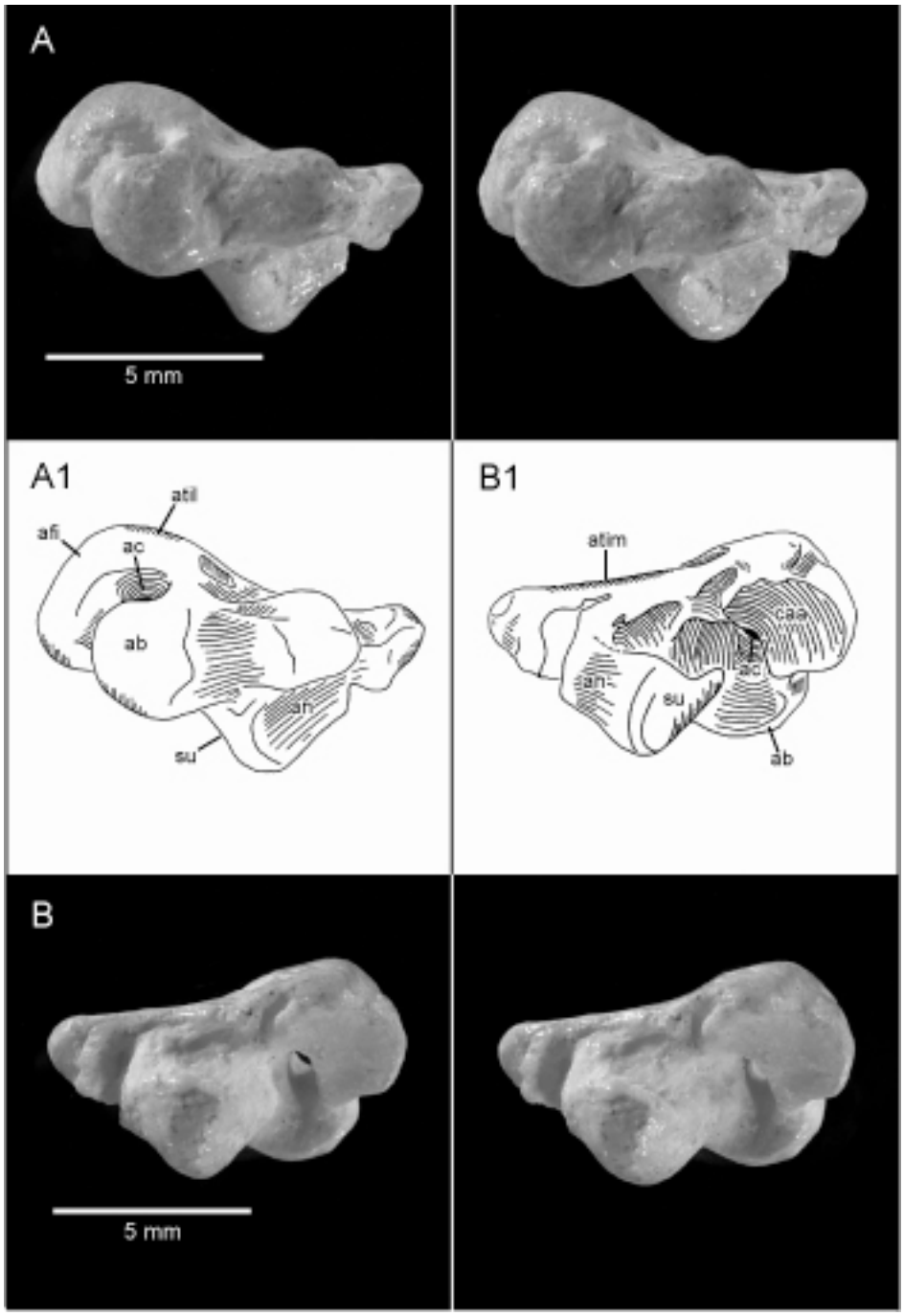

Fig. 52. Left astragalus of the Udan Multi (PSS-MAE 141): **(A)** stereophotographs of the caudal side, **(A1)** interpretive drawing of the same, **(B)** stereophotographs of the distal side, **(B1)** interpretive drawing of the same. In **A** and **A1** medial is towards the right while in **B** and **B1** it is towards the left of the page.

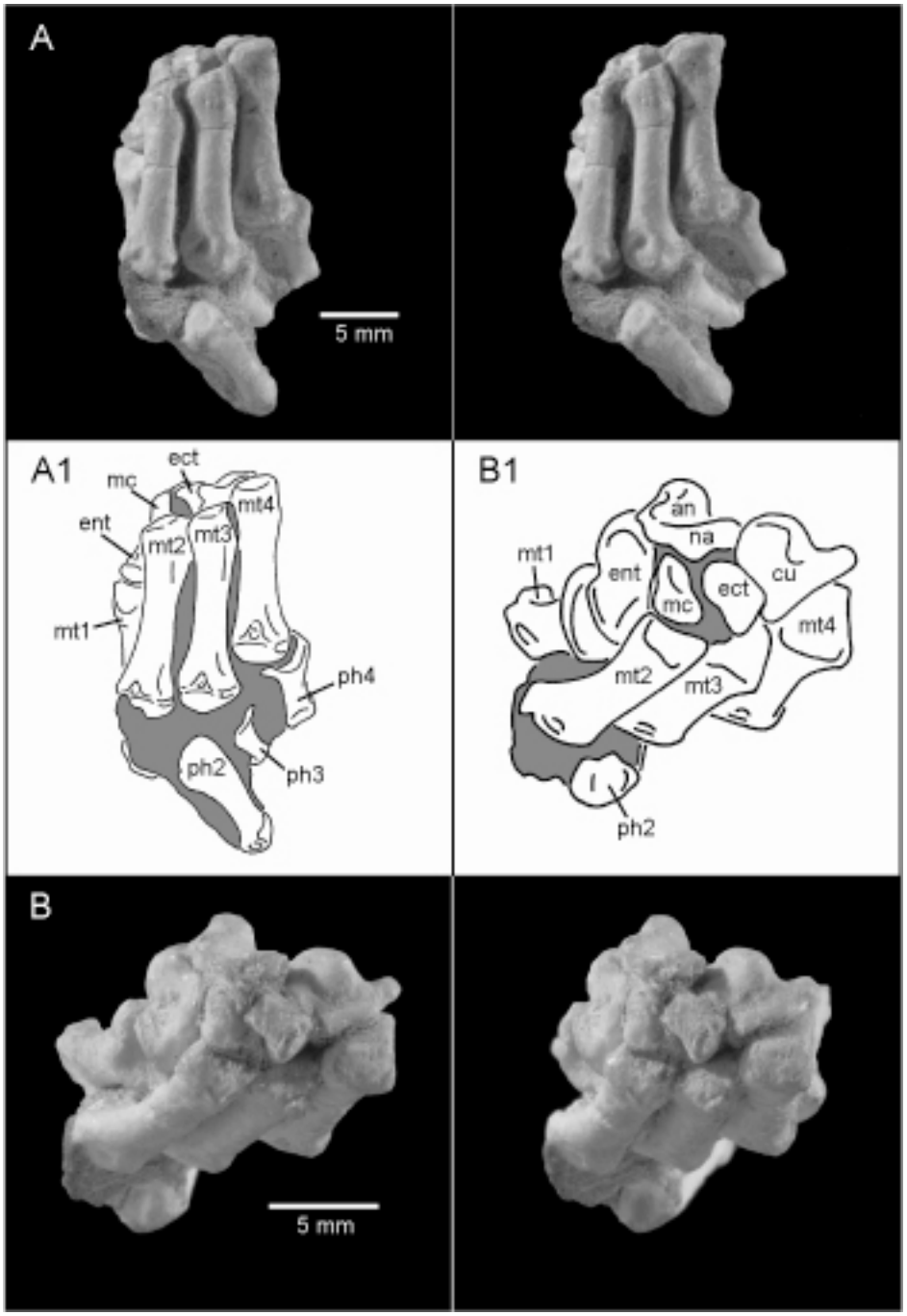

Fig. 53. Left pes of the Udan Multi (PSS-MAE 141): **(A)** stereophotographs of the dorsal side of the metatarsals and phalanges, **(A1)** interpretive drawing of the same, **(B)** dorsal view of ankle and proximal view of metatarsals, and **(B1)** interpretive drawing of the same.

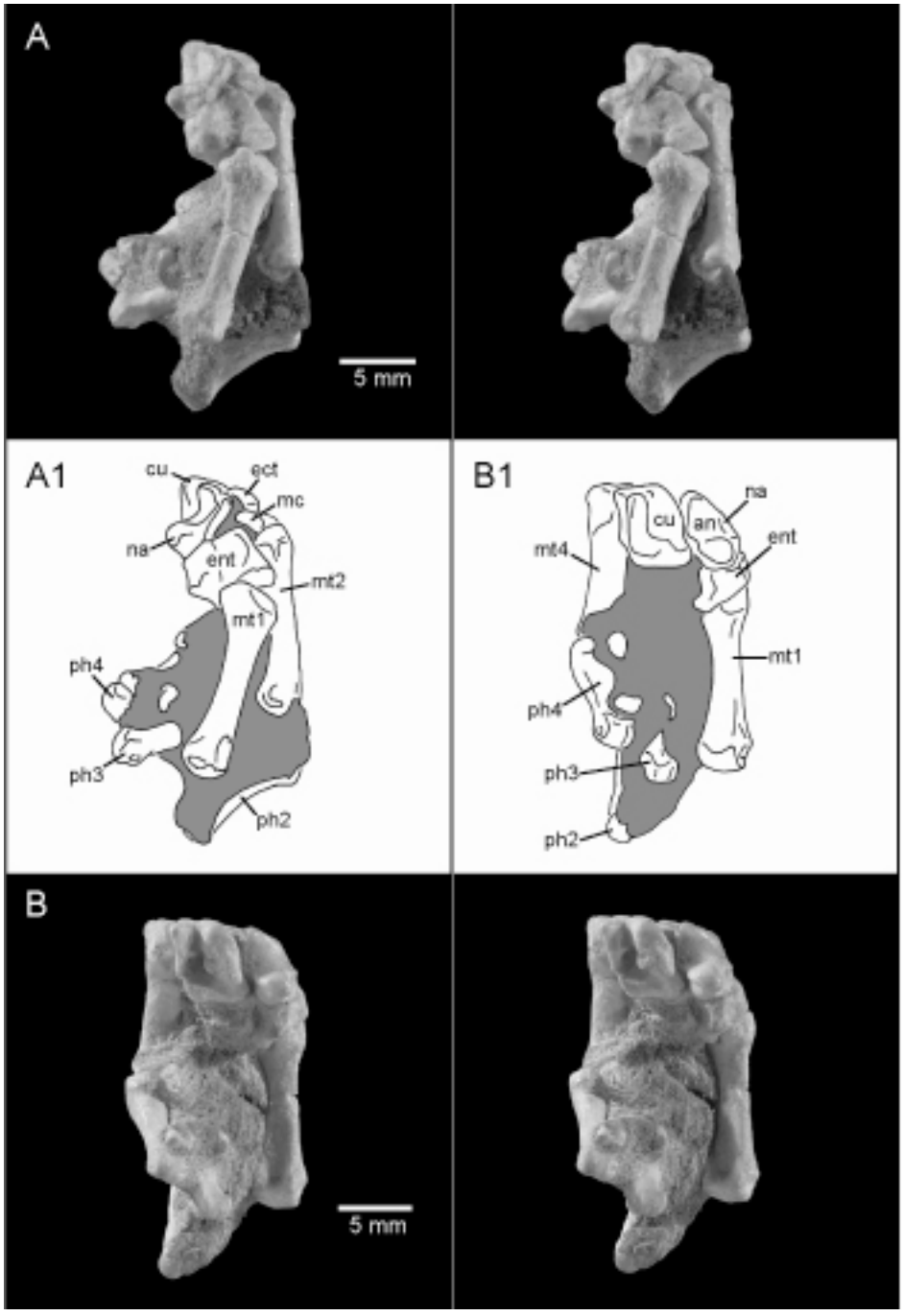

Fig. 54. Left pes of the Udan Multi (PSS-MAE 141): **(A)** stereophotographs of medial side, **(A1)** interpretive drawing of the same, **(B)** plantar view of the metatarsals and proximal view of the ankle, and **(B1)** interpretive drawing of the same.

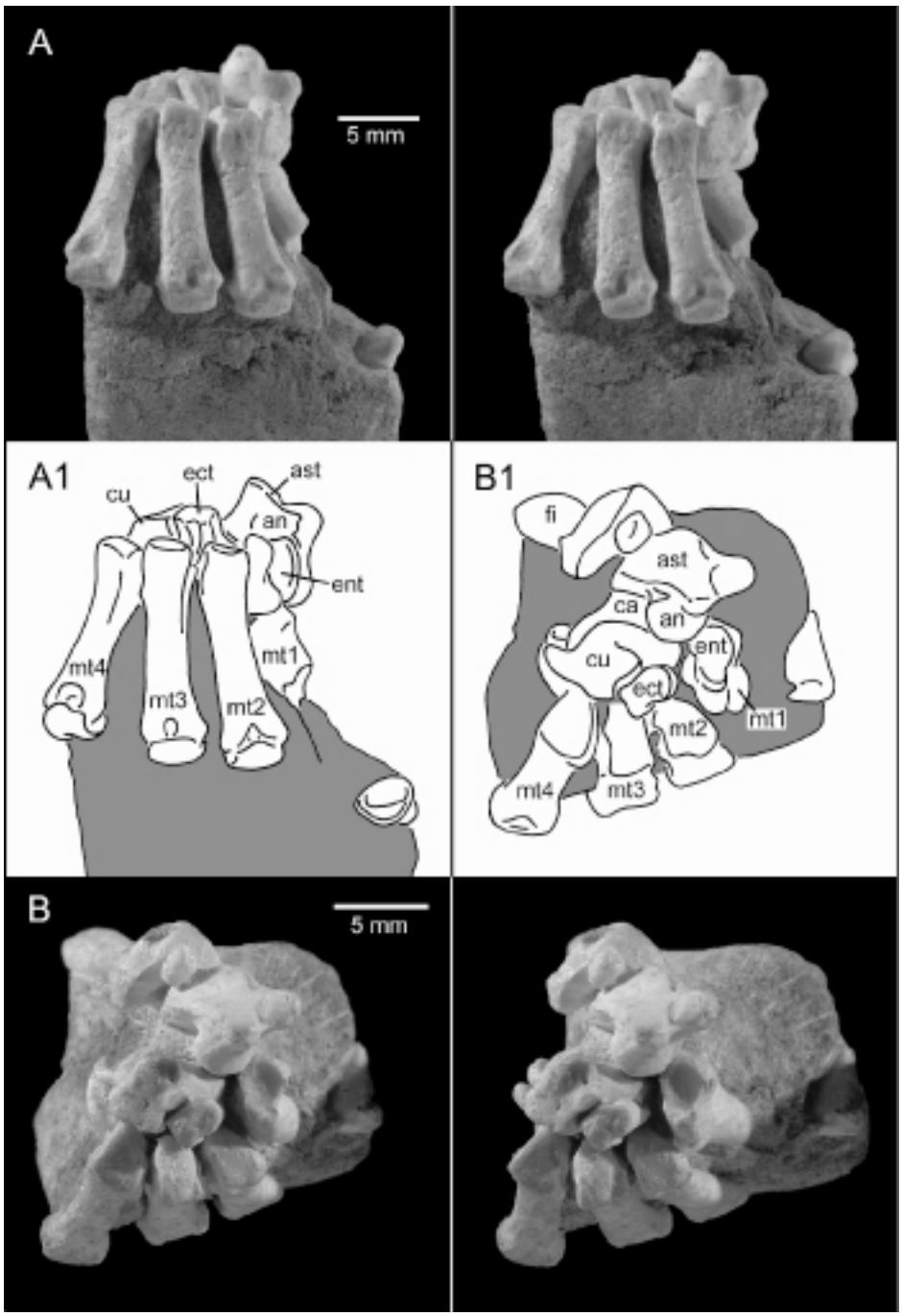

Fig. 55. Right pes of the Udan Multi (PSS-MAE 141): **(A)** stereophotographs of the dorsal side of the metatarsals and phalanges, **(A1)** interpretive drawing of the same, **(B)** dorsal view of ankle and proximal view of metatarsals, and **(B1)** interpretive drawing of the same.

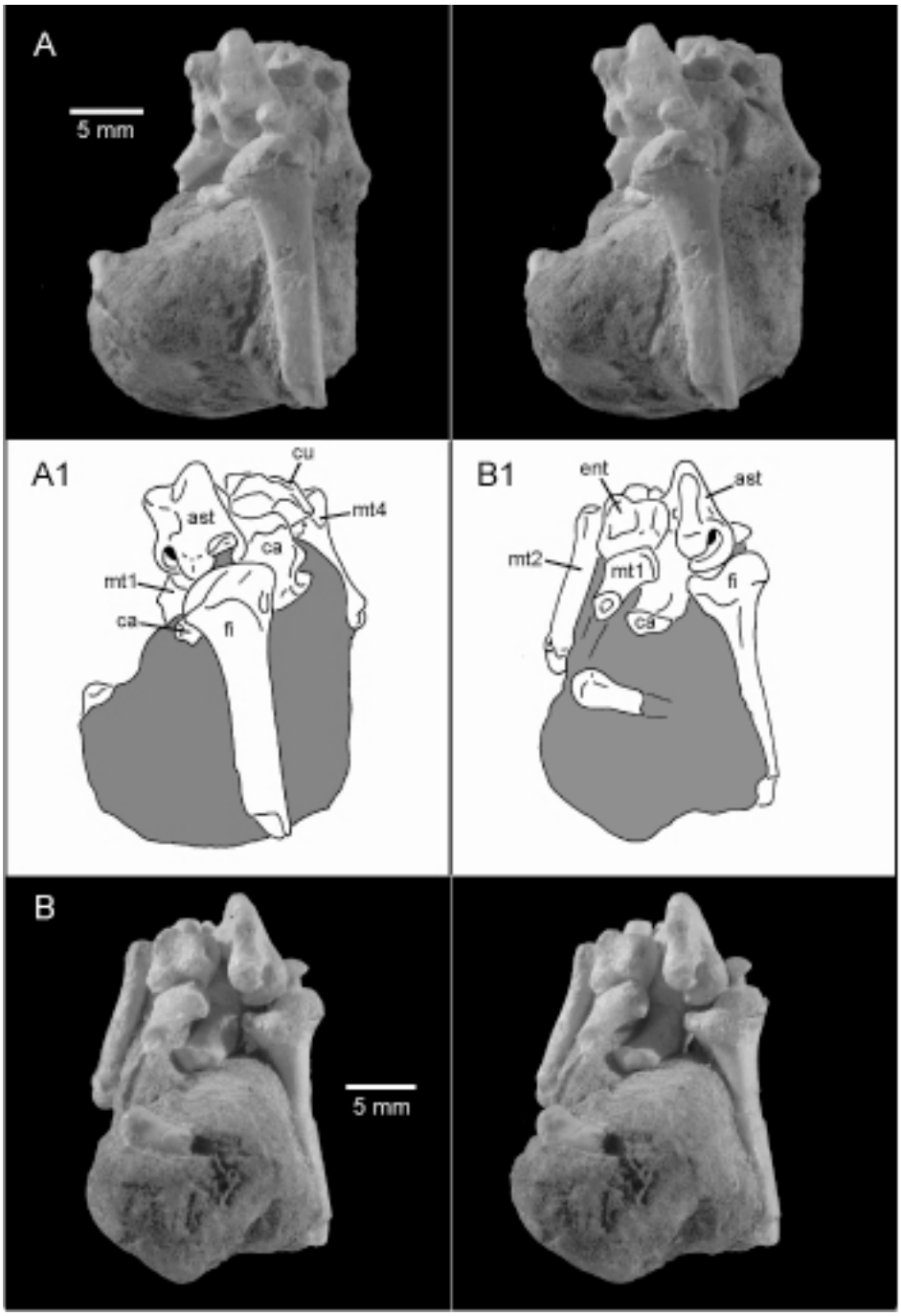

Fig. 56. Right pes of the Udan Multi (PSS-MAE 141): **(A)** stereophotographs of the lateroplantar side of the metatarsals and the dorsolateral side of the ankle, **(A1)** interpretive drawing of the same, **(B)** medioplantar side of the metatarsals and proximal view of the ankle, and **(B1)** interpretive drawing of the same.

Fig. 57. Left metatarsal of the Udan Multi (PSS-MAE 141): **(A)** dorsolateral view, **(B)** medioplantar view. Lateral is towards the right in **1** and towards the left in **2**.

REMARKS

Both the skull and skeleton of the Udan Multi were discovered, although only the postcranial skeleton is described here. In an abstract, Spurlin et al. (2000) described the partial skull and jaw of the Udan Multi and classified it in the the Suborder Djadochtatheria, which has since been replaced by Superfamily Djadochtatheroidea (Kielan-Jaworowska and Hurum, 2001). Spurlin et al., (2000) also indicated that among described taxa, the Udan Multi is most closely related to *Tombaatar*, a Mongolian multituberculate described by Rougier et al (1997). The Udan Multi and *Tombaatar* are similar in size and both share the absence of a P2, an elaborated palatal torus, and an extremely depressed infraorbital foramen (Spurlin, et al., 2000). They differ from each other by different molar proportion (Spurlin, et al., 2000). A detailed description of the skull and jaw of the Udan Multi is underway (Rougier et al., in prep).

PHYLOGENETIC ANALYSES

The goals of the phylogenetic analysis were to test previous hypotheses for the phylogeny of Multituberculata based on craniodental data, to develop a phylogenetic hypothesis for those multituberculates that have postcrania based on postcranial data, and to determine where isolated multituberculate postcrania from North America fit into multituberculate phylogeny.

TAXON SAMPLING

A total of 19 taxa and 16, representative, isolated, individual postcranial bones were included in the phylogenetic analyses. The most critical multituberculate taxa included are those that have postcrania associated with craniodental elements. These include *Djadochtatherium matthewi* (Simpson, 1928; McKenna, 1961), *Ptilodus kummae* (Krause and Jenkins, 1983), *Kryptobaatar dashzevegi*, *Nemegtbaatar gobiensis*, *Chulsanbaatar vulgaris* (Kielan-Jaworoska and Gambaryan, 1994), and *Catopsbaatar catopsaloides* (Kielan-Jaworowska et al., 2000; Kielan-Jaworowska and Hurum, 2005). Character codings for these eight taxa were based on direct observations of specimens. Three taxa that have postcranial data associated with craniodental remains were not included because they could only be coded for 5% or less of the 95 characters in appendix I: *Sloanbaatar* (Kielan-Jaworowska and Gambaryan, 1994), *Sinobaatar* (Hu and Wang, 2002), and *Taeniolabis*. In each case, the original posctcranial specimens of these taxa were examined, but poor preservation prevented them from being coded for nearly all the detailed characters in the present study.

In addition to the above taxa, I included a partial multituberculate skeleton (AMNH 16325) not associated with craniodental material that was described by and referred to *Eucosmodon* sp. by Granger and Simpson (1929). Assigning this specimen to *Eucosmodon* is probable but remains uncertain. Granger and Simpson (1929) tentatively assigned these postcranial bones to *Eucosmodon* sp. based on size, the fact that craniodental remains of *Eucosmodon* had been collected from the same stratigraphic level, and that the bones were similar to fragmentary postcranial bones of "*Eucosmodon" teilhardi* (Granger and Simpson, 1929). Given what little is known of the postcranial skeleton of "*Eucosmodon" teilhardi*, it is not clear if these similarities are informative. Furthermore, "*E." teilhardi* has since been referred to *Stygimys teilhardi* by Sloan and Van Valen (1965). Even so, *Eucosmodon* seems to be the only likely candidate to which this skeleton can be referred. In addition to these previously described postcranial specimens, data from three new multituberculate skeletons associated with craniodental material, which are described in this dissertation, were included: the neoplagiaulacid *Ectypodus* sp. (BT03049) and two djadochtatheroideans *Kryptobaatar dashzevegi* (MAE 00-22) and an undescribed taxon the Udan Multi (PSS-MAE 142). The OTU's (operational taxonomic units) of *Ectypodus* and the Udan Multi are entirely based on these specimens while the OTU for *Kryptobaatar* is a combination of the new skeleton with previously published data (i.e. Kielan-Jaworowska, 1998; Kielan-Jaworoska and Gambaryan, 1994).

Two more taxa are based on the unpublished masters thesis of Deischl (1964). He studied over 300 isolated postcranial bones of multituberculates from the Bug Creek Anthills locality of Montana and assigned many of them to five taxa known only by

craniodental remains (i.e. *Cimexomys minor*, *Mesodma formosa*, *Mesodma thompsoni*, *Stygimys kuszmauli*, *Catopsalis joyneri*) based on relative size and abundance. Deischl (1964) confidently assigned many bones to *Mesodma* and *Stigymys,* and composite skeletons he developed were also included in the analyses. Specifically, characters were coded by direct observation from the following specimens as well as from the figures and specimens described by Deischl (1964); for *Mesodma*: UMVP 1400, 1402, 1403, 1419, 1420, 1428, 1432 and for *Stygimys*: UMVP 1407, 1433, 1434. The two astragali referred to *Stygimys kuszmauli* by Deischl (1964) could not be found in the vertebrate paleontology collections of the University of Minnesota, so an uncatalogued specimen that is virtually identical to the one he figured was included instead (UM Calc 202).

In addition to the specimens at the University of Minnesota, I also studied isolated postcranial bones in the collections of the Museum of Comparative Zoology, National Museum of Natural History, and the University of Alberta (tables 9, 10). Some isolated astragali and calcanei were included in some of the analyses because these bones are the most variable among multituberculates and likely have important information for determining the phylogeny. Astragali were not common in the collections I examined, so all four isolated specimens (USNM 2894, UM Astr. 262, UA Astr. 29, UM Astr.263) were included in one of the analyses. In contrast, calcanei were quite common and to simplify the analyses, they were grouped into 10 morphotypes based on size, morphology, and geographic and stratigraphic occurrences (table 10). Based on comparisons to the specimens identified by Deischl (1963), morphotype V is almost certainly *Mesodma* and morphotype VII is almost certainly *Stygimys*. The identifications of the other specimens are highly speculative, but based on size and occurrence, I suggest

that morphotype VI could be a species of *Mesodma*, morphotype IV could be *Cimexomys*, and morphotype X could be another species of *Stygimys*.

I included 8 outgroups for this study: the monotremes *Ornithorhynchus anatinus*, *Tachyglossus aculeata*, and *Zaglossus bruijni*; triconodont *Jeholodens jenkensi* (Ji et al., 1999); the symmetrodont *Zhangheotherium quinquecuspidens* (Hu et al., 1997; Luo and Ji, 2005); the eutherians *Ukhaatherium nessovi* (Novacek et al., 1997; Horovitz, 2000, 2003) and *Eomaia scansoria* (Ji et al., 2002); and the metatherian *Didelphis virginiana*. Characters codings were based on direct examination of specimens for monotremes (see Table 9), *Ukhaatherium* (PSS-MAE 102), and *Didelphis* (UF33 and uncatalogued specimens in the Georgia Southern Museum collections). For other taxa, I consulted the references listed above. Previous studies have strongly supported monophyly of Multituberculata to the exclusion of these taxa (e.g. Simmons, 1993; Rougier et al., 1997, Kielan-Jaworowska and Hurum, 2001), thus they are all viable outgroups. Recent phylogenetic studies on the higher-level phylogeny of mammals place Trechnotheria as the sister-group to Multituberculata, which includes symmetrodonts and therian mammals (Luo et al., 2002; Luo and Wible, 2005).

Table 9. Taxa and specimens studied except isolated calcanei and astragali.

Taxon	Element(s)	Institution	Number
Monotremata			
Zaglossus bruijni	Skeleton	AMNH	66194
Tachyglossus aculeatus	Skeleton	AMNH	65833
Ornithorhynchus anatinus	Skeleton	AMNH	150101
Marsupialia			
Didelphis virginiana	Skeleton	AMNH	146532
Didelphis virginiana	Skeleton	GSM	no number
Placentalia			
Ukhaatherium nessovi	Partial Skeleton	PSS-MAE	106
Multituberculata			
Eucosmodon sp.	Partial Skeleton	AMNH	16325
Kryptobaatar dashzevegi	Partial Skeleton	MAE	00-22
Udan Multi	Partial Skeleton	PSS-MAE	142
Catopsbaatar catopsaloides	Partial Skeleton	PM	120/107
Kryptobaatar dashzevegi	Partial Skeleton	ZPAL MgM	I/41
Nemegtbaatar gobiensis	Partial Skeleton	ZPAL MgM	I/82
Chulsanbaatar vulgaris	Partial Skeleton	ZPAL MgM	I/83
Chulsanbaatar vulgaris	Partial Skeleton	ZPAL MgM	I/99b
Sinobaatar lingyuanensis	Skeleton	IVPP	V12517
Ptilodus kummae	Partial Skeleton	UA	9001
cf. ?*Catopsalis joyneri*	Distal end of humerus	MCZ	19529
cf. ?*Stygimys kuszmauli*	Distal end of humerus	UA	11994
Genus and species indet.	Scapulocoracoid	MCZ	20959
Genus and species indet.	Scapulocoracoid	MCZ	20785
Genus and species indet.	Scapulocoracoid	UA	11992
Genus and species indet.	Scapulocoracoid	UA	11993
Genus and species indet.	Scapulocoracoid	UCMP	148112
Genus and species indet.	Scapulocoracoid	UCMP	148122
Genus and species indet.	Scapulocoracoid	UCMP	148293
Genus and species indet.	Humeri (29 specimens)	MCZ	20962
Genus and species indet.	Humerus	UA	11300
Genus and species indet.	Ulna	UA	11302
Genus and species indet.	Femur	UA	11301
Genus and species indet.	Parafibula	UA	11996
Genus and species indet.	Tibia (30 specimens)	MCZ	18397
Genus and species indet.	Tibia	UA	11995

Table 10. Geographical and temporal distribution of isolated calcanei and astragali examined in this study. Abbreviations: BCA = Bug Creek Anthills Fauna, probably Early Paleocene. Pask. Fm. = Paskapoo Formation, exact locality uncertain. Morphotypes were developed for calcanei only.

Tentative ID	Morphotype	Institution	Number	Element	Locality
?Catopsalis	I	UM	Calc.253	calcaneus	BCA?
?Catopsalis	II	UCMP	111159	calcaneus	Bushy tailed blowout
?Catopsalis	III	MCZ	20960-1	calcaneus	BCA
?Cimexomys	IV	MCZ	20960-4	calcaneus	BCA
?Cimexomys	IV	MCZ	20960-6	calcaneus	BCA
?Mesodma 1	V	UM	Calc.258	calcaneus	BCA?
?Mesodma 1	V	UMVP	1432	calcaneus	BCA
?Mesodma 2	VI	MCZ	20960-5	calcaneus	BCA
?Mesodma 2	VI	UM	Calc.171	calcaneus	BCA
?Mesodma 2	VI	UM	Calc.177	calcaneus	BCA
?Mesodma 2	VI	UM	Calc.179	calcaneus	BCA?
?Stygimys	VII	MCZ	20783	calcaneus	BCA
?Stygimys	VII	MCZ	20784	calcaneus	?
?Stygimys	VII	MCZ	20960-2	calcaneus	BCA
?Stygimys	VII	MCZ	20960-3	calcaneus	BCA
?Stygimys	VII	UM	Calc.180	calcaneus	BCA
?Stygimys	VII	UM	Calc.181	calcaneus	BCA
?Stygimys	VII	UM	Calc.186	calcaneus	BCA?
?Stygimys	VII	UMVP	1433	calcaneus	BCA
Unknown	VIII	UM	Calc.183	calcaneus	BCA
?Didelphodon	IX	UCMP	111158	calcaneus	Bushy tailed blowout
Unknown	X	UM	Calc.175	calcaneus	BCA
?Mesodma	NA	UA	Astr.29	astragalus	Pask. Fm.
?Mesodma	NA	UM	Astr.262	astragalus	BCA?
?Stygimys	NA	UM	Astr.263	astragalus	BCA?
?Cimolomys	NA	USNM	2894	astragalus	Type Lance

CHARACTERS

There are 95 postcranial characters in this study: 17 from the pectoral girdle with forelimbs and 78 from the pelvic girdle with hind limbs (Appendix 1). Of the 95 characters, 22 of them are ordered. Only those characters where all states could be easily arranged into a linear morphocline were ordered. The assignment of morphologies to states within the morphocline was done so that the most different morphologies were given the most different states (e.g. states 0 and 3 in a four state character) and states in between were arranged to put the most similar morphologies next to each other. Seven characters (characters 20, 23, 25, 32, 48, 52, 93) are continuous and were coded using Thiele's (1993) formula (see methods below). Of the 95 characters, 77 characters are original to this work while the remaining 18 are from the following references: Schaeffer (1941), Jenkins (1971), Simmons (1993), Kielan-Jaworowska and Gambaryan (1994), Hu et al. (1997), Ji et al. (1999), Horovitz (2000), Ji et al. (2002), and Sereno (2006). In all of these publications, these characters were used at a higher-taxonomic level, not to resolve relationships within Multituberculata. The 95 postcranial characters and the distributions of their character states are described below.

SCAPULA

Character 1. *Spine of scapula relative to the plane of the scapular blade (ordered): (0) inclined, spine projects cranially or craniolaterally, (1) forms a 90˚ angle, spine projects directly laterally, (2) inclined, spine projects caudolaterally, (3) inclined, spine projects caudally and runs almost parallel to the plane of the blade.* The scapula

spine is located on the lateral surface of the scapula and divides this surface into two fossae, the infraspinatus and supraspinatus fossae, which form the respective origins for muscles that bear the same names (Evans, 1993). Based primarily on embryology, Sanchez-Villagra and Maier (2003) suggested that the ventral part of the spine, which includes the acromion, is homologous to the anterior margin of the scapula in monotremes while the dorsal portion is formed from the ossification of connective tissues between the supraspinatus and infraspinatus muscles. This contradicts early views (e.g. Romer, 1956), that hypothesized that the entire scapular spine of therians is homologous to the anterior margin of the scapula of monotremes and sauropsids. Given the uncertainty in the homology of the dorsal portion of the scapular spine of multituberculates with those of other mammals, this character is based only on the ventral part of the spine, which seems to be homologous across all ingroup and outgroup taxa. The most primitive state "state 0" is to have the spine in the same plane as the scapular blade, which is seen in all monotremes. Inclination of the spine varies among multituberculate taxa. Some multituberculates, like the Udan Multi, *Djadochtatherium*, and *Ectypodus*, have a spine that is directed laterally (state 1), while in others, like *Nemegtbaatar*, *Chulsanbaatar*, and *Mesodma*, it is inclined caudolaterally (state 2). A spine that is bent over so that it runs parallel and lateral to the scapular blade is an autapomorphy of *Ukhaatherium* (Horovitz, 2003) (state 3).

Character 2. *Position of coracoid process/metacoracoid relative to the center of the glenoid fossa of the scapula in caudal view (ordered): (0) medial to center, (1) aligned with center, (2) lateral to center.* Although monotremes have two distinct coracoids, a procoracoid and a metacoracoid, multituberculates (Sereno and McKenna,

1995; Sereno, 2006) and therians lack coracoids and instead the glenoid fossa is composed entirely of the scapula. Even so, embryological evidence indicates that the coracoid process of therians is homologous to the metacoracoid and that the procoracoid does not contribute to the scapula (Klima, 1987; Vickaryous and Hall, 2006).

The above character description is based on a glenoid fossa that faces ventrocaudally, as is seen in multituberculates and therians. In monotremes, the glenoid fossa faces laterally and the base of the coracoid process originates caudal to the craniocaudal center of the glenoid fossa. Assuming that the glenoid fossa and coracoid process rotated together, then the comparable state in multituberculates to the condition seen in monotremes is state (0), caudal to center. A probably homologous state occurs in most djadochtatheroids (e.g. Udan Multi, *Nemegtbaatar*, *Kryptobaatar*), where the base of the coracoid process originates medial to the transverse center of the glenoid fossa (state 0). *Djadoctatherium* and *Ectypodus* have a coracoid process that is aligned with the center of the glenoid fossa, with the scapula in caudal view (state 1). In contrast, *Didelphis* has a coracoid process that originates lateral to the center of the glenoid fossa (state 2).

Character 3. *Shape of glenoid fossa, not including the portion on the coracoid process: (0) ovoid, with long axis oriented craniocaudally, (1) circular, (2) subrectangular, long axis of rectangle oriented transversely.* The glenoid fossa occurs on the scapula, and in some cases, on the metacoracoid as well and articulates with the head of the humerus. This character is based only on the shape of the scapula's contribution to the glenoid fossa. In monotremes, where the suture between the metacoracoid and the scapula is clear, the scapular glenoid is subrectangular with the long axis oriented

craniocaudally. As mentioned in the description for character 2, the monotreme morphology can be homologized with that of other mammals if the glenoid and surrounding structures are rotated so that the glenoid faces ventrocaudally. In this case, the long axis would be oriented transversely, thus monotremes are coded as "2" for this character. With this rotation, monotremes resemble the morphology in *Kryptobaatar*, *Nemegtbaatar*, and the Udan Multi (fig. 41.4: gl) (state 2). In multituberculates and therians, the metacoracoid is not a discrete element and merges with the scapula, where it may contribute to the glenoid fossa (Grossman et al., 2002). For this character, it is assumed that in therians and multituberculates, those parts of the glenoid on the coracoid process are homologous to those on the metacoracoid of monotremes, and are thus not considered in determining the shape of the fossa. *Ectypodus* (fig. 8: gl) and *Djadoctatherium* are similar to *Didelphis* in having a circular shaped glenoid fossa without a long axis (state 1). *Ukhaatherium* has an ovoid fossa with the long axis oriented craniocaudally (state 2).

Character 4. *Lateral rim of the glenoid fossa in lateral view: (0) straight, (1) concave. This is character is based on the ventral part of the scapula (part near the humerus) being in direct lateral view.* In monotremes, *Didelphis*, *Nemegtbaatar*, and *Mesodma*, the lateral rim of the glenoid fossa is straight in lateral view (state 0). Based on its occurrence in monotremes, this is presumably the primitive state for Multituberculata. In contrast, the Udan Multi, *Ptilodus*, *Djadochtatherium*, and *Ectypodus* (fig. 8.2) have a lateral rim that is concave and bowed dorsally in lateral view (state 1).

Character 5. *Posterior (caudal) process of the coracoid/metcoracoid: (0) present and points caudally, (1) small and points medially, (2) absent, coracoid process comes to*

a ventral point. In monotremes, the body of the metacoracoid forms a process that projects caudoventrally to approach (i.e. *Ornithorhynchus*) or contact (e.g. *Tachyglossus*) the sternum (state 0). In multituberculates the metacoracoid does not form a distinct element from the scapula. In all multituberculates included in this study for which this region is preserved, except *Kryptobaatar*, the distal end of the coracoid process bears a medially projecting flange, most evident in cranial view of the Udan Multi (fig. 41: cop). As described in characters 2 and 3, rotation of this entire part of the scapula would support the hypothesis that this flange is homologous with the caudally projecting metacoracoid of monotremes. The primary difference is that in these multituberculates the process is small (state 1). In *Kryptobaatar* and *Didelphis* the coracoid process does not have a medially projecting flange on its distal end (state 2), although the coracoid process is much larger in the former taxon.

Character 6. *Ridge for fourth aponeurosis of m.subscapularis on scapula (sensu Kielan-Jaworowska and Gambaryan, 1994): (0) absent, (1) present, on ventral end of medial side and is oriented cranioventrally to caudodorsally (2) present, weakly developed.* As described by Kielan-Jaworowska and Gambarayn (1994: 23), this ridge is located "on the ventral part of the medial side of the blade, lying in prolongation of the coracoid edge, there is a ridge that extends in an arch towards the ventral margin. The ridge is more prominent ventrally than dorsally, with a shallow pit behind it, just above the glenoid fossa". This ridge is labeled with the number 13 in their figure 13H. In this same work they suggested that this ridge is an origin for one of four aponeuroses of the subscapularis muscle (Kielan-Jaworowska and Gambaryan, 1994: 41). Among the outgroups for which this region can be observed, the ridge is entirely absent (state 0) (i.e.

monotremes and *Didelphis*). The ridge is present in all multituberculates included in the matrix (state 1), although it is noticeably less developed in *Nemegtbaatar*. Thus *Nemegtbaatar* is coded as autapomorphic (state 2) for this character.

Character 7. *Supraspinous fossa along anterior margin of scapular blade: (0) absent or rudimentary; (1) present (Rowe, 1988; Sereno, 2006).* Sereno (2006) homologizes the supraspinous fossa in therians with the incipient supraspinous fossa in multituberculates, and this approach is followed here. This incipient supraspinous fossa occurs at the base of the acromion process of the scapula in multituberculates (fig. 8.2: ifo). Based on an embryological study of *Monodelphis*, Sanchez-Villagra and Maier (2003) argued that the supraspinous fossa originated from the dorsal side of the blade and extended ventrally through evolution, unlike the rudimentary ventrally-placed fossa in mutltituberculates. Despite this difference in opinion among authors, because of the coding employed here, which follows (Sereno, 2006), a rudimentary fossa as in multituberculates and no fossa, as in monotremes, is coded the same (state 0). A fully developed supraspinous fossa occurs in *Ukhaatherium* and *Didelphis* (state 1).

Character 8. *Glenoid fossa of scapula, orientation: (0) posterolateral, (1) lateral, (2) posteroventral. (Sereno and McKenna, 1995; Sereno, 2006).* This character has been described in some detail by previous studies, so it will not be discussed any further here.

Character 9. *Procoracoid: (0) present, (1) reduced/fused with manubrium sterni. (Rowe, 1988; Sereno, 2006).* This character has been described in some detail by previous studies, so it will not be discussed any further here.

Character 10. *Interclavicle size: (0) Larger, (1) smaller, than the sternum (anteroposterior and transverse dimensions) (modified from Rowe, 1988; Sereno, 2006).*

This character has been described in some detail by previous studies, so it will not be discussed any further here.

Character 11. *Interclavicle-sternum coossification: (0) absent, (1) present (claviculosternal contact) (Rowe, 1988; Sereno, 2006).* This character has been described in some detail by previous studies, so it will not be discussed any further here.

HUMERUS

Character 12. *Shape of the humeral head in proximal view: (0) round, (1) ovoid, long axis of head oriented craniomedially to caudolaterally, (2) ovoid, long axis of head aligned craniocaudally.* The humeral head is round in *Ukhaatherium*, *Kryptobaatar*, and *Chulsanbaatar* (state 0). An ovoid head with the long axis oriented craniomedially to caudolaterally occurs in *Nemegtbaatar* and the Udan Multi (fig. 42.3: hh). In contrast, an ovoid head with the axis aligned craniocaudally occurs in *Didelphis* and monotremes (state 2). This character is related to, but different from, the degree of humeral torsion as measured by previous authors. Kielan-Jaworowska (1998) and Kielan-Jaworowska and Gambaryan (1994) measured torsion by determining the angle between a line through the epicondyles of the distal humerus and another through the center of the humeral head. In the current character, the orientation of the head is based on the proximal end of the humerus only, with the shaft rotated so that lesser and greater tubercles are facing cranially. The distal end was not used because few multituberculates are represented by humeri that have proximal and distal ends attached.

Character 13. *Fossa between deltopectoral and posterior (caudal) crests of humerus (sensu Poplewski, 1948, cited in Kielan-Jaworowska and Dashzeveg, 1978), the*

latter being the crest centered on the caudal side of the shaft and oriented proximodistally (ordered): (0) absent, (1) well defined, (2) cavernous, undercuts greater tubercle. Based on the reconstruction of Kielan-Jaworowska and Gambaryan (1994) this fossa was the probable origin for a large brachialis muscle. It is absent in monotremes and *Didelphis* (state 0). In contrast, all multituberculates for which this region is preserved have a fossa, although it is either just well defined, as in *Kryptobaatar* (state 1), or cavernous and extending into the body of the greater tubercle, as in the Udan Multi (fig. 42.1), *Chulsanbaatar*, and *Nemegtbaatar* (state 2).

Character 14. *Head of humerus in lateral or medial view: (0) aligned with shaft, (1) offset caudally from shaft.* Whereas nearly all taxa examined in this study have a humeral head that extends caudally beyond the level of the shaft (state 1) (i.e. monotremes, *Ukhaatherium*, *Didelphis*, Udan Multi, *Nemegtbaatar*, and *Chulsanbaatar*), *Kryptobaatar* (fig. 23: hu) is autapomorphic in having the head of the humerus aligned with the shaft (state 0).

Character 15. *Intertubercular (bicipital) groove of humerus, in proximal view: (0) clearly present, (1) absent or poorly defined. (modified from Rowe, 1988).* The intertubercular groove occurs on the proximal end of the humerus between the greater and lesser tubercles. It forms an open channel for the biceps tendon, as seen in the dog (Evans, 1993). When the tubercles are well developed, a clear intertubercular groove occurs, as seen in monotremes, *Zhangheotherium*, *Ukhaatherium*, and the Udan Multi (fig. 42: itg) (state 0). In *Didelphis*, *Nemegtbaatar*, *Kryptobaatar*, and *Chulsanbaatar* the groove is present but is very shallow and poorly defined (state 1). The development of the

groove was determined by observing the humerus in proximal view and comparing the width of the groove (i.e. distance between the tubercles) to its depth.

Character 16. *Cranial projection of greater tuberosity of humerus: (0) absent, (1) present and helps define intertubercular groove, most evident in proximal view.* In *Didelphis* the greater tubercle projects cranially causing the intertubercular groove to look deeper when the humerus is in proximal view (state 1). This cranial projection is not developed in other taxa included in the character/taxon matrix (i.e. Udan Multi, *Kryptobaatar*, *Nemegtbaatar*, *Chulsanbaatar*, and monotremes) (state 0).

Character 17. *Supinator crest (on lateral edge of humerus above ectepicondyle): (0) in cranial or caudal view, the edge of the crest is concave, (1) expanded proximally up the shaft, in cranial or caudal view, the edge of the crest is straight or convex.* In *Ukhaatherium*, *Didelphis*, and the Udan Multi (fig. 43: suc) the lateral edge of the humerus just proximal to the capitulum is sharp and expanded laterally (state 1). In the same taxa, the edge of the humerus is either convex or straight due to its lateral expansion, in cranial and caudal views. On the cranial side of the supinator crest, the humerus is distinctly concave. Kielan-Jaworowska and Gambarayan (1994) reconstructed this concave area as the origins for the extensor carpi radialis longus, extensor carpi radialis brevis, and extensor digitorum communis muscles in multituberculates. In *Kryptobaatar*, *Nemegtbaatar*, *Stygimys*, *Mesodma*, and monotremes the edge is rounded over, not expanded, and concave in cranial view (state 0). In these taxa the origins of the muscles listed above are greatly reduced.

PELVIS

Character 18. *Ischial tuber (i.e. ischiatic tuberosity): (0) present, (1) absent (Ji et al., 2002).* The ischial tuber occurs at the caudodorsal corner of the ischium. It is most pronounced when the dorsal and caudal edges of the ischium and highly concave. A well-developed ischial tuber occurs in *Zhangheotherium*, *Ukhaatherium*, *Kryptobaatar*, *Eucosmodon*, *Ptilodus*, *Ectypodus*, and all monotremes examined. In contrast, a distinct tuber is absent in *Didelphis* and the Udan Multi (fig. 45).

Character 19. *Postobturator notch: (0) absent, (1) present, ischiatic table narrow, (2) absent, ischiatic table wide (Kielan-Jaworowska and Gambaryan, 1994).* The postobturator notch is a feature that has only been observed in multituberculates, and it is a probable synapomorphy of this group (Kielan-Jaworowska and Gambaryan, 1994). It occurs as a shallow to deep notch on the ventrocaudal margin of the ischiu, and the strut of ischium forming the caudal border of the obturator foramen is pinched between the obturator foramen cranially and the postobturator notch caudally. The notch cuts into the dorsoventrally deep symphysis between the ischia. Although Krause and Jenkins (1983) speculated that the notch is preservational remnant of a true foramen, the well preserved pelvis of *Ectypodus* described in the present study confirms that this structure is a notch, not a foramen. Krause and Jenkins (1983) thought the notch and surrounding bone was the origin of an adductor muscle, and Kielan-Jaworowska and Gambaryan (1994) reconstructed the adductor brevis muscle as originating along the margin of the postobturator notch. The notch is absent in all outgroups that have this region preserved, including *Zhangheotherium*, *Ukhaatherium*, *Didelphis*, and all three monotremes (state 0). The postobturator notch is present in all multituberculates examined (i.e.

Kryptobaatar, *Nemegtbaatar*, *Eucosmodon*, *Ptilodus*, *Ectypodus*, *Mesodma* comp) (state 1), except the Udan Multi. The Udan Multi, unlike taxa with state (0), has a very wide ischiatic table (fig. 45: itb), which is the strut of ischium caudal to the postobturator notch. Based on its unique morphology, it was coded as state (2). There does seem to be some variation in the degree of closure of the postobturator notch in multituberculates; however, this variation was not coded because it is unclear how much of the differences are due to poor preservation versus true differences in morphology.

TIBIA

Character 20. *Width of distal epiphysis of tibia (ordered): continuous character, see table 11.* The ratio of the transverse width of the distal epiphysis/its maximum proximodistal depth is greatest in the Udan Multi (2.26), and this taxon is coded as "9" for this character. The same ratio is smallest in *Ptilodus* (1.13), and this taxon is coded as "0" for this character. Intermediate morphologies are coded as indicated in table 11.

Character 21. *Shaft of tibia in lateral or medial view: (0) fairly straight, (1) bowed cranially.* The shaft of tibia is fairly straight in *Didelphis*, *Chulsanbaatar*, *Ptilodus, Ectypodus*, *Mesodma*, and the monotremes examined in the present study. In contrast, the shaft is clearly bowed in the Udan Multi (fig. 62: D2), *Kryptobaatar* (fig. 29), and *Nemegtbaatar* (state 1). The direction that is tibia is bowed in these taxa is sensitive to the orientation of the hind limbs and the view of the observer. If the limbs are held in a in an exact parasagittal orientation, such as in Z-PAL MgM-I/41 (Kielan-Jaworowska and Gambaryan, 1994: fig. 6C), then the tibia is bowed cranially and may

even appear to be bowed slightly medial. In a more natural position, a slight component of the bend may appear to be lateral in direction, although again the vast majority is cranial.

Table. 11. Measurements (in mm) and codings for character 20. See methods for Thiele's (1993) formula. The result from Thiele's formula was rounded to the nearest integer. Abbreviations: A = transverse width of distal epiphysis of tibia; B = proximodistal depth of epiphysis on cranial side, where medial malleous is; Ca- ?*Catopsalis*; Ci- ?*Cimexomys*; Me1- *Mesodma* 1; Me2- *Mesodma* 2; St- *Stygimys*; Di- ?*Didelphodon*.

TAXON	A	B	A/B	Thiele's Result	Codings
Tachyglossus	-	-	-	-	-
Zaglossus	-	-	-	-	-
Ornithorhynchus	-	-	-	-	-
Zhangheotherium	-	-	-	-	-
Ukhaatherium	-	-	-	-	-
Didelphis	6.84	6.01	1.14	0.065	0
"Udan Multi"	7.72	3.41	2.26	9.03	9
Catopsbaatar	-	-	-	-	-
Kryptobaatar	2.41	1.7	1.42	2.29	2
Eucosmodon	7.28	5.97	1.22	0.71	1
Ptilodus	3.59	3.18	1.13	0.00	0
UM Calc. 253^{Ca}	-	-	-	-	-
V5711-111159^{Ca}	-	-	-	-	-
MCZ 20960-1^{Ca}	-	-	-	-	-
MCZ 20960-4^{Ci}	-	-	-	-	-
MCZ 20960-6^{Ci}	-	-	-	-	-
UM Calc. 258^{Me1}	-	-	-	-	-
UMVP 1432^{Me1}	-	-	-	-	-
UM Calc. 171^{Me2}	-	-	-	-	-
UM Calc. 177^{Me2}	-	-	-	-	-
UM Calc. 183St	-	-	-	-	-
MCZ 20784St	-	-	-	-	-
UMVP 1433St	-	-	-	-	-
UCMP 111158^{Di}	-	-	-	-	-

Character 22. *Tibial tuberosity: (0) absent, (1) cranially positioned and not hooked, (2) hooked and its end points distolaterally, (3) hooked and its end points distally (modified from Kielan-Jaworowska and Gambaryan, 1994).* The tibial tuberosity is typically situated on the cranial side of the tibial shaft, originates at the proximal end of the tibia, extends distally for a short distance down the shaft, and is the point of insertion for the quadriceps femoris and biceps femoris muscles in the dog (Evans, 1993) or the ligamentum patellae in man (Schaeffer, 1953). The tibial tuberosity is absent in *Zhangheotherium* (state 0), while a cranially positioned, low tibial tuberosity occurs in *Ukhaatherium*, *Didelphis*, and monotremes. In multituberculates, the medial and lateral tibial condyles for articulation with the femoral condyles are not parasagittal but are instead oriented craniolaterally to caudomedially. The space between the condyles is aligned with a laterally-positioned, elongate, hook-like process (fig. 14, 29, 46: ttu) that is considered here to be homologous to the tibial tuberosity (state 3). This interpretation differs from Kielan-Jaworowska and Gambaryan (1994). They labeled an indistinct region on the cranial face of the tibia as the tuberosity and considered the hook-like process a separate structure (Kielan-Jaworowska and Gambaryan, 1994: fig. 17). The final character state (state 3) is a modification of state 2 and occurs in *Ptilodus*. In this taxon, the tibial process is particularly elongate and its distal end runs parallel to the tibial shaft for a short distance.

Character 23. *Width of tibial shaft (ordered): continuous character, see table 12.* The ratio of maximum length of tibia/minimum transverse diameter of tibial shaft is found in *Didelphis* (16.04), and this taxon is coded as state 9. The smallest value for the

same ratio is found in *Zhangheotherium* (3.96), and this taxon is coded as state 0 for this character. Intermediate morphologies were scored as indicated in table 12.

Table 12. Measurements (in mm) and codings for character 23. See methods for Thiele's (1993) formula. The result from Thiele's formula was rounded to the nearest integer. Abbreviations: A = tibia shaft length; B = minimum transverse diameter of shaft; Ca- ?*Catopsalis*; Ci- ?*Cimexomys*; Me1- *Mesodma* 1; Me2- *Mesodma* 2; St- *Stygimys*; Di- ?*Didelphodon*.

TAXON	A	B	A/B	Thiele's Result	Coding
Tachyglossus	64.4	5.9	11.01	5.26	5
Zaglossus	80.2	7.5	10.75	5.06	5
Ornithorynchus	43.7	4.0	11.00	5.25	5
Zhangheotherium	21	5.3	3.96	0.00	0
Ukhaatherium	21.2	-	-	-	-
Didelphis	90.1	5.6	16.04	8.99	9
"Udan Multi"	40.9	6.9	5.89	1.44	1
Catopsbaatar	-	-	-	-	-
Kryptobaatar	19.7	2.4	8.17	3.14	3
Eucosmodon	-	-	-	-	-
Ptilodus	27.8	2.9	9.59	4.19	4
UM Calc. 253^{Ca}	-	-	-	-	-
V5711-111159^{Ca}	-	-	-	-	-
MCZ 20960-1^{Ca}	-	-	-	-	-
MCZ 20960-4^{Ci}	-	-	-	-	-
MCZ 20960-6^{Ci}	-	-	-	-	-
UM Calc. 258^{Me1}	-	-	-	-	-
UMVP 1432^{Me1}	-	-	-	-	-
UM Calc. 171^{Me2}	-	-	-	-	-
UM Calc. 177^{Me2}	-	-	-	-	-
UM Calc. 183St	-	-	-	-	-
MCZ 20784St	-	-	-	-	-
UMVP 1433St	-	-	-	-	-
UCMP 111158^{Di}	-	-	-	-	-

Character 24. *Lateral articular surface for astragalus on tibia: (0) flat and medial malleolus absent, (1) caudolateral to medial malleolus, (2) crescent-shaped in distal view and cranial part is directly lateral to medial malleolus.* In *Zhangheotherium* the lateral articular surface for the astragalus is flat and the medial malleolus absent (state 0). In contrast, all other taxa examined have a medial malleous, but the morphology of the lateral articular facet varies. In the Udan Multi, *Mesodma*, and tachyglossids the lateral articular facet is flat or slightly concave and is situated caudolateral to the medial malleolus (state 1). In *Didelphis*, *Nemegtbaatar*, *Eucosmodon*, *Ptilodus* and *Ornithorhynchus* the lateral articular surface for the astragalus is crescent-shaped and is situated caudolateral and lateral to the medial malleolus (state 2). This morphology in *Eucosmodon* was described in some detail by Krause and Jenkins (1983). There the lateral articular facet partially spirals around the medial malleolus, facilitating abduction and eversion of the foot.

Character 25. *Length of tibia relative to femur (ordered): continuous character, see table 13.* The maximum value for the ratio of maximum length of the tibia/maximum length of the femur is seen in *Ornithorhynchus* (1.46), which is coded as state 9 for this character. The smallest value for the same ratio is 0.72, which occurs in the Udan Multi (state 0). Intermediate morphologies and their codings are listed in table 13.

Table 13. Measurements (in mm) and codings for character 25. See methods for Thiele's (1993) formula. Abbreviations: A = tibia length; B = length of femur; Ca- ?*Catopsalis*; Ci- ?*Cimexomys*; Me1- *Mesodma* 1; Me2- *Mesodma* 2; St- *Stygimys*; Di- ?*Didelphodon*.

TAXON	A	B	A/B	Thiele's Result	Coding
Tachyglossus	64.4	67.5	0.95	2.85	3
Zaglossus	80.2	71.1	1.13	4.96	5
Ornithorhynchus	43.7	30.0	1.46	8.96	9
Zhangheotherium IVPP7466	23.5	22	1.07	4.23	4
Zhangheotherium CAGS97-07352	21	22	0.95	2.85	3
Ukhaatherium	21.2	17.3	1.22	6.15	6
Didelphis	90.14	86.6	1.04	3.90	4
"Udan Multi"	40.94	56.99	0.72	0.00	0
Catopsbaatar	-	-	-	-	-
Kryptobaatar ZPAL MgM I/41	17.9	24.9	0.72	0.00	0
Kryptobaatar MAE 00-22	19.7	24.1	0.82	1.18	1
Eucosmodon	-	-	-	-	-
Ptilodus	27.8	35.99	0.77	0.63	1
UM Calc. 253^{Ca}	-	-	-	-	-
V5711-111159^{Ca}	-	-	-	-	-
MCZ 20960-1^{Ca}	-	-	-	-	-
MCZ 20960-4^{Ci}	-	-	-	-	-
MCZ 20960-6^{Ci}	-	-	-	-	-
UM Calc. 258^{Me1}	-	-	-	-	-
UMVP 1432^{Me1}	-	-	-	-	-
UM Calc. 171^{Me2}	-	-	-	-	-
UM Calc. 177^{Me2}	-	-	-	-	-
UMVP 1428^{MeCo}	16.33	20.58	0.79	0.89	1
UM Calc. 183St	-	-	-	-	-
MCZ 20784St	-	-	-	-	-
UMVP 1433St	-	-	-	-	-
UCMP 111158^{Di}	-	-	-	-	-

FIBULA

Character 26. *Fibula in craniolateral view: (0) extends distally to same level as tibia, (1) terminates well proximal to distal end of tibia.* In most taxa included the phylogenetic analysis, the fibula is shorter than the tibia. The proximal ends of these bones are approximately aligned, so the distal end of the fibula terminates well proximal to the distal end of the tibia. This morphology occurs in *Zhangheotherium*, *Ukhaatherium*, *Eomaia*, *Didelphis*, Udan Multi (fig. 46: D2, 3), *Kryptobaatar*, *Nemegtbaatar*, and all monotremes, and is best seen in craniolateral view (state 1). Having the fibula shorter than the tibia likely causes the foot to be slightly abducted and everted, unless cartilage or a supernumerary bone, like the lunula ossification of marsupials, fills the gap (Szalay, 1994). In *Ptilodus*, the fibula extends distally to the same level as tibia when viewed cranially, and this morphology optimizes as an autapomorphy of this genus (state 0). Krause and Jenkins (1983) describe a lunule in *Ptilodus* that is situated between the fibula and the lateral astragalotibial facet of the astragalus, and the lunule must thin cranially because it is not visible in cranial view. A fibula that is similar in length to the tibia also occurs in a variety of mammals not included in the matrix (e.g. *Canis*, see Evans, 1993) and presumably these instances are convergent to the morphology observed in *Ptilodus*.

Character 27. *Hook-like lateral process of the fibula (ordered): (0) absent, (1) short, projects from craniolateral side of the proximal end of the fibula and situated just lateral to the articular facet with the tibia, (2) long and its end is recurved to then parallel the shaft for a short distance (modified from Kielan-Jaworowska and*

Gambaryan, 1994). In multituberculates, the lateral side of the proximal end of the fibula has a hook-like process, similar to and positioned caudal to the hook-like tibial tuberosity of the tibia (see character 22). Kielan-Jaworowska and Gambaryan (1994) reconstruct 3 muscles as originating from this process: tibialis anterior from its cranioproximal side, peroneus longus from its caudoproximal side, and the peroneus brevis along its distal side. In the Udan Multi (fig. 46: hlp), *Nemegtbaatar*, and *Chulsanbaatar* the hook-like lateral process of the fibula points laterally and slightly distally (state 1). In *Kryptobaatar* and *Ptilodus* the process is longer and curves so that it runs parallel to the shaft of the tibia for a short distance (state 2). *Zhangheotherium*, *Didelphis*, and monotremes lack a process on this part of the fibula (state 0).

CALCANEUS

Character 28. *Tuber calcis in dorsal view: (0) straight, (1) curved medially.* In most taxa examined in this study, the tuber calcis is fairly straight and projects caudally from the articular region of this bone (e.g. *Eomaia*, *Didelphis*, *Kryptobaatar* (fig. 39: A), *Eucosmodon*, *Ptilodus*, *Stygimys*) (state 0). In the Udan Multi (fig. 47: A), *Catopsbaatar*, *Ukaatherium*, and both echidnas, the tuber calcis is bent so that in dorsal view, its distal end points caudomedially (state 1). This character cannot be coded for taxa that have a very short tuber, such as *Ornithorhynchus*.

Character 29. *Tuber calcis, in dorsal view: (0) widens towards tip, (1) the same width towards tip.* In monotremes and the multituberculates *Catopsbaatar*, Udan Multi (fig. 47:A), *Eucosmodon*, and *Ptilodus* the tuber calcis widens, transversely, at its distal (i.e. caudal) end (state 0). In *Ukhaatherium*, *Didelphis*, *Kryptobaatar* (fig. 39:A),

Stygimys, and *Mesodma* the distal end is approximately the same width at its proximal base (the part adjacent to the calcaneoastragalar facet) (state 1). This character is based on the dorsal face of the tuber calcis, not more plantar portions.

Character 30. *Shallow fossa on caudoplantar corner of medial side of tuber calcis: (0) present, (1) absent.* In *Ptilodus* and several isolated calcanei from North America (e.g. UM Calc.171, UM Calc.186), the medial side of the tuber has a very shallow, small fossa on its caudoplantar corner, just cranial to its tip (state 0). Based on comparison to the dog, this could be the insertion for the superficial digital flexor muscle (Evans, 1993). The fossa is absent in most taxa examined in the present study (state 1) (i.e. monotremes, *Ukhaatherium*, *Didelphis*, Udan Multi, *Catopsbaatar*, *Kryptobaatar*, *Eucosmodon*, *Stygimys*, and *Mesodma*).

Character 31. *Caudal end of tuber calcis in lateral view: (0) convex, (1) almost straight.* The caudal (distal) end of the tuber calcis is convex in some taxa and bowed caudally in lateral view (e.g. *Zaglossus*, *Ornithorhynchus*, *Didelphis*, *Kryptobaatar* (fig. 40: B), *Eucosmodon*, *Ptilodus*) (state 0). In *Tachyglossus*, *Ukhaatherium*, and the multituberculates the Udan Multi (fig. 47: B), *Catopsbaatar*, *Stygimys*, and *Mesodma* the caudal end of the tuber is flat dorsoventrally and thus appears straight in lateral view.

Character 32. *Tuber calcis height, relative to total length of calcaneus (ordered): continuous character, for codings see table 14.* The length of the tuber calcis was measured from the caudal (distal) end of the tuber to the caudal end of the calcaneoastragalar facet, while the maximum craniocaudal length of the calcaneus was taken as this bone's length. The ratio of tuber length/calcaneus length is greatest in *Zaglossus* (0.87), which is coded as state "9". The same ratio is smallest in *Ukhaatherium*

(0.23), which is coded as state "0". Intermediate morphologies and their codings are shown in table 14.

Table 14. Measurements (in mm) and codings for character 32. See methods for Thiele's (1993) formula. The result from Thiele's formula was rounded to the nearest integer. Abbreviations: A = craniocaudal length of tuber calcis; B = length of calcaneus; Ca- ?*Catopsalis*; Ci- ?*Cimexomys*; Me1- *Mesodma* 1; Me2- *Mesodma* 2; St- *Stygimys*; Di- ?*Didelphodon*.

TAXON	A	B	A/B	Thiele's Result	Coding
Tachyglossus	12.5	15.7	0.79	7.88	8
Zaglossus	16.2	18.5	0.87	9.00	9
Ornithorhynchus	4.4	9.2	0.48	3.42	3
Zhangheotherium	2.1	6.5	0.32	1.27	1
Ukhaatherium	0.7	3.0	0.23	0.00	0
Didelphis	6.5	12.2	0.53	4.21	4
"Udan Multi"	5.7	11.4	0.50	3.77	4
Catopsbaatar	5.8	11.6	0.50	3.75	4
Kryptobaatar	2.3	5.0	0.46	3.15	3
Eucosmodon	7.2	15.7	0.46	3.14	3
Ptilodus	3.9	7.9	0.49	3.73	4
UM Calc. 253^{Ca}	-	-	-	-	-
V5711-111159^{Ca}	-	-	-	-	-
MCZ 20960-1^{Ca}	3.8	8.5	0.44	2.96	3
MCZ 20960-4^{Ci}	1.2	3.8	0.32	1.27	1
MCZ 20960-6^{Ci}	1.7	3.8	0.45	3.11	3
UM Calc. 258^{Me1}	1.5	3.8	0.40	2.39	2
UMVP 1432^{Me1}	1.7	4.2	0.41	2.54	3
UM Calc. 171^{Me2}	2.5	4.6	0.55	4.48	5
UM Calc. 177^{Me2}	1.7	4.2	0.41	2.50	3
UM Calc. 183St	-	-	-	-	-
MCZ 20784St	3.9	8.9	0.44	2.94	3
UMVP 1433St	4.5	8.8	0.51	3.95	4
UCMP 111158^{Di}	6.8	12.0	0.56	4.66	5

Character 33. *Peroneus brevis fossa on calcaneus: (0) wide and similar in width along entire length, (1) constricted transversely at the middle of its length, (2) absent.* The peroneus brevis fossa (fig. 47 A1: bf) is a shallow irregular depression bounded medially by the calcaneoastragalar facet and its cranial continuation the dorsiflexion stop (see char. 52), cranially by the raised rim of the cuboid facet, laterally by the trochlear ridge and the peroneal process, and caudally by the cranial ridge (fig. 47 A: cr). The cranial ridge is a low structure that runs craniomedially across the calcaneal body from the lateral border caudal to the peroneal process to just cranial to the caudolateral corner of calcaneoastragalar facet. The peroneus brevis fossa is probably for the attachment of the peroneus brevis muscle. A wide and unrestricted peroneus brevis fossa occurs in *Zhangheotherium*, the Udan Multi, *Catopsbaatar*, and *Kryptobaatar* (state 0). The peroneus brevis fossa also occurs in *Eucomodon* and *Mesodma*, although in these taxa the dorsiflexion stop is wide transversely and constricts the peroneus brevis fossa at the middle of its anteroposterior lengths (state 2). The peroneus brevis fossa is absent in monotremes, *Ukhaatherium*, and *Didelphis* (state 0).

Character 34. *Trochlear ridge of calcaneus (on dorsal surface, medially borders the peroneal groove) (ordered): (0) narrow and high, (1) wide and low, (2) absent.* In multituberculates, a well defined ridge on the dorsal face of the calcaneus medially borders the peroneal groove (fig. 47 A1: trc). Based on its position separating the peroneus brevis fossa, which is likely for the peroneus brevis muscle, and the peroneal groove, which transmits the peroneus longus muscle, it is similar to the variable trochlear process in man (Schaeffer, 1953). Given that the structure in multituberculates is probably not homologous to that in *Homo* and is more of a ridge instead of a process, it is

here called the trochlear ridge. In the Udan Multi and *Catopsbaatar* the trochlear ridges are high and narrow (state 0). A lower and transversely wider trochlear ridge occurs in *Kryptobaatar*, *Eucosmodon*, *Ptilodus*, and *Mesodma* (state 1).The trochlear ridge is absent in monotremes, *Ukhaatherium*, and *Didelphis* (state 2).

Character 35. *Floor of the peroneal groove of calcaneus: (0) visible in dorsal view, (1) not visible in dorsal view, but visible in plantar view.* The floor of the peroneal groove is on the lateral side of the astragalus, between the peroneal process and the trochlear ridge. When the groove is oriented straight dorsoventrally or dorsomedially to plantolaterally then the groove is visible in dorsal view. This occurs in monotremes, *Didelphis*, *Kryptobaatar* (fig. 39: A), and *Ptilodus* (state 0). By contrast, the groove is visible in plantar, but not dorsal view, in *Ukhaatherium* and in the multituberculates *Catopsbaatar*, Udan Multi (fig. 47: A), *Eucosmodon*, *Stygimys*, and *Mesodma* (state 1).

Character 36. *Peroneal process of calcaneus (ordered): (0) cranially and slightly laterally directed, (1) craniolaterally directed, (2) laterally directed (modified from Simmons, 1993).* The peroneal process is a large distinct structure in all multituberculates and projects laterally from the body of the calcaneus near its cranial end. The cranial side of the peroneal process forms the caudal side of the peroneal groove. In *Kryptobaatar* (fig. 39: A), *Eucosmodon*, *Ptilodus*, *Stygimys*, and *Mesodma* the peroneal process is directed cranially (distally) and slightly laterally, causing the peroneal groove to be nearly enclosed cranially (state 0). In *Ukhaatherium*, the Udan Multi (fig. 47: A), and *Catopsbaatar* the peroneal process is directed craniolaterally, and differs from state 0 in being more laterally directed than state 1 (state 0). In monotremes and *Zhangheotherium* the peroneal process is a laterally directed (state 2). *Didelphis*, which

also has a peroneal process, was coded as "?" for this character because it has a broad flange that is neither pointing laterally nor craniolaterally.

Character 37. *Cranial end of peroneal groove of calcaneus: (0) flat or turns smoothly into the cranial face of the calcaneus, (1) forms a laterally projecting tubercle, (2) forms a thickened lip that borders the calcaneocuboid facet.* The lateral side of the cranial end of the calcaneus forms the medial border of the peroneal groove. In most taxa examined in this study, the cranial end of the lateral side of the calcaneus is featureless (state 0), such as in *Ukhaatherium*, *Didelphis*, *Kryptobaatar* (fig. 39: A), *Eucosmodon*, *Ptilodus,* and *Mesodma*. In the Udan Multi, the peroneal groove is well developed and the cranial side of the calcaneus has a concave region that likely articulated with metatarsal V (fig. 47 A1: cm5). Between the peroneal groove and this articulating facet is a laterally projecting tubercle (state 1). In monotremes, the lateral side of the calcaneus ends in a thickened lip that separates an indistinct peroneal groove from the calcaneocuboid facet (state 2).

Character 38. *Cranioplantar side of the peroneal process of calcaneus: (0) convex or gently concave, (1) bears a deep circular fossa.* In nearly all taxa examined in this study (e.g. *Didelphis*, *Kryptobaatar*, *Eucosmodon*, *Stygimys*, and *Mesodma*), the cranial and plantar sides of the peroneal process are either convex or gently concave (state 0). In contrast, the Udan Multi has a unique morphology. The cranioplantar side of the peroneal process bears a deep circular fossa of unknown function (fig. 48 B1: just above "pg") (state 1). Given the orientation of the peroneal groove (see character 35), this fossa is not visible in dorsal view, partially visible in plantar view, and clearly visible in cranial view.

Character 39. *Calcaneal lateral crest/flange (ordered): (0) weakly developed, calcaneal lateral ridge is closely appressed to the body of the calcaneus, (1) present and forms a prominent crest that juts medially away from the calcaneal body, but ends cranial to caudal edge of the calcaneoastragalar facet, (2) present and extends beyond the caudal edge of the calcaneoastragalar facet (modified from Jenkins, 1971, Horovitz, 2000).* This character was briefly described by Jenkins (1971), although he used the term lateral flange instead of lateral crest. Horovitz (2000) described the morphology and reduction of the lateral crest among mammals in some detail, and little needs to be added here. Absence or weak development of the crest occurs in most taxa examined, including monotremes, *Didelphis*, *Kryptobaatar* (fig. 39 A1: lc), *Eucosmodon*, *Ptilodus*, *Stygimys*, and *Mesodma* (state 0). A well developed crest occurs in *Zhangheotherium* and the multituberculates *Catopsbaatar* and the Udan multi, although the morphology slightly differs. In *Zhangheotherium*, the lateral crest extends caudally from the peroneal process and terminates well before reaching the level of the calcaneoastragalar facet (Luo and Ji, 2005: fig. 7) (state 1). In *Catopsalis* and the Udan Multi (fig. 47 A1: lc), the lateral crest is much longer and extends caudally well beyond the calcaneoastragalar facet and borders most of the calcaneal tuber (state 2), converging upon the morphology of *Oligokyphus* (Szalay, 1994) and the Manda cynodont (Jenkins, 1971).

Character 40. *Tip of the peroneal process of calcaneus, if viewed head-on: (0) rounded, (1) ovoid and dorsoplantarly deep, (2) lacks a distinct tip, the process is a long flange, (3) ovoid but long axis is craniocaudal.* This character is based on the calcaneus in lateral or craniolateral view, depending upon the orientation of the peroneal process (see character 36). In *Kryptobaatar*, *Ptilodus*, *Stygimys*, and *Mesodma* the tip of the

peroneal process is round (state 0). In the Udan Multi, *Catopsbaatar*, and *Eucosmodon* the dorsoplantar diameter of the peroneal process is much greater than its craniocaudal diameter, giving it an ovoid shape (state 1). In *Ornithorhynchus*, *Ukhaatherium*, and *Didelphis*, the peroneal process forms a dorsoplantarly flattened, craniocaudally elongate flange (state 2). State 3 occurs in both tachyglossids, and here the peroneal process is rod-like and ovoid but unlike state 1, the craniocaudal diameter is greater than its dorsoplantar diameter.

Character 41. *Calcaneocuboid facet on calcaneus: (0) concave, (1) nearly flat.* In most taxa examined in this study (e.g. *Ukhaatherium*, *Didelphis*, *Eucosmodon*, *Ptilodus*, *Stygimys*, and *Mesodma*) the calcaneocuboid facet is clearly concave (0). Although the calcaneocuboid facet is slightly concave in *Zhangheotherium*, the Udan Multi, and *Kryptobaatar*, it is much less so than taxa with state 0, thus these taxa were coded as state 1.

Character 42. *Long axis of calcaneocuboid facet on calcaneus: (0) oriented caudomedially to craniolaterally, (1) dorsoplantarly, (2) transversely.* The long axis of the calcaenocuboid facet is oriented caudomedial to craniolateral in the Udan Multi (fig. 47), *Kryptobaatar*, *Eucosmodon*, *Ptilodus*, and *Stygimys* (state 0). In contrast, the long axis is dorsoplantar, or nearly 90° from state 0, in *Tachyglossus*, *Ornithorhynchus*, and *Mesodma* (state 1). The long axis of the facet in state 2 is transverse, or orthogonal to the axes in states 0 and 1, and this morphology occurs in *Zhangheotherium*, *Ukhaatherium* and *Didelphis* (state 2). In some taxa the calcaenocuboid facet is nearly round (see character 44), although in all these cases, one axis was slightly longer than the others, and I was able to code character 42.

Character 43. *Calcaneocuboid facet on calcaneus faces: (0) primarily medially, (1) craniomedially, (2) oriented craniomedially and slightly plantarly, (3) cranially (modified from Kielan-Jaworowska and Gambaryan, 1994).* Kielan-Jaworowska and Gambaryan (1994:84) listed a "Mediodistal calcaneocuboid facet" as an autapomorphy of Multituberculata. A medially or craniomedially-facing calcaneocuboid facet on the calcaneus does occur in all multituberculates examined in the present study, although it also occurs in monotremes, raising the possibility that the multituberculate morphology is plesiomorphic. For the present character, the orientation of the calcaneocuboid facet was subdivided into more states. A facet that faces primarily medially, and maybe slightly cranial as well, occurs in *Tachyglossus*, *Ornithorhynchus*, *Eucosmodon*, *Ptilodus*, and *Mesodma* (state 0). In the Udan Multi (fig. 47 B: ccf), *Catopsbaatar*, and *Kryptobaatar* the calcaneocuboid facet faces approximately as much cranial as it does medial, thus craniomedial (state 1). State 2 is similar to state 1 but the calcaneocuboid facet faces slightly plantar as well, so that it is not visible in dorsal view. This morphology occurs in *Ukhaatherium*, *Didelphis*, and *Stygimys* (state 2). In *Zhangheotherium* the calcaneocuboid facet faces directly cranial (state 3).

Character 44. *Shape of the calcaneocuboid facet on the calcaneus: (0) round or nearly so, (1) oval.* In *Ukhaatherium*, *Ptilodus*, and *Mesodma* the calcaneocuboid facet is nearly round when viewed head-on (state 0). The exact view depends upon the direction that this facet faces (see character 43). In the Udan Multi, *Kryptobaatar*, *Eucosmodon*, and *Stygimys* the dorsoplantar axis of the calcaneocuboid facet is noticeably longer giving the entire facet an oval shape (state 1).

Character 45. *Sustentacular and calcaneocuboid facets on calcaneus: (0) only the cranial tip of former contacts the latter, (1) former broadly contacts the latter along its cranial side, (2) do not contact each other.* This character is broadly related to the craniocaudal length of the calcaenus between the sustentacular and calcaneocuboid facets. When this length is substantial, these two facets do not contact each other, as in *Zhangheotherium* and monotremes (state 2). In *Didelphis* and *Stygimys* the two facets are very close to each other and it appears that the cranial tip of the sustentacular facet barely contacts the calcaneocuboid facet (state 0). In the Udan Multi (fig. 47 B1: su and ccf), *Kryptobaatar*, *Eucosmodon*, *Ptilodus*, and *Mesodma* the sustentacular and calcaneocuboid facets share a common edge (state 1).

Character 46. *Shape of sustentacular facet on calcaneus: (0) round, (1) ovoid and craniocaudally elongate.* In nearly all taxa examined in the present study, the sustentacular facet is noticeably ovoid with the long axis oriented approximately craniocaudally (state 1). This state occurs in *Zhangheotherium*, *Ukhaatherium*, *Didelphis*, the Udan Multi (fig. 49 B: su), *Kryptobaatar*, *Eucosmodon*, *Ptilodus*, and *Mesodma*. In *Stygimys* and several isolated calcanei from North America (e.g. UM Calc. 180-183, MCZ 20960-2 and 3) the sustentacular facet is nearly round (state 0).

Character 47. *Sustentacular facet on calcaneus faces: (0) medial, (1) dorsomedially (Schaeffer, 1941, Horovitz, 2000).* This character has been described by previous studies and little needs to be added here except that the derived state "medially and slightly dorsally" differs from that of Horovitz (2000) in stating that the sustentacular facet faces dorsally and medially. In monotremes, *Zhangheotherium*, *Stygimys*, and *Mesodma* the sustentacular facet faces almost entirely medially (state 0). In

Ukhaatherium, *Didelphis*, the Udan Multi (fig. 47 B: su), *Kryptobaatar*, *Eucosmodon* and *Ptilodus* the sustentacular faces dorsomedially (state 1).

Character 48. *In dorsal view, the angle formed if the long axes of the sustentacular and calcaneoastragalar facets are extrapolated (ordered): continuous character, see table 15.* The largest angle was observed in *Didelphis* (35º) and this was coded as state 2. The smallest angle of 8º was observed in an isolated calcaneus from North America (UMVP 1432), which was coded as state 0. Intermediate morphologies and their codings are shown in table 15. This character can not be scored for taxa, such as monotremes, where the sustentacular facet faces medially.

Character 49. *Caudal edge of sustentacular facet on calcaneus: (0) cranial to the caudal edge of the calcaneoastragalar facet on calcaneus, (1) at the same level as the caudal edge of the calcaneoastragalar facet.* This character is based on the calcaneus in dorsal view. In *Zhangheotherium*, *Ukhaatherium*, *Didelphis*, the Udan Multi (fig. 47: A), *Stygimys,* and *Mesodma* the sustentacular facet is craniolateral to the calcaneoastragalar facet (state 0). Thus the caudal edges of both facets are not aligned. In monotremes, *Kryptobaatar*, *Eucosmodon*, and *Ptilodus* the sustentacular facet is lateral to the calcaneoastragalar facet and their caudal edges are aligned (state 1).

Character 50. *Sulcus calcanei (between sustentacular and calcaneoastragalar facets): (0) narrow and crescent-shaped, (1) wide with sustentacular and calcaneoastragalar facets parallel, (2) wide caudally and narrow cranially, (3) absent.* The sulcus calcanei is the nonarticular, slightly depressed area between the sustentacular and calcaneoastragalar facets (fig. 39 A: sc). In monotremes, *Zhangheotherium*, *Kryptobaatar*, *Eucosmodon*, and *Stygimys* the sulcus calcanei is narrow and crescent-

shaped (state 0). The sulcus calcanei is also present in *Ptilodus* and *Mesdoma*, although in these taxa it is wide and rectangular with the medial margin of the calcaneoastragalar facet and the lateral margin of the sustentacular facet parallel to each other. In *Ornithorhynchus* and the Udan Multi (fig. 47 B: sc) the sulcus calcanei widens caudally, with the margins of the calcaneoastragalar and sustentacular facets diverging (state 2). The sulcus calcanei is absent in *Didelphis*, with the sustentacular facet abutting the calcaneoastragalar facet (state 3).

Character 51. *Cranial edge of the sulcus calcanei: (0) extends cranially beyond the cranial edge of the calcaneoastragalar facet, (1) level with the cranial edge of calcaneoastragalar facet.* In monotremes, *Ukhaatherium*, and *Ptilodus* the cranial margin of the sulcus calcanei is cranial to the cranial margin of the calcaneoastragalar facet (state 0). In contrast, the cranial margins of these two facets are roughly aligned in the Udan Multi, *Kryptobaatar*, *Eucosmodon*, *Stygimys*, and *Mesodma* (state 1). In *Didelphis* this character is coded as "-" (inapplicable) because the sulcus calcanei is absent (see character 50).

Character 52. *Relative length of the dorsiflexion stop, which is a smooth, fairly flat area of bone located on the dorsal side just cranial to the calcaneoastragalar facet (ordered): continuous character, see table 16.* The ratio of the craniocaudal length of calcaneoastragalar facet on calcaneus/craniocaudal length of dorsiflexion stop is greatest in *Catopsbaatar* (4.7), which is coded as state 9. The smallest value for the same ratio is 0.8, which is observed in an isolated calcaneus MCZ 20960-4. This morphology is coded as state 0, and intermediate morphologies and their states are listed in table 16. The

character can not be scored for taxa that lack a well-defined dorsiflexion stop, such as monotremes.

Table. 15. Measurements (in degrees) and codings for character 48. See methods for Thiele's (1993) formula. The result from Thiele's formula was rounded to the nearest integer. Given the substantial uncertainty in making this measurement, it was spread across 3 states instead of 9. Abbreviations: A = angle between calcaneoastragalar and sustentacular facets; Ca- ?*Catopsalis*; Ci- ?*Cimexomys*; Me1- *Mesodma* 1; Me2- *Mesodma* 2; St- *Stygimys*; Di- ?*Didelphodon*.

TAXON	**A**	**Thiele's Result**	**Codings**
Zhangheotherium	-	-	-
Ukhaatherium	-	-	-
Didelphis	35	2	2
"Udan Multi"	32	1.7	2
Catopsbaatar	-	-	-
Kryptobaatar	30	1.6	2
Eucosmodon	19	0.8	1
Ptilodus	-	-	-
UM Calc. 253^{Ca}	15	0.5	1
V5711-111159^{Ca}	24	1.2	1
MCZ 20960-1^{Ca}	10	0.1	0
MCZ 20960-4^{Ci}	10	0.1	0
MCZ 20960-6^{Ci}	12	0.3	0
UM Calc. 258^{Me1}	14	0.4	0
UMVP 1432^{Me1}	8	0	0
UM Calc. 171^{Me2}	18	0.7	1
UM Calc. 177^{Me2}	14	0.4	0
UM Calc. 183St	14	0.4	0
MCZ 20784St	11	0.2	0
UMVP 1433St	15	0.5	1
UCMP 111158^{Di}	35	2	2

Table 16. Measurements (in mm) and codings for character 52. See methods for Thiele's (1993) formula. The result from Thiele's formula was rounded to the nearest integer. Abbreviations: A = craniocaudal length of calcaneoastragalar facet on calcaneus; B = length of dorsiflexion stop on calcaneus; Ca- ?*Catopsalis*; Ci- ?*Cimexomys*; Me1- *Mesodma* 1; Me2- *Mesodma* 2; St- *Stygimys*; Di- ?*Didelphodon*.

TAXON	A	B	A/B	Thiele's Result	Coding
Zhangheotherium	2	-	-	-	-
Ukhaatherium	1	0.9	1.1	0.6	1
Didelphis					
"Udan Multi"	4.3	1	4.3	7.9	8
Catopsbaatar	4.3	0.9	4.7	9.0	9
Kryptobaatar	1.5	1.3	1.1	0.6	1
Eucosmodon	4.3	3.4	1.3	0.9	1
Ptilodus	2.0	-	-	-	-
UM Calc. 253^{Ca}	2.7	1.3	2.1	2.9	3
V5711-111159^{Ca}	3.9	1.7	2.3	3.4	3
MCZ 20960-1^{Ca}	3.4	1.5	2.3	3.3	3
MCZ 20960-4^{Ci}	1.0	1.2	0.9	0.0	0
MCZ 20960-6^{Ci}	1.0	0.7	1.4	1.2	1
UM Calc. 258^{Me1}	0.9	0.8	1.0	0.4	0
UMVP 1432^{Me1}	1.3	0.9	1.3	1.1	1
UM Calc. 171^{Me2}	1.3	0.9	1.6	1.6	2
UM Calc. 177^{Me2}	1.4	0.9	1.6	1.7	2
UM Calc. 183St	2.1	1.4	1.4	1.3	1
MCZ 20784St	2.4	2.1	1.1	0.6	1
UMVP 1433St	2.4	1.7	1.4	1.2	1
UCMP 111158^{Di}	4.4	2.4	1.9	2.3	2

Character 53. *Calcaneal body cross-section, at the level of the caudal margin of the calcaneoastragalar facet: (0) wide transversely, (1) narrow transversely (Horovitz, 2000).* For this character the width of the calcaneus is compared to its dorsoplantar depth. In *Ornithorhynchus*, *Ukhaatherium*, the Udan Multi, and *Catopsbaatar* the width the

calcaneus is much greater than its depth (state 0). The opposite occurs in the following taxa with state 1, tachyglossids, *Zhangheotherium*, *Didelphis*, *Kryptobaatar*, *Eucosmodon*, *Ptilodus*, *Stygimys,* and *Mesodma*. For additional details on this character and its distribution across mammaliforms, see Horovitz (2000).

Character 54. *Fibular/lunule contact on calcaneus (ordered): (0) present large, (1) present small, (2) absent (Hu et al., 1997).* In mammals the fibula may contact the calcaneus, the astragalus, or both. In *Eucosmodon*, which has fairly complete right and left pes, the calcaneus has a large articular surface centered on the dorsal side. This surface is divided by a faint longitudinal ridge that separates the calcaneofibular facet on the lateral side from the calcaneoastragalar facet on the medial side. Based on the relation of this ridge to the facets, the presence and size of the calcaneofibular facet can be inferred for the isolated calcanei examined in the present study. Krause and Jenkins (1983) described a lunule between the fibula and the astragalus, and it seems possible that this bone, not the fibula could be contacting the calcaneus is *Ptilodus* and other multituberculates. For the present character, a lunule or fibula contact is not coded separately because of the difficulty in distinguishing these two morphologies in isolated specimens. In *Ornithorhynchus*, *Jeholodens*, *Zhangheotherium*, and *Didelphis* the fibular facet is large, being subequal to or larger than the calcaneoastragalar facet (state 0). The calcaneofibular facet is present but smaller in *Kryptobaatar*, *Eucosmodon*, *Stygimys*, and *Mesdoma*, where it is distinctly smaller than the calcaneoastragalar facet (state 1). In the Udan Multi and *Catopsbaatar* the fibula does not appear to have contacted the calcaneus (state 2). In these two taxa it is possible that a small part of the fibula articulates with the calcaneus, but this does not seem to be the case because there is no ridge subdividing the

large central articular region on the calcaneus, and the lateral side of the astragalus is inflated, which would separate the distal fibula from the calcaneus.

Character 55. *Orientation of the calcaneoastragalar facet relative to the long axis of tuber calcis in dorsal view, (0) craniomedially to caudolaterally, (1) craniocaudally, (2) caudomedially to craniolaterally.* The Udan Multi (fig. 47 A1: caa) and *Catopsbaatar* are distinctive in having the long axis of the calcaneoastragalar facet oriented craniomedial to caudolateral (state 0). Having the calcaneoastragalar facet aligned with the calcaneal tuber and its long axis running craniocaudally occurs in the majority of taxa examined, including *Zhangheotherium*, *Ukhaatherium*, *Kryptobaatar*, *Eucosmodon*, *Stygimys*, and *Mesodma* (state 1). In *Didelphis* the calcaneoastraglar facet is also not aligned with the tuber, although in this case the facet is oriented caudomedial to craniolateral (state 2). This character is distinct from 28 (orientation of caudal end of tuber) because the orientation of the facet is relative to the entire calcaneal tuber, not just its distal end.

Character 56. *Tubercle on proximal edge of sustentacular tali on calcaneus (visible in dorsal or caudal view): (0) absent, (1) present.* In the Udan Multi, *Kryptobaatar*, and *Eucosmodon* there is a low tubercle on the caudoplantar side of the sustentacular tali, at the point where the tali joins the main body of the calcaneus (state 1). In the Udan Multi, the tubercle forms a short ridge that extends distally on the plantar side of the calcaneus. The tubercle is absent in *Ukhaatherium*, *Didelphis*, *Ptilodus* *Stygimys*, and *Mesdoma* (state 0). The function, if any, of this tubercle is unclear, although it could be an attachment point for a ligament that joins the calcaneus to the astragalus or tibia.

Character 57. *Ventrodistal fossa of calcaneus (ventrodistal groove of Horovitz, 2000): (0) well developed, but does not reach the sustentacular facet, (1) fossa elongate and reaches sustentacular facet, (2) well developed, only present next to sustentacular facet, (3) poorly developed or absent (Horovitz, 2000).* Horovitz (2000) referred to this feature as the ventrodistal groove, although fossa is used here because the structures in the taxa examined in the present study are typically wide and shallow, more like fossae than grooves. The ventrodistal fossa/groove occurs just caudal or caudolateral to the calcaneocuboid facet. Szalay and Decker (1974) speculated that the plantar calcaneocuboid ligament may have attached in this fossa. A ventrodistal fossa occurs in most taxa examined in this study, although its size and development varies. In *Tachyglossus*, *Ornithorhynchus*, *Ukhaatherium*, *Eomaia*, the Udan Multi, and *Kryptobaatar* the ventrodistal fossa is present on the plantar side, but there is a distinct area of flat bone between the medial margin of the sustentacular facet and the medial margin of the ventrodistal fossa (state 0). In *Eucosmodon* and *Ptilodus*, the ventrodistal fossa extends medially so that it is just shy of the sustentacular margin (state 1). Even though the sustentacular facet and the ventrodistal facets are on opposite sides of the calcaneus, they converge on the medial edge of the calcaneus. State 2 is similar to state 1 in being adjacent to the sustentacular facet, but the ventrodistal fossa is not situated directly caudal to the calcaneocuboid facet. This morphology occurs in *Didelphis* (state 2). The ventrodistal fossa/groove is absent in *Zaglossus*, *Stygimys*, and *Mesdoma* (state 3).

Character 58. *Cranioplantar tuberosity of the calcaneus, occurs on craniolateral margin of the calcaneocuboid facet and extends onto plantar side: (0) in cranial view,*

wide dorsally but narrows plantarly, (1) same width dorsally and plantarly, (2) absent. The cranioplantar tuberosity is an inflated area of bone that forms the lateral or craniolateral margin of the calcaneocuboid facet (fig. 39: cpt), depending upon the way the calcaneocuboid facet faces (see character 43). It extends to some degree onto the plantar side of the calcaneus and is situated cranial to the ventrodistal fossa, if the latter is present. In *Kryptobaatar* and *Eucosmodon* the cranioplantar tuberosity is widest dorsally and narrows plantarly, when the calcaneus is in cranial (distal) view (state 0). In contrast, the tubersosity appears to be the same width dorsally and plantarly in *Zhangheotherium*, *Ukhaatherium*, and the Udan Multi (state 1). The cranioplantar tuberosity is absent in monotremes, *Didelphis*, *Stygimys*, and *Mesodma* (state 2). In multituberculates the cranioplantar tuberosity is often smooth and likely articulates with metatarsal V.

ASTRAGALUS

Character 59. *Buttress and astragalonavicular articular surface on astragalus: (0) as seen in plantar view, do not contact each other, (1) contact each other, in caudal view, the buttress can be seen to be deflected plantarly, (2) buttress absent.* In multituberculates, the astragalar foramen is near the caudal edge of the bone. The arch of bone that encircles the foramen and protrudes from the caudal side of the astragalus is called the astragalar buttress (fig. 36 A: ab). The astragalonavicular facet starts on the cranial side of the astragalus, extends medially onto the medial side of the astragalus, and then curves caudolaterally to approach the base of the buttress. In plantar view, the astragalonavicular facet and the buttress are clearly separate in the Udan Multi (fig. 50 B:

an and ab), *Kryptobaatar*, *Ptilodus*, and *Ectypodus* (state 0). In contrast, the caudolateral end of the astragalonavicular facet just touches the medial side of the base of the buttress in *Stygimys* (state 1). This condition appears to be the result of a ventral deflection of the entire buttress, best seen with the astragalus in caudal view. The buttress is absent in most mammals, including tachyglossids, *Jeholodens*, *Zhangheotherium*, *Ukhaatherium*, *Eomaia*, and *Didelphis* (state 3).

Character 60. *The shape of the buttress on astragalus: (0) square in dorsal and plantar views, bears a groove on its caudal side that is oriented dorsoplantarly, (1) square in dorsal and plantar views, bears a groove on its caudal side that is oriented laterodorsally to medioplantarly, (2) arched and rounded in dorsal and plantar views, no groove on the caudal side.* The profile of the astragalar buttress in dorsal or plantar view varies depending on whether a short groove occurs on its caudal face. In *Kryptobaatar* (fig. 38: A), *Ptilodus*, *Ectypodus*, and *Stygimys* there is a short, dorsoplantarly oriented groove on the caudal face of the buttress. The groove causes the caudal side to have distinct caudolateral and caudomedial corners, giving the buttress an overall square shape (state 0). The buttress is also square in two isolated astragali from North America (UA Astr. 29 and UM Astr. 262), but in these taxa the groove is oriented laterodorsally to medioplantarly (state 1). In the Udan Multi the groove is absent and the caudal face of the buttress is convex. As a result, the buttress is more arched and rounded in dorsal or plantar views (state 2). This character could not be coded for taxa that lack a buttress (see character 59).

Character 61. *Groove between buttress and calcaneoastragalar facet in plantar view of astragalus: (0) absent, (1) present.* In *Kryptobaatar* (fig. 36: B) and *Mesodma* the

caudal end of the calcaneoastragalar facet is upturned and this borders a shallow transverse groove that separates the facet from the lateral base of the astragalar buttress (state 1). In contrast, the groove is absent in the Udan Multi, *Eucosmodon*, *Ptilodus*, and *Ectypodus* (state 0). This character cannot be scored for taxa that lack a buttress.

Character 62. *Position of ridge defining caudal edge of tibial articular surface on astragalus (ordered): (0) in cranial position, well separate from astragalar foramen, with a small fossa between the two, (1) in caudal position along the edge of the astragalar foramen, fossa absent, (2) no foramen, but fossa present.* With the astragalus in dorsal view, the caudal edge of the tibial articular surface is defined either by a faint ridge, a slight change in elevation, or a change in the smoothness of the bone. This character codes for the position of the caudal edge and whether it is partially defined by a fossa that is caudal to it. If the astragalar foramen is absent, state 0 and 1 are based on the distance between the tibial articular surface and the caudal edge separating the dorsal and plantar sides of the astragalus. In monotremes, the Udan Multi, *Kryptobaatar*, and *Stygimys* the tibia articular surface is well separate from the astragalar foramen, and a shallow fossa occurs caudal to the articular surface and runs transversely, paralleling the surface's caudal edge (state 0). In *Eucosmodon*, *Ptilodus*, and *Ectypodus* the tibial articular surface is extended caudally so that it terminates just cranial to the astragalar foramen, and there is no space for a transverse fossa (state 1). *Didelphis* lacks an astragalar foramen but the caudal edge of the tibial articular surface is defined by a fossa. This morphology is coded as state 2.

Character 63. *Caudolateral surface of astragalus: (0) has a groove that laterally borders the buttress and then a flat or slightly convex area lateral to this groove, (1) a*

broad, flat or slightly concave region, (2) a distinctly concave region that helps to define the caudolateral process of the astragalus, (3) strongly convex and articulates with fibula. The caudolateral part of the astragalus is situated lateral to the astragalar foramen and/or buttress and caudal to the calcaneoastragalar facet. In the Udan Multi (fig. 51: B), the caudolateral surface is separated from the lateral base of the buttress by a distinct dorsoplantar groove (state 0). The caudolateral surface, which is directly lateral to the groove is slightly convex. State 1 is similar to state 0 except that the groove is absent. This morphology occurs in *Kryptobaatar*, *Eucosmodon*, *Ptilodus*, and *Stygimys* (state 1). In *Ectypodus* (fig. 17.1) the caudolateral surface is concave transversely and helps form a distinct caudolateral process of the astragalus (fig. 16.2: clp) (state 2). In monotremes the entire caudolateral region of the astragalus is highly convex and articulates with the fibula (state 3).

Character 64. *Lateral astragalotibial facet on astragalus (ordered): (0) convex, (1) concave transversely but flat craniocaudally, (2) pulley-shaped, concave transversely and convex craniocaudally.* The tibial facet is divided into two parts, a medial part that articulates with the medial malleolus or homologous region of the tibia, and the remaining lateral part that is usually, but not always, more elevated. In monotremes, *Jeholodens*, *Ukhaatherium*, *Didelphis*, the Udan Multi (fig. 50 A: atil), *Kryptobaatar*, and *Ptilodus* the lateral tibial facet is convex and rounded (state 0). This type of articulation would allow for considerable movement at the upper tarsal joint. In *Eucosmodon* and *Stygimys* the lateral facet is flat craniocaudally and concave transversely (state 1). The astragalus of *Ectypodus* (fig. 15.1: atil) displays a highly derived lateral tibial facet, at least as compared to other multituberculates. The facet is pulley-shaped, being concave

transversely and convex craniocaudally (state 2). A pulley-shaped/trochleated lateral tibial articular surface is common in eutherian mammals and is best developed in cursorial taxa (Schaeffer, 1947), where it severely limits horizontal movement. However, the occurrence of this feature in *Ectypodus* should not be construed as indicating this taxon was cursorial. For one thing, the trochlea in *Ectypodus* is much shallower than in cursorial eutherians, and for another, the lower tarsal joint, as indicated by the astragalonavicular facet, allows wide rotation in a transverse plane (see character 78).

Character 65. *Medial and lateral astragalotibial facets on astragalus (ordered): (0) confluent, and distal end of tibia is smoothly curved, (1) poorly developed ridge, with distal end of tibia having a corresponding groove, (2) separated by a distinct ridge, distal end of tibia has a distinct corresponding groove, (3) medial tibial facet faces medially.* As described in character 64, the tibial articular surface of the astragalus can be divided into medial and lateral facets. In tachyglossids, the Udan Multi, *Kryptobaatar* (fig. 36 A: atil and atim), and *Ptilodus* the two facets are confluent and the exact division between the two is somewhat arbitrary (state 0). The corresponding surface on the tibia is smooth and undulatory. Two isolated astragali from North America (i.e. UMVP 263 and UM Calc 262) have a faint craniocaudal ridge on the astragalus, best seen when light is reflected off the dorsal surface (state 1). Although the tibia is not known for either specimen, it is expected that it would bear a shallow groove to receive this ridge. *Didelphis*, *Eucosmodon*, *Ectypodus* (fig. 16.1: atil and atim), and *Stygimys* have a prominent ridge that separates dorsally facing medial and lateral tibial facets, indicating that transverse movement of the upper ankle joint was limited (state 2). The morphology of other aspects of this joint varies among the taxa coded as state 2, although these

features are considered separate, independent characters (i.e. characters 64 and 66). A detailed discussion of the upper tarsal joint in *Eucosmodon*, and its functional implications, can be found in Krause and Jenkins (1983). In *Ornithorhynchus* and *Ukhaatherium* the ridge is present, but more importantly the medial tibial facet faces medially (state 3). In *Ukaatherium* and other eutherians the morphology represented by state 3 is one component of the tenon-mortise upper-ankle joint (Szalay, 1984).

Character 66. *Medial astragalotibial facet on astragalus: (0) flat or nearly so, (1) distinctly concave.* The medial astragalotibial facet (see descriptions of characters 64, 65) is typically flat or slightly concave (state 0). This morphology occurs in *Ukhaatherium*, *Didelphis*, the Udan Multi, *Kryptobaatar* (fig. 36 A: atim), *Ptilodus*, and *Ectypodus*. In contrast, the medial facet is distinctly concave transversally in *Eucosmodon* and *Stygimys* (state 1). Although part of the concavity in these taxa is likely related to the ridge separating the medial and lateral tibial facets, which was coded in character 65, the concavity is considered a separate character because it extends to the medial side of the medial astragalotibial facet as well.

Character 67. *Position of sustentacular facet on astragalus: (0) more plantarly positioned and its medial edge borders a steep, cliff-like, medially-facing astragalonavicular facet, (1) more dorsally positioned, astragalonavicular facet appears sloped.* The sustentacular facet is the craniomedial of two articulation surfaces between the astragalus and the calcaneus. Among the taxa examined in the current study, its position, dorsoplantarly, can best be described by referring to the astragalonavicular facet, which wraps around the pedestal supporting the sustentacular facet. In *Zaglossus*, the Udan Multi (fig. 52: B), and *Stygimys* the sustentacular is more plantarly positioned

(state 0), and this results in the profile of the astragalonavicular facet to appear steeper and more medially-facing, when viewed cranially. In *Didelphis*, *Kryptobaatar*, *Eucosmodon*, *Ptilodus*, and *Ectypodus* the sustentacular is more dorsally positioned, and as a result, the profile of the astragalonavicular facet is more sloped.

Character 68. *Shape of sustentacular facet on astragalus: (0) elongate craniocaudal strip, (1) circular, (2) ovoid.* The sustentacular facet in monotremes is rectangular, being long craniocaudally and narrow transversally (state 0). By contrast, the same facet is nearly circular in *Kryptobaatar* (fig. 36: su), *Ptilodus*, and *Stygimys* (state 1). *Ukhaatherium*, *Didelphis*, the Udan Multi, *Eucosmodon*, and *Ectypodus* (fig. 16.2: su) have an ovoid facet (state 2) that is similar in shape to those in state 1, but the long axis is craniocaudal, similar to state 0.

Character 69. *Lateral edge of the calcaneoastragalar facet on astragalus in plantar view (ordered): (0) convex, (1) straight, (2) concave.* In *Zaglossus*, *Ornithorhynchus*, *Ukhaatherium*, and *Ectypodus* (fig. 16.2: caa) the lateral margin of the calcaneoastragalar facet is convex and bowed laterally (state 0). By contrast, *Tachyglossus*, the Udan Multi, *Kryptobaatar* (fig. 36 B: caa), *Eucosmodon* and *Stygimys* have a lateral margin that is straight or nearly so (state 1). State 2 is the opposite of state 0 and occurs in *Didelphis*.

Character 70. *Craniomedial corner of the astragalus: (0) protrudes, (1) does not protrude.* This character relates to the craniomedial corner of the astragalus in multituberculates that is visible in dorsal view, which corresponds to the craniomedial corner of the medial tibial articular surface in all mammals. In *Didelphis*, the Udan Multi, *Kryptobaatar*, *Ectypodus* (fig. 16.1), and *Stygimys* the craniomedial corner protrudes

(state 0). This morphology is correlated with an astragalonavicular facet that faces more plantarly. In *Ukhaatherium* and *Ptilodus* the craniomedial corner does not noticeably protrude (state 1).

Character 71. *Sustentacular and calcaneoastragalar facets of astragalus: (0) run parallel to each other, (1) if the long axes are extrapolated, form an acute angle, calcaneoastragalar facet oriented caudolaterally to craniomedially.* In all taxa examined in this study, the long axis of the calcaneoastragalar facet is oriented more or less craniocaudally. In some taxa the sustentacular facet is nearly round, making it difficult to determine the long axis, although even in these situations (i.e. character 69, state 2), it generally appears that the craniocaudal axis is the longest one. In most taxa examined in this study, both facets are oriented craniocaudally and run parallel (state 0), as is seen in monotremes, *Didelphis*, the Udan Multi (fig. 50: caa and su), *Kryptobaatar*, *Eucosmodon*, and *Ptilodus*. By contrast, in *Stygimys* and particularly in *Ectypodus* (fig. 16.2: caa and su) the calcaneoastragalar facet is shifted so that its long axis is not strictly craniocaudal, but instead is angled caudolateral to craniomedial (state 1). Thus if the long axes of both facets were extrapolated, they would meet to form an acute angle cranial to the astragalus.

Character 72. *Caudomedial corner of dorsal surface of astragalus: (0) does not protrude, (1) protrudes and forms what may be homologous to the astragalar medial plantar tuberosity.* In *Zaglossus*, *Zhangheotherium*, *Kryptobaatar*, *Ectypodus* (fig. 16.1), and *Stygimys* the caudomedial corner of the astragalus is not inflated, meaning that in dorsal view the junction of the caudal and medial sides forms a 90° or obtuse angle and that the plantar side is not expanded into a distinct tuberosity (state 0). By contrast, the

caudomedial corner is inflated in *Tachyglossus*, *Ornithorhynchus*, *Ukhaatherium*, *Eomaia*, *Didelphis*, the Udan Multi (fig. 50: A), *Eucosmodon*, and *Ptilodus* (state 1). The inflation in taxa like *Ukhaatherium* and *Didelphis* is on the plantar side and is commonly called the astragalar medial plantar tuberosity (e.g. Szalay, 1994).

Character 73. *Nonarticulating groove between medial astragalotibial facet and astragalonavicular facet: (0) present, (1) absent, a thick lip separates the two facets, (2) absent, a thin lip separates the two facets.* In multituberculates, the astragalonavicular facet is on the cranial and medial side of the astragalus and the medial astragalotibial facet is on the dorsal side, and these two facets approach each other on the dorsocranial and dorsomedial edges of the astragalus. In therians and monotremes, the morphologies of the astragali are significantly different causing the astragalonavicular facet to be closest to the medial astragalotibial facet on the cranial or medial side, but not both. A nonarticulating groove or fossa separates the two fossae on the dorsocranial edge in *Ornithoryhnchus*, the dorsomedial edge in both tachyglossids, the dorsocranial edge in *Didelphis*, and the dorsocranial and craniomedial edges in *Ptilodus* (all coded as state 0). In *Kryptobaatar* (fig. 38 B: atim and an) and *Stygimys*, the groove is absent and instead the dorsocranial and dorsomedial edges of the astragali are thickened to form a lip (state 1). A similar lip occurs in the Udan Multi and *Ectypodus* (fig. 16.2: atim and an), although in these taxa the lip is thin (state 2).

Character 74. *Interarticular bulge of astragalus (located caudomedial to the sustentacular facet) (ordered): (0) absent, (1) present and very low, (2) present and high but not undercut, (3) prominent bulge that is undercut by the interarticular sulcus.* When present, the interarticular bulge occurs on the plantar side of the astragalus and is

craniomedial to the plantar opening of the astragalar canal and caudolateral to the sustentacular facet (fig. 16.2: iab). In plantar view, the bulge is convex and may parallel the interarticular sulcus for a short distance. The bulge is most prominent in *Stygimys* (state 3), and in this taxon the bulge is undercut laterally by the interarticular sulcus. In the Udan Multi, the bulge is similarly high, but is not undercut (state 2). A weakly developed and low bulge occurs in *Kryptobaatar* (fig. 36 B: iab), *Eucosmodon*, and *Ectypodus* (state 1), while it is absent in *Didelphis* and monotremes (state 0).

Character 75. *Astragalar foramen in dorsal view (ordered): (0) large, (1) medium, (2) small, (3) absent.* The astragalar canal is a widespread feature in mammals, although its function remains unknown (Schaeffer, 1947). The size of the astragalar foramen on the dorsal side of the astragalus is described qualitatively in this character and compared to the size of the surrounding astragalar buttress. In the Udan Multi (fig. 50 A: ac) the astragalar foramen is large and its diameter exceeds the width of the osseous arch (i.e. buttress) on its medial, lateral, and caudal sides (state 0). The astragalar foramen is smaller in *Kryptobaatar*, *Eucosmodon*, *Ectypodus*, and *Stygimys*, having a diameter less than the thickness of the surrounding bone (state 1). In *Ptilodus* the bone around the foramen is much thicker than the diameter of the foramen (state 2), while the astragalar foramen is absent in monotremes and *Didelphis* (state 3).

Character 76. *Astragalar canal in plantar view: (0) small, (1) large.* This character is based on the size of the plantar opening of the astragalar canal. The codings for this and the preceding characters are quite different, indicating that they are independent characters. In the Udan Multi (fig. 50 B: ac), *Kryptobaatar*, and *Stygimys* the plantar astragalar foramen is large allowing the entire length of the canal, including the

dorsal foramen, to be visible in plantar view (state 0). The plantar astragalar foramen is much smaller in *Ukhaatherium*, *Eucosmodon*, *Ptilodus* and *Ectypodus* (state 0).

Character 77. *Sustentacular facet of astragalus orientation: (0) faces plantolaterally but more plantarly than laterally, (1) faces plantolaterally but more laterally than plantarly.* This character is subtle and best coded by comparing the morphologies among taxa. In *Ukhaatherium*, *Didelphis*, *Ectypodus*, and *Stygimys* the sustentacular faces more plantarly than laterally (state 0). By contrast, in monotremes, the Udan Multi, *Kryptobaatar*, *Eucosmodon*, and *Ptilodus* the sustentacular faces more laterally than plantarly (state 1).

Character 78. *Location of astragalonavicular facet on astragalus (ordered): (0) extends from the cranial to the medioplantar side of the astragalus, astragalus lacks a neck, (1) restricted to cranial side of astragalus, astragalus lacks a neck, (2) on cranial side of astragalus and astragalus has a well or weakly developed neck (Ji et al., 1999; Luo et al., 2003).* The present character formulation takes a conservative approach and combines characters treated as independent by Luo et al (2003: 214 and 217). Their character 214 coded for the presence or absence of the astragalar neck and 217 coded for the expansion of the astragalonavicular facet onto the medial side. Readers are referred to the above cited publications for more details regarding these characters. For the present character, monotremes and all multituberculates are coded as state 0, lacking a neck but having the astragalonavicular facet wrap around onto the medial side. State 1, lacking the neck and medial expansion of the facet, occurs in *Jeholodens* and *Zhangheotherium*. In *Ukhaatherium*, *Eomaia*, and *Didelphis* the astragalonavicular facet is primarily on the cranial side of the astragalus and a well-developed neck is present (state 2).

Character 79. *Astragalonavicular facet on astragalus: (0) saddle-shaped, concave dorsoplantarly and convex transversally, occurs on cranial and the medial sides, (1) convex transversally and flat to convex dorsoplantarly, occurs on cranial and the medial sides, (2) restricted to cranial side, (3) forms a complex interlocking joint, lateral portion is concave but medial portion convex (modified from Kielan-Jaworowska and Gambaryan, 1994).* Kielan-Jaworowska and Gambarayan (1994) stated that a saddle-shaped astragalonavicular facet on the astragalus is a synapomorphy of Multituberculata (state 0 of the present character). I can confirm that this morphology occurs in all multituberculate astragali examined (fig. 38 B: an), as well as in the monotreme *Zaglossus*. In *Tachyglossus* and *Didelphis* the astragalonavicular facet has a similar position on the astragalus as in state 0, but it is flat to convex dorsoplantarly (state 1). In *Zhangheotherium*, *Eomaia*, and *Ukhaatherium* the astragalonavicular facet is restricted to the cranial side only (state 2), while in *Ornithorhynchus* it forms a complex interlocking joint with the navicular (state 3).

Character 80. *Sustentacular facet relative to the calcaneoastragalar facet: (0) medial to calcaneoastragalar facet, (1) primarily cranial to it, but also slightly medial.* In monotremes, the Udan Multi (fig. 50 B: caa and su), *Kryptobaatar*, *Eucosmodon*, *Ptilodus*, *Ectypodus*, and *Stygimys* the sustentacular facet is situated near and medial to the calcaneoastragalar facet. By contrast, in *Ukhaatherium*, *Eomaia*, and *Didelphis* the sustentacular facet is well separated from and craniomedial to the calcaneoastragalar facet. This is partially related to the fact that these taxa have an astragalar neck, which is one component of character 79, because the development of the astragalar neck allows for the space between the sustentacular and the astragalonavicular facet to develop.

However, it is still considered a separate character because the development of the neck does not require that the sustentacular facet shift its position.

CUBOID

Character 81. *Dorsoplantar diameter of cuboid in lateral view: (0) greater than proximodistal length, (1) less than proximodistal length.* This character is based on the cuboid being oriented with the foot plantigrade and the animal in a standing position. In this orientation, proximodistal = craniocaudal. State 0, having the dorsoplantar diameter greater than the proximodistal length, occurs only in the Udan Multi. In all the rest of the taxa for which this character could be scored (e.g. *Tachyglossus*, *Ornithorhynchus*, *Didelphis*, *Kryptobaatar*, *Eucosmodon* and *Ptilodus*), the dorsoplantar diameter is less than the proximodistal length (state 1). The maximum proximodistal length and greatest dorsoplantar diameter were considered when scoring taxa for this character.

Character 82. *Transverse width of the cuboid in dorsal view (ordered): (0) greater than proximodistal length, (1) equal to proximodistal length, (2) less than proximodistal length.* As with the previous character, the maximum dimensions of the cuboid were considered. In the Udan Multi (fig. 53 B: cu), the cuboid is rectangular in shape with the transverse width greater than its proximodistal length (state 0). The cuboid is roughly square-shaped in *Catopsbaatar*, with subequal transverse and proximodistal dimensions (state 1). In *Tachyglossus*, *Ornithorhynchus*, *Didelphis*, *Kryptobaatar*, *Chulsanbaatar*, *Eucosmodon*, and *Ptilodus* the cuboid is rectangular, although unlike state 0 the proximodistal length is greater than the transverse width. Although the

functional significance of this character is unclear, a proximodistally long cuboid occurs in some cursorial mammals (e.g. *Canis*, Evans, 1993).

Character 83. *Groove for tendon of peroneus longus on cuboid, located just plantar to articular surface for metatarsals IV and V: (0) extends slightly onto lateral side, (1) restricted to plantar side.* On the cuboid of *Eucosmodon*, Szalay (1994: fig. 5.10A) referred to a short, dorsoplantar groove near the cranio(disto)plantar corner of the lateral side as the groove for the tendon of the peroneus longus muscle. Following the figure of Szalay (1994) and confirmed by inspection of the actual specimen, *Eucosmodon* is coded as state 0 for this character. By contrast, the groove is restricted to the plantar side of the cuboid in *Didelphis* and the Udan Multi (state 1).

Character 84. *Articular surface for metatarsal V on cuboid: (0) concave dorsoplantarly, (1) flat in all directions.* The distal (cranial) face of the cuboid has an articular surface for metatarsal V (state 0). In *Tachyglossus*, *Eucosmodon*, and *Ptilodus* this facet is concave dorsoplantarly, potentially allowing for greater flexion of the foot. In *Ornithorhynchus*, *Didelphis*, and the Udan Multi this facet is flat (state 1).

Character 85. *Nonarticular area on lateral side of cuboid between contact for calcaneus and craniolateral corner (ordered): (0) narrow and very deep, (1) narrow and shallow, (2) wide and shallow.* In *Eucosmodon* the lateral side of the cuboid has a broad and shallow nonarticular area between the calcaneocuboid facet and the edge formed by the junction of the cranial and lateral sides (state 2). In *Didelphis* (state 1) a similar nonarticular area occurs, although it much narrower than in state 2. The cuboid of the Udan Multi is highly unusual as compared to other taxa examined in the present study. Its cuboid is roughly diamond-shaped, and the proximal and lateral sides are merged to form

a single proximolateral-facing side. The most notable feature of this side is a very deep, dorsoplantarly-oriented groove (fig. 54 B: cu) that occurs lateral to the calcaneocuboid facet (state 2).

NAVICULAR

Character 87. *Dorsal end of astragalar contact as compared to plantar end, with navicular in medial or lateral view (ordered): (0) taller than plantar end, (1) same height as plantar end, (2) shorter than plantar end.* The astragalonavicular articular surface on the navicular is usually concave dorsoplantarly with elevated dorsal and plantar margins. This character codes for which margin is more elevated. In an animal with a plantigrade foot, "taller" means that the edge extends more proximally/caudally, in dorsal view. The dorsal end is taller than the plantar end in *Kryptobaatar*, *Eucosmodon*, and *Ectypodus* (fig. 18: A) (state 0). The dorsal and plantar ends are subequal in *Ornithorhynchus*, *Didelphis*, and the Udan Multi (fig. 54 A: na) (state 1). *Ptilodus* has the opposite condition from state 0. Here the plantar end is taller than the dorsal end (state 2).

Character 88. *Dorsoplantar groove on the medial side of the navicular: (0) present, (1) absent.* In *Eucosmodon*, *Ptilodus*, and *Ectypodus* (fig. 18: A2) there is a short, non-articular, dorsoplantar groove on the medial side of the navicular between the astragalonavicular facet and the facet for the mesocuneiform (state 0). This groove is absent in *Tachyglossus*, *Ornithorhynchus*, *Didelphis*, and the Udan Multi (state 1).

ECTOCUNEIFORM

Character 89. *Contact surface for navicular on ectocuneiform: (0) concave dorsoplantarly and fairly flat transversely, (1) flat dorsoplantarly and transversely, (2) convex transversely, morphology along dorsoplantar axis unclear.* The contact surface for the navicular facet is concave dorsoplantarly (fig. 18 B2: nfe) but nearly flat transversely in *Eucosmodon* and *Ectypodus* (state 0). This morphology is best seen in lateral or medial view. In *Ornithorhynchus*, *Didelphis*, and the Udan Multi the facet is fairly flat in all directions. The ectocuneiform of *Ptilodus* is only visible in dorsal view, making it difficult to determine its shape dorsoplantarly. However, in dorsal view it can be seen that it is strongly convex transversely (state 2).

MESOCUNEIFORM

Character 90. *Size of mesocuneiform in dorsal view: (0) small, proximodistal length is less than 75% of that of the ectocuneiform, (1) proximodistal lengths of meso- and ectocuneiforms are subequal.* A small mesocuneiform occurs in *Tachyglossus*, *Zhangheotherium*, *Didelphis*, *Catopsbaatar*, *Kryptobaatar*, *Chulsanbaatar*, *Eucosmodon*, and *Ptilodus*. By contrast, a much larger mesocuneiform that is subequal in length to the ectocuneiform occurs in *Ornithorhynchus* and the Udan Multi (fig. 53 B: mc).

ENTOCUNEIFORM

Character 91. *Contact for navicular on entocuneiform: (0) concave, large, and bowl-shaped with sharp medial and lateral edges, (1) weakly concave, small, and defined by broad rounded-over edges.* The proximal (caudal) face of the entocuneiform articulates with the navicular. In the Udan Multi, the articulation facet is large and clearly concave with sharp edges delimiting the articular facet (state 0). The navicular facet in *Ornithorhynchus*, *Didelphis*, *Eucosmodon*, and *Ptilodus* is also concave, although much less so than in the Udan Multi (fig. 55 B: ent), and the edges are low, thick, and rounded-over (state 1).

METATARSALS

Character 92. *Dorsal sides of distal ends of metatarsals II through V: (0) each bears a distinct pit just proximal to the distal articular facet, (1) pits are absent, may have a shallow transverse trough instead.* In the Udan Multi (fig. 55: A) there is a small but distinct circular put on the dorsal side of each metatarsal (fig. 53 A: mt1-4), just proximal to the distal articular facet for the proximal phalanx (state 0). In the other taxa examined in this study (i.e. *Tachyglossus*, *Ornithorhynchus*, *Didelphis*, *Kryptobaatar* (fig. 35), *Eucosmodon*, and *Ptilodus*) these pits are absent, although there may be a shallow transverse trough that parallels the edge of the articular facet for the proximal phalanx.

Character 93. *Length of metatarsal V measured relative to metatarsal IV (ordered): continuous character, see table 17.* The length of metatarsal V/length of metatarsal IV is greatest in *Ornithoryhnchus* (1.17), which is coded as state 9. The same

ratio is smallest in *Ptilodus* (0.68), which is coded as state 0. Intermediate morphologies and their states are listed in table 17.

Character 94. *Proximal end of metatarsal V: (0) dorsal face faces directly dorsally, (1) dorsal face actually faces dorsolaterally.* In *Tachyglossus*, *Didelphis*, *Eucosmodon*, *Ptilodus*, and *Ectypodus* (fig. 20.2) the proximal end of metatarsal V faces dorsally (state 0), while in *Ornithorhynchus*, the Udan Multi (fig. 57.1), and *Kryptobaatar* the dorsal side is turned to face dorsolaterally (state 1).

Character 95. *Peroneal process of metatarsal V: (0) absent, (1) at the proximal end of metatarsal V, (2) distal to the proximal end.* The peroneal process of metatarsal V is the attachment site for the peroneus longus muscle, which in eutherian mammals acts to flex and evert the foot (Evans, 1993; Schaeffer, 1953). Despite previous assertions, the size of the peroneal process is not correlated with grasping ability (Sargis et al., 2007). The process projects laterally from the shaft of the metatarsal V. In *Eucosmodon*, *Ptilodus*, and *Ectypodus* (fig. 20.4) the peroneal process is most visible because it is clearly separate from the proximal end of the metatarsal (state 2). The peroneal process also occurs in *Eomaia*, *Didelphis*, the Udan Multi (fig. 57), *Kryptobaatar* and *Chulsanbaatar*, although in these taxa the process is at the proximal end (i.e. base) and causes it to appear much wider than normal (state 1). The peroneal process is absent in *Tachyglossus*, *Ornithorhynchus*, *Jeholodens*, and *Zhangheotherium* (state 0).

Table 17. Measurements (in mm) and codings for character 93. See methods for Thiele's (1993) formula. The result from Thiele's formula was rounded to the nearest integer. Abbreviations: A = length of metatarsal V; B = length of metatarsal IV; Ca- ?*Catopsalis*; Ci- ?*Cimexomys*; Me1- *Mesodma* 1; Me2- *Mesodma* 2; St- *Stygimys*; Di- ?*Didelphodon*.

TAXON	A	B	A/B	Thiele's Result	Codings
Tachyglossus	10.6	9.6	1.10	7.77	8
Ornithoryhnchus	12.7	10.8	1.17	9.01	9
Zhangheotherium	5.8	5.7	1.02	6.25	6
Ukhaatherium	-	-	-	-	-
Didelphis	13	18	0.72	0.94	1
"Udan Multi"	10.41	11.87	0.88	3.73	4
Catopsbaatar	-	11.47	-	-	-
Kryptobaatar ZPAL MgM I/41	5.4	7.3	0.74	1.26	1
Kryptobaatar MAE 00-22	4.91	7.29	0.67	0.06	1
Eucosmodon	13.62	15.99	0.85	3.27	3
Ptilodus	7.35	10.83	0.68	0.16	0
UM Calc. 253^{Ca}	-	-	-	-	-
V5711-111159^{Ca}	-	-	-	-	-
MCZ 20960-1^{Ca}	-	-	-	-	-
MCZ 20960-4^{Ci}	-	-	-	-	-
MCZ 20960-6^{Ci}	-	-	-	-	-
UM Calc. 258^{Me1}	-	-	-	-	-
UMVP 1432^{Me1}	-	-	-	-	-
UM Calc. 171^{Me2}	-	-	-	-	-
UM Calc. 177^{Me2}	-	-	-	-	-
UMVP 1428^{MeCo}	-	-	-	-	-
UM Calc. 183St	-	-	-	-	-
MCZ 20784St	-	-	-	-	-
UMVP 1433St	-	-	-	-	-
UCMP 111158^{Di}	-	-	-	-	-

METHODS

As mentioned in the CHARACTERS section, seven characters (i.e. 20, 23, 25, 32, 48, 52, 93) displaying continuous variation were coded using Thiele's formula (Thiele, 1993), which incorporates the relative values of the traits as well as their magnitudes. Each of these 7 characters codes for the relative size of a feature as expressed by a ratio between two measurements. To determine the coding for a character, the ratio for a single taxon was put into the following formula…

$$\text{Character state for taxon A} = n * [(\text{Ratio}_A - \text{Ratio}_{min}) / (\text{Ratio}_{max} - \text{Ratio}_{min})]$$

Where n is the total number of available states, x is the ratio for taxon A, Ratio_{min} is the minimum ratio for all taxa in the matrix, Ratio_{max} is the maximum ratio for all the taxa in the matrix. Since the program NONA (Goloboff, 1994) was used to find most parsimonious trees, n was 9, the number of states available in this program minus one (although n = 3 for character 48, see table 15). Other programs with more states could have been used, but ten seemed sufficient to cover the variation in the fairly small matrix analyzed here. One problem with using Thiele characters is that the minimum length for these characters is 9, while that for most other characters, which are binary, is one. This gives too much weight to continuous characters in the phylogenetic analyses, so all other characters were given a weight of nine, following a suggestion by Wiens (2001). Tree lengths were then divided by 9 so that a change from one state to the other in a binary

character was one step. This caused some of tree lengths and Bremer support values to be non-integers.

Most parsimonious trees were found using the computer program NONA (Goloboff, 1994) and some support analyses were conducted in PAUP* (Swofford, 2002). With NONA, TBR (tree bisection and reconnection) branch swapping was done on trees found by 1,000 random-taxon-addition heuristic searches using the following commands: *mult*1000* and *max**. Lists for unequivocal apomorphies for nodes common to all most parsimonious trees was generated using the command *apo/*. Given the fairly small number of OTU's and the small number of most parsimonious trees found, more exhaustive heuristic searches were not needed, although for the TAX analysis (see below), the heuristic result was confirmed by a branch and bound analysis conducted in PAUP*.

Two separate phylogenetic analyses were conducted, and although the number of OTU's differed, *both analyses included the same 95 postcranial characters* described in Appendix I. The first analysis, referred to as TAX for taxa, included all taxa with postcranial data, while isolated specimens were excluded (19 OTU's). The second analysis, called the ALL analysis because all OTU's in Appendix 2 were included, has all the taxa from the TAX analysis as well as 3 isolated astragali and 16 isolated calcanei. The character/taxon matrix for the ALL analysis is shown in Appendix 2. The matrix for the TAX analysis is the same as that in Appendix 2, except all non-bolded taxa were excluded.

Support for individual nodes in the strict consensus of most parsimonious trees was quantified using Bremer support (Bremer, 1988, 1994) and bootstrap percentages

(Felsenstein, 1985). Bremer support analyses were done in PAUP* with command files generated and processed using the program TreeRot (Sorenson, 1996). The command files from TreeRot were changed following the suggestions of Geisler (2001). For the ALL analysis, two different reduced cladistic consensus trees (Wilkinson, 1994) were generated from all most parsimonious trees. The first reduced consensus included all OTU's coded for features of the calcaneus (25 OTU's), including isolated calcanei but excluding isolated astragali. The second reduced consensus included all OTU's that were coded for astragali characters (16 OTU's); therefore, isolated astragali were retained while isolated calcanei were pruned from all most parsimonious trees. This was done because some of unresolved nodes in the strict consensus of the ALL analysis were the result of isolated calcanei and astragali having non-overlapping character codings, and generating the reduced consensus yielded much better resolved trees. The two reduced consensus trees were then used to generate two command files in TreeRot, essentially using a simplified version of the methodology of double decay analyses (Wilkinson et al., 2000). Each command file was executed separately, and while all OTU's were included in the analyses, the constraints generated by TreeRot were loaded as backbone constraints. So for the reduced cladistic consensus that included all taxa coded for the calcaneus, a clade was considered monophyletic in suboptimal trees even if an isolated astragalus moved in and out of it. Similarly, for the reduced cladistic consensus that included all taxa with an astragalus, a clade was considered monophyletic in suboptimal trees even if an isolated calcaneus moved in and out of it. By comparing the strict consensus and the Bremer support values for its nodes to the reduced consensus trees and the Bremer support values for their nodes, it can be determined whether missing data (i.e.

non-overlapping character codings) or homoplasy is primarily responsible for the lack of resolution and low support in the strict consensus for the ALL analysis.

Bootstrap percentages were derived from most parsimonious trees from 1000 bootstrap replicates. Uninformative characters were removed from data matrices before conducting bootstrap analyses, removing the small affects that these characters can have as shown by previous studies (Harshman, 1994; Carpenter, 1996).

Two phylogenetic hypotheses were evaluated using the postcranial data collected in the present study: that of Rougier et al (1997) and a composite phylogeny from Kielan-Jaworowska and Hurum (2001, 1997), the earlier paper providing the phylogeny within Djadochtatheroidea. The relationships among outgroups for the "Rougier et al. tree" were based on Rougier et al. (1996c)**,** while the relationships for the "Kielan-Jaworowska and Hurum tree" were based on the analysis of Luo et al. (2002) where they constrained monophyly of Multituberculata and Haramiyida. Kielan-Jaworowska and Hurum (2001) considered Haramiyida to be the most likely sister-group to Multituberculata. Both of these studies included many more taxa than the current study, so their trees were pruned until the taxon sampling matched that of the current study. Previous phylogenies understandably did not include the undescribed Udan Multi, so it was placed in the phylogenetic position of the djadochtatheroid *Tombaatar*, which it is very closely related to (Spurlin et al., 2000; Rougier et al., in prep). In the tree of Kielan-Jaworowska and Hurum (2001), the relationships among several cimolodontan families were not resolved. To map characters onto their tree, branches were manually moved to resolve the node within Cimolodonta, and the arrangement that was most parsimonious according to the dataset set of the present study was selected. This was not difficult to do by hand because

only three unresolved lineages joined at the politomy. For their tree, Taeniolabidoidea was placed closer to Eucosmodontidae than to Djadochtatheroidea.

RESULTS

TAX (TAXON) ANALYSIS

The heuristic analyses in NONA and the branch-and-bound analyses in PAUP found three most parsimonious trees, each 243.9 steps (2195/9) in length. Several taxa are monophyletic in the strict consensus of these three trees: Tachyglossidae, Monotremata, Theria, Trechnotheria, and Multituberculata (fig. 58). There is also a clade of Mongolian multituberculates (fig. 58: Mm); however, Djadochtatheroidea is not an appropriate name for this clade as its type genus, *Djadochtatherium*, is in a clade with North American taxa. Most clades have relatively low Bremer support and bootstrap values, although there are a few exceptions. The best supported clades are Monotremata (fig. 58: Mo) and Theriiformes, with Bremer support values of 3.2 and a bootstrap of 90%. The value for both clades is the same because this is the position of the root of the trees. Other well supported clades include Tachyglossidae (Bremer support= 1.9, Bootstrap= 82%), Multituberculata (2, 79%), and the Udan Multi + *Catopsbaatar* (0.8, 64%). Some of the low support values could be caused by the inclusion of taxa with large amounts of missing data. To determine if this was the case, the three taxa with the largest number of missing entries (i.e. those not bolded in fig. 58) were pruned from the constraint trees developed with TreeRot, and then these trees were employed as backbone constraints. Specifically the taxa excluded in this form of a double decay analysis were *Jeholodens* (only coded for 8 characters), *Chulsanbaatar* (coded for 14), and *Djadochtatherium*

(coded for just 6). Overall this has little effect on most nodes except for Multituberculata, where the Bremer support increased from 3.7 to 5.7 steps.

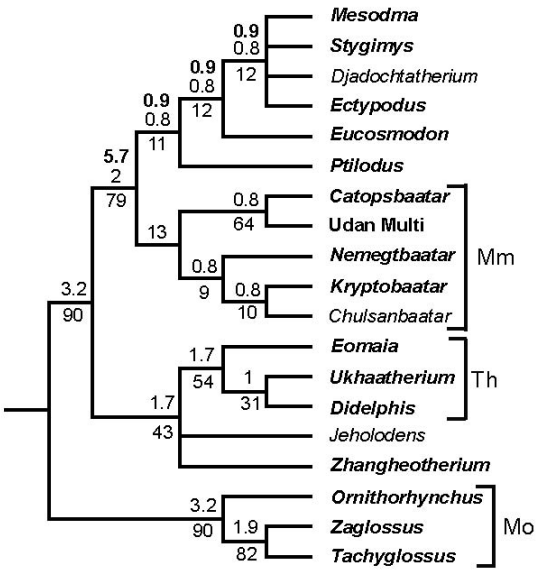

Fig. 58. Results of phylogenetic analyses of the postcranial data in appendix II with isolated specimens excluded (i.e. TAX analysis). Shown here is a strict consensus of 3 most parsimonious trees, each 243.9 (2195/9) steps in length. Bremer support values are placed above each node and bootstrap percentages are placed below. As with tree lengths, Bremer support values were divided by 9. Taxonomic abbreviations: **Th**, Theria; **Mm**, Mongolian Late Cretaceous Multituberculates Clade; **Mo,** Monotremata.

ALL ANALYSIS

Heuristic analyses in NONA recovered 848 most parsimonious trees, each 325.4 steps (2929/9) in length. As in the TAX analysis, Tachyglossidae, Monotremata, Trechnotheria, and Multituberculata are monophyletic in the strict consensus (fig. 59). However, the phylogeny within Multituberculata is very different. *Kryptobaatar* no longer groups with other Mongolian taxa but is instead is closer to a clade of primarily North America taxa. In the TAX analysis, *Ptilodus* was the most basal member of a North America clade of multituberculates, while in the ALL analysis, it is in a more apical position. The vast majority of isolated calcanei and astragali from the Bug Creek Anthills fauna form a large unresolved clade, except for two calcanei that form a clade that branches off between *Ptilodus* and a *Djadochtatherium* + *Eucosmodon* + *Ectypodus* clade. Based on size, age, and geographic distribution, this clade may represent species of *Catopsalis* (fig. 59: ?Ca]. Three clades were well supported: Tachyglossidae (Bremer support = 2.6 steps, bootstrap = 79%), Monotremata, and Theriiformes (both 3.1, 92%). The remaining clades occurred in < 50% of bootstrap replicates and have a Bremer support of 1 or less.

The low support values were expected since the analysis included isolated calcanei and astragali, which have completely non-overlapping character codings. To determine the affect this had on the support values and the number of most parsimonious trees, the constraint trees for Bremer support created by TreeRot were modified into two sets (see METHODS). The first set only includes those taxa and specimens that are coded for most of the calcaneal characters (25 OTU's). The second set includes only those taxa

and specimens that could be coded for most of the astragalar characters (16 OTU's). Two reduced cladistic consensus trees were created from the pool of 848 most parsimonious trees using these two sets of taxa. When OTU's that did not have the calcaneus coded were pruned in PAUP, all trees reduced to 5 different topologies, with the strict consensus having all but one node fully resolved (fig. 60). At the base of Multituberculata is an isolated calcaneus from the Bushy Tailed Blowout exposure of the Lance Formation (Niobara County, Wyoming), that based on morphology is very similar to stagodontid marsupials described by Szalay (1993). Two calcanei, which based on size and stratigraphic occurrence may belong to *Cimexomys* (fig. 60: ?Ci) formed the sister-group to three calcanei that likely represent one or more species of *Stygimys* (fig. 60: ?St). Small calcanei from the Bug Creek Anthills fauna that based on size and morphology could be referred to *Mesodma* sp. are paraphyletic and arranged as stem taxa to the ?*Cimexomys* and *Stygimys* clade. The Bremer support values in this reduced cladistic consensus tree were similar to those in the strict consensus. Nodes not present in the strict consensus including all taxa (fig. 59) were relatively weakly supported (i.e. Bremer support < 1) with one notable exception. An Udan Multi + Catopsbaatar clade had a Bremer support of 5.9, and even though it did not occur in the strict consensus with all taxa, it did occur in 79% of bootstrap replicates.

When all taxa that lack astragali or are coded for few astragalar characters were pruned from the 848 most parsimonious trees, only 6 distinct trees are left. The strict consensus of these trees only varies in the position on an isolated astragalus (USNM 2984) from the type locality of the Lance Formation (fig. 61). In some of the trees this specimen is more closely related to Multituberculata while in others it is closer to

Theriiformes. Astragali from the Bug Creek Anthills fauna form two clades that are sister-groups to each other. Based on size and morphology, one of these is probably *Mesodma* (UM Astr. 262 and UA Astr. 29) while the other is likely *Stygimys* (*Stygimys* and UM Astr. 263). Bremer support values are on average slightly higher than when all taxa are included (i.e. fig. 59).

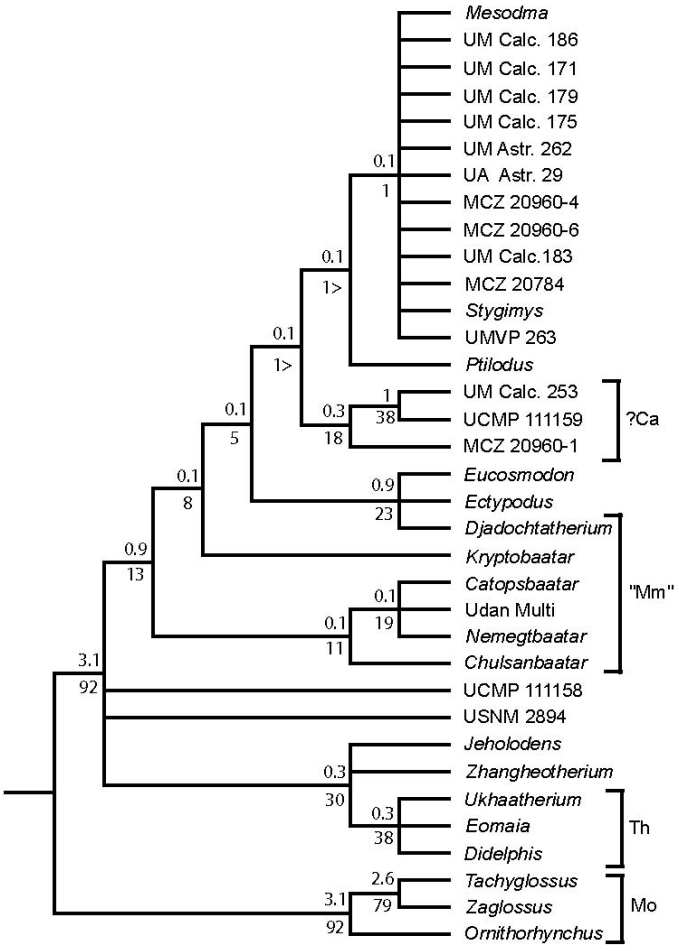

Fig. 59. Results of phylogenetic analyses of the postcranial data in appendix II (ALL analysis). Shown here is a strict consensus of 848 most parsimonious trees, each 325.4 steps (2929/9) in length. Bremer support values are placed above each node and bootstrap percentages are placed below. As with tree lengths, Bremer support values were divided by 9. Taxonomic abbreviations: **?Ca**, ?*Catopsalis*; **Th**, Theria; "**Mm"**, Paraphyletic Mongolian Late Cretaceous Multituberculates Clade; **Mo,** Monotremata.

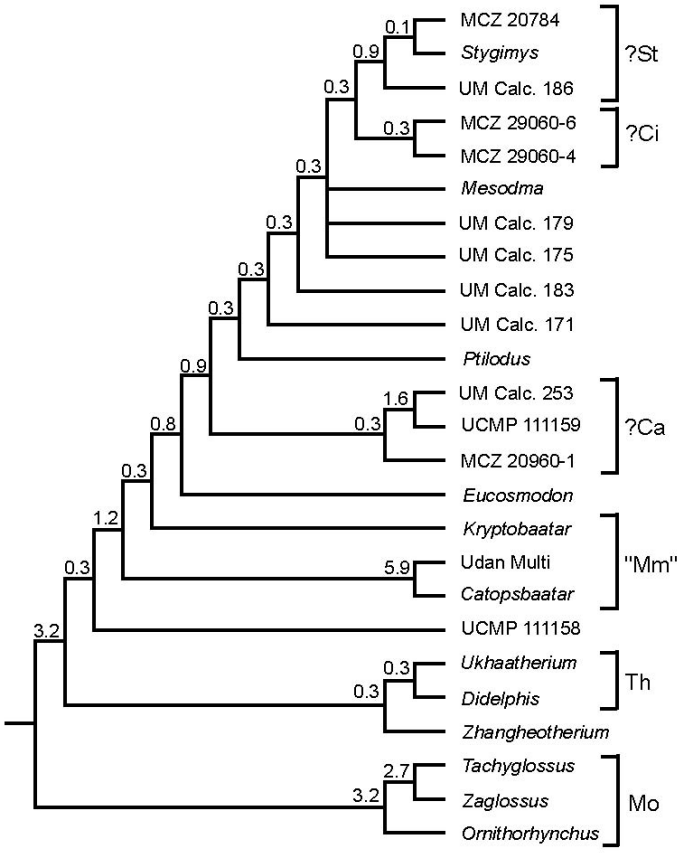

Fig. 60. Reduced cladistic consensus of the 848 most parsimonious trees from the ALL analysis. Taxa without character codings for calcanei were pruned from all most parsimonious trees, leaving 5 distinct trees of which this is the strict consensus. Double decay values with the subset of taxa shown here are placed above each node. As with tree lengths, double decay values were divided by 9. Taxonomic abbreviations: **?Ca**, ?*Catopsalis*; **?Ci**, ?*Cimexomys*; **?St**, *Stygimys*, **Th**, Theria; "**Mm"**, Paraphyletic Mongolian Late Cretaceous Multituberculates Clade; **Mo,** Monotremata.

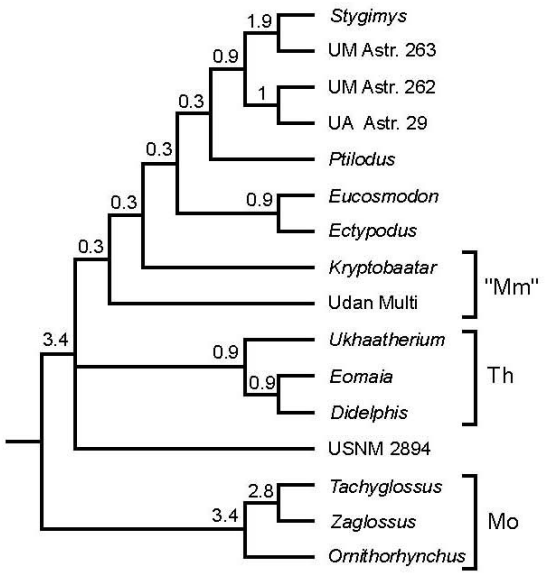

Fig. 61. Reduced cladistic consensus of the 848 most parsimonious trees from the ALL analysis. Taxa without character codings for astragali were pruned from all most parsimonious trees, leaving 6 distinct trees of which this is the strict consensus. Double decay values with the subset of taxa shown here are placed above each node. As with tree lengths, double decay values were divided by 9. Taxonomic abbreviations: **Th**, Theria; "**Mm"**, Paraphyletic Mongolian Late Cretaceous Multituberculates Clade; **Mo,** Monotremata.

PREVIOUS HYPOTHESES

Two composite previous hypotheses were evaluated with the TAX matrix. The composite phylogeny of Kielan-Jaworowska and Hurum (1997, 2001) was 263.7 (2374/9) or 19.8 (179/9) steps longer than the most parsimonious trees from the TAX analysis (fig. 62: B). The hypothesis of Rougier et al. (1997) was much more congruent with the current dataset (fig. 62: A). It was 254.7 (2292/9) steps, or 10.7 (97/9) steps longer than the shortest trees for this matrix.

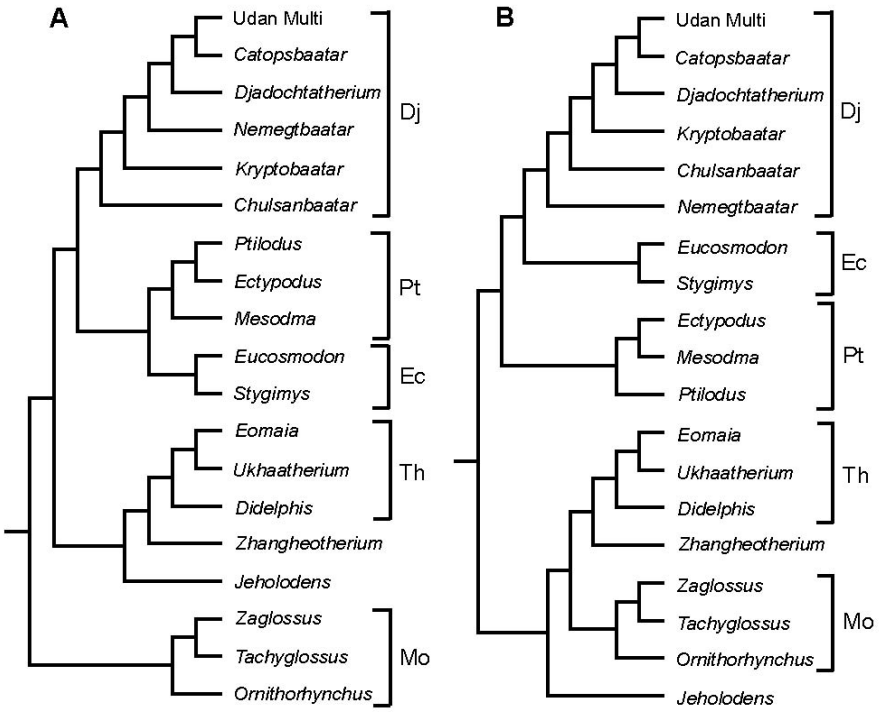

Fig. 62. Simplified versions of phylogenetic trees from previous studies evaluated with the postcranial data in Appendix II. **(A)** The shortest tree that is also consistent with a simplified version of the phylogeny of Kielan-Jaworowska and Hurum (1997, 2001), with outgroup relationships from Luo et al. (2002).Tree length = 263.7 (2374/9) or 19.8 (179/9) steps longer than the most parsimonious trees from the TAX analysis. **(B)** Simplified cladogram from Rougier et al, (1997) with outgroups relationships from Rougier et al. (1996c). Tree length = 254.7 (2292/9) steps, or 10.7 (97/9) steps longer than the shortest trees for this matrix.

DISCUSSION

EVALUATION OF MULTITUBERCULATE AUTAPOMORPHIES

Although not the main focus of the present study, the analyses conducted allowed for previously suggested postcranial synapomorphies of Multituberculata to be evaluated. Kielan-Jaworowska and Gambaryan (1994) listed 18 postcranial autapomorphies of Multituberculata based on their own work as well as that of previous authors (i.e. Granger and Simpson, 1929; Krause and Jenkins, 1983; Szalay, 1993; Sereno and McKenna, 1990). Of the 18 characters they listed, I was able to confirm five to six of them in some of the phylogenetic analyses (the characters coding for the peroneal process and groove in their study are here not considered independent): presence of postobturator notch, hook-like lateral process of tibia (considered here to be the homologue of the tibial tuberosity), hook-like lateral process of fibula, craniolaterally directed peroneal process of the calcaneus, and calcaneocuboid facet faces distomedially,. Although their other characters were not directly evaluated in the parsimony analyses, less formal observations corroborate some of them. Based on observations of the new specimens described in the present study, five other characters Kielan-Jaworowska and Gambaryan (1994) listed are likely autapomorphies of Multituberculata: long ischiopubic symphysis with ventral keel, medially protruding and plate-like lesser trochanter of femur, posttrochanter fossa of femur, contact or close approximation of metatarsal V and calcaneus, and astragalar buttress.

Five of the characters Kielan-Jaworowska and Gambaryan (1994) listed seem questionable: process-like ischial tuber, dorsoventrally oriented ilium/sacrum contact,

subtrochanter tubercle of femur, saddle-shaped astragalonavicular facet, and horizontal astragalonavicular joint. An ischial tuberosity occurs in *Ukhaatherium* but does not occur in the Udan Multi; however, one aspect of this character may turn out to be a multituberculate synapomorphy if the depth of the ischial notch, and not the tuber itself, is focused on instead. The contact between the ilium and sacrum does not appear to be dorsoventrally oriented in the multituberculates studied here, and the subtrochanter tubercle of the femur is absent in the Udan Multi, although this may be a reversal. Two of the synapomorphies listed by Kielan-Jaworowska and Gambaryan (1994) relate to the astragalonavicular facet. The first, saddle-shaped astragalonavicular facet, also occurs in the monotreme *Zaglossus*, and is here interpreted as the plesiomorphic condition. The other monotremes studied here (i.e. *Ornithorhynchus* and *Tachyglossus*) have different morphologies. In *Ornithorhynchus*, the astragalonavicular facet is a complex, interlocking joint, which is here interpreted as an autapomorphy of this genus. *Tachyglossus* has an astragalonavicular facet of the astragalus that is similar to metatherians, like *Didelphis*, in being convex dorsoplantarly and convex transversally; however, under the most parsimonious trees in the present study this morphology is interpreted as convergent. The second putative synapomorphy of this joint listed by Kielan-Jaworowska and Gambaryan (1994), astragalonavicular joint oriented so that movement is horizontal with abduction and adduction, occurs in all three monotremes studied here, and is considered a plesiomorphy of multituberculates, not a synapomorphy.

In addition to previously suggested autapomorphies for Multituberculata, I propose 8 more (Appendices 3 and 4): the main axis of the calcaneocuboid facet on the calcaneus is oriented caudodorsally to cranioplantarly (ALL analysis only), tip of

peroneal process is rounded (TAX analysis only), small fibular/lunule contact on calcaneus (ALL only), wide peroneus brevis fossa of the calcaneus (ALL only), sustentacular and calcaneocuboid facets contact each other (TAX only), trochlear ridge of calcaneus is wide and low (TAX and ALL), the cranial edge of the sulcus calcanei is level with calcaneoastragalar facet (ALL only), and short tibia (TAX only) (see Table 13 for a quantitative description of a short tibia). The large number of synapomorphies for Multituberculata is consistent with the relatively high support this clade received in the TAX analysis: Multituberculata was in 79% of bootstrap replicates (the 3rd highest value) and had a Bremer support of 2. The Bremer support increased to 5.7 when taxa with a high % of missing data were ignored, which is nearly twice as the next best supported node (fig. 58). Thus monophyly of Multituberculata is well supported by postcranial characters, mirroring the large number of dental autapomorphies that diagnose this clade (Kielan-Jaworoska et al., 2004).

PHYLOGENY WITHIN MULTITUBERCULATA

Traditionally, *Ectypodus* was placed in the Ptilodontoidea, a result supported by recent phylogenetic analyses (i.e. Simmons, 2993; Rougier et al., 1997). It is somewhat surprising then that the TAX and ALL analyses place *Ectypodus* as more closely related to *Eucosmodon* than to *Ptilodus* (figs. 58, 59). Two characters in particular, support a close relationship between *Stygimys* and *Ectypodus* to the exclusion of *Eucosmodon* in the TAX analysis: long axes of sustentacular and calcaneoastragalar facets on astragalus are not parallel, and sustentacular facet of astragalus facing plantarly. This is surprising

because historically *Eucomodon* and *Stygimys*, but not *Ectypodus*, were placed in the family Eucomodontidae (fig. 62: Ec). By far the most intriguing character supporting a clade including *Stygimys*, *Eucosmodon*, and *Ectypodus* but not *Ptilodus* is the morphology of the astragalotibial joint.

Krause and Jenkins (1983) created a composite reconstruction of the multituberculate ankle using the partially articulated skeleton of *Ptilodus* and the disarticulated foot of *Eucosmodon*. However, closer inspection of these specimens reveals that these taxa have very different morphologies for the distal tibia. *Eucosmodon* has well-developed, convex lateral and medial condyles of the tibia that fit into distinct, concave facets on the dorsal surface of the astragalus. Although the dorsal side of the astragalus is not visible in the type of *Ptilodus kummae*, the distal end of the left tibia is. It shows a single, concave articular surface without clear medial and lateral condyles. This morphology is very similar to that observed in the Udan Multi and corresponds to a dorsal surface of the astragalus that is gently convex laterally but concave medially (fig. 46 C, 50 A). The new specimen of *Ectypodus* sp. from the Bangtail II quarry has a highly specialized astragalotibial joint. The lateral astragalotibial articular surface on the astragalus is pulley-shaped and the medial astragalotibial surface is concave (fig. 16.1). Although unique, this morphology shares clear similarities with that seen in *Eucosmodon* and *Stygimys*, and a transversely concave lateral astragalotibial articular surface on the astragalus is one of the characters supporting the clade including *Eucosmodon*, *Ectypodus*, and *Stygimys.*

In the TAX analysis and to a lesser extent in the ALL analysis, several Mongolian multituberculates form a clade to the exclusion of North American taxa (fig. 58: Mm).

Previously, a similar clade was named Djadochtatheria by Kielan-Jaworowska and Hurum (1997) and then changed to Djadochtatheroidea by Kielan-Jaworowska and Hurum (2001); however, these names are not appropriate for the clade recovered in the present study because its namesake, *Djadochtatherium*, is instead in a clade with North American taxa. So I refer to this grouping as the Mongolian Late Cretaceous Multituberculates Clade (MLCM), which was an informal name previously used by Kielan-Jaworowska and Hurum (1997). In the TAX analysis, all Mongolian taxa form an exclusive clade, except for *Djadochtatherium*, while in the ALL analysis, *Kryptobaatar* is excluded as well (fig. 59: "Mm"). In the TAX analysis, 8 characters are optimized as synapomorphies of the MLCM (Appendix 3): wide distal epiphysis of the tibia, cranially bowed tibia, tibial shaft is wide as compared to its length (see Table 12), calcaneocuboid facet faces craniomedially, tubercle on proximal end of sustentacular shelf of calcaneus, cavernous astragalar foramen, and proximal end of metatarsal V faces dorsolaterally. For most of these characters, only a few Mongolian multituberculates could be coded, so it is important to discover and describe additional specimens to test the validity of these synapomorphies. One of these putative synapomorphies, a cranially bowed tibia, does not occur in *Chulsanbaatar* (Kielan-Jaworowska and Gambaryan, 1994: fig. 24), and it is optimized here as a synapomorphy because of its nested position within the MLCM. A more basal position for *Chulsanbaatar*, as in the most parsimonious trees of Rougier et al. (1997) (fig 62: A), would change this character to a synapomorphy of a subclade within the MLCM. *Djadochtatherium*, which is excluded from the MLCM, could not be scored for these putative synapomorphies.

All the evidence excluding *Djadochtatherium* from the MLCM is from the scapula of the holotype skeleton. The scapula of *Ectypodus* is most similar to that of *Djadochtatherium* and also shares several features with the Udan Multi. Specifically, unlike the Udan Multi and *Nemegtbaatar*, both *Djadochtatherium* and *Ectypodus* have a coraocoid process that is lateral to, not aligned with, the center of the glenoid fossa, with the scapula in caudal view. Unlike *Nemegtbaatar*; the Udan Multi, *Djadochtatherium*, and *Ectypodus* have a scapular spine that projects directly laterally and a lateral edge of the glenoid fossa that is concave in lateral view. It is interesting that among other djadochtatheroids, *Djadochtatherium* is most similar to the Udan Multi. The Udan Multi is closely related to *Tombaatar*, which is the sister-group to *Djadochtatherium* in the analyses of Rougier et al. (1997) and Kielan-Jaworowska and Hurum (1997) (fig. 62). Therefore, it seems likely that in an analysis that combines postcranial and craniodental data, several of these scapular characters may support an Udan Multi + *Djadochtatherium* + *Tombaatar* + *Catopsbaatar* clade, and the similarities in the scapula between these djadochtatheroids and *Ectypodus* will be optimized as convergence.

Across both analyses (TAX and ALL) bootstrap percentages and branch support values are generally low (figs. 58-61). This should not be surprising given the large amount of missing data and the historical difficulty that phylogenetic analyses have had in resolving the multituberculate systematics (e.g. Simmons, 1993; Rougier et al., 1997; Kielan-Jaworowska and Hurum, 2001). Despite the low values, very strong support emerged in the current study for a clade including the Udan Multi and *Catopsbaatar*. A more detailed study comparing the calcaneus of these two taxa is underway (Bolortsetseg and Kielan-Jaworowska, in prep.), but this result will be briefly discussed here. In the

ALL analysis, the Udan Multi + *Catopsbaatar* clade was in 79% of bootstrap replicates. Although these two taxa formed an unresolved trichotomy with *Nemegtbaatar* in the strict consensus, when taxa with codings for the calcaneus were not considered, this clade emerged and had a Bremer support of 5.9 (fig. 60), almost twice the Bremer support of the next best supported clades (i.e. Monotremata and Theriiformes). The Udan Multi + *Catopsbaatar* clade also received a relatively high bootstrap percentage in the TAX analysis (64%), although the Bremer support was quite low (0.8) (fig. 58). The Udan Multi and *Catopsbaatar* have highly unusual and strikingly similar calcanei. The most obvious similarity is the wide and craniocaudally extensive lateral crest, which converges upon the morphology seen in more basal taxa such as *Oligokyphus*. The Udan Multi + *Catopsbaatar* clade is not that surprising because as previously mentioned, the Udan Multi is most closely related to the djadochtatheroid *Tombaatar* (Spurlin et al., 2000). *Tombaatar* is in turn the sister-group to *Catopsbaatar* in two previous phylogenetic analyses (Rougier et al., 1997; Kielan-Jaworowska and Hurum, 1997) (fig. 62). Therefore, the postcranial data is consistent with the close relationship of *Tombaatar* and *Catopsbaatar*, which is based entirely on craniodental data.

The inclusion of isolated postcranial elements to the matrix did substantially change the phylogenetic relationships among multituberculates, as evidence by the different relationships depicted in the TAX and ALL analyses (figs. 58 and 59). While the inclusion of more data can be justified with an appeal to total evidence (e.g. Kluge, 1989), the TAX most parsimonious trees are more consistent with trees supported by craniodental data than are those most parsimonious trees supported by the ALL analysis. Specifically *Kryptobaatar* is included the clade of Mongolian multituberculates (MLCM)

in the TAX analysis, while in the ALL analysis it is the first branch of a clade that includes the North American taxa *Ptilodus*, *Eucosmodon*, *Ectypodus*, and many others. Although the exact reasons for this are complex, inspection of the optimizations of characters indicate that much of the change in topology is due to the inclusion of two isolated specimens: UCMP 111158, a calcaneus from the Bushy Tailed Blowout exposure of the Lance Formation (Niobara County, Wyoming), and USNM 2894, an astragalus from the type locality of the Lance Formation (Niobrara County, Wyoming). In the strict consensus of the ALL analysis, these two specimens form a multichotomy with Trechnotheria and Multituberculata (fig. 59). When the subset of OTU's lacking the astragalus are pruned from the most parsimonious trees, six distinct trees remain. In these trees, USNM 2984 is either a stem taxon to Theria or to Multituberculata (fig. 61). When the subset of OTU's that lack the calcaneus are pruned, UCMP 111158 is the sister-group to Multituberculata (fig. 60). Thus based on their positions near the multituberculate root, these two isolated specimens have an important influence on the character states optimized as primitive for Multituberculata.

USNM 2894 has s several features common to multituberculate astragali (i.e. buttress, saddle-shaped astragalonavicular facet, absence of astragalar neck); however, it also resembles the astragalus of the Udan Multi in having a plantarly situated sustentacular facet and a highly convex lateral astragalotibial facet. USNM 2894 is about 1.5 times the size of the astragali attributed to *Stygimys kuszmauli*. Based on this, the most likely known multituberculate from the type Lance Fm that this astragalus might belong to is *Cimolomys gracilis*. While in computer-assisted phylogenetic analyses (i.e. Simmons, 1993; Rougier et al., 1997) *Cimolomys* is usually placed in a highly nested

position within Cimolodonta, it is placed in a more basal position in the hand-drawn cladogram of Kielan-Jaworowska and Hurum (2001). Given the unusual morphology of USNM 2894 and the uncertainty surrounding its identification, additional searching for microfossils at the Type Lance Formation is warranted. More importantly, the similarity of this specimen to the astragalus of the Udan Multi changes the optimization of several characters within Multituberculata. Some of the unusual morphology of the Udan Multi, which was optimized as derived in the TAX analysis, is now optimized as primitive, thus supporting the break-up of the MLCM in the ALL analysis.

UCMP 111158, an isolated calcaneus from the Bushy Tailed Blowout exposure of the Lance Formation (Niobara County, Wyoming), is like USNM 2894 in being similar to the Udan Multi. The Udan Multi and UCMP 111158 both have a lateral crest of the calcaneus that extends caudal to the level of the calcaneoastragalar facet, a medially curved tuber calcis, and a tubercle on the sustentacular shelf. Thus like the inclusion of the isolated astragalus USNM 2984, UCMP 11158 changes the optimization of several characters and contributes to the paraphyly of the MLCM. It is tempting to hypothesize that the astragalus (USNM 2984) and the calcaneus (UCMP 111158) are from the same taxon. Supporting this is the fact that these specimens do form a clade in some of the most parsimonious trees from the ALL analysis; however, this hypothesis seems unlikely. USNM 2984 is considerably smaller than UCMP 111158, and the relative spacing between the calcaneoastragalar and sustentacular facets is very different; it is much wider in UCMP 111158.

The obvious question then is what taxon does UCMP 111158 represent? Its morphology is remarkably similar to an isolated calcaneus from the Oldman Formation

referred to *Didelphodus* and figured by Szalay (1993: fig. 6.6 A-E). The referral of the Oldman specimen to *Didelphodus* certainly makes sense in terms of size, and it also shares some similarities with the calcanei of the Paleocene marsupials *Mayulestes* and *Pucadelphys* (Muizon, 1998). Like both of these South American taxa, the Oldman calcaneus had a transversely compressed tuber, a large bulbous calcaneoastraglar facet, and a craniocaudally long peroneal process. Thus it seems likely that UCMP 111158 is a stagodontid marsupial, and based on the list of taxa reported from the Lance Formation as compiled by Kielan Jaworowska et al. (2002), *Didelphodus vorax* seems like the most likely candidate. Combining dental data from *Didelphodus* with UCMP 111158, and including craniodental characters in the matrix, would almost certainly change UCMP 111158's phylogenetic position and then could also change the phylogeny within Multituberculata. Thus although the ALL analysis includes more OTU's than the TAX analysis, the TAX analysis may represent a more accurate phylogeny of Multituberculata. This is certainly supported by the fact that the topology of the strict consensus from the TAX analysis (fig. 58) is more similar to the trees based on craniodental data only (e.g. Rougier et al., 1997) (fig. 62: A)

Finally, I have a few notes regarding the methodology used in the phylogenetic analyses. In an earlier version of this study, separate analyses were done for OTU's that lack calcanei and OTU's that lack astragali. The thinking behind this approach was that since an isolated astragalus and an isolated calcaneus have completely non-overlapping character codings, an analysis that included isolated astragali and calcanei would take a prohibitively long time and yield more most parsimonious trees than current computers could save. A reviewer of the previous study (G.W. Rougier) suggested trying an analysis

with all isolated specimens to see if in fact this would be the result. While the analyses were slow, only 848 most parsimonious trees were found. The strict consensus of these trees had 16 (46%) out of a possible 35 nodes resolved (fig. 59). Given that many of the OTU's had non-overlapping character codings, this is surprisingly good. Thus in the current age when independent data matrices are being combined to form supermatrices, matrices should be combined even if some taxa have non-overlapping character codings, instead of assuming a priori that the result will be a completely unresolved consensus tree.

APPENDIX I

POSTCRANIAL CHARACTERS FOR PHYLOGENETIC ANALYSIS

SCAPULA

1. Spine of scapula relative to the plane of the scapular blade (ordered): (0) inclined, spine projects cranially or craniolaterally, (1) forms a 90˚ angle, spine projects directly laterally, (2) inclined, spine projects caudolaterally, (3) inclined, spine projects caudally and runs almost parallel to the plane of the blade.

2. Position of coracoid process/metacoracoid relative to the center of the glenoid fossa of the scapula in caudal view (ordered): (0) medial to center, (1) aligned with center, (2) lateral to center.

3. Shape of glenoid fossa, not including the portion on the coracoid process: (0) ovoid, with long axis oriented craniocaudally, (1) circular, (2) subrectangular, long axis of rectangle oriented transversely.

4. Lateral rim of the glenoid fossa in lateral view: (0) straight, (1) concave. This is character is based on the ventral part of the scapula (part near the humerus) being in direct lateral view.

5. Posterior (caudal) process of the coracoid/metacoracoid: (0) present and points caudally, (1) small and points medially, (2) absent, coracoid process comes to a ventral point.

6. Ridge for fourth aponeurosis of m.subscapularis on scapula (sensu Kielan-Jaworowska and Gambaryan, 1994): (0) absent, (1) present, on ventral end of medial side and is oriented cranioventrally to caudodorsally (2) present, weakly developed.

7. Supraspinous fossa along anterior margin of scapular blade: (0) absent or rudimentary; (1) present (Rowe, 1988; Sereno, 2006).

8. Glenoid fossa of scapula, orientation: (0) posterolateral, (1) lateral, (2) posteroventral. (Sereno and McKenna, 1995; Sereno, 2006).

9. Procoracoid: (0) present, (1) reduced/fused with manubrium sterni. (Rowe, 1988; Sereno, 2006).

10. Interclavicle size: (0) Larger, (1) smaller, than the sternum (anteroposterior and transverse dimensions) (modified from Rowe, 1988; Sereno, 2006).

11. Interclavicle-sternum coossification: (0) absent, (1) present (claviculosternal contact) (Rowe, 1988; Sereno, 2006).

HUMERUS

12. Shape of the humeral head in proximal view: (0) round, (1) ovoid, long axis of head oriented craniomedially to caudolaterally, (2) ovoid, long axis of head aligned craniocaudally.

13. Fossa between deltopectoral and posterior (caudal) crests of humerus (sensu Poplewski, 1948, cited in Kielan-Jaworowska and Dashzeveg, 1978), the latter being the crest centered on the caudal side of the shaft and oriented proximodistally (ordered): (0) absent, (1) well defined, (2) cavernous, undercuts greater tubercle.

14. Head of humerus in lateral or medial view: (0) aligned with shaft, (1) offset caudally from shaft.

15. Intertubercular (bicipital) groove of humerus, in proximal view: (0) clearly present, (1) absent or poorly defined. (modified from Rowe, 1988).

16. Cranial projection of greater tuberosity of humerus: (0) absent, (1) present and helps define intertubercular groove, most evident in proximal view.

17. Supinator crest (on lateral edge of humerus above ectepicondyle): (0) in cranial or caudal view, the edge of the crest is concave, (1) expanded proximally up the shaft, in cranial or caudal view, the edge of the crest is straight or convex.

PELVIS

18. Ischial tuber (i.e. ischiatic tuberosity): (0) present, (1) absent (Ji et al., 2002).

19. Postobturator notch: (0) absent, (1) present, ischiatic table narrow, (2) absent, ischiatic table wide (Kielan-Jaworowska and Gambaryan, 1994).

TIBIA

20. Width of distal epiphysis of tibia (ordered): continuous character, see table 11.

21. Shaft of tibia in lateral or medial view: (0) fairly straight, (1) bowed cranially.

22. Tibial tuberosity: (0) absent, (1) cranially positioned and not hooked, (2) hooked and its end points distolaterally, (3) hooked and its end points distally (modified from Kielan-Jaworowska and Gambaryan, 1994).

23. Width of tibial shaft (ordered): continuous character, see table 12.

24. Lateral articular surface for astragalus on tibia: (0) flat and medial malleolus absent, (1) caudolateral to medial malleolus, (2) crescent-shaped in distal view and cranial part is directly lateral to medial malleolus.

25. Length of tibia relative to femur (ordered): continuous character, see table 13.

FIBULA

26. Fibula in craniolateral view: (0) extends distally to same level as tibia, (1) terminates well proximal to distal end of tibia.

27. Hook-like lateral process of the fibula (ordered): (0) absent, (1) short, projects from craniolateral side of the proximal end of the fibula and situated just lateral to the articular facet with the tibia, (2) long and its end is recurved to then parallel the shaft for a short distance (modified from Kielan-Jaworowska and Gambaryan, 1994).

CALCANEUS

28. Tuber calcis in dorsal view: (0) straight, (1) curved medially.

29. Tuber calcis, in dorsal view: (0) widens towards tip, (1) the same width towards tip.

30. Shallow fossa on caudoplantar corner of medial side of tuber calcis: (0) present, (1) absent.

31. Caudal end of tuber calcis in lateral view: (0) convex, (1) almost straight.

32. Tuber calcis height, relative to total length of calcaneus (ordered): continuous character, for codings see table 14.

33. Peroneus brevis fossa on calcaneus: (0) wide and similar in width along entire length, (1) constricted transversely at the middle of its length, (2) absent.

34. Trochlear ridge of calcaneus (on dorsal surface, medially borders the peroneal groove) (ordered): (0) narrow and high, (1) wide and low, (2) absent.

35. Floor of the peroneal groove of calcaneus: (0) visible in dorsal view, (1) not visible in dorsal view, but visible in plantar view.

36. Peroneal process of calcaneus (ordered): (0) cranially and slightly laterally directed, (1) craniolaterally directed, (2) laterally directed (modified from Simmons, 1993).

37. Cranial end of peroneal groove of calcaneus: (0) flat or turns smoothly into the cranial face of the calcaneus, (1) forms a laterally projecting tubercle, (2) forms a thickened lip that borders the calcaneocuboid facet.

38. Cranioplantar side of the peroneal process of calcaneus: (0) convex or gently concave, (1) bears a deep circular fossa.

39. Calcaneal lateral crest/flange (ordered): (0) weakly developed, calcaneal lateral ridge is closely appressed to the body of the calcaneus, (1) present and forms a prominent crest that juts medially away from the calcaneal body, but ends cranial to caudal edge of the calcaneoastragalar facet, (2) present and extends beyond the caudal edge of the calcaneoastragalar facet (modified from Jenkins, 1971, Horovitz, 2000).

40. Tip of the peroneal process of calcaneus, if viewed head-on: (0) rounded, (1) ovoid and dorsoplantarly deep, (2) lacks a distinct tip, the process is a long flange, (3) ovoid but long axis is craniocaudal.

41. Calcaneocuboid facet on calcaneus: (0) concave, (1) nearly flat.

42. Long axis of calcaneocuboid facet on calcaneus: (0) oriented caudomedially to craniolaterally, (1) dorsoplantarly, (2) transversely.

43. Calcaneocuboid facet on calcaneus faces: (0) primarily medially, (1) craniomedially, (2) oriented craniomedially and slightly plantarly, (3) cranially (modified from Kielan-Jaworowska and Gambaryan, 1994).

44. Shape of the calcaneocuboid facet on the calcaneus: (0) round or nearly so, (1) oval.

45. Sustentacular and calcaneocuboid facets on calcaneus: (0) only the cranial tip of former contacts the latter, (1) former broadly contacts the latter along its cranial side, (2) do not contact each other.

46. Shape of sustentacular facet on calcaneus: (0) round, (1) ovoid and craniocaudally elongate.

47. Sustentacular facet on calcaneus faces: (0) medial, (1) dorsomedially (Schaeffer, 1941, Horovitz, 2000).

48. In dorsal view, the angle formed if the long axes of the sustentacular and calcaneoastragalar facets are extrapolated (ordered): continuous character, see table 15.

49. Caudal edge of sustentacular facet on calcaneus: (0) cranial to the caudal edge of the calcaneoastragalar facet on calcaneus, (1) at the same level as the caudal edge of the calcaneoastragalar facet.

50. Sulcus calcanei (between sustentacular and calcaneoastragalar facets): (0) narrow and crescent shaped, (1) wide with sustentacular and calcaneoastragalar facets parallel, (2) wide caudally and narrow cranially, (3) absent.

51. Cranial edge of the sulcus calcanei: (0) extends cranially beyond the cranial edge of the calcaneoastragalar facet, (1) level with the cranial edge of calcaneoastragalar facet.

52. Relative length of the dorsiflexion stop, which is a smooth, fairly flat area of bone located on the dorsal side just cranial to the calcaneoastragalar facet (ordered): continuous character, see table 16.

53. Calcaneal body cross-section, at the level of the caudal margin of the calcaneoastragalar facet: (0) wide transversely, (1) narrow transversely (Horovitz, 2000).

54. Fibular/lunule contact on calcaneus (ordered): (0) present large, (1) present small, (2) absent (Hu et al., 1997).

55. Orientation of the calcaneoastragalar facet relative to the long axis of tuber calcis in dorsal view, (0) craniomedially to caudolaterally, (1) craniocaudally, (2) caudomedially to craniolaterally.

56. Tubercle on proximal edge of sustentacular tali on calcaneus (visible in dorsal or caudal view): (0) absent, (1) present.

57. Ventrodistal fossa of calcaneus (ventrodistal groove of Horovitz, 2000): (0) well developed, but does not reach the sustentacular facet, (1) fossa elongate and reaches sustentacular facet, (2) well developed, only present next to sustentacular facet, (3) poorly developed or absent (Horovitz, 2000).

58. Cranioplantar tuberosity of the calcaneus, occurs on craniolateral margin of the calcaneocuboid facet and extends onto plantar side: (0) in cranial view, wide dorsally but narrows plantarly, (1) same width dorsally and plantarly, (2) absent.

ASTRAGALUS

59. Buttress and astragalonavicular articular surface on astragalus: (0) as seen in plantar view, do not contact each other, (1) contact each other, in caudal view, the buttress can be seen to be deflected plantarly, (2) buttress absent.

60. The shape of the buttress on astragalus: (0) square in dorsal and plantar views, bears a groove on its caudal side that is oriented dorsoplantarly, (1) square in dorsal and plantar views, bears a groove on its caudal side that is oriented laterodorsally to medioplantarly, (2) arched and rounded in dorsal and plantar views, no groove on the caudal side.

61. Groove between buttress and calcaneoastragalar facet in plantar view of astragalus: (0) absent, (1) present.

62. Position of ridge defining caudal edge of tibial articular surface on astragalus (ordered): (0) in cranial position, well separate from astragalar foramen, with a small fossa between the two, (1) in caudal position along the edge of the astragalar foramen, fossa absent, (2) no foramen, but fossa present.

63. Caudolateral surface of astragalus: (0) has a groove that laterally borders the buttress and then a flat or slightly convex area lateral to this groove, (1) a broad, flat or slightly concave region, (2) a distinctly concave region that helps to define the caudolateral process of the astragalus, (3) strongly convex and articulates with fibula.

64. Lateral astragalotibial facet on astragalus (ordered): (0) convex, (1) concave transversely but flat craniocaudally, (2) pulley-shaped, concave transversely and convex craniocaudally.

65. Medial and lateral astragalotibial facets on astragalus (ordered): (0) confluent, and distal end of tibia is smoothly curved, (1) poorly developed ridge, with distal end of tibia having a corresponding groove, (2) separated by a distinct ridge, distal end of tibia has a distinct corresponding groove, (3) medial tibial facet faces medially.

66. Medial astragalotibial facet on astragalus: (0) flat or nearly so, (1) distinctly concave.

67. Position of sustentacular facet on astragalus: (0) more plantarly positioned and its medial edge borders a steep, cliff-like, medially-facing astragalonavicular facet, (1) more dorsally positioned, astragalonavicular facet appears sloped.

68. Shape of sustentacular facet on astragalus: (0) elongate craniocaudal strip, (1) circular, (2) ovoid.

69. Lateral edge of the calcaneoastragalar facet on astragalus in plantar view (ordered): (0) convex, (1) straight, (2) concave.

70. Craniomedial corner of the astragalus: (0) protrudes, (1) does not protrude.

71. Sustentacular and calcaneoastragalar facets of astragalus: (0) run parallel to each other, (1) if the long axes are extrapolated, form an acute angle, calcaneoastragalar facet oriented caudolaterally to craniomedially.

72. Caudomedial corner of dorsal surface of astragalus: (0) does not protrude, (1) protrudes and forms what may be homologous to the astragalar medial plantar tuberosity.

73. Nonarticulating groove between medial astragalotibial facet and astragalonavicular facet: (0) present, (1) absent, a thick lip separates the two facets, (2) absent, a thin lip separates the two facets.

74. Interarticular bulge of astragalus (located caudomedial to the sustentacular facet) (ordered): (0) absent, (1) present and very low, (2) present and high but not undercut, (3) prominent bulge that is undercut by the interarticular sulcus.

75. Astragalar foramen in dorsal view (ordered): (0) large, (1) medium, (2) small, (3) absent.

76. Astragalar canal in plantar view: (0) small, (1) large.

77. Sustentacular facet of astragalus orientation: (0) faces plantolaterally but more plantarly than laterally, (1) faces plantolaterally but more laterally than plantarly.

78. Location of astragalonavicular facet on astragalus (ordered): (0) extends from the cranial to the medioplantar side of the astragalus, astragalus lacks a neck, (1) restricted to cranial side of astragalus, astragalus lacks a neck, (2) on cranial side of astragalus and astragalus has a well or weakly developed neck (Ji et al., 1999; Luo et al., 2003).

79. Astragalonavicular facet on astragalus: (0) saddle-shaped, concave dorsoplantarly and convex transversally, occurs on cranial and the medial sides, (1) convex transversally and flat to convex dorsoplantarly, occurs on cranial and the medial sides, (2) restricted to cranial side, (3) forms a complex interlocking joint, lateral portion is concave but medial portion convex (modified from Kielan-Jaworowska and Gambaryan, 1994).

80. Sustentacular facet relative to the calcaneoastragalar facet: (0) medial to calcaneoastragalar facet, (1) primarily cranial to it, but also slightly medial.

CUBOID

81. Dorsoplantar diameter of cuboid in lateral view: (0) greater than proximodistal length, (1) less than proximodistal length.

82. Transverse width of the cuboid in dorsal view (ordered): (0) greater than proximodistal length, (1) equal to proximodistal length, (2) less than proximodistal length.

83. Groove for tendon of peroneus longus on cuboid, located just plantar to articular surface for metatarsals IV and V: (0) extends slightly onto lateral side, (1) restricted to plantar side.

84. Articular surface for metatarsal V on cuboid: (0) concave dorsoplantarly, (1) flat in all directions.

85. Nonarticular area on lateral side of cuboid between contact for calcaneus and craniolateral corner (ordered): (0) narrow and very deep, (1) narrow and shallow, (2) wide and shallow.

NAVICULAR

87. Dorsal end of astragalar contact as compared to plantar end, with navicular in medial or lateral view (ordered): (0) taller than plantar end, (1) same height as plantar end, (2) shorter than plantar end.

88. Dorsoplantar groove on the medial side of the navicular: (0) present, (1) absent.

ECTOCUNEIFORM

89. Contact surface for navicular on ectocuneiform: (0) concave dorsoplantarly and fairly flat transversely, (1) flat dorsoplantarly and transversely, (2) convex transversally, morphology along dorsoplantar axis unclear.

MESOCUNEIFORM

90. Size of mesocuneiform in dorsal view: (0) small, proximodistal length is less than 75% of that of the ectocuneiform, (1) proximodistal lengths of meso- and ectocuneiforms are subequal.

ENTOCUNEIFORM

91. Contact for navicular on entocuneiform: (0) concave, large, and bowl-shaped with sharp medial and lateral edges, (1) weakly concave, small, and defined by broad rounded-over edges.

METATARSALS

92. Dorsal sides of distal ends of metatarsals II through V: (0) each bears a distinct pit just proximal to the distal articular facet, (1) pits are absent, may have a shallow transverse trough instead.

93. Length of metatarsal V measured relative to metatarsal IV (ordered): continuous character, see table 17.

94. Proximal end of metatarsal V: (0) dorsal face faces directly dorsally, (1) dorsal face actually faces dorsolaterally.

95. Peroneal process of metatarsal V: (0) absent, (1) at the proximal end of metatarsal V, (2) distal to the proximal end.

APPENDIX II: MATRIX FOR PHYLOGENETIC ANAYLSIS

A= 0+1, B= 3+5, C= 3+4, D= 0+1+2. Taxa in bold are used in TAX analysis. Underlined OTU's are isolated calcanei.

	10	20	30	40	50	60	70	80
Tachyglossus	0020000000	0201000000	0151310101	1822022003	1101210-10	0-1210022-	-030012011	01003-1010
Zaglossus	0020000000	0201000000	0151510101	0922022003	1?-1210-10	0-1210322-	-030010001	00003-1000
Ornithorhynchus	0020000000	0201000000	0152910-01	0322022002	1101210-12	0-001002--	-03031?001	01003-1030
Jeholodens	??????111?	??????????	??????????	??????????	??????????	???0????2?	???0??????	???????1??
Zhangheotherium	??????1111	0???0??00-	?000C100??	??0???2??1?	123?210?00	??101??12?	??????????	?0?????12?
Ukhaatherium	3?0???1111	10?10?100?	?1??61?111	1022110?02	0220011?0?	0?0?10012?	???030?201	?1??D00221
Eomaia	??????1111	1?????????	??????1?0??	??????????	??3???????	???????0?2?	??????????	?1?????221
Didelphis	0210201111	1201111100	0192410011	04220?0002	0221011203	??10202?2?	?2?0201220	01003-0211
Udan Multi	10?11101??	?121001129	1311011101	1400111121	1011111202	1802010102	0000000210	0122011000
Catopsbaatar	??????????	??????????	???????101	140011??21	??1???????	?9020?????	??????????	??????????
Djadochtatherium	1111?1?1??	??????????	??????????	??????????	??????????	??????????	??????????	??????????
Kryptobaatar	?02?2?0111	0010100012	12B?A12011	0301000000	1011111210	1111110000	1010001110	0011111000
Nemegtbaatar	20201201??	?121100?14	1232?11???	??????????	??????????	??????????	??????????	??????????
Chulsanbaatar	2???1??1??	?02110????	0??????1???	??????????	??????????	??????????	??????????	????????0?
Eucosmodon	??????????	???????011	???2???001	0311100001	0001111110	111111102?	0111211?1?	01?1101000
Ptilodus	???1?1????	???????010	0342102000	04?1000?00	0000111?11	0?1??01?00	0110011?1	010?201000
Ectypodus	11111101??	???????01?	02?????????	??????????	??????????	????????00	0122201200	1021100010
Stygimys	??????????	??????0???	???????011	14??10?000	0021000100	1111103210	1011210110	1013110000
Mesodma	2020?101??	??????0?17	02611??011	1311100000	0100110001	111110322	??????????	??????????
MCZ 20784	??????????	??????????	???????011	0311000000	0000000000	0111103022	??????????	??????????
UM Calc 171	??????????	??????????	???????000	152?000000	0100111102	1211103022	??????????	??????????
UM Calc 175	??????????	??????????	??????????	??11000000	1110010201	1111102022	??????????	??????????
UM Calc 179	??????????	??????????	???????010	1311000000	0120110002	0111113022	??????????	??????????
UM Calc 183	??????????	??????????	???????01?	??01000000	0120001001	1111103022	??????????	??????????
UM Calc 253	??????????	??????????	??????????	??001???0?	1101001101	-310201022	??????????	??????????
UA 111158	??????????	??????????	???????1??	?522120022	1121111201	0210113222	??????????	??????????
UA 111159	??????????	??????????	???????001	1???21?0?0?	0120001101	1310211122	??????????	??????????
MCZ 20960-1	??????????	??????????	???????001	0301001001	0101111011	1300201122	??????????	??????????
MCZ 20960-4	??????????	??????????	???????010	0111000000	1001011001	1011103022	??????????	??????????
MCZ 20960-6	??????????	??????????	???????010	032?100000	1001110001	1111103???	??????????	??????????
UM Calc 186	??????????	??????????	???????010	131101000?	0001001000	1111103122	??????????	??????????
USNM 2894	??????????	??????????	??????????	??????????	??????????	????????12	0000000111	0102200000
UM Astr 262	??????????	??????????	??????????	??????????	??????????	????????11	0021101121	1101101000
UA Astr 29	??????????	??????????	??????????	??????????	??????????	????????11	1021211121	1001201000
UM Astr 263	??????????	??????????	??????????	??????????	??????????	????????10	1011111101	1113011000

	90 95
Tachyglossus	12?0-?21?0 ?1800
Zaglossus	?????????? ?????
Ornithorhynchus	12?1-11111 11910
Jeholodens	?????????? ??5?0
Zhangheotherium	?????????0 ??6?0
Ukhaatherium	?????????? ?????
Eomaia	?????????? ??7?1
Didelphis	1211111110 11101
Udan Multi	0011011111 00411
Catopsbaatar	?1???????0 ?????
Djadochtatherium	?????????? ?????
Kryptobaatar	12????0??0 ?1A11
Nemegtbaatar	?????????? ?????
Chulsanbaatar	?2????????0 ????1
Eucosmodon	1200200000 11302
Ptilodus	12?0?02020 11002
Ectypodus	??????000? ???02
Stygimys	?????????? ?????
Mesodma	?????????? ?????
MCZ 20784	?????????? ?????
UM Calc 171	?????????? ?????
UM Calc 175	?????????? ?????
UM Calc 179	?????????? ?????
UM Calc 183	?????????? ?????
UM Calc 253	?????????? ?????
UA 111158	?????????? ?????
UA 111159	?????????? ?????
MCZ 20960-1	?????????? ?????
MCZ 20960-4	?????????? ?????
MCZ 20960-6	?????????? ?????
UM Calc 186	?????????? ?????
USNM 2894	?????????? ?????
UM Astr 262	?????????? ?????
UA Astr 29	?????????? ?????
UM Astr 263	?????????? ?????

APPENDIX III

APOMORPHY LIST FOR "TAX" ANAYLSIS

Strict consensus of 3 trees. Nona chooses as its default the first taxon in the matrix to be the outgroup, which in this case is *Tachyglossus*. If the trees are rooted on the internal branch above *Ornithorhynchus*, then monotremes are monophyletic and the length remains the same.

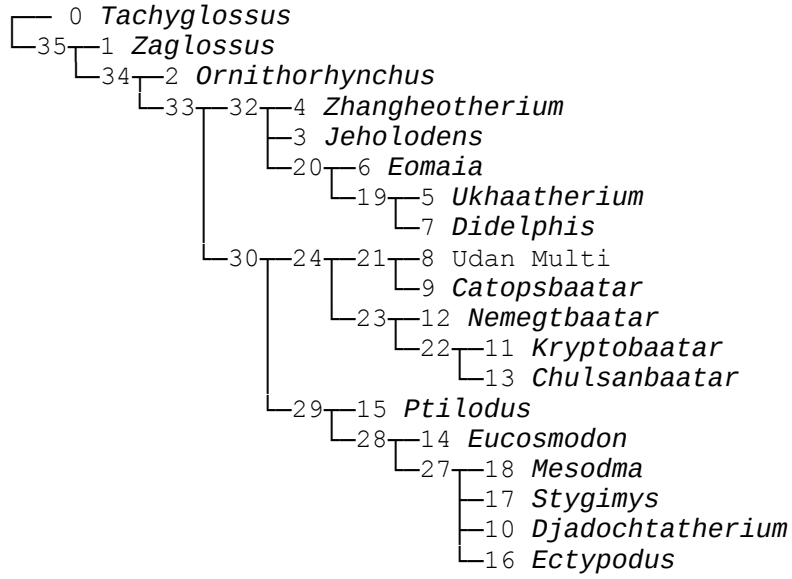

Zaglossus

```
In all trees:
   char 57: 0 --> 3
   char 72: 1 --> 0
```

Ornithorhynchus

```
In all trees:
   char 25: 45 --> 9
   char 50: 0 --> 2
   char 53: 1 --> 0
   char 65: 0.2 --> 3
   char 79: 0 --> 3
```

```
     char 90: 0 --> 1
     char 93: 8 --> 9
     char 94: 0 --> 1
```

Jeholodens

```
  In all trees:
     no autapomorphies!
```

Zhangheotherium

```
  In all trees:
     char 22: 1 --> 0
     char 23: 45 --> 0
     char 24: 2 --> 0
     char 39: 0 --> 1
     char 72: 1 --> 0
```

Ukhaatherium

```
  In all trees:
     char 1: 01 --> 3
     char 12: 2 --> 0
     char 25: 4 --> 6
     char 28: 0 --> 1
     char 31: 0 --> 1
     char 35: 0 --> 1
     char 44: 1 --> 0
     char 53: 1 --> 0
     char 65: 2 --> 3
```

Eomaia

```
  In all trees:
     char 93: 56 --> 7
```

Didelphis

```
  In all trees:
     char 15: 0 --> 1
     char 18: 0 --> 1
     char 55: 1 --> 2
     char 57: 0 --> 2
     char 69: 01 --> 2
     char 79: 2 --> 1
```

Udan Multi

```
  In all trees:
     char 82: 1 --> 0
     char 90: 0 --> 1
```

Catopsbaatar

```
  In all trees:
     char 52: 8 --> 9
```

Djadochtatherium

```
In all trees:
   no autapomorphies!
```

Kryptobaatar

```
In all trees:
   char 5: 1 --> 2
   char 13: 2 --> 1
   char 14: 1 --> 0
   char 27: 1 --> 2
```

Nemegtbaatar

```
In all trees:
   no autapomorphies!
```

Chulsanbaatar

```
In all trees:
   char 21: 1 --> 0
```

Eucosmodon

```
In all trees:
   char 40: 0 --> 1
   char 56: 0 --> 1
```

Ptilodus

```
In all trees:
   char 22: 2 --> 3
   char 30: 1 --> 0
   char 44: 1 --> 0
   char 50: 0 --> 1
   char 68: 2 --> 1
   char 87: 1 --> 2
   char 93: 3 --> 0
```

Ectypodus

```
In some trees:
   no autapomorphies!
   char 63: 1 --> 2
   char 64: 1 --> 2
   char 69: 1 --> 0
   char 79: 0 --> 1
```

Stygimys

```
In some trees:
   char 43: 0 --> 2
   char 45: 1 --> 0
   char 46: 1 --> 0
   char 59: 0 --> 1
   char 61: 0 --> 1
```

```
     char 62: 1 --> 0
     char 67: 1 --> 0
     char 68: 2 --> 1
     char 74: 1 --> 3
     char 76: 0 --> 1
```

Mesodma

```
  In all trees:
     char 42: 0 --> 1
     char 44: 1 --> 0
     char 48: 1 --> 0
     char 50: 0 --> 1
  In some trees:
     char 1: 1 --> 2

Node 19 of Current Tree

  In all trees:
     char 43: 3 --> 2

Node 20 of Current Tree [Theria]

  In all trees:
     char 78: 1 --> 2
     char 95: 0 --> 1
  In some trees:
     char 11: 0 --> 1

Node 21 of Current Tree

  In all trees:
     char 28: 0 --> 1
     char 31: 0 --> 1
     char 34: 1 --> 0
     char 35: 0 --> 1
     char 39: 0 --> 2
     char 40: 0 --> 1
     char 52: 1 --> 8
     char 53: 1 --> 0
     char 54: 1 --> 2
     char 55: 1 --> 0
     char 82: 2 --> 1

Node 22 of Current Tree

  In all trees:
     char 12: 1 --> 0

Node 23 of Current Tree

  In all trees:
     char 1: 1 --> 2
     char 15: 0 --> 1

Node 24 of Current Tree
```

```
  In all trees:
     char 20: 01 --> 2.4
     char 21: 0 --> 1
     char 23: 45 --> 3
     char 43: 0 --> 1
     char 56: 0 --> 1
     char 76: 0 --> 1
     char 94: 0 --> 1

Node 27 of Current Tree

  In some trees:
     char 29: 0 --> 1
     char 31: 0 --> 1
     char 47: 1 --> 0
     char 49: 1 --> 0
     char 57: 1 --> 3
     char 71: 0 --> 1
     char 72: 1 --> 0
     char 77: 1 --> 0

Node 28 of Current Tree

  In all trees:
     char 35: 0 --> 1
     char 64: 0 --> 1
     char 87: 1 --> 0

Node 29 of Current Tree

  In all trees:
     char 41: 1 --> 0
     char 57: 0 --> 1
     char 84: 1 --> 0
     char 86: 1 --> 0
     char 88: 1 --> 0

Node 30 of Current Tree [Multituberculata]

  In all trees:
     char 6: 0 --> 1
     char 19: 0 --> 1
     char 22: 1 --> 2
     char 25: 4 --> 1
     char 27: 0 --> 1
     char 34: 2 --> 1
     char 40: 2 --> 0
     char 45: 2 --> 1
     char 59: 2 --> 0
     char 74: 0 --> 1
     char 93: 56 --> 34

Node 32 of Current Tree [Trechnotheria]

  In all trees:
     char 7: 0 --> 1
     char 78: 0 --> 1
```

```
  In some trees:
     char 43: 0 --> 3
     char 49: 1 --> 0
     char 79: 0 --> 2

Node 33 of Current Tree [Theriiformes]

  In all trees:
     char 8: 0 --> 1
     char 9: 0 --> 1
     char 10: 0 --> 1
     char 37: 2 --> 0
     char 66: 1 --> 0
     char 68: 0 --> 2
     char 93: 8 --> 56

Node 34 of Current Tree

  In all trees:
     char 24: 1 --> 2
     char 40: 3 --> 2
     char 54: 2 --> 01

Node 35 of Current Tree

  In all trees:
     char 25: 3 --> 45
     char 31: 1 --> 0
     char 79: 1 --> 0
```

APPENDIX IV

APOMORPHY LIST FOR "ALL" ANAYLSIS

Strict consensus of 898 trees. Nona chooses as its default the first taxon in the matrix to be the outgroup, which in this case is *Tachyglossus*. If the trees are rooted on the internal branch above *Ornithorhynchus*, then monotremes are monophyletic and the length remains the same.

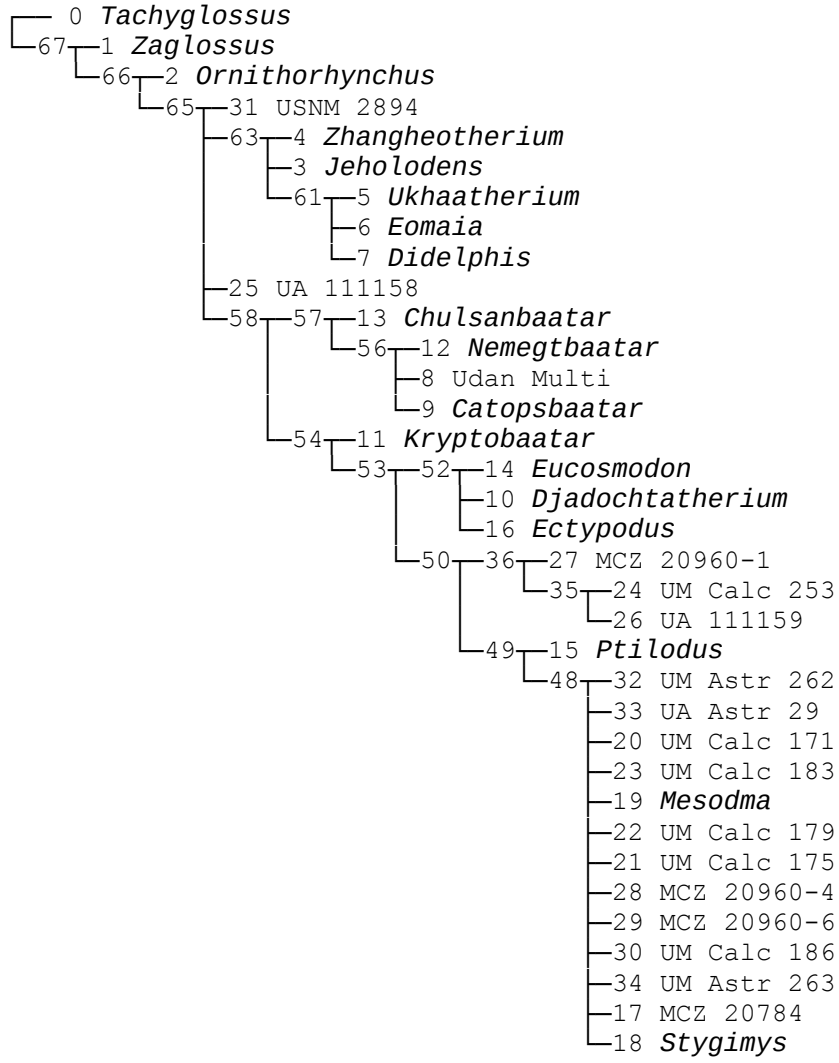

Zaglossus

```
In all trees:
   char 57: 0 --> 3
   char 72: 1 --> 0
```

Ornithorhynchus

```
In all trees:
   char 25: 45 --> 9
   char 50: 0 --> 2
   char 53: 1 --> 0
   char 65: 0.2 --> 3
   char 79: 0 --> 3
   char 90: 0 --> 1
   char 93: 8 --> 9
```

Jeholodens

```
In all trees:
   no autapomorphies!
```

Zhangheotherium

```
In some trees:
   no autapomorphies!
   char 22: 1 --> 0
   char 23: 45 --> 0
   char 24: 2 --> 0
   char 33: 2 --> 0
   char 43: 2 --> 3
   char 72: 1 --> 0
```

Ukhaatherium

```
In some trees:
   char 1: 0.2 --> 3
   char 25: 4 --> 6
   char 28: 0 --> 1
   char 31: 0 --> 1
   char 44: 1 --> 0
   char 53: 1 --> 0
   char 65: 2 --> 3
   char 69: 1 --> 0
```

Eomaia

```
In some trees:
   char 43: 2 --> 3
   char 93: 56 --> 7
```

Didelphis

```
In all trees:
   char 57: 0 --> 2
```

```
     char 79: 2 --> 1
  In some trees:
     char 15: 0 --> 1
     char 18: 0 --> 1
     char 55: 1 --> 2
     char 69: 01 --> 2
     char 70: 1 --> 0
     char 75: 2 --> 3
     char 93: 56 --> 1

Udan Multi

  In some trees:
     char 15: 1 --> 0
     char 17: 0 --> 1
     char 19: 1 --> 2
     char 20: 4 --> 9
     char 22: 2 --> 3
     char 23: 3 --> 1
     char 24: 2 --> 1
     char 82: 1 --> 0
     char 90: 0 --> 1
```

Catopsbaatar

```
  In some trees:
     no autapomorphies!
     char 52: 8 --> 9
```

Djadochtatherium

```
  In all trees:
     no autapomorphies!
```

Kryptobaatar

```
  In all trees:
     char 21: 0 --> 1
     char 29: 0 --> 1
     char 40: 1 --> 0
     char 61: 0 --> 1
     char 72: 1 --> 0
     char 73: 02 --> 1
```

Nemegtbaatar

```
  In some trees:
     no autapomorphies!
     char 6: 1 --> 2
```

Chulsanbaatar

```
  In all trees:
     no autapomorphies!
```

Eucosmodon

In some trees:
no autapomorphies!
char 66: 0 --> 1

Ptilodus

In all trees:
char 20: 12 --> 0
char 22: 2 --> 3
char 32: 3 --> 4
char 51: 1 --> 0
char 75: 1 --> 2

Ectypodus

In some trees:
no autapomorphies!
char 63: 1 --> 2
char 64: 1 --> 2
char 69: 1 --> 0
char 71: 0 --> 1
char 72: 1 --> 0
char 77: 1 --> 0
char 79: 0 --> 1

MCZ 20784

In some trees:
no autapomorphies!
char 31: 1 --> 0
char 44: 1 --> 0
char 51: 1 --> 0

Stygimys

In some trees:
char 32: 3 --> 4
char 35: 0 --> 1
char 43: 0 --> 2
char 48: 0 --> 1
char 58: 0 --> 2
char 65: 1 --> 2
char 67: 1 --> 0
char 70: 1 --> 0
char 72: 1 --> 0
char 77: 1 --> 0

Mesodma

In some trees:
no autapomorphies!
char 30: 0 --> 1
char 35: 0 --> 1
char 58: 0 --> 2

UM Calc 171

```
  In some trees:
     no autapomorphies!
     char 32: 3 --> 5
     char 33: 0 --> 2
     char 50: 1 --> 2

UM Calc 175

  In some trees:
     no autapomorphies!
     char 41: 0 --> 1
     char 43: 0 --> 1
     char 48: 0 --> 2
     char 57: 3 --> 2

UM Calc 179

  In some trees:
     no autapomorphies!
     char 43: 0 --> 2
     char 50: 1 --> 2
     char 51: 1 --> 0
     char 56: 0 --> 1

UM Calc 183

  In some trees:
     no autapomorphies!
     char 43: 0 --> 2
     char 45: 1 --> 0
     char 46: 1 --> 0

UM Calc 253

  In all trees:
     char 34: 1 --> 0
     char 41: 0 --> 1

UA 111158

  In some trees:
     no autapomorphies!
     char 32: 34 --> 5
     char 50: 0 --> 1
     char 57: 0 --> 3

UA 111159

  In all trees:
     char 34: 1 --> 2
     char 43: 0 --> 2
     char 44: 1 --> 0
     char 56: 0 --> 1

MCZ 20960-1

  In all trees:
```

```
     char 37: 0 --> 1
     char 48: 1 --> 0
     char 53: 1 --> 0

MCZ 20960-4

  In some trees:
     no autapomorphies!
     char 32: 3 --> 1
     char 47: 0 --> 1
     char 52: 1 --> 0

MCZ 20960-6

  In some trees:
     no autapomorphies!
     char 33: 1 --> 2
     char 35: 0 --> 1
     char 45: 0 --> 1

UM Calc 186

  In some trees:
     no autapomorphies!
     char 36: 0 --> 1
     char 47: 0 --> 1
     char 58: 0 --> 1

USNM 2894

  In some trees:
     no autapomorphies!
     char 59: 2 --> 1
     char 74: 01 --> 2

UM Astr 262

  In all trees:
     no autapomorphies!

UA Astr 29

  In some trees:
     no autapomorphies!
     char 65: 1 --> 2
     char 72: 1 --> 0
     char 75: 1 --> 2

UM Astr 263

  In some trees:
     no autapomorphies!
     char 69: 1 --> 0
     char 75: 1 --> 0

Node 35 of Current Tree
```

```
  In all trees:
     char 45: 1 --> 0
     char 46: 1 --> 0
     char 49: 1 --> 0

Node 36 of Current Tree

  In all trees:
     char 52: 12 --> 3
     char 54: 1 --> 0
     char 55: 1 --> 2

Node 49 of Current Tree

  In all trees:
     char 30: 1 --> 0
     char 40: 1 --> 0
     char 44: 1 --> 0

Node 50 of Current Tree

  In all trees:
     char 50: 0 --> 1
     char 56: 1 --> 0

Node 52 of Current Tree

  In some trees:
     char 2: 0 --> 1
     char 3: 2 --> 1
     char 65: 01 --> 2

Node 53 of Current Tree

  In all trees:
     char 41: 1 --> 0
     char 48: 2 --> 1
     char 57: 0 --> 1
     char 95: 1 --> 2
  In some trees:
     char 43: 1 --> 0

Node 54 of Current Tree

  In all trees:
     char 27: 1 --> 2
     char 28: 1 --> 0
     char 36: 1 --> 0
     char 49: 0 --> 1
     char 60: 2 --> 0
     char 63: 0 --> 1
     char 67: 0 --> 1
     char 93: 4 --> 1.3

Node 56 of Current Tree

  In some trees:
```

```
     char 12: 0 --> 1
     char 21: 0 --> 1
     char 82: 2 --> 1

Node 57 of Current Tree

  In all trees:
     char 13: 1 --> 2

Node 58 of Current Tree [Multituberculata]

  In some trees:
     char 33: 2 --> 0
     char 34: 2 --> 1
     char 36: 2 --> 1
     char 42: 1 --> 0
     char 43: 2 --> 1
     char 51: 0 --> 1
     char 54: 0 --> 1
     char 70: 1 --> 0
     char 75: 2 --> 1

Node 61 of Current Tree [Theria]

  In all trees:
     char 78: 1 --> 2
  In some trees:
     char 11: 0 --> 1
     char 41: 1 --> 0
     char 45: 2 --> 0
     char 95: 0 --> 1

Node 63 of Current Tree [Trechnotheria]

  In all trees:
     char 78: 0 --> 1
  In some trees:
     char 7: 0 --> 1
     char 28: 1 --> 0
     char 42: 1 --> 2
     char 79: 0 --> 2

Node 65 of Current Tree [Theriiformes]

  In all trees:
     char 8: 0 --> 1
     char 9: 0 --> 1
     char 10: 0 --> 1
     char 37: 2 --> 0
     char 49: 1 --> 0
     char 66: 1 --> 0
     char 93: 8 --> 56
  In some trees:
     char 43: 0 --> 2
     char 63: 3 --> 0
     char 68: 0 --> 12
     char 75: 3 --> 2
```

```
Node 66 of Current Tree

  In all trees:
     char 24: 1 --> 2
     char 40: 3 --> 2
     char 54: 2 --> 0

Node 67 of Current Tree

  In all trees:
     char 25: 3 --> 45
     char 31: 1 --> 0
     char 67: 2 --> 0
     char 79: 1 --> 0
```

REFERENCES

Archibald, J.D. 1982. A study of Mammalia and geology across the Cretaceous–Tertiary boundary in Garfield County, Montana. University of California Publications in Geological Sciences 122: 1–286.

Benton, M.J., M.A. Shishkin, E.N. Kurochkin, and D.M. Unwin, 2000. The Age of Dinosaurs in Russia and Mongolia. Cambridge University Press, Cambridge.

Broom, R. 1914. On the structure and affinities of the Multituberculata. Bulletin of American Museum of Natural History 33: 115-134.

Butler, P.M. and G.T. MacIntyre. 1994. Review of the British Haramiyidae (?Mammalia, Allotheria), their molar occlusion and relationships. Philosophical Transactions of the Royal Society of London 345: 433-458.

Butler, P.M. 2000. Review of the early allotherian mammals. Acta Palaeontologica Polonica 45: 317-342.

Bremer, K. 1988. The limits of amino acid sequence data in angiosperm phylogenetic reconstruction. Evolution 42: 795-803

Bremer, K. 1994. Branch support and tree stability. Cladistics 10: 295-304.

Carpenter, J.M. 1996. Uninformative bootstrapping. Cladistics.12: 177-181.

Clark, J.M, M.A. Norell, and L. Chiappe. 1999. An oviraptorid skeleton from the Late Cretaceous of Ukhaa Tolgod, Mongolia, preserved in an avian-like brooding position over an oviraptorid nest. American Museum Novitates 3265: 1-36.

Clark, J.M. , M A. Norell, and T. Rowe 2002. Cranial anatomy of *Citipati osmolskae* (Theropoda, Oviraptorosauria), and a reinterpretation of the holotype of *Oviraptor philoceratops*. American Museum Novitates 3364: 1-24.

Clarke, J.A. and M.A. Norell. 2002. The morphology and phylogenetic position of *Apsaravis ukhaana* from the Later Cretaceous of Mongolia. American Museum Novitates.3387: 1-46.

Clemens, W.A. 1963. Fossil mammals of the type Lance Formation, Wyoming. Part I. Introduction and Multituberculata. University of California Publications in Geological Sciences 48: 1-105.

Clemens, W.A. and Z. Kielan-Jaworowska. 1979. Multituberculata. *In*: J.A. Lillegraven, Z. Kielan-Jaworowska, and W.A. Clemens (eds.), Mesozoic Mammals: The First Two-thirds of Mammalian History. 99-149. University of California Press, Berkeley.

Dashzeveg, D., M.J. Novacek, M.A. Norel., J.M. Clark, L.M. Chiappe, A. Davidson, M.C. McKenna, L. Dingus, C. Swisher, and A. Perle. 1995. Extraordinary preservation in a new vertebrate assemblage from the Late Cretaceous of Mongolia. Nature 374: 446-449.

Dashzeveg, D. , L. Dingus, D.B. Loope, C.C. Swisher III, T. Dulam, and M.R. Sweeney. 2005. New Stratigraphic Subdivision, Depositional Environment, and Age Estimate for the Upper Cretaceous Djadochta Formation, Southern Ulan Nur Basin, Mongolia. American Museum Novitates. 3498: 1-31.

Deischl, G.D. 1964. The postcranial Anatomy of Cretaceous Multituberculate Mammals. Unpublished M.Sc. thesis. University of Minnesota, Minneapolis. 85pp.

Evans, H.E. 1993. Miller's Anatomy of the Dog. 3rd edition. W B Saunders Co.

Felsenstein, J. 1985. Confidence Limits on Phylogenies: An Approach Using the Bootstrap. Evolution 39(4): 783-791

Gambaryan, P.P., and Z. Kielan-Jaworowska. 1997. Sprawling versus parasagittal stance in multituberculate mammals. Acta Palaeontologica Polonica 42: 13–44.

Geisler, J.H. 2001. New Morphological Evidence for the Phylogeny of Artiodactyla, Cetacea, and Mesonychidae. American Museum Novitates. 3344: 1-53.

Gidley, J.W. 1909. Notes on the fossil mammalian genus *Ptilodus*, with description of a new species. Proceedings of the United States National Museum 36: 611-626.

Gingerich, P.D., P. Houde, and D.W. Krause. 1983. A new earliest Tiffanian (Late Paleocene) mammalian fauna from Bangtail Plateau, western Crazy Mountain Basin, Montana. Journal of Paleontology, 57: 957-970.

Goloboff, P. 1994. NONA version 1.9. Computer program and documentation. Available at ftp.unt.edu.ar/pub/parsimony.

Granger, W., and GG.Simpson. 1929. A revision of Tertiary Multituberculata. Bulletin of the American Museum of Natural History 56: 601-676.

Grossmann, M., M.R. Sánchez-Villagra, and W. Maier. 2002. On the development of the shoulder girdle in *Crocidura russula* (Soricidae) and other placental mammals: evolutionary and functional aspects. Journal of Anatomy 201: 371-381.

Hahn, G. 1973. Neue Zähne von Haramiyiden aus der Deutschen Ober-Trias und ihre beziehungen zu den Multituberculaten. Palaeontolographica, Abteilung A 142: 1-15.

Harshman, J. 1994. The Effect of Irrelevant Characters on Bootstrap Values. Systematic Biology 43(3): 419-424.

Horovitz, I. 2000. The tarsus of *Ukhaatherium nessovi* (Eutheria, Mammalia) from the Late Cretaceous of Mongolia: an appraisal of the evolution of the ankle in basal therians. Journal of Vertebrate Paleontology 20(3). 547-560.

Horovitz, I. 2003. Postcranial skeletal morphology of *Ukhaatherium nessovi* (Eutheria, Mammalia) from the Late Cretaceous of Mongolia. Journal of Vertebrate Paleontology 23: 857-868 .

Hu, Y.-M., Y.-Q. Wang, Z.-X. Luo, and C.-K. Li. 1997. A new symmetrodont mammal from China and its implications for mammalian evolution. Nature 390: 137–142.

Hu, Y-M., Y. Wang, C-K. Li, and Z. Luo. 1998. Morphology of dentition and forelimb *Zhangheotherium*. Vertebrata PalAsiatica 38: 102-125.

Hu, Y-M., and Y. Wang. 2002. *Sinobaatar* gen. nov.: First multituberculate from the Jehol biota of Liaoning, Northeast China. Chinese Science Bulletin 47 (11): 933-937.

Hu, Y.−M., J. Meng, Y.−Q. Wang, and Ch.−K. Li. 2005. Large Mesozoic mammals fed on young dinosaurs. Nature 433: 149–152.

Hurum, J. H., Z.−X. Luo, and Z. Kielan−Jaworowska. 2006. Were mammals originally venomous? Acta Palaeontologica Polonica 51: 1–11.

Jenkins, F.A.Jr. 1971. The postcranial skeleton of African cynodonts. Peabody Museum of Natural History Bulletin 36: 1–216.

Jenkins, F.A. Jr. 1973. The functional anatomy and evolution of the mammalian humero-ulnar joint. The American Journal of Anatomy 137: 281-298.

Jenkins, F.A.Jr, and D.W. Krause. 1983. Adaptations for climbing in North American multituberculates (Mammalia). Science 220: 713-715.

Jenkins, F.A.Jr., S.M. Gatesy, N.H. Shubin, and W.W. Amaral. 1997. Haramiyids and Triassic mammalian evolution. Nature 385: 715–718.

Jepsen, G.L. 1930. Stratigraphy and paleontology of the Paleocene of northeastern Park County, Wyoming. Proceedings of the American Philosophical Society 69: 463–528

Jepsen, G.L. 1940. Paleocene faunas of the Polecat Bench Formation, Park County, Montana. Proceedings of the American Philosophical Society 83: 217–341.

Ji,Q., Z.-X. Luo, and S. Ji. 1999. A Chinese triconodont mammal and mosaic evolution of the mammalian skeleton. Nature 398. 328-330.

Ji, Q., Z.-X. Luo, C.-X.Yuan, J.R. Wible, J.-P. Zhang, and J.A. Georgi. 2002. The earliest known eutherian mammal. Nature 416: 816–822.

Joyce, W.G., and M.A. Norell. 2005. *Zangerlia ukhaachelys*, new species, a nanhsiungchelyid turtle from the late Cretaceous of Ukhaa Tolgod, Mongolia. American Museum Novitates 3481: 1-19.

Kielan-Jaworowska, Z. 1970. New Upper Cretaceous multituberculate genera from Bayan Dzak, Gobi Desert. Palaeontologica Polonica 21: 35-49.

Kielan-Jaworowska, Z. 1971. Skull structure and affinities of the Multituberculata. Palaeonotologia Polonica 25: 5-41.

Kielan-Jaworowska, Z. 1977. Evolution of the therian mammals in the Late Cretaceous of Asia. Part II. Postcranial skeleton in *Kennalestes* and *Asioryctes*. Palaeontologia Polonica 37: 65–83.

Kielan- Jaworowska, Z. and D. Dahszeveg, 1978. New Late Cretaceous mammal locality in Mongolia and a description of a new multituberculate. Acta Palaeontologica Polonica 23: 115-130.

Kielan-Jaworowska, Z. 1979. Pelvic structure and nature of reproduction in Multituberculata. Nature 277: 402-403.

Kielan-Jaworowska, Z. 1986. Brain evolution in Mesozoic mammals. Contributions to Geology, University of Wyoming, Special Paper 3, 21-34.

Kielan-Jaworowska, Z. 1989. Postcranial skeleton of a Cretaceous multituberculate mammal. Acta Palaeontologica Polonica 34: 75-85.

Kielan-Jaworowska, Z., and T. Qi. 1990. Fossorial adaptations of a taeniolabidoid multituberculate mammal from the Eocene of China. Vertebrata Palasiatica 28: 81-94.

Kielan-Jaworowska, Z. 1992. Interrelationships of Mesozoic mammals. Historical Biology 6: 185-202.

Kielan-Jaworowska, Z., and P.P. Gambaryan. 1994. Postcranial anatomy and habits of Asian multituberculate mammals. Fossils and Strata 36: 1–92.

Kielan-Jaworowska, Z. 1997. Characters of multituberculates neglected in phylogenetic analyses of early mammals. Lethaia 29: 249-266.

Kielan-Jaworowska, Z. 1998. Humeral torsion in multituberculate mammals. Acta Palaeontologica Polonica 43: 131-134.

Kielan-Jaworowska, Z., and J. H. Hurum. 1997. Djadochtatheria-a new suborder of multituberculate mammals. Acta Palaeontologica Polonica 42: 201-242.

Kielan-Jaworowska, Z., M.J. Novacek, B.A. Trofimov, and D. Dashzeveg. 2000. Mammals from the Mesozoic of Mongolia. *In* M. J. Benton, M. A. Shishkin, E. N. Kurochkin, and D. M. Unwin (eds.), The Age of Dinosaurs in Russia and Mongolia, 573–652. Cambridge University Press, Cambridge.

Kielan-Jaworowska, Z., and J.H. Hurum. 2001. Phylogeny and systematics of multituberculate mammals. Paleontology 44: 389-429.

Kielan-Jaworowska, Z., J.H. Hurum, P.J. Currie, and R. Barsbold. 2002. New data on anatomy of the Late Cretaceous multituberculate mammal *Catopsbaatar*. Acta Palaeontologica Polonica 47: 557-560.

Kielan−Jaworowska, Z., R.L. Cifelli, and Z.−X Luo. 2004. Mammals from the Age of Dinosaurs: Origins, Evolution, and Structure. 620 pp. Columbia University Press, New York.

Kielan−Jaworowska, Z. J.H. Hurum, and A. Lopatin. 2005. Skull structure in *Catopsbaatar* and the zygomatic ridges in multituberculate mammals. Acta Palaeontologica Polonica 50: 487–512.

Kielan-Jaworowska, Z., and J. H. Hurum, 2006. Limb Posture in Early Mammals: Sprawling or Parasagittal. Acta Palaeontologica Polonica 51: 393-406.

Klima, M. 1987. Early development of the shoulder girdle and sternum in marsupials (Mammalia: Metatheria). Advances in Anatomy, Embryology and Cell Biology 109: 1–91

Kluge, A. 1989. A concern for evidence and a phylogenetic hypothesis of relationships among *Epicrates* (Boidae, Serpentes). Systematic Zoology 38: 7–25.

Krause, D.W., and D. Baird. 1979. Late Cretaceous mammals east of the North American Western Inferior Seaway. Journal of Paleontology 53: 562-565.

Krause, D.W., and F.A.Jr. Jenkins.1983. The postcranial skeleton of North American multituberculates. Bulletin of the Museum of Comparative Zoology 150: 199-246.

Krause, D.W. 1987. Systematic revision of *Prochetodon* (Multituberculata, Mammalia) from the late Paleocene and early Eocene of western North America. Contributions from the Museum of Paleontology, University of Michigan 27: 221–236.

Kurzanov, S.M. 1992. A giant protoceratopsid from the Upper Cretaceous of Mongolia (in Russian). Palaeontological Journal: 81–93.

Lillegraven, J.A. and G. Krusat. 1991. Cranio-mandibular anatomy of *Haldanodon exspectatus* (Docodonta; Mammalia) from the Late Jurassic of Portugal and its implications to the evolution of mammalian characters. Contributions to Geology, University of Wyoming 28: 39-138.

Luo, Z-X., Z. Kielan-Jaworowska, and R.L. Cifelli. 2002. In quest for a phylogeny of Mesozoic mammals. Acta Palaeontologica Polonica 47(1): 1-78.

Luo, Z.-X., Q. Ji, J.R. Wible, and C.-X. Yuan. 2003. An Early Cretaceous tribosphenic mammal andmetatherian evolution. Science 302: 1934-1940.

Luo, Z.-X., and Q. Ji. 2005. New study on dental and skeletal features of the Cretaceous mammal *Zhangheotherium*. Journal of Mammalian Evolution 12: 337-357.

Luo, Z.-X., and J.R. Wible. 2005. A Late Jurassic digging mammal and early mammalian diversification. Science 308:103-107.

Makovicky, P. J., M.A. Norell, J.M. Clark, and T. Rowe. 2003. Osteology and Relationships of *Byronosaurus jaffei* (Theropoda: Troodontidae) American Museum Novitates 3402: 1-32.

Makovicky, P. J. 2007. Telling time from fossils: a phylogeny-based approach to chronological ordering of paleobiotas. Online early article.

Matthew, W. D., and W. Granger.1921. New genera of Paleocene mammals. American Museum Novitates 13: 1–7.

Maddison, W.P., and D.R. Maddison. 1992. MacClade: Analysis of Phylogeny and Character Evolution. Version 3.0. Sinauer Associates, Sunderland, Massachusetts. xi + 398 pp + computer program.

McKenna, M.C. 1961. On the shoulder girdle of the mammalian subclass Allotheria. American Museum Novitates 2066: 1-27.

McKenna, M.C. 1987. Molecular and morphological analysis of high-level mammalian relationships. *In* Patterson, C. (ed.): Molecules and Morphology in Evolution: Conflict or Compromise?, 55-93. Cambridge University press, Cambridge.

Meng, J. 1992. The stapes of *Lambdopsalis bulla* (Multituberculata) and transformational analyses on some stapedial features in Mammaliaformes. Journal of Vertebrate Paleontology 12: 459–471

Meng, J., and D. Miao. 1992. The breast-shoulder apparatus of Lambdopsalis bulla (Multituberculata) and its systematic and functional implications. Journal of Vertebrate Paleontology 12: 43A.

Meng, J., and A.R. Wyss. 1995. Monotreme affinities and low frequency hearing suggested by multituberculate ear. Nature 377: 141-144.

Miao, D. 1993. Cranial Morphology and Multituberculate Relationships. Pp.63-74. *In* F. S. Szalay, M. J. Novacek, and M. C. McKenna (Eds.), Mammalian Phylogeny. Volume 1. Springer Verlag, New York.

Minjin, B. 2001. Evidence from the hand of Kryptobaatar dashzevegi for the phylogenetic position of Multituberculata. Journal of Vertebrate Paleontology 21(3): 80A-81A.

Minjin, B. 2003. The tarsus of a new djadochtatherian multituberculate from Mongolia. Journal of Vertebrate Paleontology 23(3):79A.

Muizon C. de 1998. *Mayulestes ferox*, a borhyaenoid (Metatheria, Mammalia) from the early Palaeocene of Bolivia. phylogenetic and paleobiologic implications. Geodiversitas 20 (1): 19-142.

Novacek, M.J., G. Rougier, J.R. Wible, M.C. McKenna, D. Dashzeveg, and I. Horovitz. 1997. Epipubic bones in eutherian mammals from the Late Cretaceous of Mongolia. Nature 389: 483-485.

Norell, M.A., P. Makovicky, and J.M. Clark. 2000. A new troodontid from Ukhaa Tolgod, Late Cretaceous, Mongolia. Journal of Vertebrate Paleontology 20(1): 7-11.

Norell, M.A., J.M. Clark, and L.M. Chiappe. 2001. An embryonic oviraptorid (Dinosauria, Theropoda) from the Upper Cretaceous of Mongolia. American Museum Novitates 3315: 1-17.

Poplewski, R. 1948. Anatomia ssaków. Czytelnik, Warszawa, 2. 1-890.

Rigby, J.K.Jr. 1980. Swain Quarry of the Fort Union Formation, middle Paleocene (Torrejonian), Carbon County, Wyoming: geologic setting and mammalian fauna. Evolutionary Monographs 3: 1-178.

Romer, A.S. 1956. Osteology of the Reptiles. University of Chicago Press. Chicago. 772 pp.

Rougier, G.W., J.R. Wible, and M.J Novacek. 1996a. Middl-Ear Ossicles of the Multituberculate *Kryptobaatar* from the Mongolian Late Cretaceous: Implications for Mammaliamorph Relationships and the Evolution of the Auditory Apparatus. American Museum Novitates 3187: 1-43.

Rougier, G.W., J.R. Wible, and M.J.Novacek.1996b. Multituberculate phylogeny. Nature 379:406.

Rougier, G.W., J.R. Wible, and J.A. Hopson. 1996c. Basicranial anatomy of *Priacodon fruitaensis* (Triconodontidae, Mammalia) from the Late Jurassic of Colorado, and a reappraisal of mammaliaform interrelationships. American Museum Novitates 3187: 1-43.

Rougier, G.W., M.J. Novacek, and D. Dashzeveg. 1997. A New Multituberculate from the Late Cretaceous Locality Ukhaa Tolgod, Mongolia. Considerations on Multituberculate Interrelationships. American Museum Novitates 3191: 1-26.

Rougier, G., J.R. Wible, and M.J. Novacek. 1998. Implications of *Deltatheridium* specimens for early marsupial history. Nature 396: 459-463.

Rougier, G.W., and J.R. Wible. 2006. Major changes in the ear region and basicranium of early mammals. *In* M. Carrano, T.J. Gaudin, R. Blob, and J.R. Wible (editors), Amniote Paleobiology: Phylogenetic and Functional Perspectives on the Evolution of Mammals, Birds and Reptiles: 269-311. University of Chicago Press, Chicago.

Rowe, T.B. 1988. Definition, diagnosis, and origin of Mammalia. Journal of Vertebrate Paleontology 8:241-264.

Rowe, T.B. 1993. Phylogenetic systematics and the early history of mammals. *In* F.S. Szalay, M.J. Novacek, and M.C. McKenna (eds.), Mammal Phylogeny: Mesozoic Differentiation, Multituberculates, Monotremes, Early Therians, and Marsupials, 129–145. Springer-Verlag, New York.

Sahni, A.1972. The vertebrate fauna of the Judith River Formation, Montana. Bulletin of the American Museum of Natural History 147: 323-412.

Sanchez-Villagra, M.R., and W. Maier. 2003. Ontogenesis of the scapula in marsupial mammals, with special emphasis on perinatal stages of didelphids and remarks on the origin of the therian scapula. Journal of Morphology 258(2): 115-129.

Sargis, E.J., D.M. Boyer, J.I. Bloch, and M.T. Silcox. 2007. Evolution of pedal grasping in Primates. Journal of Human Evolution 53: 103-107.

Schaeffer, B. 1941. The morphological and functional evolution of the tarsus in amphibians and reptiles. Bulletin of the American Museum of Natural History 78: 395–472.

Schaeffer, B. 1947. Notes on the origin of the artiodactyls tarsus. American Museum Novitates 1356: 1-24.

Schaeffer, J.P. 1953. Morris' Human Anatomy: A Complete Systematic Treatise. Eleventh Edition. The Blakiston Company, New York and Toronto: 1-1718.

Scott, G.S. 2005. New Neoplagiaulacid multituberculates (Mammalia: Allotheria) from the Paleocene of Alberta, Canada. Journal of Paleontology 79(6): 1189-1213.

Sereno, P.C., and M.C. McKenna. 1995. Cretaceous multituberculate skeleton and the early evolution of the mammalian shoulder girdle. Nature 377: 144-147.

Sereno, P. 2006. Shoulder Girdle and Forelimb in Multituberculates: Evolution of Parasagittal Forelimb Posture in Mammals. *In* M. Carrano, T.J. Gaudin, R. Blob, and J.R. Wible (editors), Amniote Paleobiology: Phylogenetic and Functional Perspectives on the Evolution of Mammals, Birds and Reptiles: 315-366. University of Chicago Press, Chicago.

Simmons, N.B., and D. Miao. 1986. Paraphyly of *Catopsalis* (Mammalia: Multituberculata) and its biogeographic implications. Contributions to Geology, University of Wyoming, Special Paper 3: 87–94.

Simmons, N.B. 1993. Phylogeny of Multituberculata. *In* F.S. Szalay. M.J. Novacek, and M.C. McKenna (eds.), Mammalian phylogeny: Mesozoic differentiation, multiutberculates, monotremes, early therians, and marsupials. 146-164. New York: Springer-Verlag.

Simpson, G.G. 1926. Mesozoic Mammalia. IV. The multituberculates as living mammals. American Journal of Sciences 2: 228-250.

Simpson, G.G. 1928. Further notes on Mongolian Cretaceous mammals. American Museum Novitates 329: 1-14.

Simpson, G.G., and H.O. Elftman. 1928. Hind limb musculature and habits of a Paleocene multituberculate. American Museum Novitates 333: 1-19.

Simpson, G.G. 1945. The principles of classification and a classification of mammals. Bulletin of the American Museum of Natural History 85: 1-350.

Simpson, G.G. 1947. *Haramiya*, new name, replacing *Microcleptes* Simpson, 1928. Journal of Paleontology 21: 497.

Sloan, R.E., and L. Van Valen. 1965. Cretaceous mammals from Montana. Science 148: 220-227.

Smith, T., D.-Y. Guo, and Y. Sun. 2001. A new species of *Kryptobaatar* (Multituberculata): the first Late Cretaceous mammal from Inner Mongolia (P. R. China). Bulletin de l'Institut Royal des Sciences Naturelles de Belgique, Sciences de la Terre 71, supplement: 29–50.

Spurlin, B.K., M.J. Novacek, and G.W. Rougier. 2000. Ear region evolution in multituberculates: a new taxon from the Late Cretaceous locality Udan Sayr, Mongolia. Journal Vertebrate Paleontology 21(3): 70-71.

Stafford, B.J., and R.W. Thorington. 1998. Carpal development and morphology in archontan mammals. Journal of Morphology 235(2): 135-155.

Szalay, F.S., and R.L. Decker. 1974. Origin, evolution, and function of the tarsus in Late Cretaceous Eutheria and Paleocene Primates. *In* F. A. Jenkins, Jr. (ed.), Primate Locomotion, 223–259. Academic Press, London.

Szalay, F.S. 1993b. Pedal evolution of mammals in the Mesozoic: tests for taxic relationships. *In* F.S. Szalay, M.J. Novacek, and M.C. McKenna (eds.), Mammal Phylogeny: Mesozoic Differentiation, Multituberculates, Monotremes, Early Therians, and Marsupials, 108–128. Springer-Verlag, New York.

Szalay, F.S. 1994. Evolutionary History of the Marsupials and an Analysis of Osteological Characters. 481 pp. Cambridge University Press, Cambridge.

Szalay, F.S., and B.A. Trofimov.1996. The Mongolian Late Cretaceous *Asiatherium*, and the early phylogeny and paleobiogeography of Metetheria. Journal of Vertebrate Paleontology 16: 474-509.

Swofford, D.L. 2000. PAUP. Phylogenetic Analysis Using Parsimony. Version 4.0. Sinauer Associates, Sunderland.

Swofford, D.L. (2002). PAUP,∗ Phylogenetic Analysis Using Parsimony (∗ and Other Methods), Version 4.0b10, Sinauer Associates, Sunderland, MA. Available at http://paup.csit.fsu.edu/.

Thiele, K. 1993. The holy grail of the perfect character: the cladistic treatment of morphometric data. Cladistics 9: 275-304.

Van Valen, L., and R.E. Sloan. 1966. The extinction of the multituberculates. Systematic Zoology 15: 261–278.

Vickaryous, M.K., and K.H. Hall. 2006. Homology of the reptilian coracoid and a reappraisal of the evolution and development of the amniote pectoral apparatus. Journal of Anatomy 208(3): 263-285.

Wang, Y.-Q., Y.-M. Hu, J. Meng, and C.-K. Li. 2001. An ossified Meckel's cartilage in two Cretaceous mammals and origin of the mammalian middle ear. Science 294: 357–361.

Weil, A. 1999. Multituberculate phylogeny and mammalian biogeography in the Late Cretaceous and earliest Paleocene Western Interior of North America. Ph.D. dissertation, University of California, Berkeley.

Wible, J.R., and J.A. Hopson. 1993. basicranial evidence for early mammal phylogeny. Pp. 45-62. *In* F.S. Szalay, M.J. Novacek, and M.C. McKenna (eds.) Mammalian Phylogeny. Volume 1. Springer Verlag, New York.

Wible, J.R., G.W. Rougier, M.J. Novacek, and M.C. McKenna, and D. Dashzeveg. 1995. A mammalian petrosal from the Early Cretaceous of Mongolia: implications for the evolution of the ear region and mammaliamorph relationships. American Museum Novitates 3149:1-19.

Wible, J.R., and G.W. Rougier, 2000. Cranial anatomy of *Kryptobaatar dashzevegi* (Mammalia, Multituberculata) and its bearing on the evolution of mammalian characters. Bulletin of the American Museum of Natural History 247: 1-124.

Wiens, J.J. 2001. Character Analysis in Morphological Phylogenetics: Problems and Solutions. Systematic Biology 50(5): 689-699.

Wilkinson, M. 1994. Common cladistic information and its consensus representation: reduced Adams and reduced cladistic consensus trees and profiles. Systematic Biology 43: 343–368.

Wilkinson, M. 1995. Coping with abundant missing entries in phylogenetic inference using parsimony. Systematic Biology 44: 501-514.

Wilkinson, M., J.L. Thorley and P. Upchurch. 2000. A Chain Is No Stronger than Its Weakest Link: Double Decay Analysis of Phylogenetic Hypotheses. Systematic Biology 49 (4): 754-776.